

# **Experimental Measurement and Modelling of Heat Transfer in Spiral and Curved Channels**

by

©Mehdi Ghobadi

A Thesis submitted to the School of Graduate Studies in partial fulfillment of the requirements for the degree of

**Doctor of Philosophy**

**Faculty of Engineering and Applied Science**

Memorial University of Newfoundland

**May 2014**

St. John's

Newfoundland

# Abstract

Heat transfer enhancement is desired in most thermal applications. In general, there are two methods to improve the heat transfer rate: active and passive techniques. Active techniques are based on external forces such as electro-osmosis, magnetic stirring, etc. to perform the augmentation. Active techniques are effective; however, they are not always easy to implement with other components in a system. They also increase the total cost of the system manufacturing. On the other hand, passive techniques employ fluid additives or special surface geometry. Using the surface geometry approach is easier, cheaper and does not interfere with other components in the system. Surface modification or additional devices incorporated in the stream are two passive augmentation techniques. With these techniques, the existing boundary layer is disturbed and the heat transfer performance is improved. However, pressure drop is also increased. Curved geometry is one of the passive heat transfer enhancement methods that fit several heat transfer applications such as: compact heat exchangers, steam boilers, gas turbine blades, electronics cooling, refrigeration and etc. This dissertation contains eight chapters.. Chapter one is the introduction and shows the originality, novelty and importance of the work. Chapter two reviews the literatures on the heat transfer and the pressure drop correlations in curved circular tubes. In chapters three and four, two heat sinks having spiral and straight channel geometry engraved on them are examined experimentally. Heat transfer and pressure drop inside them are

measured, and reduced to apply two existing correlations to predict their behaviour analytically. In chapters five, six and seven, thermal and flow behaviour inside curved geometry are studied experimentally. The calculated heat transfer coefficient and pressure drop are compared to the existing models. Comparing the predicted Nusselt number from the existing models, poor accuracy was observed in the region of  $5 < Pr < 15$ . Finally, in chapters six and seven two new asymptotic correlations are proposed to calculate the heat transfer and the pressure drop inside mini scale curved and coiled tubes.

# Acknowledgements

I would like to express the deepest appreciation to my supervisor, Dr. Yuri S. Muzychka, who has the attitude and the substance of a great mentor. Without his guidance and persistent help this dissertation would not have been possible.

I would also like to express my gratitude to Dr. Serpil Kocabiyik, the co-supervisor of this thesis, for her useful comments, remarks and engagement.

Last but not the least, I would like to thank my lovely wife, Nikoo. This work could not have been possible without her continuous support and encouragement.

# Table of Contents

Abstract	ii
Acknowledgments	iv
Table of Contents	ix
List of Tables	xi
List of Figures	xvi
Nomenclature	xvii
<b>1 Introduction</b>	<b>1</b>
1.1 Overview . . . . .	1
1.2 Curved Geometry . . . . .	3
1.3 Objectives . . . . .	5
1.4 Methodology . . . . .	6
1.5 Organization of the Thesis . . . . .	7
1.6 References . . . . .	10
<b>2 A Review of Heat Transfer and Pressure Drop Correlations for Laminar Flow in Curved Circular Ducts*</b>	<b>14</b>

2.1	Introduction . . . . .	15
2.2	Problem Formulation . . . . .	20
2.3	Developing Flow . . . . .	25
2.3.1	Hydrodynamically Developing Flow . . . . .	25
2.3.2	Thermally Developing and Hydrodynamically Developed Flow	28
2.3.3	Thermally and Hydrodynamically Developing . . . . .	31
2.4	Critical Reynolds Number . . . . .	32
2.5	Review of The Fluid Flow Correlations in Fully Developed Flow . . .	35
2.6	Review of the Heat Transfer Correlations in Fully Developed Flow . .	42
2.6.1	Constant Temperature . . . . .	48
2.6.2	Constant Heat Flux . . . . .	50
2.7	Conclusions . . . . .	59
2.8	Acknowledgement . . . . .	60
2.9	References . . . . .	61
<b>3</b>	<b>Heat Transfer and Pressure Drop in a Spiral Square Channel*</b>	<b>82</b>
3.1	Introduction . . . . .	83
3.2	Experimental Setup . . . . .	86
3.3	Benchmarking and Uncertainty . . . . .	88
3.4	Graetz flow for Constant Wall Temperature . . . . .	90
3.5	Data Analysis . . . . .	93
3.6	Results and Discussion . . . . .	94
3.7	Analytical Prediction . . . . .	97
3.8	Pressure Drop . . . . .	101
3.9	Conclusion . . . . .	103
3.10	References . . . . .	105

<b>4</b>	<b>Heat Transfer and Pressure Drop in Mini Channel Heat Sinks*</b>	<b>110</b>
4.1	Introduction . . . . .	111
4.2	Heat Sinks and Experimental Setup . . . . .	116
4.3	Benchmarking and Uncertainty . . . . .	118
4.4	Analytical Model . . . . .	119
4.5	Data Analysis . . . . .	122
4.6	Results and Discussion . . . . .	123
	4.6.1 Heat Transfer . . . . .	124
	4.6.2 Pressure Drop . . . . .	127
4.7	Conclusion . . . . .	131
4.8	References . . . . .	133
<b>5</b>	<b>Effect of Entrance Region and Curvature on Heat Transfer in Mini Scale Curved Tubing at Constant Wall Temperature*</b>	<b>137</b>
5.1	Introduction . . . . .	138
5.2	Experimental Setup . . . . .	144
5.3	Data Analysis . . . . .	146
5.4	Results and Discussion . . . . .	149
5.5	Conclusion . . . . .	160
5.6	References . . . . .	162
<b>6</b>	<b>Pressure Drop in Mini-Scale Coiled Tubing*</b>	<b>166</b>
6.1	Introduction . . . . .	167
6.2	Experimental Setup . . . . .	171
6.3	Data Analysis . . . . .	175

6.4	Results and Discussion . . . . .	177
6.5	Conclusion . . . . .	188
6.6	References . . . . .	190
<b>7</b>	<b>Fully Developed Heat Transfer in Mini Scale Coiled Tubing for Constant Wall Temperature*</b>	<b>193</b>
7.1	Introduction . . . . .	194
7.2	Experimental Setup . . . . .	199
7.3	Data Analysis . . . . .	201
7.4	Results and Discussion . . . . .	205
7.5	Conclusion . . . . .	216
7.6	References . . . . .	218
<b>8</b>	<b>Summary and Conclusions</b>	<b>222</b>
8.1	Objectives of The Present Thesis . . . . .	222
8.1.1	Heat Transfer and Pressure Drop in a Spiral Square Channel .	222
8.1.2	Heat Transfer and Pressure Drop in Mini Channel Heat Sinks	223
8.1.3	Effect of Entrance Region and Curvature on Heat Transfer in Mini Scale Curved Tubing at Constant Wall Temperature . . .	224
8.1.4	Pressure Drop in Mini-Scale Coiled Tubing . . . . .	226
8.1.5	Fully Developed Heat Transfer in Mini Scale Coiled Tubing for Constant Wall Temperature . . . . .	227
8.2	Recommendations for Future Studies . . . . .	228
8.2.1	Two-Phase Flow inside Curved Ducts . . . . .	228
8.2.2	Particle Image Velocimetry . . . . .	228
8.2.3	Flow in Micro Scale Curved Ducts . . . . .	229

8.3	References . . . . .	229
<b>A</b>	<b>Appendix</b>	<b>230</b>
A.1	Experimental Method . . . . .	230
A.1.1	Heat Sinks . . . . .	230
A.1.2	Curved and Coiled Tubes . . . . .	233
A.2	Benchmarking Tests . . . . .	235
A.2.1	Heat Transfer . . . . .	235
A.2.2	Pressure Drop . . . . .	236
A.2.3	Viscosity Benchmarking . . . . .	237
A.3	Uncertainty Analysis . . . . .	240
A.3.1	Reynolds Number Uncertainty . . . . .	240
A.3.2	$L^*$ Uncertainty . . . . .	241
A.3.3	$q^*$ Uncertainty . . . . .	242

# List of Tables

2.1	Prandtl, Reynolds and Dean range for the different fluids . . . . .	37
2.2	Experimental Friction Factor Correlations Curved Tubes for Laminar Flow . . . . .	44
2.3	Numerical and Analytical Friction Factor Correlations Curved Tubes for Laminar Flow . . . . .	45
2.4	Experimental Studies on Heat Transfer Correlations Curved Tubes for Constant Wall Temperature . . . . .	51
2.5	Numerical and Theoretical Studies on Heat Transfer Correlations Curved Tubes for Constant Wall Temperature . . . . .	52
2.6	Experimental Studies on Heat Transfer Correlations Curved Tubes for Constant Heat Flux . . . . .	56
2.7	Numerical and Theoretical Studies on Heat Transfer Correlations Curved Tubes for Constant Heat Flux . . . . .	57
3.1	Prandtl, Reynolds, and Peclet Numbers for Examined Fluids . . . . .	96
3.2	RMS of the Dravid Correlation Prediction . . . . .	98
4.1	Prandtl, Reynolds, and Peclet Numbers for Examined Fluids . . . . .	123
5.1	Curved tubes lengths in cm . . . . .	143
5.2	Prandtl, Reynolds and Dean range for the different fluids . . . . .	150

6.1	Tubing outer and Inside Diameter . . . . .	172
6.2	Tubing outer and Inside Diameter . . . . .	177
7.1	Tubing outer and Inside Diameter . . . . .	198
7.2	Prandtl, Reynolds and Dean Range for the Different Fluids . . . . .	206
A.1	RMS of heat transfer benchmarking test . . . . .	236
A.2	Silicone oils benchmarking results . . . . .	240

# List of Figures

1.1	Secondary flow field at low and high Dean numbers [24]. . . . .	5
2.1	Different type of curved tube geometries: (a) helical coil, (b) bend tube, (c) serpentine tube, (d) spiral and (e) twisted tubes . . . . .	16
2.2	Secondary flow field at low and high Dean numbers [33] . . . . .	19
2.3	The influence of Prandtl number on the Nusselt numbers in the en- trance region of a curved circular tube for the T boundary condition [46] . . . . .	29
2.4	Critical Reynolds number reported by different researchers [99] . . . .	34
2.5	The influence of Prandtl number on the Nusselt numbers in the en- trance region of a curved circular tube for the T boundary condition .	35
2.6	The influence of the Dean number on axial velocity profiles in a hori- zontal curved tube: (a) horizontal plane, (b) vertical plane [46] . . . .	38
2.7	Fully Developed $(fRe)_p/(fRe)_s$ , as a function of the Dean number [33]	38
2.8	Experimental friction factor correlations comparison [33] . . . . .	41
2.9	Numerical friction factor correlations comparison . . . . .	42
2.10	The dimensionless horizontal temperature profile for T boundary con- dition as a function of a) Dean number and b) Prandtl number for a curved tube . . . . .	46

2.11	A comparison of the Manlapaz Correlation for the Nusselt Prediction for Constant Wall Temperature [175] . . . . .	53
2.12	A comparison of the Manlapaz Correlation for the Nusselt Prediction for Constant Heat Flux [175] . . . . .	58
2.13	Effectiveness of curved circular tubes as compared to straight tubes [186]	59
3.1	Experimental test setup and the spiral channel . . . . .	88
3.2	Pressure drop and heat transfer benchmarking test in straight circular tubes with 10% error bars . . . . .	90
3.3	Different fluid performance for the middle inlet spiral channel . . . . .	95
3.4	Different fluid performance for the side inlet spiral channel . . . . .	95
3.5	a) Inlet effect on heat transfer for 3 cSt silicone oil, b) Heat transfer enhancement ratio for 0.65 cSt silicone oil . . . . .	97
3.6	Program flow chart . . . . .	99
3.7	Dravid model predictions for 1 cSt silicone oil . . . . .	100
3.8	Dravid model predictions for 3 cSt silicone oil . . . . .	100
3.9	Dravid prediction for examined fluids . . . . .	101
3.10	Pressure drop for the spiral channel with middle and side inlet com- parison to the straight channel of an identical size . . . . .	103
3.11	Pressure drop and heat transfer performance comparison of spiral chan- nel and an identical straight channel . . . . .	104
4.1	Spiral and straight heat sinks used in the experiments . . . . .	116
4.2	Experimental test setup . . . . .	117
4.3	Pressure drop and heat transfer benchmarking test in straight circular tubes . . . . .	119
4.4	Different fluid performance for the middle inlet spiral channel heat sink	124

4.5	Different fluid performance for the side inlet spiral channel heat sink .	125
4.6	Different fluid performance for the straight channel heat sink . . . . .	126
4.7	The configuration effect of channel pattern for 1 cSt silicon oil . . . . .	127
4.8	The entrance effect in the spiral heat sink for 10 cSt silicon oil . . . . .	128
4.9	Dimensionless pressure drop comparison between the heat sinks . . . . .	129
4.10	Pressure drop comparison of the heat sinks versus water velocity . . . . .	130
4.11	Dimensionless heat transfer versus dimensionless pressure drop comparison . . . . .	131
5.1	Curved tubing in different lengths . . . . .	143
5.2	System configuration . . . . .	145
5.3	Benchmarking results with 10 percent error bars . . . . .	146
5.4	Dravid model comparison for the experimental results for water R=4 cm, L=25.12 cm with 10 percent error bars . . . . .	151
5.5	Dravid model comparison for 1 cSt silicone oil R=2 cm, L=9.42 cm with 10 percent error bars . . . . .	152
5.6	Different radius of curvature for water with L=6.28 cm . . . . .	153
5.7	Different radius of curvature for 1 cSt silicone oil with L=25.12 cm . . . . .	154
5.8	Nusselt analysis for different radius of curvature for water at L=6.28 cm . . . . .	155
5.9	Nusselt analysis for different radius of curvature for 1 cSt silicone oil with L=25.12 cm . . . . .	155
5.10	Nusselt analysis for different lengths for 0.65 cSt silicone oil with R=4 cm . . . . .	157
5.11	Nusselt analysis for different lengths for 3 cSt silicone oil with R=2 cm . . . . .	157
5.12	Normalized Reynolds analysis for different lengths for 0.65 cSt silicone oil with R=4 cm . . . . .	158

5.13	Normalized Reynold analysis for different lengths for 3 cSt silicone oil with R=2 cm . . . . .	159
5.14	Viscosity effect on the curved tube with R=2 cm and L=9.42 cm . . .	160
5.15	Viscosity effect on the curved tube with R= 8 cm and L=25.12 cm . .	162
6.1	Experimental Setup . . . . .	173
6.2	Benchmarking results for a straight tube, with error bars represent $\pm 10\%$	174
6.3	$f_c Re$ vs Re for 1.016 mm tube diameter and 0.5 m length . . . . .	179
6.4	$f_c Re$ vs Re for 1.27 mm tube diameter and 1 m length . . . . .	180
6.5	$f_c Re$ vs Re for 1.27 mm tube diameter and 0.5 m length . . . . .	180
6.6	$f_c Re$ vs Re for 1.59 mm tube diameter and 1 m length . . . . .	181
6.7	$f_c Re$ vs Re for 1.59 mm tube diameter and 0.5 m length . . . . .	181
6.8	Manlapaz-Churchill correlation for different D/R ratios . . . . .	184
6.9	$f_c Re$ vs De for 1.016 mm tube diameter and 0.5 m length . . . . .	184
6.10	$f_c Re$ vs De for 1.27 mm tube diameter and 1 m length . . . . .	186
6.11	$f_c Re$ vs De for 1.27 mm tube diameter and 0.5 m lengt . . . . .	186
6.12	$f_c Re$ vs De for 1.59 mm tube diameter and 1 m length . . . . .	187
6.13	$f_c Re$ vs De for 1.59 mm tube diameter and 0.5 m length . . . . .	187
6.14	$f_c Re$ vs De for all of the experimental results . . . . .	188
7.1	System configuration . . . . .	200
7.2	Benchmarking results for a straight tube, with error bars represent $\pm 10\%$	202
7.3	Heat transfer performance of different curvatures for constant length of 0.26 m with 0.65 cSt oil . . . . .	207
7.4	Heat transfer performance of different curvatures for constant length of 0.13 m with 1 cSt oil . . . . .	208

7.5	Heat transfer performance of different curvatures for constant length of 0.26 m with water . . . . .	208
7.6	Proposed model prediction for constant length of 0.26 m and different curvatures with 0.65 cSt oil . . . . .	211
7.7	Proposed model prediction for constant length of 0.13 m and different curvatures with 1 cSt oil . . . . .	212
7.8	Proposed model prediction for constant length of 0.26 m and different curvatures with water . . . . .	212
7.9	Model prediction for 1 cm curvature and 0.65 cSt oil . . . . .	214
7.10	Model prediction for 4 cm curvature and 1 cSt oil . . . . .	214
7.11	Model prediction for 2 cm curvature and water . . . . .	215
7.12	Viscosity effect on the curved tubing with three turns of 2 cm radius	216
7.13	Viscosity effect on the curved tubing with three turns of 1 cm radius	217
A.1	Heat sinks channel patterns . . . . .	231
A.2	Experiment configurations of the heat sinks tests . . . . .	232
A.3	A heat sink inside the insulation box . . . . .	233
A.4	Coiled tubes used for the heat transfer experiments in Chapter 7 . . .	234
A.5	A coiled tube used for the pressure drop tests . . . . .	234
A.6	The straight tube used for the heat transfer benchmarking test . . . .	236
A.7	Heat transfer benchmarking results for water and different silicone oils with 10% error bars . . . . .	237
A.8	Pressure drop benchmarking results for water with 10% error bars . .	238
A.9	Viscosity of the silicon Oils given by the company (Clear Co.) . . . .	239

## Nomenclature

$A$	=	area, $m^2$
$a$	=	tube radius, $m$
$b$	=	coil pitch, $m$
$C_p$	=	specific heat capacity, $J/kg.K$
$D_h$	=	hydraulic diameter, $m$
$De$	=	Dean number, $\equiv Re\sqrt{(a/R)}$
$Eu$	=	Euler number, $\equiv \frac{\Delta p}{\frac{1}{2}\rho V^2}$
$f$	=	Fanning friction factor, $\equiv \frac{\Delta p}{L} \frac{D}{4} \frac{1}{\frac{1}{2}\rho U^2}$
$Gr$	=	Graetz number, $\equiv \frac{Pe}{L/D}$
$h$	=	thermal convection coefficient, $W/m^2K$
$ID$	=	inner diameter of tubing, $m$
$k$	=	thermal conductivity, $W/mK$
$L$	=	length of curved tubing, $m$
$L^*$	=	dimensionless thermal length
$m$	=	power for the empirical approach
$m_1$	=	experimental correlation constant
$m_2$	=	experimental correlation constant
$\dot{m}$	=	mass flow rate, $(kg/s)$
$n$	=	power for the Asymptotic approach
$Nu$	=	Nusselt number, $\equiv hD/k$

$OD$	=	outer diameter of tubing, $m$
$P$	=	tube perimeter, $m$
$Pe$	=	Peclet number, $\equiv UD/\alpha$
$Pr$	=	Prandtl number, $\equiv \nu/\alpha$
$q$	=	heat flux, $W/m^2$
$q^*$	=	Dimensionless mean wall flux
$R$	=	radius of curvature, $m$
$R_c$	=	effective radius of curvature, $m$
$R$	=	radius of curvature, $m$
$R_c$	=	effective radius of curvature, $m$
$R_{thermal}$	=	thermal resistance, $W/m.K$
$1/R$	=	curvature, $1/m$
$Re$	=	Reynolds number, $\equiv UD/\nu$
$T$	=	temperature, $K$
$U$	=	average liquid velocity, $m/s$
$x$	=	axial position

### ***Greek Symbols***

$\alpha$	=	thermal diffusivity, $m^2/s$
$\theta$	=	angel of the length from the entrance, $rad$
$\delta$	=	boundary layer thickness, $m$
$\zeta$	=	boundary layers ratio, $\delta_t h/\delta$
$\eta$	=	torsion, $\eta = \frac{(b/2\pi)}{R_c^2 + (b/2\pi)^2}$
$\mu$	=	dynamic viscosity, $Ns/m^2$
$\rho$	=	fluid density, $kg/m^3$

### ***Superscripts***

\* = dimensionless

$\overline{(\cdot)}$  = mean value

### ***Subscripts***

*a* = ambient

*ave* = average

*c* = curved

*crit* = critical

*H1* = *H1* boundary condition

*H2* = *H2* boundary condition

*i* = inlet

*m* = mean

*o* = outlet

*p* = peripheral

*p* = straight

*T* = constant temperature

*th* = thermal

*x* = local

*w* = wall

# Chapter 1

## Introduction

### 1.1 Overview

The prevailing trend of miniaturization in electronic devices is aligned with the increasing demand for higher performance and reliability, requires new methods for the removal of heat. Thermal management of these miniature electronic devices has attracted many researchers to develop efficient and cost competitive heat removal systems. Thermal management for heat fluxes up to  $10,000 \text{ W/cm}^2$ , which are generated by state-of-the-art chips in very small volume is needed. Conventional air-cooled heat sinks have limited the heat transfer coefficient that should be improved. Liquid cooled micro channel flow networks, as heat sinks are known to be a promising approach to this heat transfer problem because of its ease of manufacture at the chip level. Micro-fabrication technologies also allow production of miniature liquid cooled heat sinks that are suitable for microprocessor cooling. However, even the upper range of heat fluxes achieved in such micro-channel heat sinks will not meet the increasing demands of the electronics industry.

A micro-channel or mini channel heat sink is a device that removes heat by fluid flowing in channels over a heated substrate (e.g. a computer chip). Single-phase

flow in micro-channels and mini channels is often laminar, and additional means to increase the mass and heat transfer rates in micro-channels is desired. Tuckerman and Pease [1] were pioneers to introduce the micro-channel heat sink cooling concept [2]. A rectangular micro-channel with a width of  $50 \mu m$  and depth of  $302 \mu m$  was fabricated on  $1 \times 1 cm^2$  silicon wafer. Using water as working fluid, they demonstrated an impressive heat removal rate of  $790 W/cm^2$  with their integrated single phase microchannel heat sink, however at the expense of significant pressure losses of over 2 bar for one square centimeter of chip. The topic attracted many other researchers who mainly worked on straight channels [3-7]. However new methods for heat transfer enhancement are needed to improve the performance of heat sink. In general, there are two methods to improve the heat transfer: active and passive techniques [8, 9].

The active techniques base on external forces such as electro-osmosis [10], magnetic stirring [11], bubble induced acoustic actuation [12] and ultrasonic effects [13] to perform the augmentation. The active technique is effective; however, it is not always easy to perform the compatible design with other component in a system. It also increases the total cost of the system.

On the other hand, passive techniques employ fluid additives or special surface geometry. Using the geometry approach is easier, cheaper and does not interfere with other components in the system. Surface modification and additional devices incorporated into the equipment are two passive augmentation techniques. In these techniques, the existing boundary layer is disturbed and the heat transfer performance is improved, however pressure drop is also increased significantly [14].

Curved geometries fits several practical applications, because of lack of moving parts, compactness in structure, ease of manufacture and arrangement and high efficiency in heat transfer. The various types of curved tube geometries can be classified as follows: (a) torus (constant curvature and zero pitch), coiled or helical tube (constant

curvature and pitch), serpentine tubes (periodic curved tubes with zero pitch) with bends or elbows, spirals (Archimedian spirals), and twisted tubes.

## 1.2 Curved Geometry

Using curved geometries is preferred to other conventional agitation techniques due to their similar and sometimes better performance. Lower energy consumption and maintenance cost make them even more attractive. Heat transfer augmentation due to secondary flow and providing a higher heat and mass transfer area per unit volume of space are two main advantages that are achieved in heat and mass transfer applications. Curved tubes can provide homogenization of feed streams with a minimum residence time and are available in most materials of construction.

Curved geometry application in nanofluidics attracted many researchers [16, 17, 18]. Naphon et al. [16] investigated heat transfer in nanofluidics in mini heat sinks. Hashemi et al. [17] experimentally studied on heat transfer and pressure drop of nanofluid flow in a horizontal helically coiled tube in constant heat flux. Razi et al. [18] accomplished an empirical study on the pressure drop characteristics of nanofluid inside helically coiled tubes.

From a heat transfer point of view, helically coiled exchangers offer certain advantages. Compact size provides a distinct benefit. Higher film coefficients, the rate at which heat is transferred through a wall from one fluid to another, and more effective use of available pressure drop result in efficient and less-expensive designs. True counter-current flow fully utilizes available LMTD (logarithmic mean temperature difference). Helical geometry permits handling of high temperatures and extreme temperature differentials without high induced stresses or costly expansion joints. High-pressure capability and the ability to fully clean the service-fluid flow area add

to the exchanger's advantages.

Coiled geometry also finds applications in flow through porous media [19], chemical reactors, evaporators and steam generators [20]. The idea has been widely used in biomedical studies such as protein separation and emulsification [21], blood vessels blood oxygenators [22], and drug delivery systems [23]. Reviewing all current and potential applications of curved geometry is beyond the scope of this study.

Unlike the flow in straight pipes, fluid motion in a curved pipe is not parallel to the curved axis of the bend, owing to the presence of a secondary motion caused by secondary flow. As the flow enters a curved bend, centrifugal forces act outward from the center of curvature on the fluid elements. Because of the no-slip condition at the wall, the axial velocity in the core region is much greater than that near the wall. To maintain the momentum balance between the centrifugal forces and pressure gradient, slower moving fluid elements move toward the inner wall of the curved tube. This leads to the onset of a secondary flow such that fluid near the wall moves along upper and lower halves of the torus wall while fluid far from it flows to the outer wall. The curvature,  $1/R$ , affects the flow patterns, and even slight curvature was observed to modify the critical velocity of the fluid [15].

It has been well established that for high Dean numbers,  $De > 100$ , the secondary flow field consists of a relatively inviscid core and a viscous boundary layer is initiated. Fig. 1.1 depicts the secondary flow field at low and high Dean numbers. The secondary flow increases the heat and mass transfer rates in addition to the rate of momentum transfer, the latter resulting in an increased pressure drop [24].

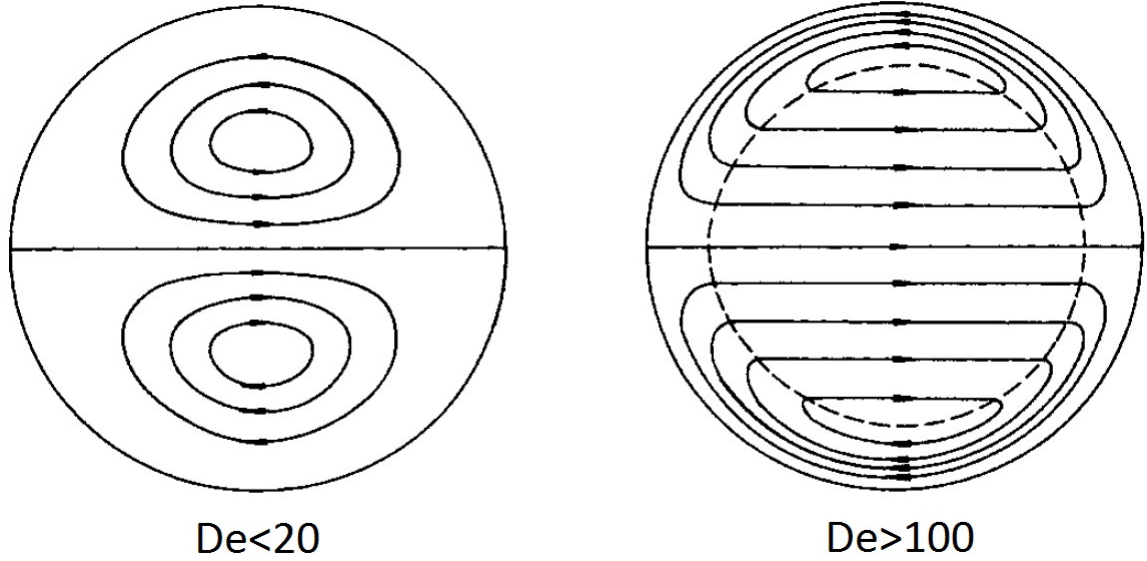


Figure 1.1: Secondary flow field at low and high Dean numbers [24].

### 1.3 Objectives

My PhD studies began with investigating the heat transfer and pressure drop characteristics of the flow inside a spiral and straight with 90 degree bends heat sinks that may be used as a heat removal system. Unlike many heat sinks using parallel channels, I examined a channel that is formed in spiral and straight geometry. I began to use only water as the working fluid, however, later silicone oils with viscosity smaller than water, the same as water and higher than water were employed to expand the heat transfer results for a wider range of Prandtl number.

Comparing the spiral heat sink results with the available correlations showed there is not a correlation that can be used to predict the heat transfer and the pressure drop of the flow inside curved tubes. The curved tubes studies began with investigating the length and curvature effects on the heat transfer augmentation. Short tubes were curved with different radius of curvature and in 90, 180, 270 and 360 degree angle of tube curvature. Hence, tubes with a same curvature and different length were

available to study the length effect on the heat transfer augmentation. Furthermore, the radii of curvature were chosen so that curved tubes with the same length and different radii of curvature were available to investigate the effect of curvature on the heat transfer enhancement.

The most important objective of the current study is developing two models for the heat transfer (Nusselt number) and pressure drop (friction factor). Long tubes were coiled with the least possible pitch. Different tube diameter and radii of curvature were used. Water and two low viscosity silicone oils were employed as working fluids. Using an empirical correlation and asymptotic concept, two asymptotic model were proposed to predict the heat transfer and pressure drop in curved and coiled tubes..

## 1.4 Methodology

All of the results presented in this dissertation are based on experimental results collected in the microfluidics lab at Memorial University of Newfoundland. As stated before, I started by designing two heat sinks, and after collecting the results from them, new experiments were designed to study the curved tubes heat transfer enhancement and pressure drop further. All of the experimental apparatus were designed in the microfluidics lab and were manufactured in the machine shop of Memorial University. Different thermocouples, pressure gages, pumps and syringes were ordered to perform the experiments with the best accuracy. Besides water, 0.65 cSt, 1 cSt, 3 cSt, 10 cSt and 100 cSt silicone oils were bought and used as a working fluid. The temperature dependent properties were provided by the manufacturer, and were confirmed in the room temperature.

Benchmarking tests were conducted before performing the experiments to ensure that the experimental apparatus are calibrated as well as for experiment design assessment.

Different methods were employed to reduce the collected data. Nusselt number and Reynolds analysis were used as well as dimensionless heat and length analysis. Discretization method was used to apply the models to the spiral heat sink. The spiral channel was divided to small cells, where the radius of curvature in each cell can be assumed to be constant.

In Chapters 6 and 7 empirical correlation and asymptotic concepts are employed to derive two new correlations to predict the heat transfer and pressure drop in curved tubes.

## 1.5 Organization of the Thesis

This dissertation contains eight chapters, including six journal papers. Chapter 2 reviews the available literatures on the heat transfer and pressure drop correlations for curved circular tubes. Chapter 2 reviews the different correlations to calculate critical Reynolds number for the flow transition from laminar to turbulent inside curved tubes. Numerical and experimental Fanning friction factor correlations are also reviewed. Heat transfer enhancement due to the curvature is also studied and numerical and empirical correlations to calculate Nusselt number are presented. Chapter 2 is submitted to *Heat Transfer Engineering Journal* for publication.

A spiral heat sink is experimentally and analytically is examined in Chapter 3. The spiral channel was fabricated in a copper plate. The cross section of the channel is square with 1 mm sides. A copper cap plate was bolted tight to seal the channel. Water and four silicone oils (0.65 cSt, 1 cSt, 3 cSt and 10 cSt) were used as the working fluid; thus Prandtl numbers from 5 to 110 were examined. The heat transfer enhancement is observed from the data reduction from the experimental results. The spiral channel is discretized to assume the same curvature in each cell and a well-known

correlation is applied to each cell to calculate the average heat transfer coefficient through the spiral channel. Two models were used to predict the Nusselt number. However, the accuracy of them was questioned for the low Prandtl numbers fluids. Chapter 3 is submitted to *Journal of Experimental Heat Transfer* for publication.

In Chapter 4 heat transfer and pressure drop for two types of square mini-channel heat sinks for the purpose of cooling are investigated: one with spiral geometry and other with straight geometry which has 90 degree bends. The cross section of the channels for both heat sinks is a 1 mm square channel and fabricated on a copper base plate. A copper cap plate is used to seal the channel. Water and five low viscosity silicon oils (0.65 cSt, 1 cSt, 3 cSt, 10 cSt and 100 cSt) were used as a coolant; thus a Prandtl number from 5 to 100 was examined. Heat transfer behaviour over a range of flow rates from laminar to turbulent has been examined for all the fluids; only water was examined as a working fluid for pressure drop measurements. It has been shown that heat transfer is increased in comparison to the straight channel of similar length due to the disturbance of the boundary layer. This disturbance also results in increasing the pressure drop. The dimensionless mean wall flux and the dimensionless thermal flow length were used to analyze the experimental data instead of conventional Nusselt number and channel length. Chapter 4 is accepted for publication in *Heat Transfer Engineering Journal* for publication.

An experimental study on heat transfer enhancement in short curved tubes for the constant wall temperature boundary condition is presented in Chapter 5. Copper tubing with four different radii of curvature (1 cm, 2 cm, 4 cm, and 8 cm) and in four lengths were used. Tubing radii were chosen, so that a constant tube length occurs in different curvatures. Hence, the effect of curvature on heat transfer at a constant length can be studied as well as the effect of heat transfer enhancement by changing the length in a constant curvature. Experimental results are also compared

with an existing model for curved tubing. Water and three different silicone oils (0.65 cSt, 1 cSt and 3 cSt) were used in the experiments to examine the effect of Prandtl number on curved tubing heat transfer augmentation. This Chapter is published in *International Journal of Heat and Mass Transfer*; 2013; 65: 357-365.

In Chapter 6 laminar, steady state flow in mini-scale coiled tubes is studied experimentally. Three different tube diameters: 1.6 mm, 1.27 mm and 1.016 mm with different lengths of 1 m and 0.5 m were coiled with different radius of curvature to provide data over a wide range of Reynolds numbers from 5 to 2300. An asymptotic model is developed based on the experimental results to predict the pressure drop increase based on Dean number. The results and simple model are also compared to a well-known existing model for circular tubing. The coiled tube lengths used in this study were long enough to consider the flow to be fully developed. The effects of varying curvature and tube length are also studied. The pitch of the coils is restricted to the diameter of the tube to minimize the effect of coiling. Dean number is used instead of Coiled number (modified Dean number) which allows the results to be expanded to spiral and curved tubing. Chapter 6 is submitted to *Experimental Thermal and Fluid Science* for publication.

An experimental study on heat transfer enhancement in mini scale coiled tubing for constant wall temperature conditions is conducted in Chapter 7. Copper coils with three different radii of curvature (1 cm, 2 cm, and 4 cm), and in four lengths (1, 2, 3 and 4 coil turns) were used. The tube length is long enough to consider the flow to be hydro-dynamically fully developed. Hence, the effects of varying curvatures and lengths on heat transfer are studied. The pitch of the coil is restricted to the diameter of the tube to minimize the effect of coiling. Dean number is used instead of Coiled number (modified Dean number), and hence, the results can be expanded to spiral and curved tubing. Water and two different silicone oils (0.65 cSt, 1 cSt) were used

in the experiments to examine the effect of Prandtl number on coiled tubing heat transfer augmentation. Prandtl numbers from 5 to 15 are covered in this paper. A new asymptotic correlation is proposed to calculate Nusselt number in fully developed coiled tubing based on the current results. This Chapter is accepted for publication in *International Journal of Heat and Mass Transfer* for publication.

Finally, a brief summary is presented in Chapter 8. Several of suggestions to continue further investigations are presented in this chapter as well.

## 1.6 References

- [1] Tuckerman D. B., Pease R. F. W., 1981, “High performance heat sinking for VLSI”, *IEEE Electron Device Letters* 2, Vol. 4, pp. 126-129.
- [2] Xi Y., Yu J., Xie Y., Gao H., 2010, “Single-phase flow and heat transfer in swirl microchannels”, *Journal of Experimental Thermal and Fluid Science*”, Vol. 34, pp. 1309-1315.
- [3] B.X. Wang, X.F. Peng, 1994, “Experimental investigation on liquid forced-convection heat transfer through microchannels”, *International Journal of Heat and Mass Transfer* 37, pp. 73-82.
- [4] W. Owhaib, B. Palm, 2004, “Experimental investigation of single-phase convective heat transfer in circular microchannels”, *Journal of Experimental Thermal and Fluid Science* 18 (2–3), pp. 105-110.
- [5] J. Li, G.P. Peterson, P. Cheng, 2004, “Three-dimensional analysis of heat transfer in a micro-heat sink with single phase flow”, *International Journal of Heat and Mass Transfer* 47, pp. 4215–4231.
- [6] Y.Q. Xie, J.Z. Yu, Z.H. Zhao, 2005, “Experimental investigation of flow and heat transfer for the ethanol–water solution and FC-72 in rectangular microchannels”,

International Journal of Heat and Mass Transfer 41, pp. 695–702.

[7] R. Revellin, B. Agostini, T. Ursenbacher, J.R. Thome, 2008, “Experimental investigation of velocity and length of elongated bubbles for flow of R-134a in a 0.5 mm microchannel”, Journal of Experimental Thermal and Fluid Science 32 (3), pp. 870–881.

[8] Sudarsan A. P., Ugaz V. M., 2005, “Fluid mixing in planar spiral microchannels”, Journal of The Royal Society of Chemistry, Vol. 6, pp. 74-82.

[9] Wongwises S., Naphon P., 2006, “A review of flow and heat transfer characteristic in curved tubes”, Journal of Renewable and Sustainable energy reviews, Vol. 10, pp. 463-490.

[10] Oddy M. H., Santiago J. G., Mikkelsen J. C., 2001 "Electrokinetic Instability Micromixing", Analytical Chemistry, Vol. 73, pp. 5822-5832.

[11] Riahi M., Alizadeh E., 2012, "Fabrication of a 3D active mixer based on deformable Fe-doped PDMS cones with magnetic actuation", Journal of Micromechanics and Micro-Engineering, Vol. 22 (11): 115001.

[12] Xiagemeng Q., Rongsheng L., Hong C., 2011, "Microfluidic Chip Based Microarray Analysis", Progress in Chemistry, Vol. 23 (1), pp. 221-230.

[13] Bartoli F., Baffigi F., 2011, "Effects of ultrasonic waves on the heat transfer enhancement in subcooled boiling", Experimental Thermal and Fluid Science, Vol. 35 (3), pp. 423-432.

[14] Webb R. L., Kim N. H., “Principles of enhanced heat transfer”, Taylor and Francis, Philadelphia, 2005.

[15] Nigam K., Vashisth S., Kumar V., 2008, "A Review on the Potential Applications of Curved Geometries in Process Industry", Industrial Engineering Chemistry Research, Vol. 47, pp. 3291-3337, .

[16] Naphon P., Nakharintr, L., 2013, "Heat Transfer of Nanofluids in the Mini-

Rectangular Fin Heat Sinks", International Communication in Heat Mass Transfer, Vol. 40, pp. 25-31.

[17] Hashemi, S. M., and Akhavan-Behabadi, M. A., 2012, "An Empirical Study on Heat Transfer and Pressure Drop Characteristics of CuO–Base Oil Nanofluid Flow in a Horizontal Helically Coiled Tube under Constant Heat Flux", International Communication in Heat and Mass Transfer, Vol. 39, pp. 144-151.

[18] Fakoor-Pakdaman M., Akhavan-Behabadi M. A., Razi P., 2013 "An Empirical Study on the Pressure Drop Characteristics of Nanofluid Flow Inside Helically Coiled Tubes", International Journal of Thermal Science, Vol. 65, pp. 206-213.

[19] Nunge R. J., Lin T. S., Grill W. N., 1972, "Laminar Dispersion in Curved Tubes and Channels", Journal of Fluid Mechanics, Vol. 52, pp. 363-383.

[20] Kallinikos L. E., Papayannakos N. G., 2010, "Intensification of Hydrodesulphurization Process With a Structured Bed Spiral Mini-Reactor", Chemical Engineering and Processes Intensification, Vol. 49, no. 10, pp. 1025-1030.

[21] Kaur J., Agrawal G.P., 2002, "Studies on Protein Transmission in Thin Channel Flow Module: the Role of Dean Vortices for Improving Mass Transfer", Journal of Membrane Science, Vol. 196, pp. 1-11.

[22] Ito Y., 2010, "Spiral column configuration for protein separation by high-speed counter current chromatography", Chemical Engineering and Processing: Process Intensification, Vol. 49, no. 7, pp. 782-792.

[23] Pechar M., Pola R., 2013, "The coiled Motif in Polymer Drug Delivery Systems", Biotechnology Advances, Vol. 31, no. 1, pp. 90-96.

[24] Dravid, A. N., Smith, K. A., Merrill, E. W., Brian, P. L. T., 1971, "Effect of Secondary Fluid Motion on Laminar Flow Heat Transfer in Helically Coiled Tubes", American Institution of Chemical Engineers, Vol. 17, no. 5, pp. 1114-1122.

[25] Shah R. K., and London A. L., 1978, "Laminar Flow Forced Convection in Ducts",

Supplement 1 to Advances in Heat Transfer, Academic, New York.

[26] Dean, W. R., 1927, "Note on the Motion of Fluid in a Curved Pipe", The London, Edinburgh and Dublin Philosophical Magazine and Journal of Science, Vol. 4, pp. 208-223.

[27] Dean, W. R., 1928, "The streamline flow through curved pipes, 6th International Conference on Multiphase Flow", The London, Edinburgh and Dublin Philosophical Magazine and Journal of Science, Vol. 5, pp. 673-695.

[28] Truesdell Jr. L. C., and Adler R. J., 1970, "Numerical Treatment of Fully Developed Laminar Flow in Helically Coiled Tubes", American Institute of Chemical Engineers, Vol. 40, pp. 1010-1015.

[29] Muzychka Y. S., Yovanovich M. M., 2004, "Laminar forced convection heat transfer in combined entry region of non-circular ducts", Journal of Heat Transfer, Vol. 126, pp. 54-62.

# Chapter 2

## A Review of Heat Transfer and Pressure Drop Correlations for Laminar Flow in Curved Circular Ducts\*

**M.Ghobadi and Y.S. Muzychka**

Microfluidics and Multiphase Flow Lab, Faculty of Engineering and Applied Science,  
Memorial University of Newfoundland, St. John's, NL, Canada, A1B 3X5

### **ABSTRACT**

Heat transfer and pressure drop correlations for fully developed laminar Newtonian fluid flow in curved and coiled circular tubes are reviewed. Curved geometry is one of the passive heat transfer enhancement methods that fits several heat transfer applications such as power production, chemical and food industries, electronics, environment engineering, etc. Centrifugal force generates a pair or two pairs of cross-sectional secondary flow (based on the Dean number), which are known as the Dean vortices, improves the overall heat transfer performance with an amplified peripheral Nusselt number variation. The main purpose of this review paper is to provide the researchers with a comprehensive database of the correlations and concept they may need during their research. The paper begins with an introduction to the governing equations and important dimensionless numbers for the flow in curved tubes. The correlations for developing flow in curved and coiled circular tubes are also presented. The main contribution of this study is reviewing the numerical and experimental correlations to calculate friction factor and Nusselt number in curved circular tubes. Nusselt number correlations are categorized based on the thermal boundary condition as well as the method.

**Keywords:** Curved tubes, Helical Coils, Heat transfer, Pressure drop, Dean Number, Entrance Region

\* *Submitted to Heat Transfer Engineering Journal*

## 2.1 Introduction

The prevailing trend of miniaturization in electronic devices is aligned with the increasing demand for higher performance and reliability, requires new methods for the removal of heat. Thermal management of these miniature electronic devices has attracted many researchers to develop efficient and cost competitive heat removal systems. Thermal management for heat fluxes up to  $10,000 \text{ W/cm}^2$ , which are generated by state-of-the-art chips in very small volume is needed. Hence, conventional heat removal systems are not sufficient any more, and new methods for heat transfer enhancement are needed in order to improve the performance of heat sinks. In general, there are two methods to improve the heat transfer rate: active and passive techniques [1, 2].

Active techniques are based on external forces such as electro-osmosis [3], magnetic stirring [4], bubble induced acoustic actuation [5] and ultrasonic effects [6] to perform the augmentation. Active techniques while effective; are not always easy to incorporate with other components in a system. They also increase the total cost of the system manufacturing.

On the other hand, passive techniques employ fluid additives or special surface geometry. Using the surface geometry approach is easier, cheaper and does not interfere with other components in the system. Surface modification, adding small particles to the working fluid or additional devices, incorporated in the stream are three main passive augmentation techniques. In these techniques, the existing boundary layer is disturbed and the heat transfer performance is improved. However, pressure drop is also increased [7]. Consequently, their net effectiveness depends upon the balance

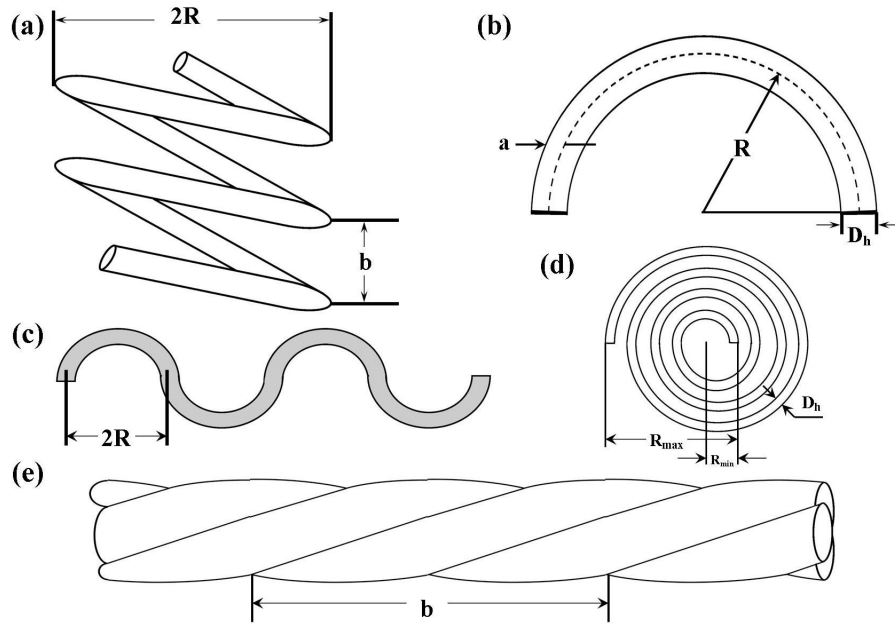


Figure 2.1: Different type of curved tube geometries: (a) helical coil, (b) bend tube, (c) serpentine tube, (d) spiral and (e) twisted tubes

between the increase in heat transfer augmentation and the pressure drop penalty. Curved geometries fits several practical applications, because of its high efficiency, lack of any moving parts, compactness in structure, ease of manufacture. The various types of curved tube geometries can be classified as follows: (a) torus (constant curvature and zero pitch), coiled or helical tube (constant curvature and pitch), serpentine tubes (periodic curved tubes with zero pitch) with bends or elbows, spirals (Archimedean spirals), and twisted tubes are shown in Fig. 2.1. The facts concerning the working principle of curved tubes and reasons for its enhanced performance are well established: (a) generation of secondary flow due to unbalanced centrifugal forces; (b) enhanced cross-sectional mixing; (c) reduction in axial dispersion; (d) improved heat-transfer coefficient; and (e) improved mass-transfer coefficient [8].

Using curved geometry is preferred to other conventional agitation techniques due to their similar and sometimes better performance. Lower energy consumption and

maintenance cost make them even more attractive. Heat transfer augmentation due to secondary flow and providing higher heat and mass transfer area per unit volume of space are two main advantages that are achieved in heat and mass transfer applications. Curved tubes can provide homogenization of feed streams with a minimum residence time and are available in most materials of construction.

From a heat transfer point of view, helically coiled heat exchangers offer certain advantages. Compact size provides a distinct benefit. Higher film coefficients, the rate at which heat is transferred through a wall from one fluid to another, and more effective use of available pressure drop, result in efficient and less-expensive designs. True counter-current flow fully utilizes available LMTD (logarithmic mean temperature difference). Helical geometry permits handling of high temperatures and extreme temperature differentials without high induced stresses or costly expansion joints. High-pressure capability and the ability to fully clean the service-fluid flow area added to the exchanger's advantages. Naphon and Wongwises [9, 10, 11, 12] studied different spiral and coiled heat exchangers heat transfer and pressure drop characteristics. Louw and Meyer [13] experimentally studied helically wound tube-in-tube heat exchangers. They quantified the effect of annular contact in terms of heat transfer coefficient and pressure drop. It was concluded that the heat transfer coefficient in the annulus increases substantially. Ghorbani et al. [14] experimentally studied the thermal performance of shell and coil heat exchangers. Ding et al. [15] simulated the performance of plate fin and tube heat exchanger. Pan et al. [16] optimized the retrofit of large scale heat exchanger networks with different intensified heat transfer techniques.

Neglecting the effect of coiled tube pitch Rennie [17] examined the double-pipe helical heat exchangers numerically and experimentally. Kumar et al. [18] numerically studied a tube-in-tube helically coiled heat exchanger for turbulent flow regime. Shok-

ouhmand et al. [19] experimentally investigated the shell and helically coiled tube heat exchangers in both parallel-flow and counter-flow configuration. They used the Wilson Plot method [20] to calculate the overall heat transfer coefficient. Wei et al. [21] studied the performance difference between straight and coiled capillary tubes. They indicated that helical effect increases with the decrease of the diameter of coiling.

Curved geometry application in nanofluidics attracted many researchers [22, 23, 24]. Naphon et al. [22] investigated heat transfer in nanofluidics in mini heat sinks. Hashemi et al. [23] experimentally studied the heat transfer and pressure drop of nanofluid flow in a horizontal helically coiled tube in constant heat flux. Razi et al. [24] accomplished an empirical study on the pressure drop characteristics of nanofluid inside helically coiled tubes. Kockmann and Roberge [25] studied transitional flow in curved micro-channels, by considering the dominance of viscous forces in micro-channels.

Coiled geometry also find applications in flow through porous media [26], chemical reactors, evaporators and steam generators [27]. The idea has been widely used in biomedical studies such as protein separation and emulsification [28], blood oxygenators [29], blood flow [30] and drug delivery systems [31]. Reviewing all current and potential applications of curved geometry is beyond the scope of this study. A review on the potential applications of curved geometries in processes engineering was accomplished by Nigam et al. [8]; However, further applications have been revealed since the time they published their work.

Unlike flow in straight pipes, fluid motion in a curved pipe is not parallel to the curved axis of the bend, owing to the presence of secondary flow. As the flow enters a curved bend, centrifugal forces act outward from the center of curvature on the fluid elements. Because of the no-slip condition at the wall, the axial velocity in the core region is much greater than that near the wall. To maintain the momentum balance

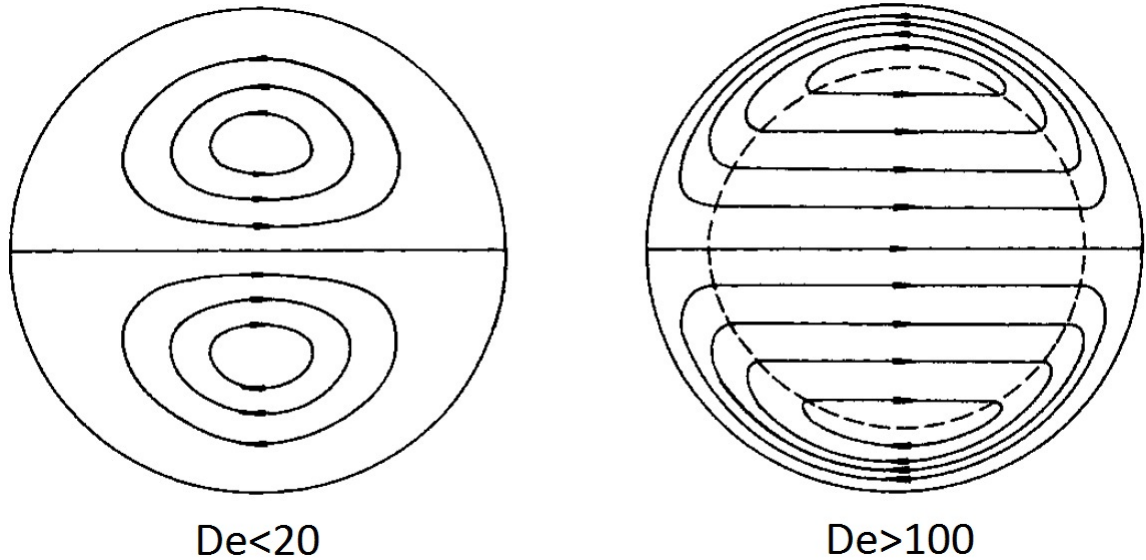


Figure 2.2: Secondary flow field at low and high Dean numbers [33]

between the centrifugal forces and pressure gradient, slower moving fluid elements move toward the inner wall of the curved tube. This leads to the onset of a secondary flow such that fluid near the wall moves along upper and lower halves of the torus wall, while fluid far from it flows to the outer wall. The curvature,  $1/R$ , affects the flow patterns, and even slight curvature was observed to modify the critical velocity of the fluid [8, 32].

It has been well established that for high Dean numbers,  $De > 100$ , the secondary flow field consists of a relatively inviscid core and a viscous boundary layer is initiated. Fig. 2.2 depicts the secondary flow field at low and high Dean numbers. The secondary flow increases the heat and mass transfer rates in addition to the rate of momentum transfer. The latter resulting in an increased pressure drop [33].

Heat transfer and pressure drop in a curved tube are dependent upon many parameters, including: Reynolds number, Prandtl number, Newtonian or non-Newtonian fluid, wall thermal boundary condition, curve-to-tube radius ratio, tube cross section,

length-to-diameter ratio, and coil pitch. These parameter effects have been described in many papers that will be mentioned later. The main purpose of this study is to summarize important experimental and theoretical results for single-phase laminar flow in curved tubes and channels. Well-known correlations for heat transfer and flow friction based on their applications are summarized in this paper. The scope of this paper is limited to steady state single-phase flows in stationary ducts. Turbulent flow inside curved ducts [34], multiphase-flow inside curved ducts [35], centrifugal instability [36, 37], transient flow [38] and swirling flow [39] are not treated here, and the reader can refer to the cited documents.

A review on friction factor and heat transfer correlations in helical and curved ducts have been presented by Naphon and Wongwises [1] and by Nigam et al. [8]. However, the experimental or numerical boundary conditions for each correlation are not always specified. In some cases, a clear distinction between tube-side and shell-side heat transfer correlations was not made. Some of the presented correlations are not valid, and not a uniform nomenclature was used for all correlations. The main purpose of this review paper is reviewing the well-know heat transfer and pressure drop correlations available for flow inside curved and coiled circular tubes. The entrance region, the critical Reynolds number for transition from laminar to turbulent flow and fully developed region are considered in this paper. Non-circular ducts, non-Newtonian fluids and turbulent flow in curved tubes are not studied.

## 2.2 Problem Formulation

The continuity, momentum and energy equations need to be solved to determine the heat transfer and pressure drop characteristics of curved coils analytically and theoretically. All three velocity components exist, even in the case of fully developed

flow, because of a curvature-induced centrifugal force that generates a secondary flow over the normal axis at any cross section.

Theoretical solutions are obtained by solving the appropriate differential equations and boundary conditions. The momentum equations for laminar flow are presented by Sankariah and Rao [40] in the toroidal coordinate system, and Patankar et al. [41] in the curvilinear cylindrical coordinate system. Patankar et al. [42] also presented the momentum equations for turbulent flow in curvilinear cylindrical coordinate system. Tyagi and Sharma [43] presented the energy equation for laminar flow in the toroidal coordinate system, and the time-average energy equation is presented for turbulent flow by Kreith [44] in the curvilinear cylindrical coordinate system. Nandakumar and Masliyah [45] employed an alternate development of a non-orthogonal coordinate system that is useful in studying fluid flow in helical tubes in the limit of large pitch. They also reported the ratio of the friction factor of a square helical tube to that of a square straight tube has been correlated through the use of the flow helical number. No slip (zero velocity components) at the wall is the usual boundary condition for the velocity problems. However, in this study we discuss three important boundary conditions for the heat transfer problems: T, H1 and H2 boundary conditions. T refers to axially and peripherally constant wall temperature. H1 refers to axially constant heat flux at the wall with peripherally constant wall temperature, and H2 refers to axially and peripherally constant heat flux at the wall. One should note that in the experimental coil heat transfer studies with constant heat flux boundary conditions, it is hard to achieve exact H1 or H2 boundary conditions. The difficulty arises because tube bending operations distort the tube wall thickness, and secondary flow alters the fluid temperature profile [46].

Most of the dimensionless groups associated with the flow inside curved ducts are in common with those for straight ducts, whereas two additional dimensionless groups for

curved tubes are Dean number and Helical coil number. Dean [47, 48] conducted the first analytical studies of fully developed laminar flow in a curved tube. He developed a series solution as a perturbation of the Poiseuille flow in a straight pipe for low values of Dean number ( $De < 17$ ). He reported that the relation between pressure gradient and the rate of flow is not dependent on the curvature to the first approximation. In order to show its dependence, he modified the analysis by including the higher-order terms and was able to show that reduction in flow due to curvature depends on a single variable, now known as the Dean number:

$$De = Re\sqrt{(D_h/2R)} \quad (2.1)$$

where  $Re$  is the Reynolds number,  $D_h$  is the tube diameter, and  $R$  is the radius of curvature of tube in Dean's notation. Various other authors have used different definitions of the Dean number for curved tube studies. It was reported that for low Dean numbers, the axial-velocity profile was parabolic and unaltered from the fully developed straight tube flow. As the Dean number is increased, the maximum velocity began to be skewed toward the outer periphery. Similarly, for high curvatures ( $1/R$ ), the secondary flow intensity is very high while for lower curvatures ( $1/R$ ), the secondary flow intensity is much less [8].

In a helical coil, the effective radius of curvature  $R_c$  of each turn is influenced by the coil pitch  $b$ , and is given by [49]:

$$R_c = R \left[ 1 + \left( \frac{b}{2\pi R} \right)^2 \right] \quad (2.2)$$

Use of  $R_c$  instead of  $R$  in Dean number definition results in a new number, referred to as a Helical coil number,  $He$ , defined as:

$$He = Re\sqrt{\frac{D_h}{2R_c}} = De \left[ 1 + \left( \frac{b}{2\pi R} \right)^2 \right]^{-1/2} \quad (2.3)$$

The definition of the peripherally and axially local and mean heat transfer coefficients and Nusselt numbers are the same as those by Shah and London [50]. The peripheral local heat transfer coefficient  $h_p$  can be written as:

$$q_p = h_p(T_w - T_m) \quad (2.4)$$

where  $T_w$  is the local temperature on the duct periphery,  $T_m$  is the fluid bulk mean temperature at the cross section, and  $q_p$  is the heat flux at the point of concern on the duct periphery. The peripherally average, but axially local, heat transfer coefficient  $h_x$  is defined by:

$$q_x = h_x(T_{w,m} - T_m) \quad (2.5)$$

where  $T_{w,m}$  is the peripheral mean wall temperature (peripheral integrated average of  $T_w$ ). The flow-length average heat transfer coefficient  $h_m$  is the integrated average of  $h_x$  from  $x = 0$  to  $x$ :

$$h_m = \frac{1}{x} \int_0^x h_x dx \quad (2.6)$$

Correspondingly, the Nusselt numbers  $Nu_{p,bc}$ ,  $Nu_{x,bc}$ ,  $Nu_{m,bc}$  and  $Nu_{bc}$  are defined below, where boundary condition denotes a specific thermal boundary condition such as T, H1 and H2. A local peripheral Nusselt number is defined as:

$$Nu_{p,bc} = \frac{h_p D_h}{k} = \frac{q_p D_h}{k(T_w - T_m)} \quad (2.7)$$

The peripheral average but axially local Nusselt number is defined as:

$$Nu_{x,bc} = \frac{h_x D_h}{k} = \frac{q_x D_h}{k(T_{w,m} - T_m)} \quad (2.8)$$

The mean (flow-length average) Nusselt number in the thermal entrance region is defined as:

$$Nu_{m,bc} = \frac{h_m D_h}{k} = \frac{1}{x} \int_0^x Nu_{x,bc} dx \quad (2.9)$$

The peripheral average Nusselt number in the hydro-dynamically and thermally fully developed region is simply defined without the first subscript  $p$ ,  $x$  or  $m$  as follows:

$$Nu_{bc} = \frac{h D_h}{k} \quad (2.10)$$

In the fully developed region,  $Nu_{m,bc}$  approaches  $Nu_{x,bc}$  and both approach  $Nu_{bc}$ .

The pressure drop inside a duct with the length of  $L$  can be expressed as:

$$\Delta P = \left( \frac{4fL}{D_h} \right) \frac{1}{2} \rho V^2 \quad (2.11)$$

where  $f$  is the Fanning friction factor. Most of the correlations for laminar flow in curved tubes are in term of the ratio of the Fanning friction factor for the curved tube to the straight tube under identical conditions,  $f_c/f_s$ . Fanning friction factor in laminar flow is defined as:  $f_s = 16/Re$ . However, one should note that the critical Reynolds number for transition from laminar to transition flow is:  $Re = 2100$ , whereas, in curved tubes, the flow persists to be laminar up to greater Reynolds number.

## 2.3 Developing Flow

Early investigations on curved geometries were conducted by Thomson [51], Williams [52], Grindley and Gibson [53] and Eustic [54]. The idea of using spiral geometry was first used in spiral plate heat exchangers in late 19th century [56], and further investigations conducted in the 1930s in Sweden [57, 58]. Taylor and Yarrow [55] studied the criterion for turbulence flow in 1929. Since then, there are now approximately 5,000 U.S. patents and more than 10,000 research articles on curved tube geometries and their applications.

In this section the well-known correlations for Nusselt number and Friction factor are reviewed. However, before reviewing the correlations, developing flow (entrance region) and critical Reynolds number are discussed.

In this section criteria for hydrodynamically developing flow, thermally developing and hydrodynamically developed flow and thermally and hydrodynamically developing flow are discussed.

### 2.3.1 Hydrodynamically Developing Flow

Kreulegan and Beiji [59] were the first who experimentally studied the flow development in curve pipes. Later Austin and Seader [60] used the angle of tube curvature to obtain fully developed flow for four different coils ( $R/a = 6.9, 9.1, 14.4$  and  $24.1$ ):

$$\phi = 49 \left( De \frac{a}{R} \right)^{0.33} \quad (2.12)$$

The equation is valid for  $190 \leq De \leq 950$ , and the flow was considered to be hydrodynamically fully developed at the coil entrance, and becoming developed because of curvature effects.  $\phi$  was found around 90 and 200 degree in the most cases that indicates a very short entrance length.

Newson and Hodgson [61] experimentally studied 32 coiled tubes, in a vertical orientation, and studied the entrance effects. Yao and Berger [62] reported the entrance length based on the boundary layer theory. However, their results were significantly different from those reported by Austin and Seader [60]. On the other hand, experimental data of Agrawal et al. [63] show good agreement with Eq (2.12). Moulin et al. [64] numerically simulated several cross sections and their results were in good agreement with the prediction of Austin and Seader [60].

Smith [65, 66] studied the influence of curvature on a pipeflow for a pipe that starts bending uniformly after an initial straight section. Singh [67] used the method of matched asymptotic expansions for the entry flow in a curved tube near the inlet. He considered two inlet conditions: (i) the condition of constant dynamic pressure at the entrance, which may be of practical interest in applications to blood flow in aorta and (ii) a uniform entry condition. He showed that the geometry and the nature of entry condition significantly affect the initial development of the flow. However, the pressure drop distribution is not significantly influenced by the secondary flow during the initial development of motion.

Humphery [68] used an elliptic form of the Navier-Stokes equations to numerically solve the laminar, incompressible, constant wall temperature boundary condition flow in curved pipes of small curvature radius and 90 degree deflection angle. He also considered the flow through curved annuli, which the presence of the inner curved wall causes the appearance of two (rather than one) pair of cross-stream vortices. Liu [69] also solved the elliptical Navier-Stokes equations in a 90 degree bend elbow, where fully developed conditions were assumed to hold. Soh and Berger [70] solved the full elliptic Navier-Stokes equations for entrance flow into a curved pipe using artificial compressibility technique.

So et al. [71] numerically studied laminar flows through 180 degree bends of circular

cross section. They considered a zero cross-stream flow at the inlet. They reported up to three secondary flow patterns in the cross-stream half-plane of a curved pipe. They were the Dean-type secondary cell, a secondary separation cell near the inner bend (closest to the center of curvature of the bend) and a third cell near the pipe center. They reported that the number of secondary cells in the cross-stream half-plane is greatly influenced by the inlet flow, and to a much lesser extent by the Dean number. Agrawal et al. [63] performed an experimental study of the development of steady, laminar, incompressible flow of a Newtonian fluid in the entry region of a curved pipe for the entry condition of uniform motion. They found an embedded vortex in addition to secondary flow separation near the inner bend. They compared their axial velocity profile with theoretical analyses of Singh [67] and Yao and Berger [62]. However, the quantitative agreement between theory and experiment was found to be poor.

Choi et al. [72] found a valley in the circumferential wall shear profile and a region of non-monotonic variation of wall shear with downstream distance. They suggested that the vortex structure in the entry region is more complicated in fully developed flow. Their results were in good agreement with the Singh [67] predictions in the developing region

Stewartson et al. [73, 74] analytically calculated the boundary layer problem for the entrance of a curved tube. They found vanishing axial shear at the inner bend at the downstream of a bend. They also studied the singular behavior near the point of vanishing axial shear.

Ebadian et al. [75] numerically showed that the velocity is almost symmetrical to center point on both horizontal and vertical centerlines near the inlet and at the inlet, and by increasing the flow length, the velocity becomes asymmetrical.

### 2.3.2 Thermally Developing and Hydrodynamically Developed Flow

The numerical studies [69-77] and experimental data [36] showed that the thermal entrance length inside curved ducts is 20 to 50 percent shorter than what observed in a straight tube. It has also been indicated that Nusselt number is oscillating in the entrance region [42, 76, 77, 80, 81, 84]. Fig. 2.3 shows the influence of Prandtl number on the Nusselt number in the entrance region of a curved circular tube at the constant wall temperature condition [76]. It has also been shown that Nusselt number oscillation is increased at the entrance for the fluids with higher Prandtl number. Furthermore, the oscillations start at higher  $Gz$  values (shorter length) [77]. Dravid et al. [77] explained the behavior as a result of secondary flow generation as a result of exposing the tube wall alternately to the hot and cold fluids. They also reported that the oscillation decreases with increasing axial position and the asymptotic value is reached for large Graetz number. It was found that the oscillation is enhanced with the increase in pitch curvature and curvature ratio decrease in the case of coiled tubes [80, 81]. Rindt et al. et al. [81, 83] also reported an oscillatory behavior for the friction factor in the case of developing flow. Rindt [84] related the oscillation phenomena to circulating secondary flow along the tube wall.

Cheng and Akiyama [36, 37] studied the thermal boundary layer development near the wall having the constant wall temperature. It develops quicker at the inner wall than at the outer wall. For a small Prandtl number,  $Pr = 0.1$ , boundary layer development along the axial length was found to be similar to that of a straight pipe. Whereas, for  $Pr = 0.7, 10$  and  $500$  the Nusselt number decreases to a minimum and then increases again and levels off to a constant value at a certain distance downstream.

Janssen and Hoogendoorn [78] proposed the following correlation to calculate pe-

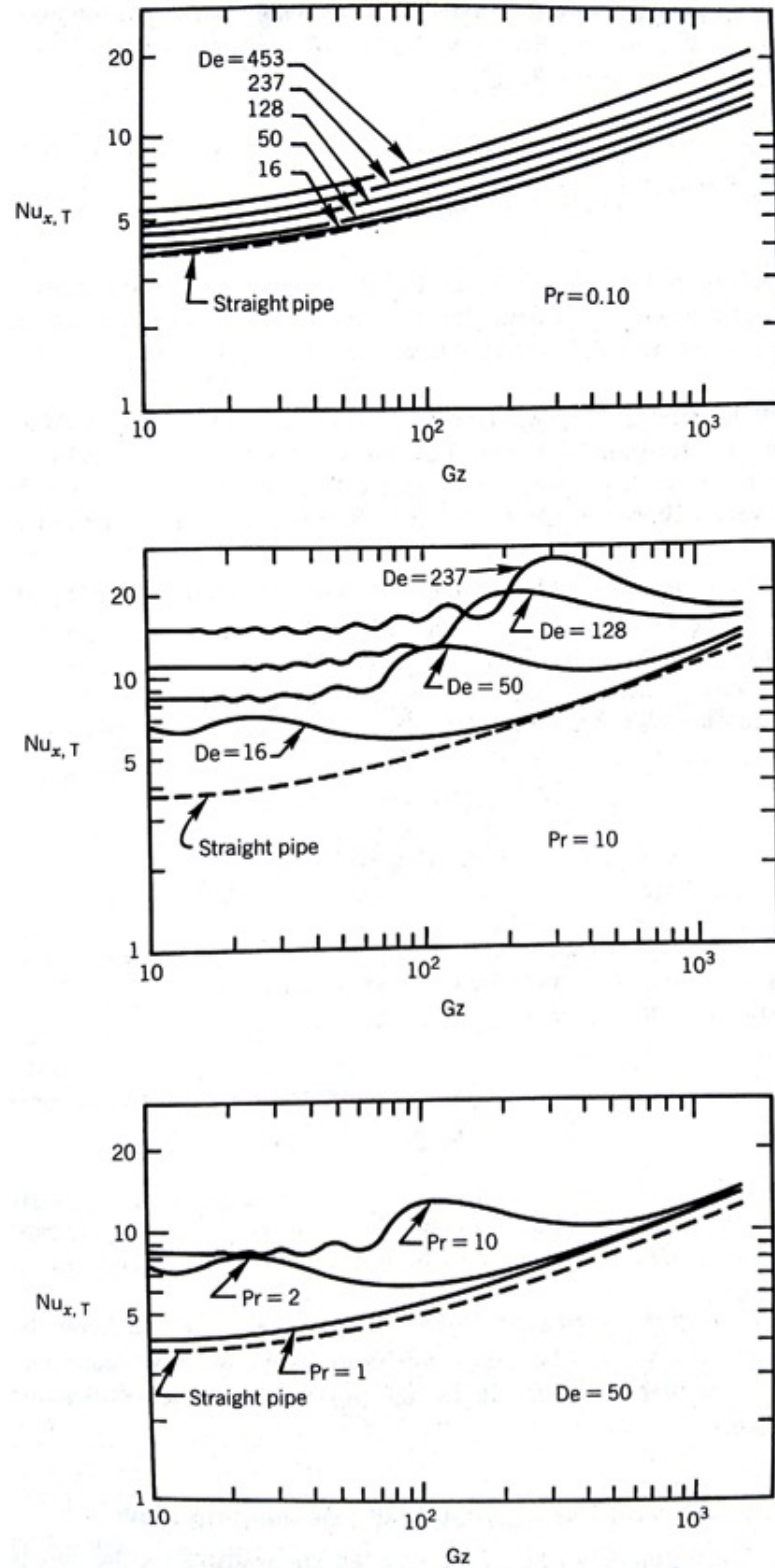


Figure 2.3: The influence of Prandtl number on the Nusselt numbers in the entrance region of a curved circular tube for the T boundary condition [46]

peripherally average thermal entrance region Nusselt numbers (it does not account the observed oscillations) for  $20 < Pr < 450$  and  $Re < Re_{crit}$ :

$$Nu_{x,T} = \left( \frac{0.32 + 3(a/R)}{0.86 - 0.8(a/R)} \right) Re^{0.5} Pr^{0.33} \left( \frac{2a}{x} \right)^{x_6} \left( \frac{\mu_m}{\mu_w} \right)^{0.14} \quad (2.13)$$

where  $x_6 = 0.14 + 0.8(a/R)$ . The validity of the correlation has been validated by the experimental results [78].

Using a glycerol solution as the working fluid inside two spirals that were enclosed in a steam chamber (constant wall temperature condition), Kubair and Kuloor [79] proposed the following correlation, which uses fluid properties calculated at an arithmetic-mean temperature:

$$Nu_{x,T} = \left( 1.98 + 1.8 \frac{a}{R_{ave}} \right) Gz^{0.7} \quad (2.14)$$

The correlation is valid for  $9 < Gz < 1000$ ,  $80 < Re < 6000$  and  $20 < Pr < 100$ . Where  $R_{ave}$  is used instead of  $R$  in the Dean number. Their proposed correlation is also applicable to the fully developed region by substituting  $Gz = 20$ .

For the H1 boundary condition, Janssen and Hoogendoorn [78] proposed the following equation to calculate peripherally average thermal entrance region Nusselt numbers:

$$Nu_{x,H1} = \left( 0.32 + 3 \frac{a}{R} \right) Re^{0.5} Pr^{0.33} \left( \frac{2a}{x} \right)^{x_6} \quad (2.15)$$

They also provided an equation to calculate the thermal entry length:

$$L_{th}^* = \frac{L_{th}}{D_h Re Pr} < \frac{15.7 Pr^{-0.8}}{De} \quad (2.16)$$

Their proposed equation indicates that the thermal entry length is mainly determined by the secondary flow, rather than by the thermal diffusivity as in straight tubes. Kalb

and Seader [85] used the novel gradient method of heat transfer investigation based on measurement of the wall internal and external surface-temperature distribution. However they focused more on the turbulent flow and the transition point from the laminar flow. They also observed a rapid transition from turbulent to laminar flow and that the Nusselt number approaches the fully developed value before two turns of the coil.

Oliver and Ashar [86] measured the heat transfer at the entrance of uniform temperature coil tubes and correlated their data by using the modified Graetz Leveque equation considering pseudoplastic behavior of liquids. Dravid et al. [77] calculated the thermal entrance length for  $H2$  condition, however no specific  $Nu_{x,H2}$  is given.

### 2.3.3 Thermally and Hydrodynamically Developing

Limited data are available for this case, because of very short entry lengths at high  $De$  and  $Pr$  value [87]. Liu and Masliyah [88] numerically studied the simultaneous development of the laminar Newtonian flow and heat transfer in helical pipes, and reported that the Nusselt number in the developing region is oscillating. They defined the torsion due to the pitch as follow:

$$\eta = \frac{(b/2\pi)}{R_c^2 + (b/2\pi)^2} \quad (2.17)$$

They reported that when torsion is dominant, the asymptotic Nusselt number decreases, while the thermal developing length increases with the flow pattern transition parameter for the high Dean numbers. When the torsion is large, the asymptotic Nusselt number tends to the limits corresponding to Poiseuille flow. They also proposed the following correlation for thermal entrance length:

$$L_{th} = \frac{0.155 + 0.00604De^{0.5}Pr^{0.25}}{1 + 0.0122DePr}Pr \quad (2.18)$$

Which is valid for  $0.01 < R/a < 0.15$  and  $20 < De < 5000$ . Janssen and Hoogerdoorn [78] gave a bound estimated on the entrance length as:

$$L_{th} = \frac{20Pr^{0.2}}{De} \quad (2.19)$$

A good agreement on the above correlations is reported [87].

Nobari et al. [89] solved the continuity, full Navier-Stokes, and energy equations by using a projection method base on the second order central difference discretization. They showed that there are two major different developing patterns of the flow which are determined based on the location of maximum axial velocity either in the semi-inner or in the semi-outer region of the curved annular pipe.

## 2.4 Critical Reynolds Number

Critical Reynolds number,  $Re_{crit}$ , identifies the transition from laminar to turbulent flow. In a curved duct flow, it is hard to identify  $Re_{crit}$  by the change in the slope of the curve for the friction factor versus Reynolds number, because of the gradual change [46]. However, it has been shown that the secondary flow in a curved tube stabilizes the laminar flow, and resulting in a higher critical Reynolds number. Sreenvisan and Strykowski [90] showed that there are two stabilization effects in flow through helically coiled pipes. First, in a certain Reynolds number range, the flow that is in turbulent in the straight pipe becomes completely laminar in the coiled section. Second, the stabilization effect of the coil persists to a certain degree even after the flow downstream of the coil has been allowed to develop in a long straight section.

They showed that the thresholds for the inner and outer wall are different. Sreenivasan and Strykowski [90] also observed that critical Reynolds number, which corresponds to the first appearance of turbulent everywhere at the chosen cross-section, reaches a maximum value and then drops as the curvature increases. Taylor and Yarrow [55] employed a colored fluid through a small hole in the side of glass helix through which water is running. Using the  $R/a = 18$ , they observed the steady stream-line motion persisted up to Reynolds number, 5830. Their results were used by Sreenivasan and McConalogue [90] in their numerical work.

Webster and Humphrey [92] reported low-frequency oscillation in half of the pipe cross-section, while the flow near the outer wall remains steady when  $5060 < Re < 6330$ . The first criterion for the transition point was introduced by Ito [93], and later Srinivasan et al. [96, 97] recommended a correlation for design purposes, which was validated by Kalb and Seader [85] experiments. Recently, Cioncolini and Santini [99, 100] proposed a piecewise correlation to calculate critical Reynolds number for different curvature ratios,  $R/a$ . Table 1 shows a summary of the proposed correlations to calculate the critical Reynolds number as a function of curvature ratio in the curved tubes. In spiral flow, the radius of curvature varies along the spiral, and therefore, the flow does not have a single critical Reynolds number. While, Kubair and Kuloor [103] suggested to use the arithmetic-average radius of curvature of the spiral in their helical coil correlation, Srinivasan et al. [97] have proposed the correlations for minimum and maximum  $Re_{crit}$  that would occur at the  $R_{max}$  and  $R_{min}$  locations in the spiral:

$$(Re_{crit})_{min} = 2100 \left[ 1 + \frac{12}{(R_{max}/a)^{0.5}} \right] \quad (2.20)$$

$$(Re_{crit})_{max} = 2100 \left[ 1 + \frac{12}{(R_{min}/a)^{0.5}} \right] \quad (2.21)$$

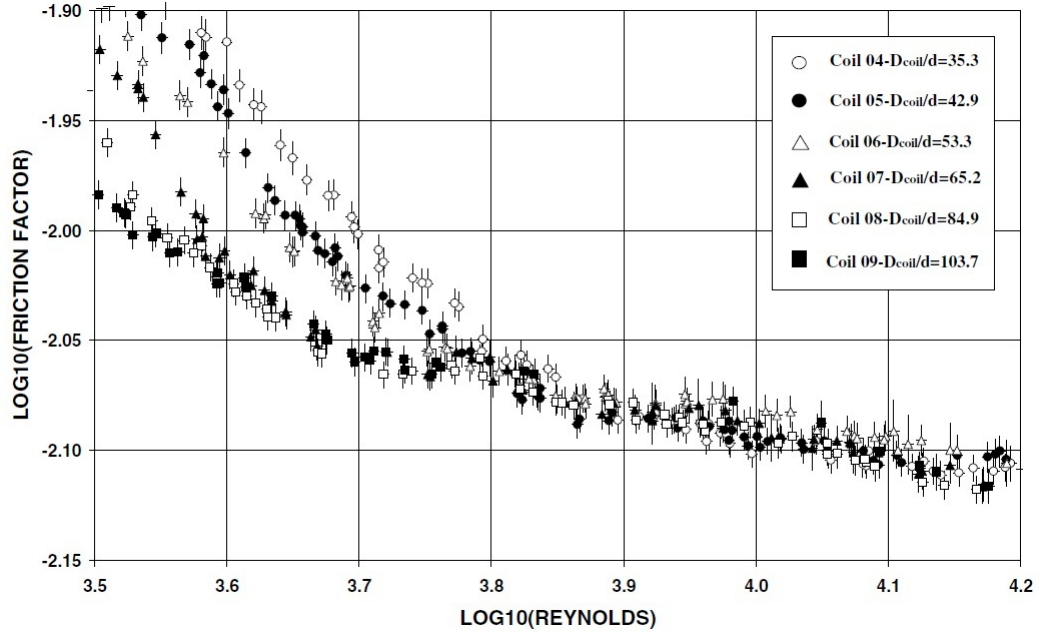


Figure 2.4: Critical Reynolds number reported by different researchers [99]

Patankar et al. [42] used Ito correlation [93] and compare it with their numerical work, and observed a good agreement between the correlation and the model. Later, Di Piazza and Ciofalo [102] used Ito [93] and Srinivasan et al. [96, 97] correlations to predict the turbulent occurrence inside the curved pipe they used.

Cioncolini and Santini [99, 100] divided the coil ducts to three different regions based on the curvature strength: strong curvature coils, medium curvature coils and mild curvature coils. They plot the friction versus Reynolds number and found the discontinuities in the plots. They proposed different correlations to predict the critical Reynolds number for each region due the breaks in the graphs. They also observed two discontinuities in the medium curvature region. Fig. 2.4 shows the experimental friction factor for the medium curvature coils observed by Cioncolini and Santini [99]. Ciofalo et al. [101, 102] used the proposed correlations in their numerical studies to predict the turbulent flow inside coiled tubes.

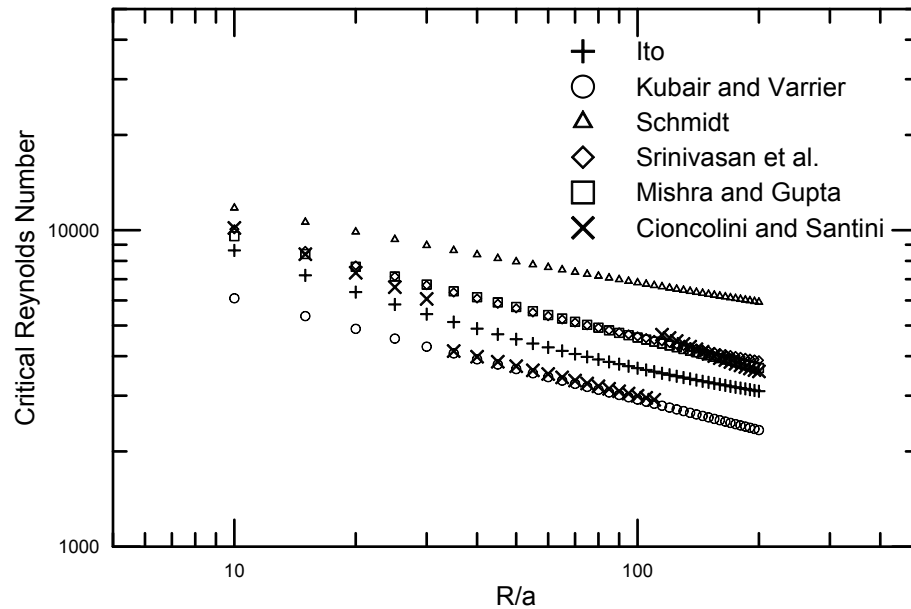


Figure 2.5: The influence of Prandtl number on the Nusselt numbers in the entrance region of a curved circular tube for the T boundary condition

Fig. 2.5 depicts the comparison for reported critical Reynolds number from Table 2.1 For the Cioncolini and Santini correlations [99, 100] the first critical Reynolds number is plotted, since the second critical Reynolds occurs for Reynolds numbers greater than 10,000. It can be observed that experimental results collected by different authors cover wide range of Reynolds number for a same curvature ratio. However, one may see that the for small curvature ratios, the critical Reynolds number is reported to be  $6,000 < Re_{crit} < 11,000$ .

## 2.5 Review of The Fluid Flow Correlations in Fully Developed Flow

The centrifugal force significantly influences the flow through a curved tube. The constant radius of curvature in the case of helically coil flow initiates a constant centrifugal force that eventually establishes fully developed flow. In the case of a

flow through a spiral tube, the radius of curvature is continuously varying, resulting in a continuous varying centrifugal force Dean number is continuously varying as well. Therefore, fully developed flow is established in a spiral coil only as a limiting condition when  $R/a$  or Dean becomes large [46].

Dean [47, 48] proposed the velocity profile based on perturbation analysis that is valid for  $De < 20$ . His solution for the velocity distribution demonstrates the shift in the maximum velocity toward the outer wall. It also indicates a secondary motion in the form of two symmetrical roll cells, with flow inward along the periphery of the tube and outward in the central region.

Mori and Nakayama [104] used boundary layer idealizations for  $De > 100$ , and obtained the fully developed velocity profiles for coils with  $R \gg a$ . Their predicted velocity profiles show good agreement with the experimental data by Adler [105] and the numerical results by Patankar [42]. Fig. 2.6 shows a typical variation in the velocity profile with the Dean number, based on the analysis of Patankar [42]. It can be seen that the velocity peak moves toward the outer wall as the Dean number increases.

The theoretical and experimental studies showed that the friction factors for coiled tubes are higher than those in a straight tube for an identical geometry and Reynolds number. Akiyama and Cheng [106] demonstrated that friction factors at the outer wall in a helical coil are substantially higher than those obtained in a straight tube. Whereas, friction factors at the inner wall are almost the same as those obtained in a straight tube. As a result, the overall effect is an increase in friction factors. This friction factors ratios can be seen in Figure 2.7.

Austin and Seader [107] numerically studied the pressure distribution inside coiled tubes. They have shown that it strongly depends on the Dean number and the pressure increases smoothly from the inner to the outer periphery.

Table 2.1: Prandtl, Reynolds and Dean range for the different fluids

Author	Technique	Correlation	Conditions
Ito [93]	Experimental	$Re_{crit} = 2,000 \left[ 1 + \frac{13.2}{(R/a)^{0.6}} \right]$	$15 < \frac{R}{a} < 860$
Kubair and varrier [94]	Experimental	$Re_{crit} = \frac{12,730}{(R/a)^{0.32}}$	$10 < \frac{R}{a} < 2,000$
Schmidt [95]	Experimental	$Re_{crit} = 2,300 \left[ 1 + \frac{8.6}{(R/a)^{0.32}} \right]$	$\frac{R}{a} < 200$
Srinivasan et al. [96, 97]	Experimental	$Re_{crit} = 2,100 \left[ 1 + \frac{12}{(R/a)^{0.5}} \right]$	$\frac{R}{a} < 200$
Mishra and Gupta [98]	Experimental	$20,000 \left[ \frac{1}{(R/a) \left[ 1 + \left( \frac{b}{2\pi D_h} \right)^2 \right]} \right]^{0.32}$ $Re_{crit} = \frac{20,000}{(R/a)^{0.32}}$	Helical Coil Tubes $\frac{R}{d} > 150$
Cioncolini and santini [99, 100]	Experimental	$Re_{crit} = \frac{30,000}{(R/a)^{0.47}}$ $Re_{crit} = \frac{12,500}{(R/a)^{0.31}}$ $Re_{crit} = \frac{120,000}{(R/a)^{0.57}}$ $Re_{crit} = 2,300 \left[ 1 + \frac{210}{(R/a)^{1.12}} \right]$	$\frac{R}{a} < 24$ $30 < \frac{R}{a} < 110$ $30 < \frac{R}{a} < 110$ $150 < \frac{R}{d}$

Bolinder and Sunden [108] employed Laser-Doppler Velocimetry measurements method to visually observe the flow pattern of laminar flow in a helical square duct with finite pitch. Ujhidy [109] used laser technique for the visualization of the flow in coiled tubes containing twisted tapes and helical static elements.

Various experimental and theoretical correlations are proposed to calculate the friction factor inside curve tubes. The main difference of these correlations is the way they account for an increase in the friction factor due to the coil curvature. The curvature can be expressed as just Dean number or combination of Dean and curvature ratio  $R/a$  [50].

Dean [47, 48] was the first researcher to investigate the pressure drop of the fully

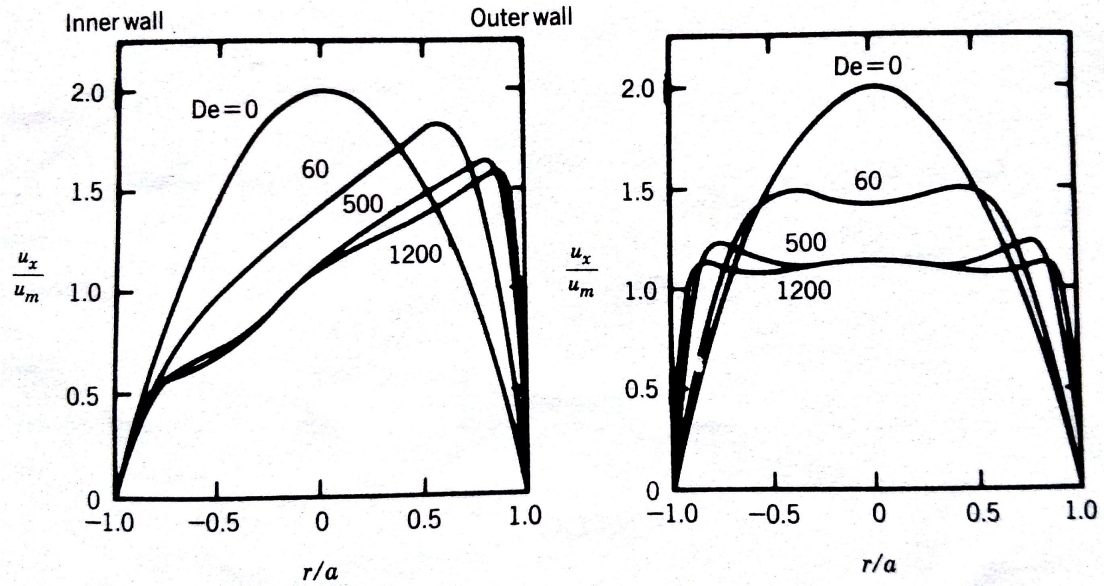


Figure 2.6: The influence of the Dean number on axial velocity profiles in a horizontal curved tube: (a) horizontal plane, (b) vertical plane [46]

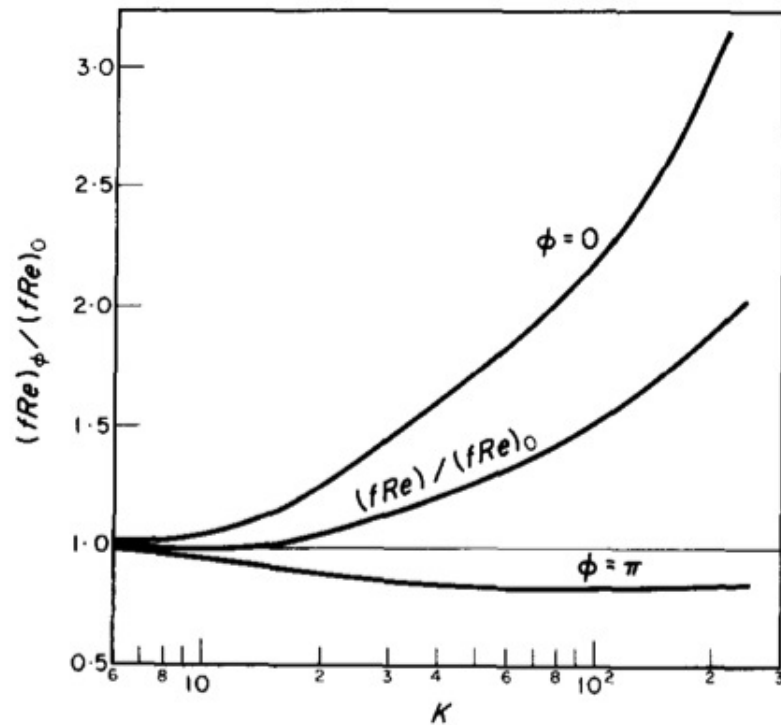


Figure 2.7: Fully Developed  $(fRe)_p / (fRe)_s$ , as a function of the Dean number [33]

developed flow in a torus for a limiting case. His solution consisted of a perturbation on the solution for Poiseuille flow through a straight tube. His solution can be rewritten in terms of friction factor ratio:

$$\frac{f_c}{f_s} = \left[ 1 - 0.03058 \left( \frac{De^2}{288} \right)^2 + 0.00725 \left( \frac{De^2}{288} \right)^4 \right]^{-1} \quad (2.22)$$

where  $f_c$  is the Fanning friction factor for the curved tube, and  $f_s$  is the Fanning friction factor for a straight tube as given by Poiseuille's law:

$$f_s = \frac{16}{Re} \quad (2.23)$$

The Dean equation is valid for  $De < 20.45$ . Topakoglu [110] extended the Dean solution to account for finite values of  $R/a$ :

$$\frac{f_c}{f_s} = \left[ 1 - 0.03058 \left( \frac{De^2}{288} \right)^2 + 0.1833 \frac{R}{a} \left( \frac{De^2}{288} \right) + \frac{(R/a)^2}{48} \right]^{-1} \quad (2.24)$$

The Topakoglu [110] solution indicates that even for small Dean numbers the friction factor ratio is still greater than one. Larrain an Bonilla [111] extended the coefficients and found that series does not converge for  $De > 16$ . Their numerical result for  $R/a < 0.2$ , do not differ significantly from the Topakoglu equation [110].

Adler [105] is another pioneer in proposing a correlation to calculate the friction factor for curved tubes. He used integral boundary layer theory to derive a solution for a torus for the mild curved tubes. The axial velocity component was postulated to increase rapidly in a boundary layer near the outer wall then decreases linearly to the inner wall. He proposed the following correlation:

$$\frac{f_c}{f_s} = 0.1064De^{0.5} \quad (2.25)$$

Ito [112] improved and extended the Adler solution to obtain:

$$\frac{f_c}{f_s} = 0.1033De^{0.5} \left[ \left( 1 + \frac{1.729}{De} \right)^{0.5} - \left( \frac{1.729}{De} \right)^{0.5} \right]^{-3} \quad (2.26)$$

Austin and Soliman [113] showed that the pitch changes affect the low Reynolds flow more than high Reynolds flow. Yamamoto et al. [114, 115] showed that at a constant  $R/a$ , the friction factor deviates from that of the torodial curved tube as torsion due to the pitch decreases toward that of the straight tube as torsion further increases. Yamamoto et al. [116] studied the secondary flow structure and stability of flow in a helical pipe with large torsion by using a numerical calculation of a fluid particle trajectory. They found an acceptable agreement with the existing experimental results.

Grundman [117] presented a practical friction diagram of helically coiled tube, which accounts for the effect of curvature ratios. Takahashi and Momazaki [118] experimentally measured the pressure drop of mercury flow inside a helical coil tube and showed that the pressure drop was almost the same as the pressure drop of the mercury flow in a straight tube.

Tables 2.2 and 2.3 depict the experimental and numerical-analytical friction factor correlations in laminar flow through curved circular tubes, respectively. As it can be seen most of correlations are presented in the form of  $f_c/f_s$ ; although, some others are in different format in the original paper, but have been converted to the base format of this paper. On the other hand, Ali [125] proposed an experimental piece wise model to calculate the heat transfer based on Euler number,  $\frac{\Delta p}{1/2\rho V^2}$ . He divided the flow in coiled helical tubes into four different regions: low laminar flow, laminar flow, mixed flow and turbulent flow. He categorized these regions with introducing a critical Reynolds number for the transition from each one to the other. He also used geometrical number for regular-helical coil,  $G_{rhc}$ , and Reynolds number to present his

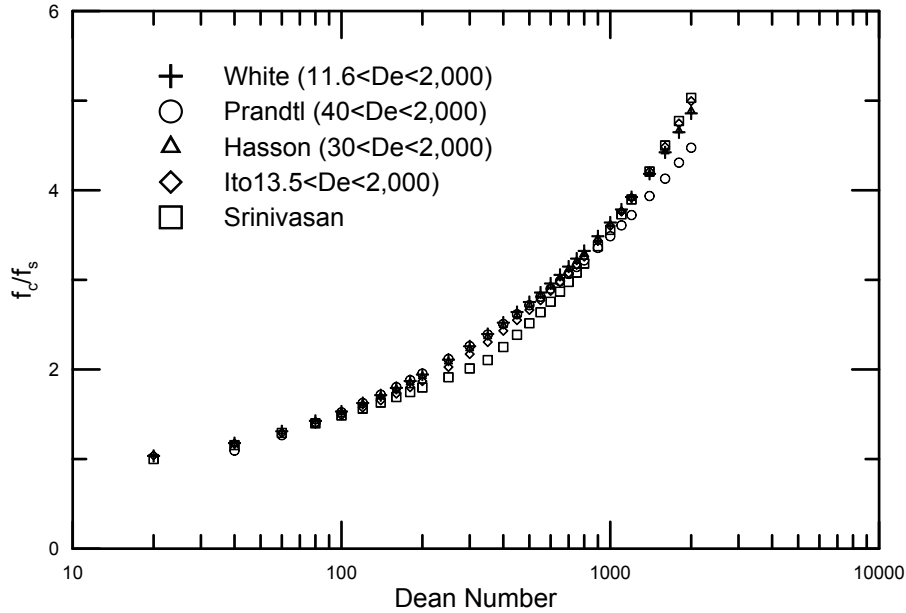


Figure 2.8: Experimental friction factor correlations comparison [33]

correlations instead of Dean number and curvature ratio.

Figs. 2.8 and 2.9 depict the comparison of the Fanning friction factor ratio correlations presented by different researchers experimentally and numerically respectively. The correlations which are only based on Dean number are depicted. It can be seen that the experimental correlations are in good agreement with each other, whereas, the Yanase correlation [134] deviates in low Dean numbers,  $De < 300$ , from other correlations, and Van Dyke correlation [130] predict the friction factor different from the other presented correlations where  $De > 300$ .

Ferng et al. [135] used a computational fluid dynamics, CFD, methodology to investigate the effects of Dean number and pitch size on the thermal-hydraulic characteristics in a helically coil-tube heat exchangers. They compared their pressure drop model by the results presented by Ju et al. [126].

Pimenta and Campos [136] experimentally studied the friction losses of Newtonian and

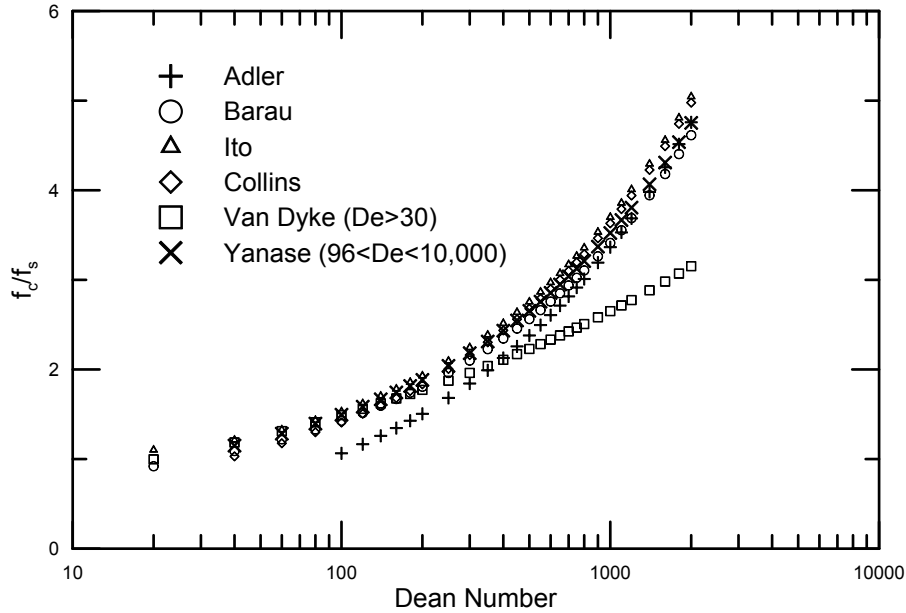


Figure 2.9: Numerical friction factor correlations comparison

non-Newtonian fluids in a helical coil. They compared their results with the Hart et al. [133] equation for Newtonian fluids. Rahimi and Beigzadeh [137] employed artificial neural networks (ANN) to predict the heat transfer and friction factor in helically coiled tubes. They compared their pressure drop results with the Ito experimental correlation [93].

## 2.6 Review of the Heat Transfer Correlations in Fully Developed Flow

The entrance region of a helical coil is about 20 to 50 percent shorter than that of a straight tube. Consequently, one may use the correlations for fully developed flow in the most of engineering applications, especially with  $De > 200$ .

In curved tubes, as with the velocity profiles, the secondary flow distorts the tempera-

ture profiles, pushing the temperature peak toward the tube outer wall. Consequently, a higher heat transfer rate at the coil outer wall than at the inner wall is expected. Cioncolini and Santini [99] showed that the secondary flow initiated inside the coiled tubes increases both hydraulic resistance and the heat transfer effectiveness in comparison to straight tubes. Hawe et al. [138] numerically found the the fully developed temperature profile in curved tubes, and also showed that the heat transfer coefficient at the outer wall is greater than the heat transfer coefficient at the inner wall. Increasing Dean number enhances secondary flow, and increasing Prandtl number enhances thermal convection. As a result a higher distortion of the temperature profile can be observed by increasing either Dean number or Prandtl number, Fig. 2.10 [76]. Balejova et al. [139, 140] experimentally studied low Reynolds number flows behavior inside curved tubes and observed cyclic behavior in their results using Newtonian and Non-Newtonian fluids. They also showed that natural convection effects can not be neglected at low Reynolds numbers.

Heat transfer characteristics of coiled tubes in heat exchangers have been studied by Ievlev et al. [141]. They reported the heat transfer and hydraulic diameter for a bundle of helical tubes in longitudinal and cross flow heat exchangers. They observed a noticeable increase in heat transfer and substantial reduction of the heat exchanger dimensions. Prasad et al. [142] studied the heat transfer coefficient for the shell and tube sides of a helical coil heat exchanger. The heat transfer values for the shell side are found to follow the classical Dittus-Boelter type relation, while a strong dependence on the coil to tube diameter is reported. Inagaki et al [143] also experimentally studied the outside heat transfer coefficient for helically coiled bundles.

Havas et al. [144] proposed a correlation for outer Nusselt number to the helical coil in an agitated vessel based for modified Reynolds number, Prandtl number, viscosity ratio and the ratio of the tube diameter to the vessel diameter.

Table 2.2: Experimental Friction Factor Correlations Curved Tubes for Laminar Flow

Authors	Correlations	Geometry	Conditions
White [119]	$\frac{f_c}{f_s} = \left[ 1 - \left( 1 - \left( \frac{11.6}{De} \right)^{0.45} \right)^{1/0.45} \right]^{-1}$	Curved Tube	$11.6 < De < 2,000$
Prandtl [120]	$\frac{f_c}{f_s} = 0.29De^{0.36}$	Helical Coil	$40 < De < 2,000$
Hasson [121]	$\frac{f_c}{f_s} = 0.556 + 0.0969\sqrt{De}$	Torus	$30 < De < 2,000$
Ito [93]	$\frac{f_c}{f_s} = \frac{21.5De}{(1.56 + \log De)^{5.73}}$ $f_c \sqrt{a/r} = 0.079 [Re(a/R)^2]^{-0.2}$	Curved Tube Curved Tube	$13.5 < De < 2000$ $Re(a/R) > 6$
Kubair and Varrier [94]	$f_c = 0.7716 \exp(3.553d/D) De^{-0.5}$	Helical Coil	$2,000 < De < 9,000$
Schmidt [95]	$\frac{f_c}{f_s} = 1 + 0.14 (R/a)^{-0.97} Re^{1-0.644(R/a)^{-0.312}}$	Helical Coil	
Topakoglu [110]	$\frac{f_c}{f_s} = \left[ 1 - 0.03058 \left( \frac{De^2}{288} \right)^2 + 0.1833 \frac{R}{a} \left( \frac{De^2}{288} \right) + \frac{(R/a)^2}{48} \right]^{-1}$	Curved Tube	
Srinivasan et al. [96]	$\frac{f_c}{f_s} = \begin{cases} 1 & \text{if } De < 30 \\ 0.419De^{0.275} & \text{for } 30 < De < 300 \\ 0.1125De^{0.5} & \text{if } De > 300 \end{cases}$	Helical Coil	$7 < R/a < 104$
Ramana Rao and Sadasivudu [122]	$f_c = \frac{1.55}{Re} \exp 14.12a/R$	Helical Coil $Re < 1,200$	$0.0159 < a/R < 0.0556$
Mishra and Gupta [98]	$\frac{f_c}{f_s} = 1 + 0.033 (\log He)^4$	Helical Coil	$1 < He < 3,000$
Gnielinski [123]	$f_c = \frac{1}{4} \left[ \frac{0.3164}{Re^{0.25}} + 0.03 \sqrt{\frac{a}{R}} \left( \frac{\mu_{wall}}{\mu_{bulk}} \right)^{0.27} \right]$	Helical Coil	
Xin et al. [124]	$f_c = 0.02985 + \frac{75.89 \left[ 0.5 - \left( \tan^{-1} \left( \frac{De - 39.88}{77.56} \right) \right) / \pi \right]}{R}$ $a_{i,out}$ is inner diameter of outer tube (m) $a_{o,in}$ is the outer diameter of inner tube(m)	Helical Coil	$35 < De < 20,000$ $1.61 < a_{i,out}/a_{o,in} < 1.67$ $R/(a_{i,out} - a_{o,in})$
Ali [125]	$Eu.G_{rhc} = 21.88Re^{-0.9}$ $Eu.G_{rhc} = 5.25Re^{-2/3}$ $Eu.G_{rhc} = 0.56Re^{-2/5}$ $Eu.G_{rhc} = 0.09Re^{-1/5}$ where: $G_{rhc} = \frac{(2a)^{0.85}(2R)^{0.15}}{L}$	Helical Coil	$Re < 500$ $500 < Re < 6,300$ $6,300 < Re < 10,000$ $10,000 < Re$
Ju et al. [126]	$\frac{f_c}{f_s} = 1$ $\frac{f_c}{f_s} = 1 + 0.015Re^{0.75} \left( \frac{a}{R} \right)^{0.4}$	Helical Coil	$De < 11.6$ $De > 11.6$
Guo et al. [127]	$f_c = 2.552Re^{-0.15} \left( \frac{a}{R} \right)^{0.51}$	Helical Coil	

Table 2.3: Numerical and Analytical Friction Factor Correlations Curved Tubes for Laminar Flow

Authors	Correlations	Geometry	Conditions
Dean [48]	$\frac{f_c}{f_s} = \left[ 1 - 0.03058 \left( \frac{De^2}{288} \right)^2 + 0.00725 \left( \frac{De^2}{288} \right)^4 \right]^{-1}$	Torus	$De < 20$
Adler [105]	$\frac{f_c}{f_s} = 0.1064De^{0.5}$	Torus	Large De
Barua [128]	$\frac{f_c}{f_s} = \frac{1.122^3}{4De} \left[ 1.181^2 + \left( 1.181^2 + \frac{De}{\sqrt{6}} \right)^{0.5} \right]^3$ $\frac{f_c}{f_s} = 0.509 + 0.0918\sqrt{De}$	Torus	Large De
Mori and Nakayam [104]	$\frac{f_c}{f_s} = 0.108 \frac{\sqrt{De}}{1 - 3.253\sqrt{De}}$	Curved Tube	$13.5 < De < 2,000$
Topakoglu [110]	$\frac{f_c}{f_s} = \left[ 1 - 0.03058 \left( \frac{De^2}{288} \right)^2 + 0.1833 \frac{R}{a} \left( \frac{De^2}{288} \right) + \frac{(R/a)^2}{48} \right]^{-1}$	Curved Tube	
Ito [112]	$\frac{f_c}{f_s} = 0.1033De^{0.5} \left[ \left( 1 + \frac{1.729}{De} \right)^{0.5} - \left( \frac{1.729}{De} \right)^{0.5} \right]^{-3}$	Curved Tube	
Tarbell and Samuel [76]	$\frac{f_c}{f_s} = 1 + \left[ 0.0008279 + \frac{0.007964}{R/a} \right] Re - 2.096 \times 10^{-7}$	Torus	$1 < De < 295$ $8.57 < R/a < 100$
Collins and Dennis [129]	$\frac{f_c}{f_s} = 0.38 + 0.1028\sqrt{De}$	Torus	Large De
Van Dyke [130]	$\frac{f_c}{f_s} = 0.47136De^{0.25}$	Torus	$De > 30$
Dennis [131]	$\frac{f_c}{f_s} = 0.388 + 0.1015\sqrt{De}$	Torus	Large De
Manlapaz and Churchill [132]	$\frac{f_c}{f_s} = \left[ \left( 1 - \frac{0.18}{[1+(35/De)^2]^{0.5}} \right)^m + \left( 1 + \frac{a/R}{3} \right)^2 \left( \frac{De}{88.33} \right) \right]^{0.5}$ $m = \begin{cases} 2 & \text{if } De < 20 \\ 1 & \text{for } 20 < De < 40 \\ 0 & \text{if } De > 40 \end{cases}$	Helical Coil	
Hart et al. [133]	$f_c = \frac{0.07725}{(\log Re/7)} \left[ 1 + \frac{0.09De^{1.5}}{70+De} \right]$	Helical Coil	
Yanase et al. [134]	$\frac{f_c}{f_s} = 0.557 + 0.0938\sqrt{De}$	Torus	$96 < De < 10,000$
Liu and Masliya [88]	$f_c Re = \left[ 16 + (0.378De\lambda^{0.25} + 12.1)De^{0.5}\lambda^{0.5}\gamma^2 \right]$ $\times \left[ \frac{1 + [(0.0908 + 0.0233\lambda^{0.5})De^{0.5} - 0.132\lambda^{0.5} + 0.37\lambda - 0.2]}{1 + 49/De} \right]$ $\lambda = \frac{R}{R^2 + (p/2\pi)^2}$ $\gamma = \eta / (\lambda De)^{0.5}, \eta = \frac{(p/2\pi)}{R^2 + (p/2\pi)^2}$	Helical Coil	Laminar Developing

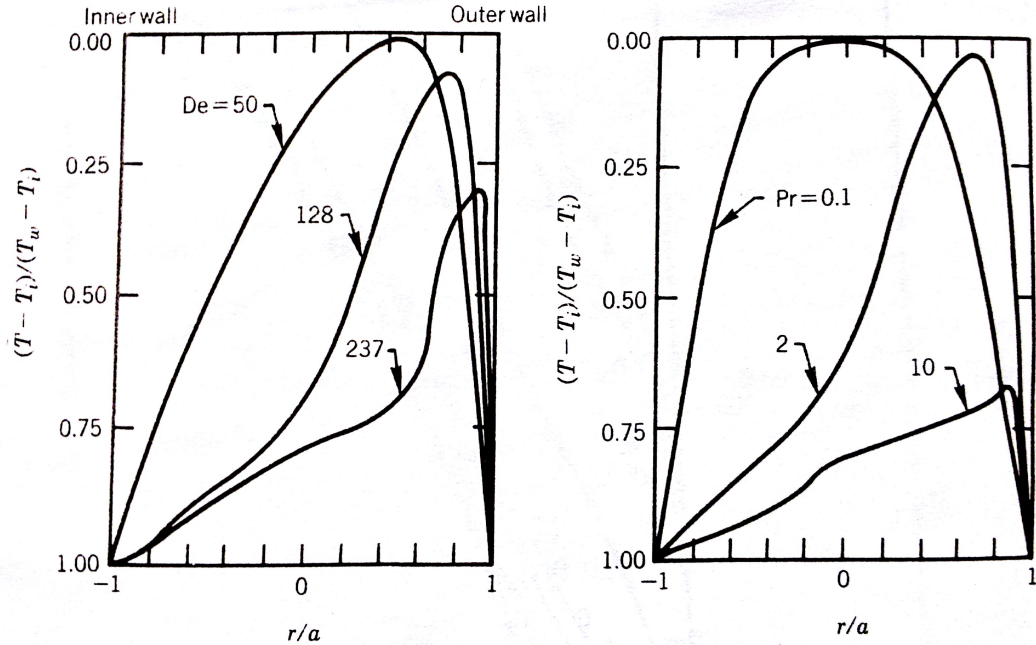


Figure 2.10: The dimensionless horizontal temperature profile for T boundary condition as a function of a) Dean number and b) Prandtl number for a curved tube

Ali [146] experimentally studied the fluids with Prandtl number,  $3 < Pr < 5$  and curvature ration,  $10 < R/a < 21$ . He showed that the heat transfer coefficient decreases with coil length with the tube diameter of 0.012 m, whereas, it increases with the coil length for tube of 0.008 m diameter. He found a critical  $R/a$  for the maximum heat transfer coefficient for tube diameter of 0.012 m with either five or ten turns of coil. Ali [147, 148] later investigated the effect of natural convection by considering the coil tube diameter as the characteristic length for the Rayleigh number. He showed that in the laminar region the average heat transfer coefficient decreases with increasing the number of coil turns, unless the flow becomes turbulent. Bai et al. [149] experimentally studied the turbulent flow in coiled tubes and showed that the contribution of the secondary flow in heat transfer augmentation decreases as the Reynolds number increases, and approaches that of a straight tube. It happens

due to the smaller boundary layer in higher Reynolds number. They also observed that the heat transfer coefficient at the outer wall is 3 to 4 times greater than that of the inner wall. Takahashi and Momozaki [118] also showed the greater heat transfer coefficient at the outer wall using mercury as the working fluid. Yang et al. [150, 151] numerically studied the effect of Prandtl number on the heat transfer coefficient increase on the outer wall and the inner wall of coiled tubes and showed that increasing the Prandtl number results in greater difference in the difference.

Jayakumar et al. [145] investigated the heat transfer in helically coiled heat exchanger experimentally and using CFD. They apply both constant wall temperature and constant heat flux, and showed that using the actual fluid properties instead of the average properties makes the modelling more accurate. The following correlation is proposed for both constant wall temperature and wall heat flux, using the temperature dependent properties:

$$Nu = 0.025De^{0.9112}Pr^{0.4} \quad (2.27)$$

The above equation is valid for  $2000 < De < 12,000$ ,  $1 < Pr < 3.5$  and  $a/R = 0.0333$ . It has been shown that heat transfer in pipes with chaotic flow, curved with alternate axis, is different from the regular coiled pipes [152, 153]. Acharya et al. [152] showed that alternating axis coils enhance the heat transfer more than the constant axis coils with the same curvature and pitch. Lemenand and Peerhossaini [153] proposed the following correlation to predict the Nusselt number pipe with chaotic flow:

$$Nu = 1.045Re^{0.303}Pr^{0.287}N_{bends}^{-0.033} \quad (2.28)$$

where the  $N_{bends}$  is the number of bends in the coil. The correlation is valid for  $100 < Re < 300$ ,  $30 < Pr < 100$ ,  $3 < N_{bends} < 13$ .

Ke et al. [154] numerically studied the heat transfer characteristic of conical spiral tube bundle. Their results showed that the cone angle and cross section have significant effect on tube heat transfer, whereas, the helical pitch has little influence on heat transfer enhancement.

The effect of natural convection induced in coiled-tube heat exchangers is studied by Zachar [155]. Natural convection induced heat transfer was studied over the outer surface of helically coiled-tube heat exchangers. It was found that the outer side heat transfer rate is slightly dependent on the inner flow rate of any helical tube in case of increasing temperature difference between the wall temperature and the coil inlet temperature. It has also been shown that the heat transfer is affected whether the fluid inside the coil is being cooled or warmed.

### 2.6.1 Constant Temperature

Several numerical works have been performed to calculate the temperature profile in constant temperature wall condition inside coiled tubes [156], however, not many experimental works have been performed to demonstrate the temperature profile in curved tubes [50]. Akiyama and Cheng [106] predicted that the heat transfer is higher for uniform wall temperature as compared to the uniform longitudinal heating for Dean numbers smaller than 200.

Jeschke [157] accomplished the first experimental research on heat transfer for two different curvature ratios,  $R/a = 6.1$  and  $18.2$ , in turbulent region. He developed an experimental correlation to calculate the Nusselt number in coiled tubes. However, his technique to perform the experiment was found to have too much uncertainty in it [8]. Merkel [158] revised the Jeschke correlation, and suggested that the heat transfer in coiled tube is  $(1 + 3.5R/a)$  times greater than the one for straight tubes.

Hawe [138] numerically found the fully developed temperature profile in curved tubes,

and also showed that the heat transfer coefficient at the outer wall is greater than the heat transfer coefficient at the inner wall in isothermal condition. Yao and Berger [87] presented a perturbation solution, but for the case of combined free and forced convection in a heated curved pipe. They considered both horizontal configurations for the curved pipes, however, they only considered a narrow range of Prandtl number,  $0.7 < Pr < 5$ .

Liu and Masliyah [159] numerically studied the effect of torsion and Prandtl number on the vortices, and the temperature profile. They predicted that for high torsion, the secondary flow is reduced to one vortex instead of the classical two vortices. The temperature distribution split into two profiles for low Prandtl (similar to two vortices), and had only one profile for high Prandtl.

Ebadian et al. [75] solved the combined effects of convective and thermal radiation heat transfer. They didn't find any influence of the thermal radiation on the velocity field. However, the heat transfer was significantly increased when the thermal radiation was taken into account.

Futagami and Aoyama [160] divided the effects of the secondary flow on the heat transfer into three types: centrifugal, buoyancy and composite range. They experimentally examined a wide range of Prandtl numbers,  $1 < Pr < 500$ , and Dean number,  $5 < De < 1000$ . Naphon and Suwagrai [161] showed that the heat transfer augmentation inside spirally coiled tubes is due to the centrifugal force that also increases the pressure drop. Zapryanov [164] proposed that the Nusselt number increases with increasing Prandtl number at a same Dean number.

Prabhanjan et al. [162] experimentally compared the heat transfer and fluid flow between a straight tube heat exchanger and a helically coiled heat exchanger. They showed that the heat transfer coefficient is affected not only by the geometry of the heat exchangers, but also by the temperature of the water bath surrounding the heat

exchanger. Later Prabhanjan et al. [163] proposed a method to predict the outlet temperatures of the helical coil by considering the flow rates and geometry of the coil. Table 2.4 summarizes the the most noticeable experimental correlations for the heat transfer inside curved tubes with constant wall temperature condition. Table 2.5 shows the available numerical and analytical correlations for the constant wall temperature boundary condition.

Manlapaz and Churchill [175] compared their numerical correlation with the available experimental results collected by the other researchers. Fig. 2.11 shows this comparison. Manlapaz and Churchill correlation [175] is the most common equation to calculate the Nusselt number for constant wall temperature condition. However, the correlation accuracy in the region of  $5 < Pr < 15$  was found to be far from convincing [176]. The correlation accuracy was also questioned for small Dean numbers [88]

## 2.6.2 Constant Heat Flux

As stated earlier there are two types of constant heat flux at the wall: H1 that refers to axially constant heat flux at the wall with peripherally constant wall temperature, and H2 that refers to axially and peripherally constant heat flux at the wall. However, it is not practical to achieve an exact H1 or H2 condition due to the fluid temperature distortion, which has been explained earlier.

Most of correlations for constant heat flux at the wall in curved tubes addressed the H1 boundary condition. Limited numerical results for H2 boundary condition by Tyagi and Sharma [43] and Manlapaz and Churchill [175] showed good agreement with the results for H1 correlations. Tyagi and Sharma [43] employed perturbation analysis to demonstrate the negligible influence of viscous dissipation on Nusselt numbers. However, their results are limited to small Dean numbers:  $De < 30$ . Manlapaz and Churchill [175] indicated no influence of the coil pitch in the Nusselt number.

Table 2.4: Experimental Studies on Heat Transfer Correlations Curved Tubes for Constant Wall Temperature

Authors	Correlations	Conditions
Kubair and Kuloor [79]	$Nu = [1.98 + 1.8a/R] Gr^{0.7}$	$10.3 < R/a < 27$ $80 < Re < 6,000$ $20 < Pr < 100$
Jha and Rao [165]	$\frac{Nu_c}{Nu_s} = 1 + 3.46R/a$	$16.6 < R/a < 37.9$
Schmidt et al. [95]	$Nu = 3.65 + 0.08 (1 + 0.87(R/a)^{0.9}) Pr^{1/3} Re^n$ where $n = 0.5 + 0.2903(R/a)^{0.194}$	$4 < R/a < 90$ $1 < De < 10$
Shchukin [166]	$Nu = \begin{cases} 0.0575Re^{0.33}De^{0.42}Pr^{0.43}\frac{Pr_m}{Pr_w} & 6.2 < R/a < 62.5 \\ 0.0266 \left[ \frac{Re^{0.85}}{(R/a)^{0.15}} + 0.225(R/a)^{1.15} \right] Pr^{0.4} & 6.2 < R/a < 104 \end{cases}$	$26 < De < 7,000$
Dravid et al. [33]	$Nu = (0.76 + 0.65De^2) Pr^{0.175}$	$50 < De < 2,000$ $5 < Pr < 175$
Janssen and Hoogendoorn [78]	$Nu = 0.616 (fRe^2)^{0.26} Pr^{1/6}$	$De > 20$ $20 < Pr < 40$
Yildiz et al. [167]	$Nu = 0.0551De^{0.864} Pr^{0.4}$	$1265 < De < 2,850$ $Pr = 0.7$
Salimpour [168]	$Nu = 0.554De^{0.496}\gamma^{-0.388} Pr^{0.151}\phi^{0.153}$ $\gamma = \frac{2b}{2\pi R}$ Correction Factor : $\phi = \frac{Pr_b}{Pr_w}$	$35 < De < 410$ $0.058 < \gamma < 0.095$ $034 < \phi < 0.6$ $160Pr < 325$ $0.113 < a/R < 0.157$
Pawar and Sunnapawar [169]	$Nu = 0.9366 (Gr)^{0.8177} Pr^{0.4}$  $Nu = 0.0472De^{0.8346} Pr^{0.4}$	$3.83 < Pr < 5.149$ $0.055 < a/R < 0.0757$ $19 < Gz < 152$ $586 < De < 4773$ $0.055 < a/R < 0.0757$ $3.83 < Pr < 7.3$
Rainieri et al. [170, 171]	$Nu = 1.168De^{0.47} Pr^{0.16}$	$12 < De < 280$ $125 < Pr < 280$

Table 2.5: Numerical and Theoretical Studies on Heat Transfer Correlations Curved Tubes for Constant Wall Temperature

Authors	Correlations	Conditions
Maekawa [172]	$Nu = 3.657 \left[ 1 + \left( \frac{De^2 Pr}{878} \right)^2 + 0.016 \left( \frac{De^2}{288} \right)^2 - \right. \\ \left. (0.0058 + 0.0269 Pr^2 + 0.0056 Pr^4) \left( \frac{De^2}{288} \right)^4 \right]$	Small Dean
Akiyama and Cheng [173]	$\frac{Nu}{3.657} = 0.27Q(1 - 1.48Q^{-1} + 23.2Q^{-2} - 120Q^{-3} + 212Q^{-4})$ $Q = De^{1/2} Pr^{1/4}$	$De \times Pr^{1/2} > 12$
Kalb and Seader [174]	$Nu = 0.836 De^{0.5} Pr^{0.1}$	$De > 80$ $0.7 < Pr < 5$
Manlapaz and Chrchill [175]	$Nu = \left[ \left( 3.657 + \frac{4.343}{x_1} \right)^3 + 1.158 \left( \frac{De}{x_2} \right)^{3/2} \right]^{1/3}$ $x_1 = \left( 1 + \frac{957}{De^2 Pr} \right)^2, x_2 = 1 + \frac{0.477}{Pr}$	$R/a > 5$
Liu and Masliyah [159]	$Nu = 3.657 + \frac{(0.75 De^{1/2} + 0.0028 Pr) Pr^{1/8}}{(1 + 0.00174 Pr^{-3})(1 + 70.6 Pr^{-0.6}/De)}$	$20 < De < 5,000$ $0.1 < Pr < 500$
Acharya et al. [152]	<p>Regular Coiled Tubes</p> $\begin{cases} \overline{Nu} = 0.69 \left( \frac{a}{R} \right)^{0.13} Re^{0.5} Pr^{0.43} & Pr < 1 \\ \overline{Nu} = 0.676 \left( \frac{a}{R} \right)^{0.13} Re^{0.5} Pr^{0.21} & Pr > 1 \end{cases}$ <p>Alternating-Axis Coils</p> $\begin{cases} \overline{Nu} = 0.7 \left( \frac{a}{R} \right)^{0.18} Re^{0.5} Pr^{0.375} & Pr < 1 \\ \overline{Nu} = 0.7 \left( \frac{a}{R} \right)^{0.18} Re^{0.5} Pr^{0.3} & Pr > 1 \end{cases}$ <p>The Relative Enhancement Ratio</p> $\begin{cases} \frac{\overline{Nu}_{Reg}}{\overline{Nu}_{Alter}} = 1.014 \left( \frac{a}{R} \right)^{0.05} Pr^{0.055} & Pr < 1 \\ \frac{\overline{Nu}_{Reg}}{\overline{Nu}_{Alter}} = 1.045 \left( \frac{a}{R} \right)^{0.05} Pr^{0.09} & Pr > 1 \end{cases}$	

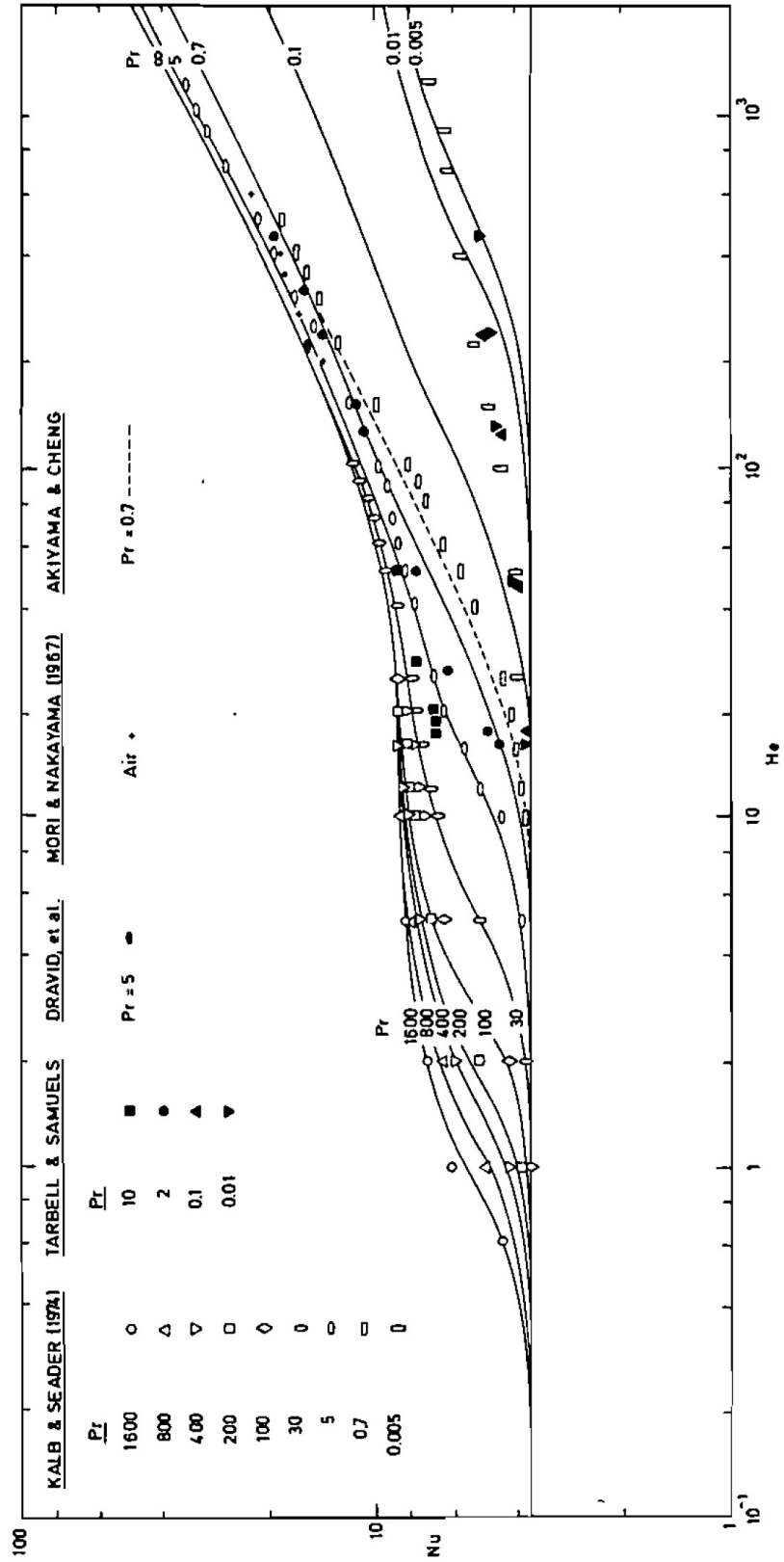


Figure 2.11: A comparison of the Manlapaz Correlation for the Nusselt Prediction for Constant Wall Temperature [175]

Berger and Bonilla [177] studied the heat transfer coefficient for heated air, water and oil in coils with condensing steam. They reported the coiled heat transfer coefficient smaller than the one in straight pipes, casting some doubt on the validity of their experiments.

Seban and McLaughlin [179] passed oil and water through tightly coiled and uniformly heated copper tubes with coil to tube ratios of 17 and 104. They indicated the peripheral conduction was significant, however, it was insufficient to maintain a peripherally uniform wall temperature in the laminar region. They also observed the oscillation at the entrance of the pipes.

Mori and Nakayama [104] measured the heat transfer to air in a uniformly heated brass pipe with a coil to tube ratio of  $R/a = 40$ . Schmidt [95] measured the heat transfer for air, water and oil at the uniform wall temperature with coil to tube ratios of  $R/a = 4.914$ ,  $R/a = 10.17$ ,  $R/a = 20.28$ ,  $R/a = 41$  and  $R/a = 81.3$ .

Jensen and Bergles [185] reported that non-uniformity occurred during the processes of making the coil resulted in large heat flux distribution on the inner wall of the tube. Austen and Soliman [113] conducted their experiments for coil to tube ratios of  $R/a = 29$  and  $R/a = 49$ , and small Prandtl numbers:  $3 < Pr < 6$ . Their results demonstrate that for the pitch changes significantly affect the heat transfer at low Reynolds number. Whereas, these effects weakened as the Reynolds number is increased. They also related these pitch effects to free convection, which consequently become less effective as the forced convection becomes more dominant at higher Reynolds.

Mori and Nakayama [104] used integral boundary layer theory to derive the following expression for H1 boundary condition:

$$Nu = \frac{0.864\sqrt{De}}{\zeta(1 + f(\zeta)De^{-1/2})} \quad (2.29)$$

where  $\zeta$  is the thermal boundary layer to hydrodynamic boundary layer ratio:  $\zeta = \delta_t h / \delta$ . As a first order approximation for large Dean numbers,  $f(\zeta)De^{-0.5}$  can be neglected, and they derived:

$$\zeta(Pr) = \begin{cases} \frac{2}{11} \left[ 1 + \left( 1 + \frac{77}{4Pr^2} \right)^{1/2} \right] & \text{if } Pr > 1 \\ \frac{1}{5} \left[ 2 + \left( \frac{10}{Pr^2} - 1 \right)^{1/2} \right] & \text{if } Pr < 1 \end{cases} \quad (2.30)$$

Mori and Nakayama [156] subsequently derived the following solution for uniform wall temperature:

$$Nu = 0.864De^{1/2} \frac{(1 + 2.35De^{-1/2})}{\zeta} \quad (2.31)$$

Dravid et al. [33] showed that the energy integrals in the above solutions were evaluated over the hydrodynamic boundary layer rather than the thermal boundary layer for  $Pr > 1$ , thereby yielding an erroneous dependence on Prandtl [175].

Tables 2.6 and 2.7 categorize the experimental and numerical correlations available for constant heat flux at the wall. Fig. 2.12 shows the Manlapaz and Churchill correlation [175] comparison with other predictions.

The relative performance of a curved tube with H1 boundary condition was studied by Kalb and Seader [186] in Fig. 2.13. The ratio  $(Nu_{H1,c}/Nu_{H1,s}) / (f_c/f_s)$  is plotted against Dean number for different Prandtl numbers. One may find a value greater than one as a better performance of curved circular tubes to straight tubes. The performance of curved tubes is improved with fluids having  $Pr > 0.7$ . The performance of coiled tubes enhances with increasing Pr. One should note that if tube-side fouling factor is significant, it may be necessary to devise a chemical cleaning method, since mechanical cleaning of a coiled tube is difficult.

Table 2.6: Experimental Studies on Heat Transfer Correlations Curved Tubes for Constant Heat Flux

Authors	Correlations	Conditions
Berger and Bonilla [177]	$\left[0.0000229 + 0.000636 \left(\frac{R}{a}\right)\right] Re^{1.29} Pr$	$30 < R/a < 100$ $1 < De < 100$
Kirpov [178]	$Nu = 0.0456 Re^{1.29} (R/a)^{0.21} Pr^{0.4}$	$10,000 < Re < 45,000$
Seban and Mclaughlin [179]	$Nu = 0.13 (f Re^2 Pr)^{1/3}$	$6,000 < Re < 65,600$ $2.9 < Pr < 5.7$
Rogers and Mayhew [180]	$Nu = 0.023 Re^{0.85} Pr^{0.4} \left(\frac{a}{R}\right)^{0.1}$	$10,000 < Re < 200,000$ $a/R = 0.0926, 0.075, 0.05$
Singh and Bell [181]	$Nu = \left[0.224 + 1.369 \frac{R}{a}\right] Re^n \left[1 + 4.8 (1 - e^{-p}) Pr^{1/3}\right] \left(\frac{\mu_b}{\mu_w}\right)^{0.14}$ $n = 0.501 + 0.318 \frac{R}{a}$ $p = 0.00946 Gr / De^2$	$6 < Re < 7,650$ $R/a = 10.2 \text{ and } 41.7$
Yildiz et al. [182]	$Nu = 0.149 Re^{0.673} Pr^{0.4} \left(\frac{a}{R}\right)^{0.337}$	$Pr = 0.7$
Xin and Ebadian [183]	$Nu = 0.00619 Re^{0.91} Pr^{0.4} \left[1 + 3.455 \left(\frac{a}{R}\right)\right]$	$5000 < Re < 10^5$ $R/a = 0.0267, 0.0884$
Moawed [184]	$Nu = 0.0345 Re^{0.48} (R/a)^{0.914} (P/a)^{0.281}$	$660 < Re < 2,300$ $7.086 < R/a < 16.142$ $1.81 < p/a < 3.205$

Table 2.7: Numerical and Theoretical Studies on Heat Transfer Correlations Curved Tubes for Constant Heat Flux

Authors	Correlations	Conditions
Mori and Nakayama [104, 187]	$\left(\frac{Nu}{Nu_s}\right)_I = 0.1979\sqrt{De}/Z$ $\left(\frac{Nu}{Nu_s}\right)_{II} = \left(\frac{Nu}{Nu_s}\right)_I + \frac{37.05}{Z} \left[ \left[ \frac{1}{40} - \frac{17Z}{120} + \left( \frac{1}{10Z} + \frac{13}{30} \right) \frac{1}{10Pr} \right] \frac{1}{\sqrt{De}} \right]^{-1}$ $Z = \frac{2}{11} \left[ 1 + \left( 1 + \frac{77}{4Pr^2} \right) \right]$ <p>I: 1st approximation, II: 2nd approximation</p>	$Pr > 1$ $Pr < 1$
Mori and Nakayama [156]	$Nu = \frac{Pr}{26.2(Pr^{2/3} - 0.074)} Re^{4/5} \left( \frac{a}{R} \right)^{0.1} \left[ 1 + \frac{0.098}{\left[ Re \left( \frac{a}{R} \right)^2 \right]^{0.2}} \right]$ $NuPr^{-0.4} = \frac{1}{41} Re^{5/6} \left( \frac{a}{R} \right)^{1/12} \left[ 1 + \frac{0.061}{\left( Re \left( \frac{a}{R} \right)^{2.5} \right)^{1/6}} \right]$	$Pr \approx 1, Re \left( \frac{a}{R} \right)^2 < 0.1$ $Pr > 1, Re \left( \frac{a}{R} \right)^2 < 0.4$
Ozisik and Topakoglu [188]	$Nu = \frac{48}{11 \left[ 1 - \left( \frac{De^2 Pr}{1303} \right)^2 \right]}$	$Pr \rightarrow \infty$ Small $De^2 Pr$
Akiyama and Cheng [106]	$\frac{Nu}{48/11} = 0.181Q(1 - 0.839Q^{-1} + 35.4Q^{-2} - 207Q^{-3} + 417Q^{-4})$ $Q = De^{1/2} Pr^{1/4}$	$DePr^{1/2} > 12$ $Pr > 12$
Kalb and Seader [186]	$Nu = 3.31De^{0.115} Pr^{0.0108}$ $Nu = 0.913De^{0.476} Pr^{0.2}$	$0.005 < Pr < 0.05$ $20 < De < 1, 200$ $0.7 < Pr < 5$ $80 < De < 1, 200$
Manlapaz and Chrchill [175]	$Nu = \left[ \left( 4.364 + \frac{4.636}{x_3} \right)^3 + 1.816 \left( \frac{De}{x_4} \right)^{3/2} \right]^{1/3}$ $x_3 = \left( 1 + \frac{1.342}{De^2 Pr} \right)^2, x_4 = 1 + \frac{1.15}{Pr}$	
Liu and Masliyeh [159]	$Nu = \begin{cases} 1.7De^{1/3} Pr^{1/6} & De < 20 \\ 0.9Re^{1/3} Pr^{1/6} & 20 < De < 100 \\ 0.7Re^{0.43} Pr^{1/6} (R/a)^{0.07} & 100 < De < 830 \end{cases}$	$0.1 < Pr < 500$

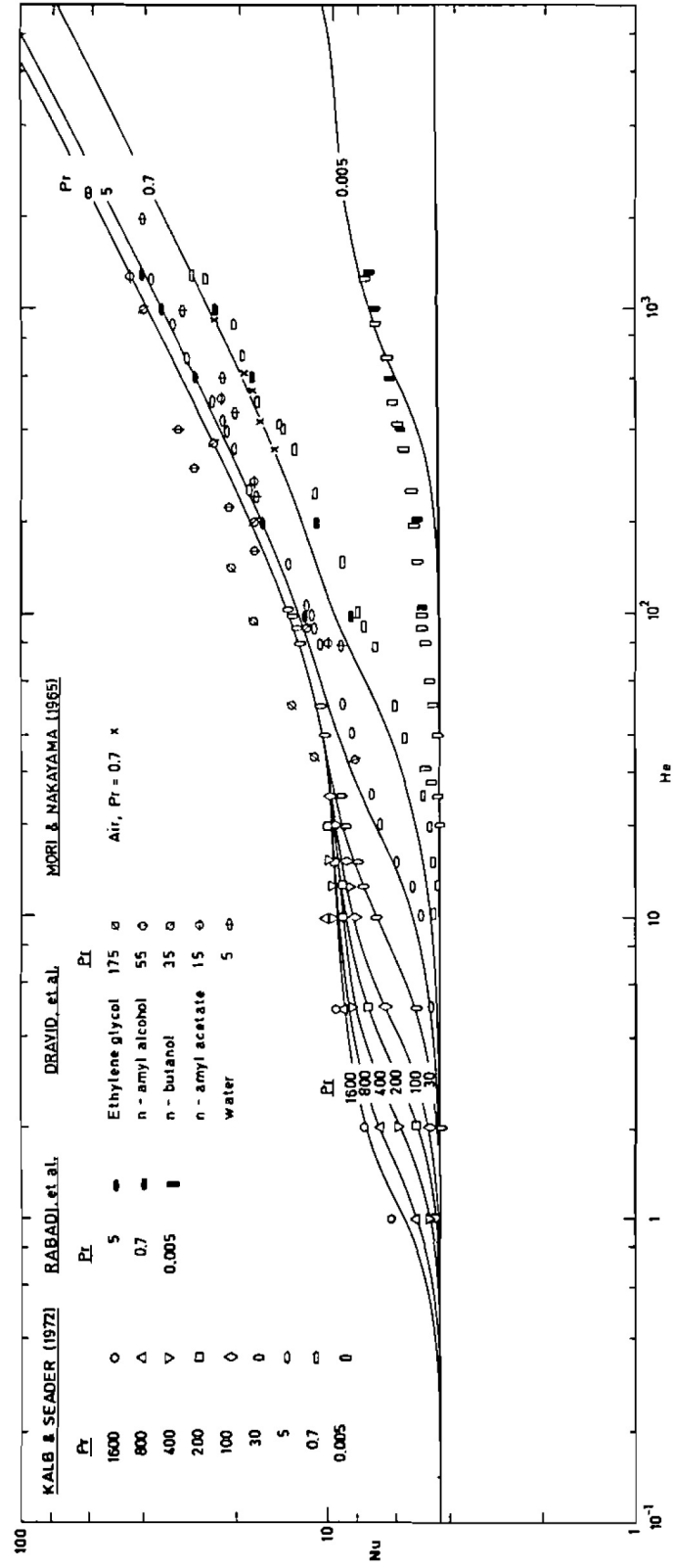


Figure 2.12: A comparison of the Manlapaz Correlation for the Nusselt Prediction for Constant Heat Flux [175]

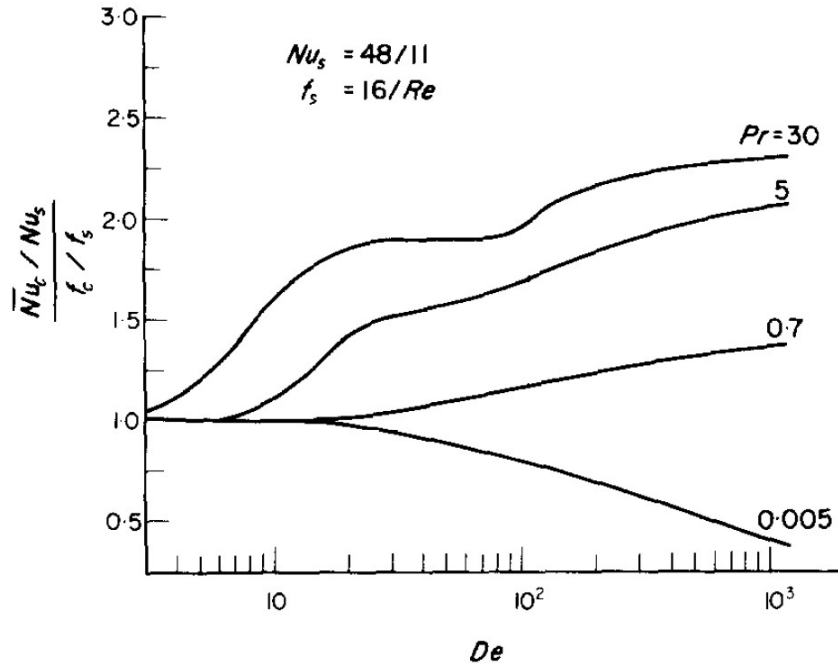


Figure 2.13: Effectiveness of curved circular tubes as compared to straight tubes [186]

## 2.7 Conclusions

Well known correlations to calculate the Nusselt number and friction factor for laminar Newtonian flow inside a curved or coiled circular tube have been reviewed. Different aspects of the flow inside curved tubes have been studied. The objectives of this review can be listed as follow:

- 1- Governing equations and important dimensionless numbers associated with curved tubes were presented. Different thermal boundary conditions of constant wall temperature,  $H1$  and  $H2$  were defined.
- 2- Available literature for the developing flow in curved tubes were reviewed. Hydro-dynamically developing, hydro-dynamically developed and thermally developed flow and hydro-dynamically and thermally developing flow inside curved tubes were studied. According to the reviewed correlation the entrance length is 20 – 50% shorter than the one in straight tubes. The researchers also observed the Nusselt number

oscillation in the entrance region of curved tubes.

3- Critical Reynolds number that identifies the transition from laminar to turbulent flow for curved tubes were studied. It was found that it is hard to identify  $Re_{crit}$  by the change in the slope of the curvature for the friction factor versus Reynolds number, because of the gradual change. However, all researchers agree that the transition happens in significantly higher Reynolds numbers in comparison to straight tubes.

4- Pressure drop correlations for fully developed flow inside curved tubes were reviewed. Centrifugal force influences the flow through a curved tube, and push the flow to the outer wall. Both numerical and empirical types of the correlations were reviewed. The correlations were presented in  $f_c/f_s$  format.

5- Heat transfer correlations in fully developed flow in curved tubes were also presented. The results were categorized for different boundary conditions: constant wall temperature,  $H1$  and  $H2$ . The well-known correlations can be found in the relevant table, where the appropriate condition (Prandtl number and Dean number) were listed as well. It was also shown that the results for  $H1$  and  $H2$  are too close.

In the end there are still gaps in the area of the flow in curved tubes. The entrance region is not yet well studied, and no accurate correlation is available to calculate the pressure drop and heat transfer for the developing flow. Most of the correlations in the fully developed region are also based on the case studied where the results were limited. Understanding the fluid flow and heat transfer behavior of the flow in circular tubes is still an interesting topic for the future investigations.

## 2.8 Acknowledgement

The authors acknowledge the financial support of the Natural Sciences and Engineering Research Council of Canada (NSERC), and AUTO 21.

## 2.9 References

- [1] Wongwises, S., and Naphon, P., A Review of Flow and Heat Transfer Characteristic in Curved Tubes, *Renewable and Sustainable energy reviews*, vol. 10, pp. 463-490, 2006.
- [2] Sudarsan, A. P., and Ugaz, V.M., Fluid Mixing in Planar Spiral Microchannels, *Journal of the Royal Society of Chemistry*, vol. 6, pp. 74-82, 2006.
- [3] Oddy, M. H., Santiago, J. G., Mikkelsen, J. C., Electrokinetic Instability Micromixing, *Analytical Chemistry*, vol. 73, pp. 5822-5832, 2001.
- [4] Lu, L. H., Ryu, K. S., Liu, C. J., Fabrication of a 3D Active Mixer Based on Deformable Fe-Doped PDMS Cones with Magnetic Actuation, *Journal of Microelectromechanical System*, vol. 11, pp. 462-469, 2002.
- [5] Liu, R. H., Yang, J., Pinder, M. Z., Athavale, M., Grodzinski P., Microfluidic Chip Based Microarray Analysis, *Lab Chip*, vol. 2, pp. 151-156, 2002.
- [6] Bartoli, C., and Baffigi, F., Effects of Ultrasonic Waves on the Heat Transfer Enhancement in Subcooled Boiling, *Experimental Thermal and Fluid Science*, vol. 35, no. 3, pp. 423-432, 2011.
- [7] Webb, R.L., and Kim, N. H., *Principles of Enhanced Heat Transfer*, Taylor and Francis, Philadelphia, 2005.

- [8] Nigam, K., Vashisth, S., Kumar, V., A Review on the Potential Applications of Curved Geometries in Process Industry, *Industrial Engineering Chemistry Research*, vol. 47, pp. 3291-3337, 2008.
- [9] Naphon, P., and Wongwises, S., Heat Transfer Coefficients Under Dry and Wet-Surface Conditions for a Spirally Coiled Finned Tube Heat Exchanger, *International Communication in Heat and Mass Transfer*, vol. 32 ,pp. 371-385, 2005.
- [10] Naphon, P., and Wongwises, S., A Study of the Heat Transfer Characteristics of a Compact Spiral Coil Heat Exchanger under Wet-Surface Conditions, *Experimental Thermal Fluid Science*, vol. 29, no. 4, pp. 511-521, 2005.
- [11] Naphon, P., and Wongwises, S., Heat Transfer Characteristics of a Spirally Coiled, Finned-Tube Heat Exchanger under Dry-Surface Conditions, *Heat Transfer Engineering*, vol. 27, no. 1, pp. 25-34, 2006.
- [12] P. Naphon, Performance and Pressure Drop of the Helical Coil Heat Exchangers With and Without Helically Crimped Fins, *International Journal of Heat and Mass Transfer*, vol. 34, pp. 321-330, 2007.
- [13] Louw, W. I., Meyer, J. P., Heat Transfer during Annular Tube Contact in a Helically Coiled Tube-in-Tube Heat Exchanger, *Heat Transfer Engineering*, vol. 26, no. 6, pp. 16-21.
- [14] Ghorbani, N., Taherian, H., Gorji, M., Mirgolbabaei, H., An Experimental Study of Thermal Performance of Shell-and-Coil Heat Exchangers, *International Communication in Heat and Mass Transfer*, vol. 37, no. 7,pp. 775-781, 2010.
- [15] Ding, W. K., Fan, J. F., He, Y. L.,Tao, W. Q., Zheng, Y. X., Gao, Y. F., Song, J., A General Simulation Model for Performance Prediction of Plate Fin-and-Tube Heat Exchanger with Complex Circuit Configuration, *Applied Thermal Engineering*, vol. 31, pp. 3106-3116, 2011.

- [16] Pan, M., Bulatov, I., Smith, R., Kim, J. K., Optimization for the Retrofit of Large Scale Heat Exchanger Networks with Different Intensified Heat Transfer Techniques, *Applied Thermal Engineering*, vol. 53, no. 2, pp. 373-386, 2013.
- [17] Rennie, T. J., Numerical and Experimental Studies of a Double-Pipe Helical Heat exchanger. Ph.D. Thesis, McGill University, Montreal, Canada, 2004.
- [18] Kumar, V., Faizee, B., Mridha, M., Nigam, K. D. P., Numerical Studies of a Tube-in-Tube Helically Coiled Heat Exchange, *Chemical Engineering Process*, vol. 47, no. 12, pp. 2287-2295, 2008.
- [19] Shokouhmand, H., Salimpour, M. R., Akhavan-Behabadi, M. A., Experimental Investigation of Shell and Coiled Tube Heat Exchangers Using Wilson Plots, *International Communication in Heat and Mass Transfer*, vol. 35, pp. 84-92, 2011.
- [20] Rose, J. W., Wilson Plot and Accuracy of Thermal Measurements, *Experimental Thermal and Fluid Science*, vol. 28, pp. 77-86, 2004.
- [21] Wei, C., Lin, Y., Wang, C., A Performance Comparison Between Coiled and Straight Capillary Tubes, *Heat Transfer Engineering*, vol. 21, no. 2, pp. 62-66, 2010.
- [22] Naphon, P., Nakharintr, L., Heat Transfer of Nanofluids in the Mini-Rectangular Fin Heat Sinks, *International Communication in Heat Mass Transfer*, vol. 40, pp. 25-31, 2013.
- [23] Hashemi, S. M., and Akhavan-Behabadi, M. A., An Empirical Study on Heat Transfer and Pressure Drop Characteristics of CuO-Base Oil Nanofluid Flow in a Horizontal Helically Coiled Tube under Constant Heat Flux, *International Communication in Heat and Mass Transfer*, vol. 39, pp. 144-151, 2012.
- [24] Fakoor-Pakdaman, M., Akhavan-Behabadi, M. A., Razi, P., An Empirical Study on the Pressure Drop Characteristics of Nanofluid Flow Inside Helically Coiled Tubes, *International Journal of Thermal Science*, vol. 65, pp. 206-213, 2013.

- [25] Kockmann, N., and Roberge, D., Transitional Flow and Related Transport Phenomena in Curved Microchannels, *Heat Transfer Engineering*, vol. 32, pp. 595-608, 2011.
- [26] Nunge, R. J., Lin, T. S., Grill, W. N., Laminar Dispersion in Curved Tubes and Channels, *Journal of Fluid Mechanics*, vol. 52, pp. 363-383, 1972.
- [27] Kallinikos, L. E., Papayannakos, N. G., Intensification of Hydrodesulphurization Process With a Structured Bed Spiral Mini-Reactor, *Chemical Engineering and Processes Intensification*, vol. 49, no. 10, pp. 1025-1030, 2010.
- [28] Kaur, J., Agrawal, G. P., Studies on Protein Transmission in Thin Channel Flow Module: the Role of Dean Vortices for Improving Mass Transfer, *Journal of Membrane Science*, vol. 196, pp. 1-11, 2002.
- [29] Ito, Y., Spiral Column Configuration for Protein Separation by High-Speed Counter Current Chromatography, *Chemical Engineering and Processing: Process Intensification*, vol. 49, no. 7, pp. 782-792, 2010.
- [30] Abdessalem, S. B., Durand, B., Aksebi, S., Chakfe, N., Kretz, J-G, Numerical Simulation of Blood flow in a Curved Textile Vascular Prosthesis, *Journal of The Textile Institute*, vol. 96, no. 2, pp. 117-122, 2005.
- [31] Pechar, M., Pola, R., The Coiled Motif in Polymer Drug Delivery Systems, *Biotechnology Advances*, vol. 31, no. 1, pp. 90-96, 2013.
- [32] Guan, X., Mathonen, T., Simulations of Flow in Curved Tubes, *Aerosol Science and Technology*, vol. 26, no. 6, pp. 485-504, 1997.
- [33] Dravid, A. N., Smith, K. A., Merrill, E. W., Brian, P. L. T., Effect of Secondary Fluid Motion on Laminar Flow Heat Transfer in Helically Coiled Tubes, *American Institution of Chemical Engineers*, vol. 17, no. 5, pp. 1114-1122, 1971.

- [34] Abdel-Aziz, M. H., Mansour, I. A. S., Sedahmed, G. H., Study of the Rate of Liquid–Solid Mass Transfer Controlled Processes in Helical Tubes Under Turbulent Flow Conditions, *Chemical Engineering and Processing: Process Intensification*, vol. 49, no. 7, pp. 643-648, 2010.
- [35] Chen., C. N., Han, J. T., Jen, T. C., Shao, L., Thermo-Chemical Characteristics of R134a Flow Boiling in Helically Coiled Tubes at Low Mass Flux and Low Pressure, *Thermochimica Acta 512*, pp. 163-169, 2011.
- [36] Cheng, K. C., and Akiyama, M., Laminar Forced Convection Heat Transfer in Curved Rectangular Channels, Microfluid Nanofluid, *Journal of Heat Transfer*, vol. 13, pp. 471-490, 1970.
- [37] Cheng, K. C., and Akiyama, M., Graetz Problem in Curved Pipes with Uniform Wall Heat Flux, *International Journal of Research and Reviews in Applied Sciences*, vol. 29, pp. 401-417, 1974.
- [38] Guo, L. J., Feng, Z. P., Chen, X., Transient Convective Heat Transfer of Steam–Water Two-Phase Flow in a Helical Tube under Pressure Drop Type Oscillations, *International Journal of Heat and Mass Transfer*, vol. 45, no. 3, pp. 533-542, 2002.
- [39] Murphy, S., Delfos, R., Pourquoi, M. J. B. M., Olujic, Z., Jansens, P. J., Nieuwstadt, F. T. M., Prediction of Strongly Swirling Flow Within an Axial Hydrocyclone Using Two Commercial CFD Codes, *Chemical Engineering Science*, vol. 62, no. 6, pp. 1619-1635, 2007.
- [40] Sankarish, M., and Rao, Y. V., Analysis of Steady Laminar Flow of an Incompressible Newtonian Fluid Through Curved Pipes of Small Curvature, *Journal of Fluids Engineering*, no. 72-WA/Fe19, 1973.

- [41] Patankar, S. V., Pratab, V. S., Spalding, D. B., Prediction of Laminar Flow and Heat Transfer in Helically Coiled Pipes, *Journal of Fluid Mechanics*, vol. 62, no. 3, pp. 539-551, 1974.
- [42] Patankar, S. V., Pratab, V. S., Spalding, D. B., Prediction of Turbulent Flow in Curved Pipes, *Journal of Fluid Mechanics*, vol. 67, no. 3, pp. 583-595, 1975.
- [43] Tyagi, V. P., and Sharma, K., An Analysis of Steady Fully Developed Heat Transfer in Laminar Flow with Viscous Dissipation in a Curved Circular Ducts, *International Journal of Heat and Mass Transfer*, vol. 18, pp. 69-78, 1975.
- [44] Kreith, F., The Influence of Curvature on Heat Transfer to Incompressible Fluids, *Transaction ASME*, vol. 79, pp. 1246-1256, 1955.
- [45] Masliyah, J. H., Nandakumar, K., Fully Developed Laminar Flow in a Helical Tube of a Finite Pitch, *Chemical Engineering Communications*, col. 29, pp. 125-138, 1984.
- [46] Kakac, S., Shah, R. K., Aung, W., Handbook of Single-Phase Convective Heat Transfer, Wiley-Inter-science, Hoboken, New Jersey, U.S.A.,1987.
- [47] Dean, W. R., Note on the Motion of Fluid in a Curved Pipe, *The London, Edinburgh and Dublin Philosophical Magazine and Journal of Science*, vol. 4, pp. 208-223, 1927.
- [48] Dean, W. R., The streamline Flow Through Curved Pipes, 6th International Conference on Multiphase Flow, *The London, Edinburgh and Dublin Philosophical Magazine and Journal of Science*, vol. 5, pp. 673-695, 1928.
- [49] Truesdell Jr., L. C., and Adler, R. J., Numerical Treatment of Fully Developed Laminar Flow in Helically Coiled Tubes, *American Institute of Chemical Engineers*, vol. 40, pp. 1010-1015, 1970.
- [50] Shah, R. K., and London, A. L., Laminar Flow Forced Convection in Ducts, *Supplement 1 to Advances in Heat Transfer*, Academic, New York, 1978.

- [51] Thompson, J., On the Origin of Windings of River and Alluvial Planes, with Remarks on The Flow of Water Round Bends in Pipes, *Proceeding R. Soc. London*, Ser. A 5(1) (1876).
- [52] Williams, G.S., Hubbell, C. W., Fenkel, G. H., On the Effect of Curvature on the Flow of Water Pipes, *Transaction of American Society Civil Engineering*, vol. 47, 1902.
- [53] Grindley, J. H., Gibson, A. H., On the Frictional Resistance of Air Through a Pipe, *Proceedings of Royal Society of London*, Serial A. 80, pp. 114-139, 1908.
- [54] Eustice, J., Experiments of Streamline Motion in Curved Pipes, *Proceedings of Royal Society of London*, Serial A. 85, pp. 114-139, 1911.
- [55] Taylor, G. I., and Yarrow, F. R. S., The Criterion for Turbulence in Curved Pipes, *Proceedings of Royal Society of London*, Serial A. 124, pp. 243-249, 1929.
- [56] Boothroyd, A., Spiral Heat Exchanger, International Encyclopedia of Heat and Mass Transfer, G. Hewitt, Y. Pulezhaev, eds., CRC Press, New York, p. 1044, 1997.
- [57] Chonwdhury, K. C., Linkmeyer, H., Bassiouny, M. Kh., Analytical Studies on the Temperature Distribution in Spiral Plate Heat Exchangers: Straightforward Design Formulate for Efficiency and Mean Temperature Difference, *Journal of Chemical Engineering Process*, vol. 19, pp. 183-190, 1985.
- [58] Burmeister, C. L., Effectiveness of Spiral-Plate Heat Exchanger with Equal Capacitance Rate, *Journal of Heat Transfer*, vol. 128, pp. 195-301, 2006.
- [59] Keulegan, G. H., and Beiji, K. H., Pressure Losses for Fluid Flows in Curved Pipes, *The Journal of Research of NIST*, vol. 18, pp. 89-144, 1937.
- [60] Austin, L. R., and Seader, J. D., Entry Region for Steady Viscous Flow in Coiled Circular Pipes, *American Institute of Chemical Engineers*, vol. 20, pp. 820-822, 1974.

- [61] Newson, I. H., Hodgson, T. D., The Development of Enhanced Heat Transfer Condenser Tubing, *Atomic Energy Research Establishment*, vol. 14, no. 3, pp. 291-323, 1974.
- [62] Yao, L. S., and Berger, S. A., Entry Flow in a Curved Pipe, *Journal of Fluid Mechanics*, vol. 67, no. 1, pp. 177-196, 1975.
- [63] Agrawal, Y., Talbot, L., Geong, K., Laser Anemometer Study of Flow Development on Curved Circular Pipes, *Journal of Fluid Mechanics*, vol. 85, no. 3, pp. 497-518, 1978.
- [64] Moulin, P., Veyretb, D., Charbit, F., Dean Vortices: Comparison of Numerical Simulation of Shear Stress and Improvement of Mass Transfer in Membrane Processes at Low Permeation Fluxes, *Journal of Membrane Science*, vol. 183, no. 2, pp. 149-162, 2001.
- [65] Smith, F. T., Pulsatile Flow in Curved Pipes, *Journal of Fluid Mechanics*, vol. 20, pp. 820-822, 1974.
- [66] Smith, F. T., Fluid Flow into a Curved Pipe, *Proceedings of Royal Society of London*, Serial A 8 October 351, pp. 71-87, 1976.
- [67] Singh, M. P., Entry Flow in Curved Pipes, *Journal of Fluid Mechanics*, vol. 65, no. 3, pp. 517-539, 1974.
- [68] Humphery, A.C., Numerical Calculations of Developing Laminar Flow in Pipes of Arbitrary Curvature Radius, *American Journal of Chemical Engineering*, vol. 56, no. 2, pp. 151-164, 1978.
- [69] Liu, N. S., Developing Flow in a Curved Pipe, *INSERM-Euromech*, vol. 92, pp. 53-64, 1977.
- [70] Soh, W. Y., and Berger, S. A., Laminar Entrance Flow in a Curved Pipe, *Journal of Fluid Mechanics*, vol. 148, pp. 109-135, 1984.

- [71] So, R. M., Zhang, H. S., Lai, Y. G., Secondary Cells and Separation in Developing Laminar Curved-Pipe Flows, *Theoretical and Computational Fluid Dynamics*, vol. 3, no. 3, pp. 141-162, 1991.
- [72] Choi, U. S., Talbot, L., Cornet, E., Experimental Study of Wall Shear Rates in the Entry Region of a Curved Tube, *Journal of Fluid Mechanics*, vol. 93, pp. 465-489, 1979.
- [73] Stewartson, K., Cebeci, T., Chang, K. C., A Boundary Layer Collision in a Curved Duct, *The Quarterly Journal of Mechanics and Applied Mathematics*, vol. 33, pp. 59-75, 1980.
- [74] K. Stewartson, K., and Simpson, C. J., On a Singularity Initiating a Boundary-Layer Collision, *The Quarterly Journal of Mechanics and Applied Mathematics*, vol. 35, pp. 1-16, 1982.
- [75] Ebadian, M. A., Zheng, B., Lin, C. X., Combined Laminar Forced Convection and Thermal Radiation in a Helical Pipe, *International Journal of Heat and Mass Transfer*, vol. 43, pp. 1067-1078, 2000.
- [76] Tarbell, J. M., and Samuels, M. R., Momentum and Heat Transfer in Helical Coils, *Chemical Engineering Journal- Lausanne (Netherland)*, vol. 5, pp. 117-127, 1973.
- [77] Dravid, A. N., Smith, K. A., Merrill, E. W., Brian, L. T., Effect of Secondary Fluid Motion on Laminar Flow Heat Transfer in Helically Coiled Tubes, *AIChE Journal*, vol. 17, pp. 1114-1122, 1971.
- [78] Janssen, L. A. M., Hoogendoorn, C. J., Laminar Convection Heat Transfer in Helical Coiled Tubes, *International Journal of Heat and Mass Transfer*, vol. 21, pp. 1197-1206, 1978.
- [79] Kubair, V., and Kuloor, N. R., Heat Transfer to Newtonian Fluids in Coiled Pipes in Laminar Flow, *International Journal of Heat and Mass Transfer*, vol. 9, pp. 63-75, 1966.

- [80] Lin, C. X., and Ebadian, M. A., Developing Turbulent Convective Heat Transfer in Helical Pipes, *International Journal of Heat and Mass Transfer*, vol. 40, pp. 3861-3873, 1997.
- [81] Lin, C. X., Zhang, P., Ebadian, M. A., Laminar Forced Convection in the Entrance Region of Helical Pipes, *International Journal of Heat and Mass Transfer*, vol. 40, pp. 3293-3304. 1997.
- [82] Lin, C. X., and Ebadian, M. A., The Effects of Inlet Turbulence on the Development of Fluid Flow and Heat Transfer in a Helically Coiled Pipe, *International Journal of Heat and Mass Transfer*, vol. 42, no. 4, pp. 739-750, 1999.
- [83] Li, L. J., Lin, C. X., Ebadian, M. A., Turbulent Heat Transfer to Near-Critical Water in a Heated Curved Pipe Under the Conditions of Mixed Convection, *International Journal of Heat and Mass Transfer*, vol. 42, no. 16, pp. 3147-3158, 1999.
- [84] Sillekens, J. J. M., Rindt, C. C. M., Steenhoven, A. A. van, Developing Mixed Convection in a Coiled Heat Exchanger, *International Journal of Heat and Mass Transfer*, vol. 41, no. 1, pp. 61-72, 1998.
- [85] Kalb, C. E., and Seader, J. D., Entrance Region Heat Transfer in a Uniform Wall-Temperature Helical Coil with Transition From Turbulent to Laminar Flow, *International Journal of Heat and Mass Transfer*, vol. 26, no. 1, pp. 23-32, 1983.
- [86] Oliver, D. R., Ashar, S. M., Heat Transfer in Newtonian and Viscoelastic Liquids During Laminar Flow in Helical Coils, *Transaction Institution Chemical Engineers*, vol. 54, pp. 218-224, 1976.
- [87] Yao, L. S., Heat Convection in a Horizontal Curved Pipe, *Journal of Heat Transfer*, vol. 106, pp. 71-77, 1984.

- [88] Liu, S., and Masliyah, J. H., Developing Convective Heat Transfer in Helical Pipes with Finite Pitch, *International Journal of Heat and Fluid Flow*, vol. 15, no. 1, pp. 66-75, 1994.
- [89] Nobari, M. R. H., Ahrabi, B. R., Akbari, G., A Numerical Analysis of Developing Flow and Heat Transfer in a Curved Annular Pipe, *International Journal of Thermal Sciences*, vol. 48, pp. 1542-1551, 2009.
- [90] Sreenivasan, K. R., and Strykowski, P. J., Stabilization Effects in Flow Through Helically Coiled Pipes, *Experiments in Fluids*, vol. 1, pp. 31-36, 1983.
- [91] Srivasata, R. S., and McConalogue, D. J., Motion of a Fluid in a Curved Tube, *Process Royal Society*, vol. A307, pp. 37-53, 1968.
- [92] Webster, D. R., and Humphery, J. A. C., Experimental Observations of Flow Instabilities in a Helical Coil, *ASME Journal of Fluids Engineering*, vol. 115, pp. 436-443, 1993.
- [93] Ito, H., Friction Factors for Turbulent Flow in Curved Pipes, *ASME Journal of Basic Engineering Transaction*, vol. 81, pp. 123-132, 1959.
- [94] Kubair, V., and Varrier, C. B. S., Pressure Drop for Liquid Flow in Helical Coils, *Transaction of Indian Institute of Chemical Engineering*, vol. 14, pp. 93-97, 1961/2.
- [95] Schmidt, D. F., Warmeubarang and Druckverlust in Rohrshlangen, *Chemical Engineering Technology*, vol. 13, pp. 781-789, 1967.
- [96] Srinivasan, P. S., Nadapurkar, S. S., Holland, F. A., Pressure Drop and Heat Transfer in Coils, *Chemical Engineering Journal*, vol. 218, pp. CE113-CE119, 1968.
- [97] Srinivasan, P. S., Nadapurkar, S. S., Holland, F. A., Friction Factors for Coils, *Transactions of the Institution of Chemical Engineers*, vol. 48, pp. T156-T161, 1970.

- [98] Mishra, P., and Gupta, S. N., Momentum Transfer in Curved Pipes 1. Newtonian Fluids; 2. Non-Newtonian Fluids, *Industrial and Engineering Chemistry Process Design and Development*, vol. 18, pp. 130-142, 1979.
- [99] A. Cioncolini, A., and Santini, L., An Experimental Investigation Regarding the Laminar to Turbulent Flow Transition in Helically Coiled Pipes, *Experimental Thermal and Fluid Science*, vol. 30, no. 4, pp. 367-380, 2006.
- [100] A. Cioncolini, A., and Santini, L., On laminar to turbulent flow transition in adiabatic helically coiled pipe flow, *Experimental Thermal and Fluid Science*, vol. 30, no. 7, pp. 653-661, 2006.
- [101] Di Piazza, I., and Ciofalo, M., Numerical Prediction of Turbulent Flow and Heat Transfer in Helically Coiled Pipe, *International Journal of Thermal Science*, vol. 49, pp. 653-663, 2010.
- [102] Stasiek, J. A., Collins, M. W., Ciofalo, M., Investigation of Flow and Heat Transfer in Corrugated Passages – I. Experimental Results, *International Journal of Heat and Mass Transfer*, vol. 39, pp. 149–164, 1996.
- [103] Kubair, and Kuloor, N. R., Flow of Newtonian fluids in Archimedean Spiral Tube Coils: Correlation of Laminar, Transition and Turbulent Flows, *Indian Journal Of Technology*, vol. 4, pp. 3-8, 1966.
- [104] Mori, Y., and Nakayama, W., Study on Forced Convective Heat Transfer in Curved Pipes (1st report, Laminar Region), *International Journal of Heat and Mass Transfer*, vol. 8, pp. 67-82, 1965.
- [105] Adler, M., Flow in Curved Tubes, *Zeitschrift fur Angewandte Mathematik und Mechanik (ZAMM)*, vol. 14, pp. 1659-1675, 1934.

- [106] Akiyama, and M. Cheng, K. C., Boundary Vorticity Method for Laminar Forced Convection Heat Transfer in Curved Pipes, *Intentional Journal of Heat and Mass Transfer*, vol. 14, pp. 1659-1675, 1971.
- [107] Austin, L. R., and Seader, J. D., Fully developed Viscous Flow in Coiled Pipes, *American Institute of Chemical Engineers* vol. 19, pp. 85-94, 1973.
- [108] Bolinder, C. J., and Sunden, B., Flow Visualization and LDV Measurements of Laminar Flow in a Helical Square Duct with Finite Pitch, *Experimental Thermal Fluid Science*, vol. 63, pp. 348-363, 1995.
- [109] Ujhidy, A., Nemeth, J., Szepvolgyi, J., Fluid Flow in Tubes with Helical Elements, *Chemical Engineering Process*, vol. 42, pp. 1-7, 2003.
- [110] Topakoglu, H. C., Steady State Laminar Flow in Incompressible Viscous Fluid in Curved Pipes, *Journal of Applied Mathematics and Mechanics* , vol. 16, no.2, pp. 1321-1338, 1967.
- [111] Larrain, J., and Bonilla, C. F., Theoretical Analysis of Pressure Drop in the Laminar Flow of a Fluid in a Coiled Pipe, *Transactions of The Society of Rheology: Journal of Rheology*, vol. 14 (2), pp. 135-148, 1970.
- [112] Ito, H., Flow in Curved Pipes, *Zeitschrift fur Angewandte Mathematik und Mechanik (ZAMM)*, vol. 49, pp. 653-662, 1969.
- [113] Austen, D. S., and Soliman, H. M., Laminar Flow and Heat Transfer in Helically Coiled Tubes with Substantial Pitch, *Experimental Thermal Fluid Science*, vol. 1, pp. 183-194, 1988.
- [114] Yamamoto, K., Yanase, S., Yoshida, T., Torsion Effect on the Flow in a Helical Pipe, *Journal of Fluid Dynamics Research*, vol. 14, pp. 259-273, 1994.

- [115] Yamamoto, K., Akita, T., Ikeuchi, H., Kita, Y., Experimental Studies of the Flow in Helical Circular Tube, *Journal of Fluid Dynamics Research*, vol. 16, pp. 237- 249, 1995.
- [116] Yamamoto, K., Aribowo, A., Hayamizu, Y., Hirose, T., Kawahara, K., Visualization of The Flow in a Helical Pipe, *Journal of Fluid Dynamics Research*, vol. 30, pp. 251-167, 2002.
- [117] Grundman, R., Friction Diagram of The Helically Coiled Tube, *Chemical Engineering and Processing: Process Intensification*, vol. 19, pp. 113-115, 1985.
- [118] Takahashi, M., and Momozaki, Y., Pressure Drop and Heat Transfer of a Mercury Single-Phase Flow and an Air-Mercury Two-Phase Flow in a Helical Tube Under a Strong Magnetic Field, *Chemical Engineering and Processing: Process Intensification*, vol. 51, pp. 869-877, 2000.
- [119] White, C. M., Fluid Friction and Its Relation to Heat Transfer, *Transactions of Institution Chemical Engineering (London)*, vol. 10, pp. 66-86, 1929.
- [120] Prandtl, L., Erzeugung von Zirkulationen beim Schütteln von Gefaßen, *Zeitschrift für Angewandte Mathematik und Mechanik*, vol. 29(1), PP. 8-9, 1949.
- [121] Hasson, D., Streamline Flow Resistance in Coils, *Reservoir Correspondence*, vol. 1, p 57, 1955.
- [122] Ramana Rao, M.V., Sadasivudu, D., Pressure Drop Studies in Helical Coils, *Indian Journal of Technology*, vol. 12, p. 473, 1974.
- [123] Gnielinski, V., Correlations for the Pressure drop in Helically Coiled Tubes, *International Journal of Chemical Engineering*, vol. 26, pp.36-44, 1986.
- [124] Xin, R. C., Awad, A., Dong, Z. F., Ebadian, M. A., An Experimental Study of Single-Phase and Two-Phase Flow Pressure Drop in Annular Helicoidal Pipes, *International Journal of Heat and Fluid Flow*, vol. 18, pp. 482-488, 1997.

- [125] Ali, S., Pressure Drop Correlations for Flow Through Regular Helical Coil Tubes, *Journal of Fluid Dynamics Research*, vol. 28, pp. 295-310, 2001.
- [126] Ju, H., Huang, Z., Xu, Y., Duan, B., Yu, Y., Hydraulic Performance of Small Bending Radius Helical Coil-pipe, *Nuclear Science Technology*, vol. 18, pp. 826-831, 2001.
- [127] Guo, L., Feng, Z., Chen, X., An Experimental Investigation of The Friction Pressure Drop of Steam-Water Two phase Flow in Helical Coils, *International Journal of Heat and Mass Transfer*, vol. 44, pp. 2601-2610, 2001.
- [128] Barua, S. N., On Secondary Flow in Stationary Curved Pipes, *The Quarterly Journal of Mechanics and Applied Mathematics*, vol. 6, pp. 61-77, 1963.
- [129] Collins, W. M., and Dennis, S. C. R., The Steady Motion of a Viscous Fluid in a Curved Tube, *The Quarterly Journal of Mechanics and Applied Mathematics*, vol. 28, pp. 133-156, 1975.
- [130] Van Dyke, M., Extended Stokes series: Laminar flow Through a Loosely Coiled Pipes, *Journal of Fluid Mechanics*, vol. 86, pp.129-145, 1978.
- [131] Dennis, S. C. R., Calculation of the Steady Flow Through a Curved Tube Using a New Finite-Difference Scheme, *Journal of Fluid Mechanics*, vol. 99, pp. 449-467, 1980.
- [132] Manlapaz, R. L., and Churchill, S. W., Fully Developed Laminar Flow in Helically Coiled of Finite Pitch, *Chemical Engineering Communication*, vol. 7, pp. 57-78, 1980.
- [133] Hart, J., Ellenberger, J., Hamersma, P. J., Single and Two-phase Flow Through Helically Coiled Tubes, *Chemical Engineering Science*, vol. 45, no.4, pp. 775-783, 1988.
- [134] Yanase, S., Goto, N., Yamamoto, K., Dual Solution of the Flow Through a curved tube, *Fluid Dynamics Research*, vol. 5, pp. 191-201, 1989.

- [135] Ferng, Y. M., Lin, W. C., Chieng, C. C., Numerical Investigated of Effects of Different Dean Number and Pitch Size on Flow and Heat Transfer Characteristics in a Helically Coiled Tube Heat Exchanger, *Applied Thermal Engineering*, vol. 36, pp. 378-385, 2012.
- [136] Pimenta, T. A., Campos, J. B. L. M., Newtonian and Non-Newtonian Fluids Flowing in Laminar Regime in a Helical Coil, *Experimental Thermal and Fluid Science*, vol. 36, pp. 194-204, 2012.
- [137] Rahimi, M., Beigzadeh, R., Prediction of Heat Transfer and Flow Characteristics in Helically Coiled Tubes Using Artificial Neural Networks, *International Communications in Heat and Mass Transfer*, vol. 39, pp. 1279-1285, 2012.
- [138] Hawe, W. B., Some Sidelights on The Heat Transfer Problems, *Transactions of Institution Chemical Engineering*, vol. 10, pp. 161-167, 1932.
- [139] Balejova, M., Cakrt, J., Mick, V., Non-Isothermal Laminar Flow in Curved Pipes, *Applied Science Reservoir*, vol. 32, p. 587, 1976.
- [140] Balejova, M., Cakrt, J., Mick, V., Heat Transfer for Laminar Flow in Curved Pipes, *international scientific journal Acta Technica*, vol. 22, 183, 1977.
- [141] Ievlev, V. M., Dzyubenko, B. V., Dreitser, G. A., Vilemas, Y. V., In-line and Cross-Flow Helical Tube Heat Exchangers, *International Journal of Heat and Mass Transfer*, vol. 25, pp. 317-323, 1982.
- [142] Prasad, B. V. S., Das, D. H., Prabhakar, A. K., Pressure Drop, Heat Transfer and Performance of a Helically Coiled Tubular Exchanger, *Journal of Heat Recovery Systems*, vol. 9, pp. 249-256, 1989.
- [143] Inagaki, Y., Koiso, H., Takumi, H., Ioka, I., Miyamoto, Y., Thermal Hydraulic Study on a High-Temperature Gas-Gas Heat Exchanger With Helically Coiled Tube Bundles, *Nuclear Engineering and Design*, vol. 185, pp. 141-155, 1998.

- [144] Havas, G., Deak, A., Sawinsky, J., Heat Transfer to Helical Coils in Agitated Vessels, *Chemical Engineering Journal*, vol. 35, pp. 61-64, 1987.
- [145] Jayakumar J. M., Mahajani, S. M., Mandal, J. C., Vijayan, P. K., Bho, R., Experimental and CFD Estimation of Heat Transfer in Helically Coiled Heat Exchangers, *Chemical Engineering Research and Design*, vol. 86, pp. 221-232, 2008.
- [146] Ali, M. E., Experimental Investigation of Natural Convection from Vertical Helical Coiled Tubes, *International Journal of Heat and Mass Transfer*, vol. 37, pp. 665-671, 1994.
- [147] Ali, M. E., Laminar Natural Convection from Constant Heat Flux Helical Coiled Tubes, *International Journal of Heat and Mass Transfer*, vol. 41, pp. 2175-2182, 1998.
- [148] Ali, M E., Natural Convection Heat Transfer from Vertical Helical Coils in Oil, *Heat Transfer Engineering*, vol. 27, no. 3, pp. 79-85, 2007
- [149] Bai, B.; Guo, L.; Feng, Z., Chen, X. Turbulent Heat Transfer in a Horizontally Coiled Tube, *Heat Transfer Asian Reservoir*, pp. 28, pp. 395-403, 1999.
- [150] Yang, V. G., Dong, Z. F., Ebdian, M. A., Laminar Forced Convection in a Helicoidal Pipe with Finite pitch, *International Journal of Heat and Mass Transfer*, vol. 38, pp. 853-862, 1995.
- [151] Yang, V. G., Ebdian, M. A., Turbulent Forced convection in a Helicoidal Pipe with Substantial Pitch, *International Journal of Heat and Mass Transfer*, vol. 39, pp. 2015-2022, 1995.
- [152] Acharya, N., Sen, M., Chang, H. C., Analysis of Heat Transfer Enhancement in Coiled-Tube Heat Exchangers, *International Journal of Heat and Mass Transfer*, vol. 44, pp. 3198-3199, 2001.

- [153] Lemenand, T., Peerhossaini, H., A Thermal Model for Prediction of the Nusselt Number in a Pipe with Chaotic Flow, *Applied Thermal Engineering*, vol. 22, pp. 1717-1730.
- [154] Ke, Y., Pei-qi, G., Hai-tao, M., Numerical Simulation on Heat Transfer Characteristic of Conical Spiral Tube Bundle, *Applied Thermal Engineering*, vol. 31, pp. 284-292, 2011.
- [155] Zachar A., Investigation of Natural Convection Induced Outer Side Heat Transfer Rate of Coiled-tube Exchangers, *International Journal of Heat and Mass Transfer*, vol. 55, pp. 7892-7901, 2012.
- [156] Mori, Y., and Nakayama, W., Study on Forced Convective Heat Transfer in Curved Pipes, (Third Report, Theoretical Analysis under the Condition of Uniform Wall Temperature and Practical Formulae), *International Journal of Heat and Mass Transfer*, vol. 10, pp. 681-695, 1967.
- [157] Jeschke, D., Heat Transfer and Pressure Loss in Coiled pipes, *Ergaenzungsheft Z. Ver. Dtsch.. Ing.*, vol. 68, pp. 24-28, 1925.
- [158] Merkel, E., *Die Grundlagen Der Wärmeübertragung*, p. 51, 1927.
- [159] Liu, S., and Masliyah, J. H., A Decoupling Numerical Method for Fluid Flow, *International Journal of Numerical Methods Fluids*, vol. 16 (8), pp. 659-682, 1993.
- [160] Futagami, K., and Aoyama, Y., Laminar Heat Transfer in a Helically Coiled Tube, *International Journal of Heat and Mass Transfer*, vol. 31, no. 2, 387-396, 1988.
- [161] Naphon, P., and Suwagrai, J., Effect of Curvature Ratios on the Heat Transfer and Flow Developments in the Horizontal Spirally Coiled Tubes, *International Journal of Heat and Mass Transfer*, vol. 50, pp. 444-451, 2007.
- [162] Prabhanjan, D. F., Raghavan, G. S. V., Rennie, T. J., Comparison of Heat Transfer Rates Between a Straight Tube Heat Exchanger and a Helically Coiled Heat Exchanger, *International Communications in Heat and Mass Transfer*, vol. 29, pp. 185-191, 2002.

- [163] Prabhanjan, D. G., Rennie, T. J., Raghavan, G. S. V., Natural Convective Heat Transfer From Helical Coiled Tubes, *International Journal of Thermal Science*, vol. 43, pp. 359-365, 2004.
- [164] Zapryanov, Z., Christon, C. H., Toshev, E. Fully developed laminar flow and heat transfer in curved tubes, *International Journal of Heat and Mass Transfer*, vol. 23, pp. 873-880, 1980.
- [165] Jha, R. K., and Rao, R., Heat Transfer through Coiled Tubes in Agitated Vessels, *International Journal of Heat and Mass Transfer*, vol. 10, pp. 395-397, 1967.
- [166] Shchukin V. K., Correlation for Experimental data on Heat Transfer in Curved Pipes, *Thermal Engineering*, vol. 16, pp. 72-76, 1969.
- [167] Yildiz, C., Bicer, Yasar, Pehlivan, D., Heat Transfer and Pressure Drop in a Heat Exchanger with a Helical Pipe Containing inside Springs, *Energy Conversion Management*, vol. 38 (6), pp. 619-624, 1997.
- [168] Salimpour, M. R., Heat Transfer Characteristics of a Temperature-Dependent-Property Fluid in Shell and Coiled Tube Heat Exchangers, *International Communications in Heat and Mass Transfer*, vol. 32, pp. 1190-1195, 2008.
- [169] Pawar, S. S., Sunnapwar, V. K., Experimental Studies on Heat Transfer to Newtonian and Non-Newtonian Fluids in Helical Coils with Laminar and Turbulent Flow, *Experimental Thermal and Fluid Science*, vol. 44, pp. 792-804, 2013.
- [170] Rainieri, S., Bozzoli, F., Pagliarini, G., Experimental Investigation on The Convective Heat Transfer in Straight and Coiled Corrugated Tubes for Highly Viscous Fluids: Preliminary Results, *International Journal of Heat and Mass Transfer*, vol. 55, pp. 498-504, 2012.

- [171] Rainieri, S., Bozzoli, F., Gattani, L., Pagliarini, G., Compound Convective Heat Transfer Enhancement, *International of Journal Heat and Mass Transfer*, vol. 59, pp. 353-362.
- [172] Maekawa, H., Heat Transfer to Fully Developed Laminar Flow in a Gently Curved Pipe, *Preprint of 1st Japan Heat Transfer Symposium*, pp. 13-16, 1964.
- [173] Akiyama, M., and Cheng, K. C., Laminar Forced Convection Heat Transfer in Curved Pipes with Uniform Wall Temperature, *International Journal of Heat and Mass Transfer*, vol. 15, pp. 1426-1431, 1972.
- [174] Kalb, C. E., and Seader, J. D., Fully Developed Viscous Flow, Heat Transfer in Curved Tubes with Uniform Wall Temperatures, *American Institute of Chemical Engineers Journal*, vol. 20, pp. 340-346, 1974.
- [175] Manlapaz, R. L., and Churchill, S. W. Fully Developed Laminar Convection From a Helical Coil. *Chemical Engineering Communication*, vol. 97, pp. 185-200, 1981.
- [176] Ghoabdi, M., Experimental Measurement and Modelling of Heat Transfer in Spiral and Curve Channels. Ph.D. thesis. Memorial University of Newfoundland, Canada, 2013.
- [177] Berger, R. R.; Bonilla, C. F. Heating of Fluids in Coils, *Academic Science: New York*, vol. 13, pp. 12-25, 1950.
- [178] Kirpov, A. V., Heat Transfer in Helically Coiled Pipes, *Trudi, Mascov Institution Khim. Mashinojtrojenija*, vol. 12, pp. 43-56, 1957.
- [179] Seban, R. A., and McLaughlin, E. F., Heat Transfer in Tube Coils With Laminar and Turbulent Flow, *International Journal of Heat and Mass Transfer*, vol. 6, 387-395, 1963.
- [180] Roger, G. F. C., and Mayhew, Y. R., Heat Transfer and Pressure Loss in Helically Tubes with Turbulent Flow, *International of Journal Heat and Mass Transfer*, vol. 7, pp. 1207-1216, 1964.

- [181] Singh, S. P. N., and Bell, K. J., Laminar Flow in Heat Transfer in a Helically Coiled Tube, *Proceeding 5th International Heat Transfer Conference*, Tokyo, vol. 2, pp. 193-197, 1974.
- [182] Yildiz, C., Bicer, Yasar, Pehlivan, D., Heat Transfer and Pressure Drops in Rotating Helical Pipes, *Applied Energy*, vol. 50, pp. 85-94, 1995.
- [183] Xin, R. C., Ebadian, M. A., The Effect of Prandtl Numbers on Local and Average Convective Heat Transfer Characteristics in Helical Pipes, *Journal of Heat Transfer*, vol. 119, pp. 463-473, 1997.
- [184] Moawed, M., Experimental Study of Forced Convection From Helical Coiled Tubes with Different parameters, *Energy Conservation Management*, vol. 52, pp. 1150-1156, 2011.
- [185] Jensen, M. K., and Bergles, A. E., Critical Heat Flux in Helical Coils with a Circumferential Heat Flux Tilt Toward the Outside Surface, *International Journal of Heat and Mass Transfer*, vol. 25, no. 9, pp. 1383-1395, 1982.
- [186] Kalb, C.E., and Seader, J.D., Heat and Mass Transfer Phenomena for Viscous Flow in Curved Circular Tubes, *International Journal of Heat and Mass Transfer*, vol. 15, pp. 801-817, 1972.
- [187] Mori, Y., and Nakayama, W. Study on Forced Convective Heat Transfer in Curved Pipes, *International Journal of Heat and Mass Transfer*, vol. 10, pp. 37-59, 1967.
- [188] Ozisik, M. N., and Topakoglu, H. C., Heat Transfer for Laminar Flow in a Curved Pipe, *Journal of Heat Transfer*, vol. 90, pp. 313-318. 1968.

# Chapter 3

## Heat Transfer and Pressure Drop in a Spiral Square Channel\*

**M.Ghobadi and Y.S. Muzychka**

Microfluidics and Multiphase Flow Lab, Faculty of Engineering and Applied Science,  
Memorial University of Newfoundland, St. John's, NL, Canada, A1B 3X5

### **ABSTRACT**

Heat transfer and pressure drop in a spiral square channel is examined experimentally and analytically. The spiral channel was fabricated in a copper plate. The cross section of the channel is square with 1 mm sides. A copper cap plate was bolted tight to seal the channel. Water and four silicone oils (0.65 cSt, 1 cSt, 3 cSt and 10 cSt) were used as the working fluid; thus Prandtl numbers from 5 to 110 were examined. The experiments were done once with the fluids entering from the side of the spiral channel and exiting from the middle of the spiral channel, and once with the fluids entering from the middle and exiting from the side. Heat transfer behaviour over a wide range of flow rates from laminar to turbulent has been examined. Heat transfer enhancement due to the spiral geometry was observed, and slight difference was reported between the side and middle inlet condition. The dimensionless mean wall flux and the dimensionless thermal flow length were used to analyze the experimental data instead of Nusselt number and Reynolds number. The spiral channel has been discretized, so that a single Dean number can be assumed in each cell, and two existing correlations were applied to obtain the average Nusselt number. The model predictions are compared with the experimental points. Pressure drop tests have only been conducted with water as the working fluid.

**Keywords:** Spiral Mini-channels, Heat Transfer, Laminar Flow, Dean Number, Graetz Flow

\* *Submitted to Experimental Heat Transfer*

### 3.1 Introduction

Heat transfer enhancement is desired in most thermal applications. In general, there are two methods to improve the heat transfer rate: active and passive techniques [1, 2]. Active techniques are based on external forces such as electro-osmosis [3], magnetic stirring [4], bubble induced acoustic actuation [5] and ultrasonic effects [6] to perform the augmentation. Active techniques are effective; however, they are not always easy to implement with other components in a system. They also increase the total cost of the system manufacturing.

On the other hand, passive techniques employ fluid additives or special surface geometry. Using the surface geometry approach is easier, cheaper and does not interfere with other components in the system. Surface modification or additional devices incorporated in the stream are two passive augmentation techniques. With these techniques, the existing boundary layer is disturbed and the heat transfer performance is improved. However, pressure drop is also increased [7].

Curved geometry is one of the passive heat transfer enhancement methods that fit several heat transfer applications such as: compact heat exchangers, steam boilers, gas turbine blades, electronics cooling, refrigeration and etc.

Early investigations on curved geometries were conducted by Thomson [8], Williams [9], Grindley and Gibson [10] and Eustic [11]. The idea of using spiral geometry was first used in spiral plate heat exchangers in the late 19th century [12] and further investigations conducted in the 1930s in Sweden [13, 14].

Dean [15, 16] conducted the first studies on flow and heat transfer in curved ducts. White [17] numerically studied the pressure drop through a constant curvature coil. Thorough investigation on heat transfer has been provided by Akiyama and Cheng [18, 19] on curved rectangular channels and curved pipes with uniform heat flux and a peripherally uniform wall temperature. Mori et al. [20] analytically and experimen-

tally studied the fully laminar flow in a curved channel with square section with a constant wall heat flux. Numerical study was performed by Yee [21] on heat transfer in a 90 degree channel with constant wall temperature. Nigam [22] accomplished a comprehensive review on the papers related to the application of curved geometry in the process industry up to 2008.

The nature of the flow inside the curved channel is completely different from the flow in a straight channel. The main reason for the heat transfer enhancement in curved channels is the initiation of secondary flows inside the channel. Cheng [23] reported that the number of the vortices inside a curved channel depends on the Dean number. Two vortices have been reported for  $De < 100$ , whereas for  $100 < De < 500$ , four vortices appear in a square curved channel. These extra vortices vanish at about  $De = 500$ . The channel aspect ratio determines the exact value of the disappearance. Centrifugal forces in a fluid are body forces and lead to secondary flow. The secondary flow changes the heat transfer and pressure drop [20]. At the central part of the flow passage, the effect of heat convection due to the secondary flow is dominated by viscosity; whereas, the conduction and viscosity effect are only important within a thin layer near the wall of the passage.

Unlike the flow in straight channels, fluid motion in curved channels is not parallel to the curved axis of the bend, owing to the presence of a secondary motion caused by secondary flow. As the flow enters a curved bend, centrifugal force acts outward from the center of curvature on the fluid elements. Pressure gradients parallel to the axis of symmetry are almost uniform along lines normal to that of the symmetry axis. Because of the no-slip condition at the wall, the axial velocity in the core region is much faster than that near the wall. To maintain the momentum balance between the centrifugal force and pressure gradient, slower moving fluid elements move toward the inner wall of the curved tube. This leads to the onset of a secondary flow such

that fluid near the wall moves along upper and lower halves of the torus wall while fluid far from it flows to the outer wall.

Manlapaz and Churchill [24] developed a general correlation for fully developed laminar convection from a helical coil for all Prandtl and Dean numbers. Their model was constructed by joining the theoretical Nusselt number for straight tubes, a theoretical asymptote for the regime of creeping secondary flow, a semi-theoretical expression for the boundary layer regime and an asymptotic value of Nu for the intermediate regime of flow.

Aoyama and Futagami [25] experimentally measured the turbulent structure in a curved circular tube for three values of the curve radius to the tube radius ratio. They showed that when R is small, turbulent generation does not balance with turbulent energy dissipation, due to a convective effect induced by secondary flow.

Measuring the temperature fluctuation for slightly heated airflow in a curved square channel, Cheng and Tinga [26] studied the relaminarization process caused by the secondary flows. Cheng [27] employed the temperature fluctuation measurements to predict the transition to turbulent flow.

Burmeister and Egner [28] numerically studied laminar flow and heat transfer in three-dimensional spiral ducts of rectangular cross section with different aspect ratio. The boundary conditions were assumed to be axially and peripherally uniform wall heat flux and a peripheral uniform wall temperature.

Hashemi and Akhavan-Behabadi [29] experimentally investigated the heat transfer and pressure drop characteristics of nanofluid flow inside horizontal helical tube under constant wall flux. They studied effect of different parameters such as Reynolds number, fluid temperature and nanofluid particle weight concentration on heat transfer coefficient and pressure drop of the flow.

The main purpose of this paper is to examine the cooling performance systems em-

ploying spiral geometry using different working fluids. Water and four silicone oils with viscosity ranging from 0.65 cSt which is less than the water's viscosity, 1 cSt, 3 cSt and 10 cSt are employed inside a square spiral mini channel to examine if the spiral geometry significantly enhances the heat removal. The results are compared to the Graetz model for straight channels of the same length, which is valid for all Prandtl numbers when the flow is hydrodynamically fully developed, and thermally developing. The pressure drop tests were performed with water as the working fluid. The results were combined with the heat transfer results to plot a diagram, which shows the pressure drop penalty incurred to reach the desired enhancement.

## 3.2 Experimental Setup

The spiral channel was fabricated on a copper base plate. The cross section of the channel is square with 1 *mm* sides and the channel length is 278 *mm*. The following equation defines the radius of curvature at each distance from the center of spiral ( $x$ ):

$$R = 2 + \frac{2x + x^2/2}{\pi} \quad (3.1)$$

A flat copper cap plate with identical size was bolted tight to seal the channel. The total heat provided by two heaters (Watlow Film Heaters), one placed on the cap, and one on the plate, which contains the channel. Five T type thermocouples were placed near the spiral channel wall to measure the surface temperature; one at the dead center and four at the center of each quadrant on one surface. Two additional thermocouples were used to measure the inlet and outlet bulk temperature using a simple T junction with a thermocouple embedded into the stream. Two Omega pressure transducers with different ranges were used to measure the pressure drop of the water flow passing through the heat sink. A Keithley Data Acquisition system (DAQ) collected the

temperatures during the experiments. The five measured temperatures from the wall were averaged to calculate the mean surface temperature. The maximum temperature difference between the five readings was found to be less than  $2^{\circ} C$ , which means less than 5% maximum deviation from the average surface temperature. The heat sink was placed inside a box surrounded by insulation material. Thermal resistance of the insulation box was measured for the case when there is no flow and variable power applied to the heat sink. The heat sink temperature for each power was collected in the steady state condition. Since conduction was the only mode of heat transfer in this case, thermal resistance of the insulation box can be calculated as:

$$R_{thermal} = \frac{T_w - T_a}{P} \quad (3.2)$$

Figure 3.1 shows a schematic configuration of the system, and the spiral channel. Four syringes (Hamilton Glass Gas Tight) were filled with the test fluid, and the pumps (Harvard Pump 33) were set to the desirable flow rate. If water is used as a medium in the experiment it was disposed of after leaving the heat sink, whereas, the silicone oils were recycled. Ten readings for each flow rate were made and averaged to account for local fluctuations.

Two pressure transducers with different ranges were used to measure the pressure drop in different ranges. Wet/wet differential pressure models from Omega Inc. with ranges of 0 – 1 psi and 0 – 15 psi with unidirectional ranges were used. Thermocouples and pressure transducer T junctions for the inlet and outlet measurements were placed as close as possible to the heat sink to minimize the effect of the straight pipe.

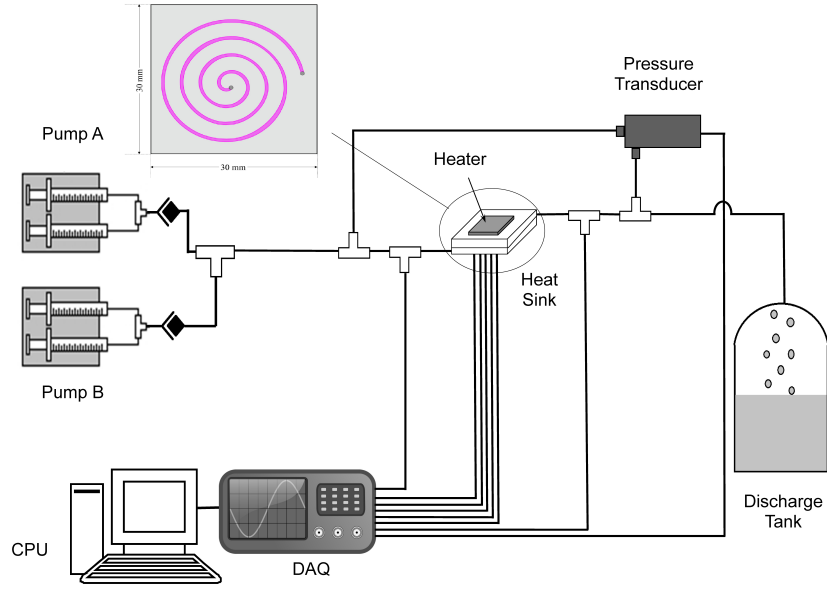


Figure 3.1: Experimental test setup and the spiral channel

### 3.3 Benchmarking and Uncertainty

In general, the uncertainty of the thermocouple reading was verified to be within  $0.1^\circ C$  using an ice bath and boiling water. The uncertainty in volumetric flow rates provided by the syringe pumps was measured at low and high flow rates and found to be on the order of  $\pm 1$  percent or better. The uncertainty of the pressure drop measurements is reported to be  $\pm 1\%$  of total pressure range. A simple uncertainty analysis was conducted using the method outlined by Kline and McClintock [30]:

$$w_F = \left[ \left( \frac{\delta F}{\delta x_1} w_1 \right)^2 + \left( \frac{\delta F}{\delta x_2} w_2 \right)^2 + \dots + \left( \frac{\delta F}{\delta x_n} w_n \right)^2 \right]^{1/2} \quad (3.3)$$

Where  $F$  is a given function of the independent variables  $x_1, x_2, \dots, x_n$ , and  $w_F$  is the uncertainty in the result and  $w_1, w_2, \dots, w_n$  are uncertainties in the independent variables.

This yields an uncertainty using the root mean squares method of  $\pm 6.36 - 7.91\%$  in the dimensionless heat transfer  $q^*$ ,  $\pm 6.04 - 7.60\%$  for  $L^*$ ,  $\pm 2.23\%$  for  $Re$  and  $\pm 1 - 5\%$  for  $dp^*$ .

Figure 3.2 depicts the pressure drop and the heat transfer benchmarking test. The pressure drop test was performed on a straight tube with 1.6 mm diameter and a 314 cm length, and 163 mm long straight copper tubing with hydraulic diameter of 1.65 mm was used for the heat transfer test. The main purpose of benchmarking tests is to determine the uncertainty of our apparatus used for the measurements. The RMS error for the benchmarking test was calculated to be 3.99% with a minimum deviation of  $\pm 1.5\%$  and maximum deviation of  $\pm 9\%$ . Three different sensors have been used to perform the tests according to the measured pressure drop. The experimental results are compared with theoretical results for laminar flow in straight tubing in Fig. 3.2. The heat transfer benchmarking test was performed with a 163 mm long straight copper tubing with the diameter of 1.65 mm. The tubing was cut precisely and the edges were filed to have smooth ends. Finally, plastic tubing was glued to the ends to avoid any leakage. Thermocouples were placed at each end with the minimum distance from the copper tubing. The constant wall temperature condition was considered with a surface temperature of  $40^\circ\text{C}$ , using a constant temperature bath. The ambient temperature and the fluid temperature at the entrance was  $25^\circ\text{C}$ . The results are shown in Fig. 3.2, and agree well with the classical Graetz Flow in a tube. The RMS error for the benchmarking test was calculated to be 5.5% with a minimum deviation of  $\pm 2.8\%$  and maximum deviation of  $\pm 9.3\%$ .

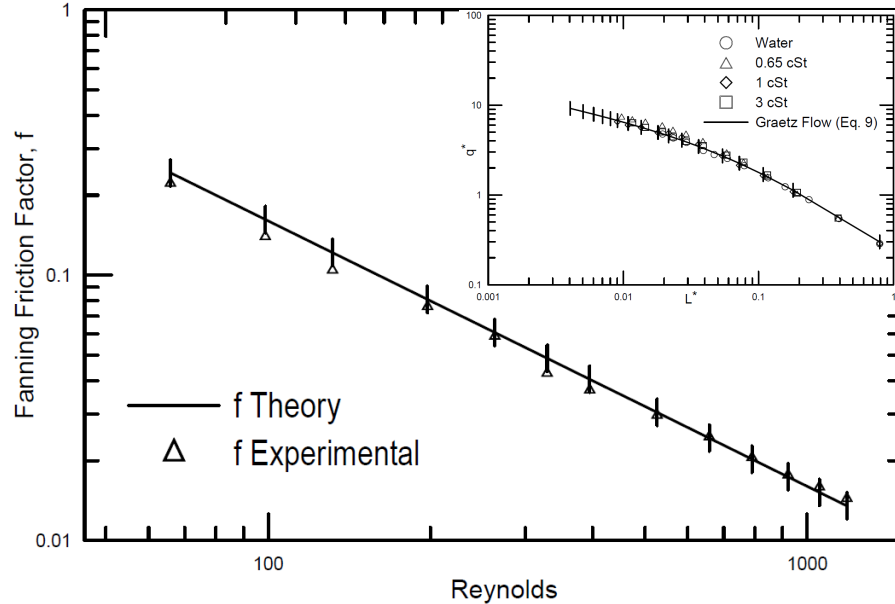


Figure 3.2: Pressure drop and heat transfer benchmarking test in straight circular tubes with 10% error bars

### 3.4 Graetz flow for Constant Wall Temperature

We begin by reviewing the classic internal flow heat transfer problem known as Graetz or Graetz-Nusselt problem and some useful alternatives for representing dimensionless heat transfer rates. Unlike external flows, where the stream temperature remains constant, i.e.  $T_\infty$ , the temperature difference between the wall and moving stream does not remain constant over the length of duct or channel.

In a duct or channel flow, we may define this wall-to-stream temperature difference in a number of ways. The correct choice should be based on the application. In a single fluid heat sink such as the current case, the best and easiest approach is to use the wall to inlet temperature difference,  $T_w - T_i$ . The most commonly used form for defining the local heat transfer coefficient in an internal flow for constant temperature has traditionally been in terms of the bulk temperature,  $T_m$ . The local heat flux,  $q_z$ , is often related to a local heat transfer coefficient,  $h_z$ , by means of some

defined characteristic temperature difference in the local flow:

$$q_z = h_z (T_w - T_m) \quad (3.4)$$

Where  $T_w - T_m$  is the local wall-to-bulk temperature difference. In a duct where the prescribed wall temperature remains constant, the heat flux varies due to changes in the bulk temperature.

Traditionally, the heat transfer rate is non-dimensionalized using a Nusselt number defined as:

$$Nu_{D_h} = \frac{q_z D_h}{k(T_w - T_m)} = \frac{h D_h}{k} \quad (3.5)$$

Hydraulic diameter is a commonly used length scale when handling flow in noncircular tubes and channels. Using this length scale one can define Nu in the same way as for a round tube. It is defined as:

$$D_h = \frac{4A}{p} \quad (3.6)$$

If a mean Nusselt number is desired, then we must integrate along the duct length:

$$\overline{Nu}_{D_h} = \frac{1}{L} \int_0^L Nu_{D_h} dz \quad (3.7)$$

In the case of constant wall temperature, one may either define a Nusselt number, and use LMTD temperature difference, or adopt a dimensionless heat transfer rate which is based on the mean wall to inlet temperature difference rather than the traditional heat transfer coefficient approach which utilizes the mean wall to bulk temperature difference. This alternative approach is more natural and more practical in the analysis of single fluid devices, such as heat sinks.

Two dimensionless parameters of interest, which need to be defined, are the dimen-

dimensionless mean wall flux:

$$q^* = \frac{\bar{q}D_h}{k(T_w - T_i)} \quad (3.8)$$

and the dimensionless thermal length:

$$L^* = Gz^{-1} = \frac{L/D_h}{Pe_{D_h}} \quad (3.9)$$

The dimensionless mean wall flux can be related to the Nusselt number using single fluid heat exchanger theory, e.g. the  $\epsilon - NTU$  method for constant wall temperature.

This leads to the following expression relating the two:

$$q^* = \frac{1}{4L^*} [1 - \exp(-4\overline{Nu}L^*)] \quad (3.10)$$

In the case of a Graetz flow in a circular tube, Muzychka et al. [31] obtained:

$$q^* = \left[ \left( \frac{1.614}{L^{*1/3}} \right)^{-3/2} + \left( \frac{1}{4L^*} \right)^{-3/2} \right]^{-2/3} \quad (3.11)$$

For non-circular micro-channels and mini-channels, we can use an alternative form of the Muzychka and Yovanovich [32] model:

$$q^* = \left[ \left( 0.641 \left( \frac{fRe_{D_h}}{L^*} \right)^{1/3} \right)^{-3/2} + \left( \frac{1}{4L^*} \right)^{-3/2} \right]^{-2/3} \quad (3.12)$$

where  $fRe_{D_h}$  is the fanning friction factor Reynolds number group for laminar flow, see Kakac et al. [33] or Bejan [34]. For a rectangular mini-channel, Muzychka and Yovanovich [32] proposed using the first term of the exact series solution:

$$fRe_{D_h} = \frac{24}{(1 + \beta)^2 \left[ 1 - \frac{192}{\pi^5} \tanh \frac{\pi}{2\beta} \right]} \quad (3.13)$$

where  $\beta = b/a$  is the aspect ratio of the rectangular channel such that  $0 < \beta < 1$ . For a square channel  $fRe_{D_h} = 14.23$ . This gives the following correlation for a Graetz flow in a square channel:

$$q^* = \left[ \left( \frac{1.553}{L^{*1/3}} \right)^{-3/2} + \left( \frac{1}{4L^*} \right)^{-3/2} \right]^{-2/3} \quad (3.14)$$

We used equation (14) as a basis for showing the degree of heat transfer enhancement in the spiral square duct.

### 3.5 Data Analysis

In all experiments, fluid enters the heat sink as a single phase liquid flow, is heated up and leaves in the same condition; hence the total heat removed by the fluid can be calculated as:

$$Q_{bulk} = \dot{m}C_p(T_o - T_i) \quad (3.15)$$

The heat sink was insulated to minimize the heat leakage due to convection, but conduction heat transfer is still present. The amount of heat received by the fluid is still different from the heat provided by the heaters:

$$Q_{bulk} = P - \frac{(T_w - T_a)}{R_{thermal}} \quad (3.16)$$

Where  $P$  is the power input, and  $R_{thermal}$  is the thermal resistant of the insulated box around the heat sink when no liquid flow is present. The second term represents the heat loss to the surroundings due to conduction. The overall bulk heat transfer using the two approaches was in good agreement, but equation (16) was used in our data reduction.

### 3.6 Results and Discussion

Water and four different silicone oils with the viscosity of 0.65 cSt, 1 cSt, 3 cSt and 10 cSt have been used as a cooling medium. Prandtl numbers from 5.7 up to 108 were tested during the experiments. Flow rates from 1.5 *ml/min* up to 200 *ml/min* were adjusted according to the viscosity of the fluid and the pump power. The Reynolds number was reported to vary from mainly laminar flow to slightly turbulent flow. It has been shown that the entrance length is 20% to 50% shorter in curved channels than for straight channels [35]. Thus, in the present work the channel is long enough to consider the fluid to be hydrodynamically developed, but thermally developing flow. Table 3.1 shows the average Prandtl number and range of Reynolds numbers for the fluids examined during the tests. Power adjustment was conducted based on the flow rate to avoid exceeding the allowable temperature of the heaters, which is about 80°C. It ranged from 5 W for the lower flow rate and increased to maximum power of (20 W) for the higher flow rates.

All fluid properties have been calculated using the mean of the inlet and outlet temperature. The manufacturer supplied viscosity and other silicone oil properties. However, the viscosity of the oils and water were measured with an accurate viscometer. Water was used as a reference fluid. The deviations between the reported viscosity, and measured viscosity were found to be less than 5%. Temperature effects on the properties have also been considered.

Fluid entered the channel from the side or from the middle of the heat sink to examine if there was any difference in the heat transfer behavior of the system. Figures 3.3 and 3.4 show  $q^*$  versus  $L^*$  for the middle and the side inlet spiral channel. The simple Graetz model for straight channels is plotted to compare the heat transfer inside spiral channel to the one in straight channel with the identical cross section and length.

Increasing the flow rate results in decreasing the  $L^*$  and increasing  $q^*$  consequently,

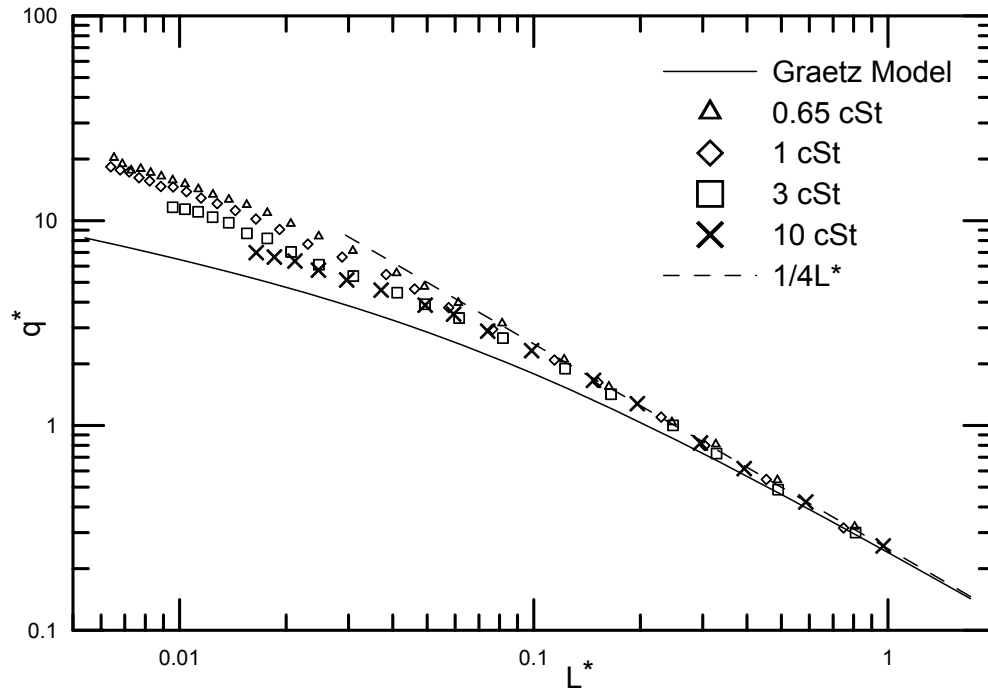


Figure 3.3: Different fluid performance for the middle inlet spiral channel

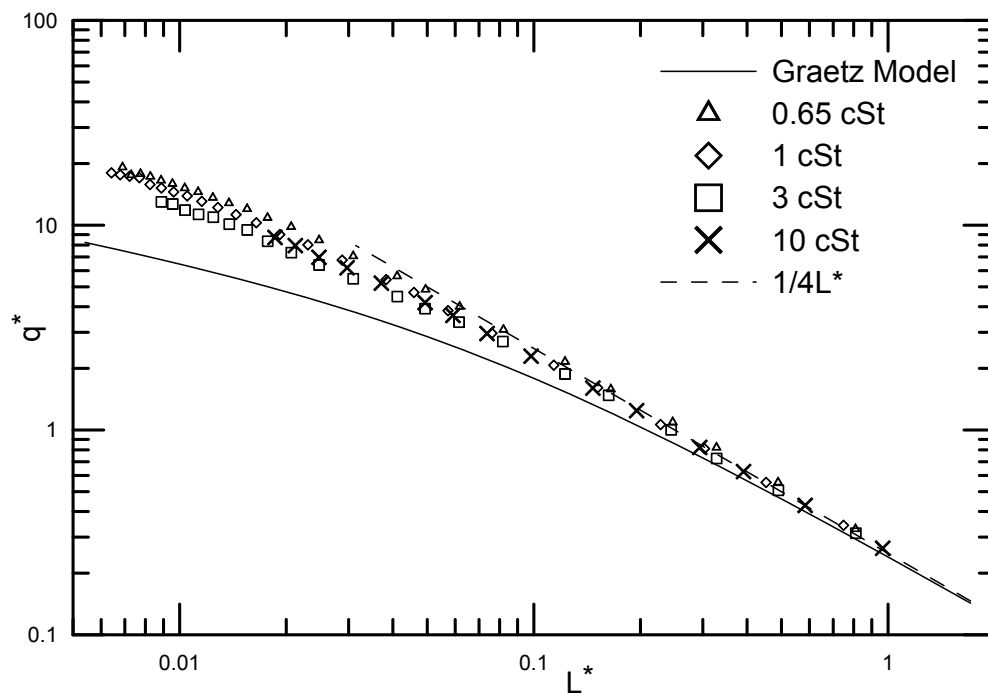


Figure 3.4: Different fluid performance for the side inlet spiral channel

Table 3.1: Prandtl, Reynolds, and Peclet Numbers for Examined Fluids

Fluid	$Pr$	$Re$	$Pe$
0.65 cSt	8.6	44 – 4481	378 – 38536
1 cSt	13.9	430 – 2907	417 – 40407
3 cSt	38.5	9.68 – 767	373 – 29529
10 cSt	108.6	2.79 – 151.42	303 – 16444

heat transfer increases with increasing the flow rate. For both configurations, thermal behaviour at very low flow rates ( $L^*$  more than one) is similar to the simple Graetz model, Eq. (14). All the results also converge to  $\frac{1}{4L^*}$  model, which is the maximum heat that can be transferred to the fluids,  $T_o \rightarrow T_w$ . In other words, the curvature does not improve the heat transfer rate when the fluid moves at very low speed. The reason is the secondary flow which enhances heat transfer in curved channels does not appear at low flow rates. Increasing the flow rate, heat transfer augmentation is observed, as compared to the equivalent straight channel.

Heat transfer is enhanced for both side and middle inlet for all fluids in comparison to the Graetz model for a straight channel of the identical size. The minimum enhancement is observed for the water and the maximum augmentation was obtained for 0.65 cSt silicone oil for both configurations. By increasing the viscosity for the silicone oils,  $q^*$  decreases.

The change in inlet of the fluid shows no significant difference in heat transfer enhancement. Figure 3.5 (a) shows the difference for 3 cSt silicone oil; plots for the other fluids are similar to Fig. 3.5 (a).

It is also helpful to see how the heat transfer enhancement ratio  $E = [(q_c^*)/(q_s^*)]$  varies by changing the flow rate. Fig. 3.5 (b) shows the enhancement ratio,  $E$ , for 0.65 cSt silicone oil as a function of  $L^*$ . Other silicone oil behaviours are identical.

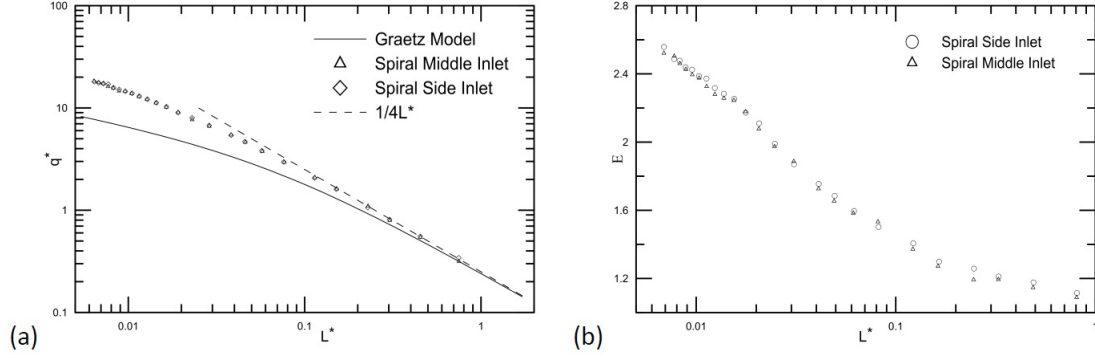


Figure 3.5: a) Inlet effect on heat transfer for 3 cSt silicone oil, b) Heat transfer enhancement ratio for 0.65 cSt silicone oil

### 3.7 Analytical Prediction

In this section, a pre-existing correlation for curved channels with constant curvature is employed to predict the heat transfer behaviour of the heat sink. Dravid et al. [35] experimentally showed the effect of the secondary flow effect on heat transfer enhancement. They proposed the following correlation for the fully developed Nusselt number and constant curvature:

$$Nu_{D_h} = (0.65\sqrt{De} + 0.76)Pr^{0.175} \quad (3.17)$$

Which is valid for  $50 < De < 2000$  and  $5 < Pr < 175$ . Dean number can be defined as:

$$De = Re\sqrt{\frac{D_h}{2R}} \quad (3.18)$$

It should be noted the curvature of a spiral channel is continuously changing with channel length; hence, the Dean number at any point is not constant. There are two ways to deal with this problem: using the mean Dean number or using channel discretization. Some earlier studies [2] have used the mean Dean number for the

calculation:

$$\overline{De} = \frac{1}{L} \int_0^L Re \sqrt{\frac{D_h}{2R}} ds \quad (3.19)$$

In the current paper, a discretization method is employed. The length of the channel was divided to 0.5 mm cells. The Dean number was calculated in each cell and the heat transfer prediction according to each correlation was calculated. Finally, the heat transfer coefficient was averaged. A program in MATLAB has been written to divide the channel length, calculate the curvature in each segment, calculate the Dean number, apply the correlations, determine the mean heat transfer rate coefficient and temperature, update the fluid properties, and lastly calculate the dimensionless heat transfer in order to compare it to the experimental results. Figure 3.6 shows the flow chart and the correlations, which have been used in the program.

Figures 3.7 and 3.8 show the models results for 1 cSt and 3 cSt silicone oil, respectively. It can be concluded that the Dravid et al. correlation [35] is able to predict the oil thermal behaviour with good accuracy. The results are the same for other silicone oils. Table 3.2 shows the root mean square error (RMS) of the Dravid et al [35] for all examined fluids.

Table 3.2: RMS of the Dravid Correlation Prediction

Fluid	$Pr$	Dravid RMS
0.65 cSt	8.6	7.2 %
1 cSt	13.9	6.3 %
3 cSt	38.5	5.2 %
10 cSt	108.6	4.5 %

Figure 3.9 shows how the Dravid et al. [35] correlation predicts the dimensionless heat transfer for fluids. Prandtl numbers of the fluids are mentioned instead of the viscosity for comparison. The Graetz model is also plotted for comparison. As expected, it

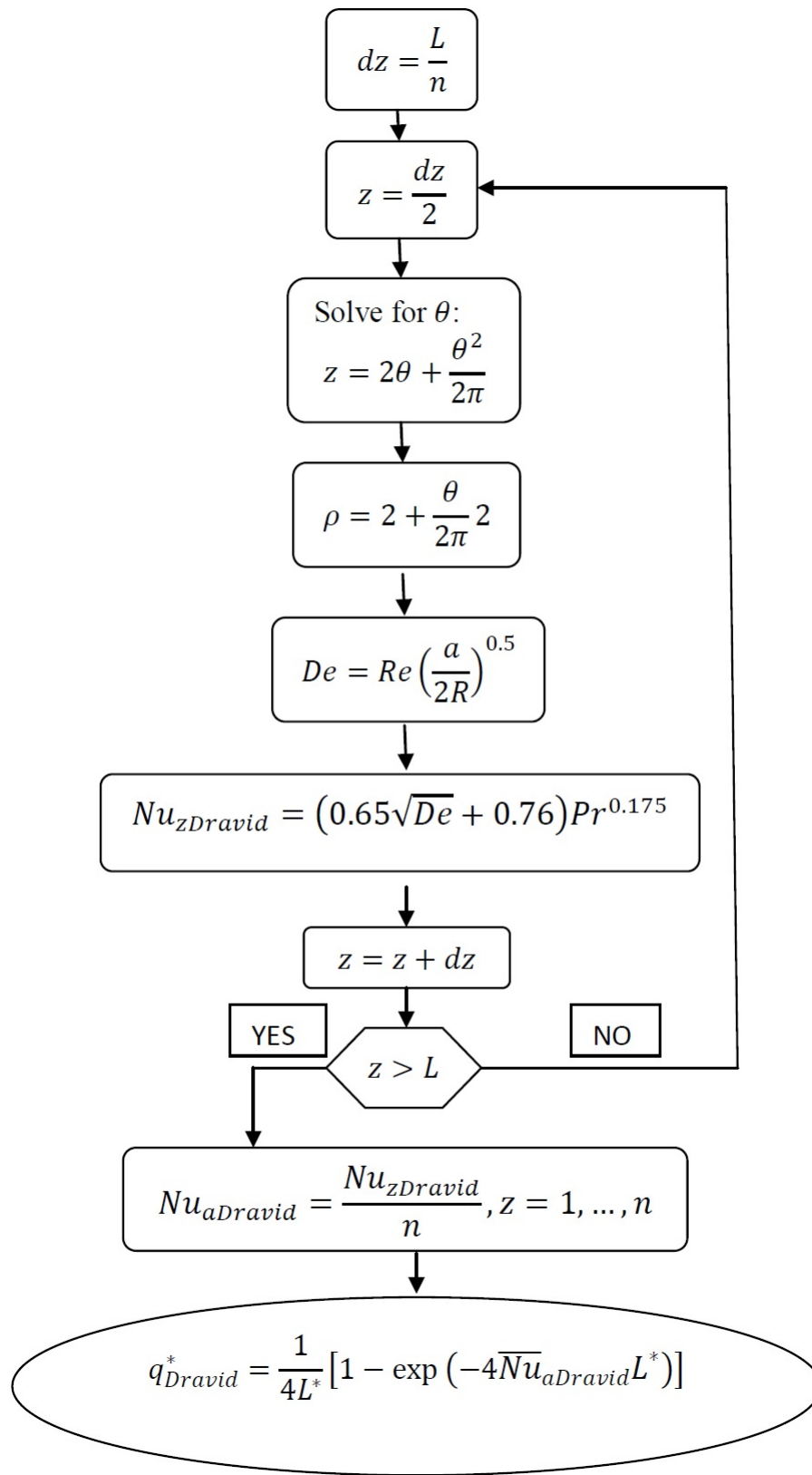


Figure 3.6: Program flow chart

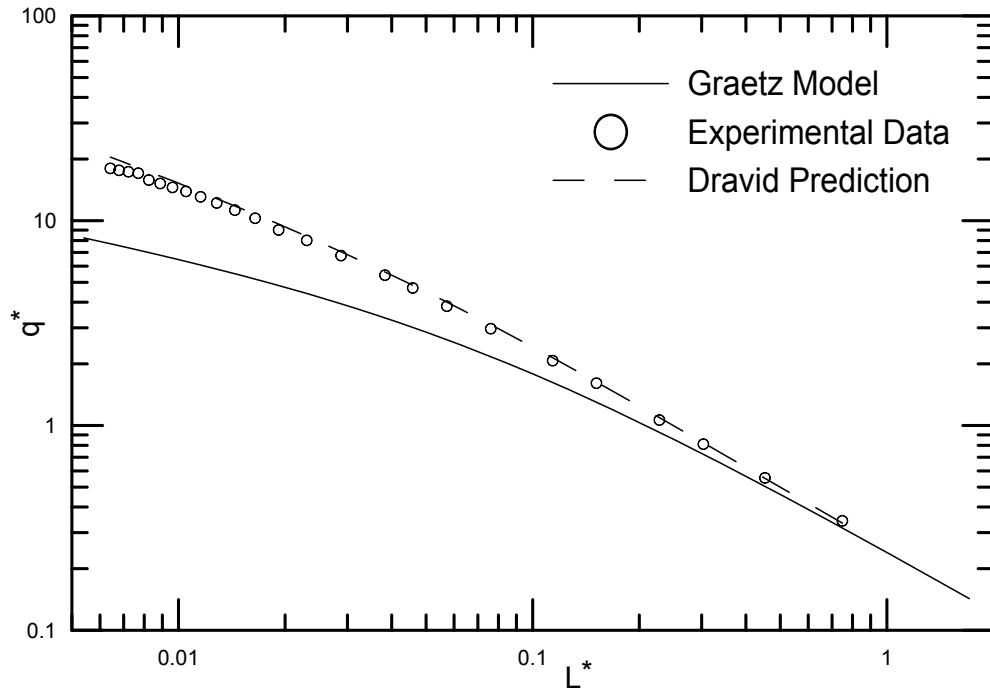


Figure 3.7: Dravid model predictions for 1 cSt silicone oil

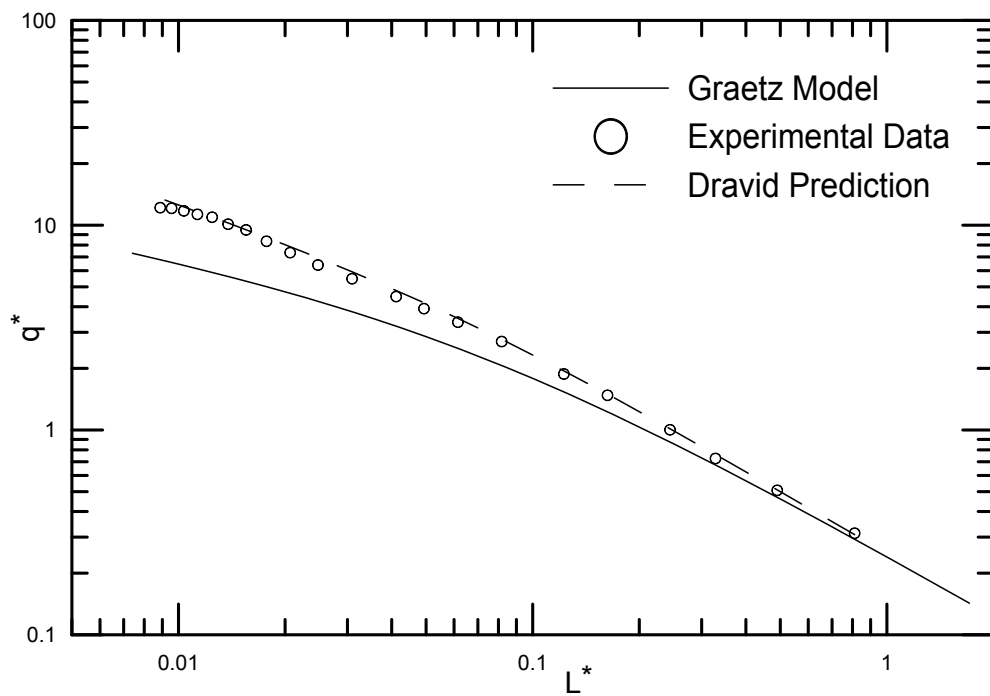


Figure 3.8: Dravid model predictions for 3 cSt silicone oil

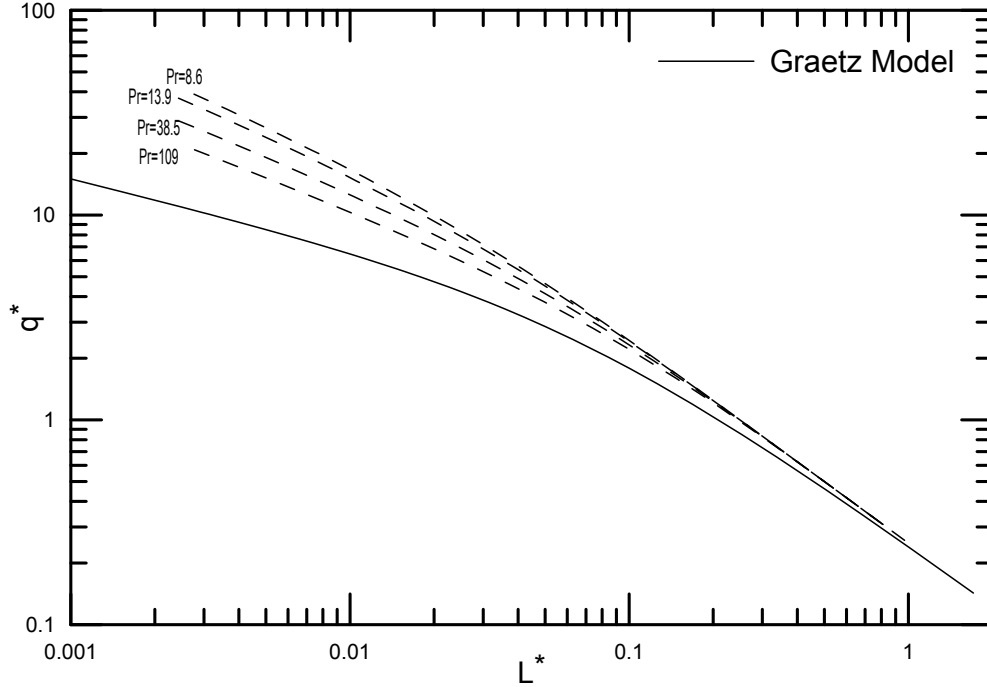


Figure 3.9: Dravid prediction for examined fluids

can be seen that  $q^*$  in low flow rates for all fluids is similar to the one for the straight channel. It is shown that all data follow the fully developed enthalpy balance ( $1/4L^*$ ). However, by increasing the flow rate and Dean number, augmentation is observed when compared to the simple Graetz model.

### 3.8 Pressure Drop

Pressure drop is also non-dimensionalized by the following equation that is based on Bejan number [34], where the length is replaced by  $D_h$ .

$$dp^* = \frac{\Delta p D_h^2}{\alpha \mu} \quad (3.20)$$

Figure 3.10 illustrates the pressure drop of the flow for both side and middle inlet

for water. It can be observed that the pressure drop for both conditions is identical. Therefore, neither of the feeding configurations has advantage over the other for the pressure drop analysis, since the flow is hydrodynamically fully developed. The theoretical calculation of pressure drop for a straight channel of the same size is also presented in the figure. It can be seen that the pressure drop in the spiral geometry increases as the flow rate increase (flow rate increase leads to smaller  $L^*$ ).

As one may see in Fig. 3.10 the pressure drop results for the flow in spiral channel follow a smooth trend, whereas, the Reynolds number is increased up to 4400, and transition to turbulent flow is observed. However, it has been shown that the transition from laminar to turbulent flow happens in higher Reynolds number in curved ducts [36]. This transition is identified by critical Reynolds number,  $Re_{crit}$ . Holland et al. [36] recommended the following correlation for design purposes:

$$Re_{crit} = 2100 \left[ 1 + 12 \left( \frac{R}{D} \right)^{-0.5} \right] \quad (3.21)$$

The lowest  $Re_{crit}$  which can be used in our experiments can be expressed as:

$$Re_{crit} = 2100 \left[ 1 + 12 \left( \frac{0.01}{0.001} \right)^{-0.5} \right] = 8,740 \quad (3.22)$$

which indicates that in the present work transition to turbulent flow does not happen until the Reynolds number is almost four times greater than the critical Reynolds for straight tubes. Since all of our results are at  $Re < 8,740$ , we can consider the results to be in the laminar region.

As discussed before, heat transfer augmentation in the spiral heat sink leads to an increase in pressure drop; hence a comparison for the enhancement in heat transfer with the pressure drop penalty is useful to find the optimum flow rates to reach the desirable heat transfer with the minimum pressure drop.

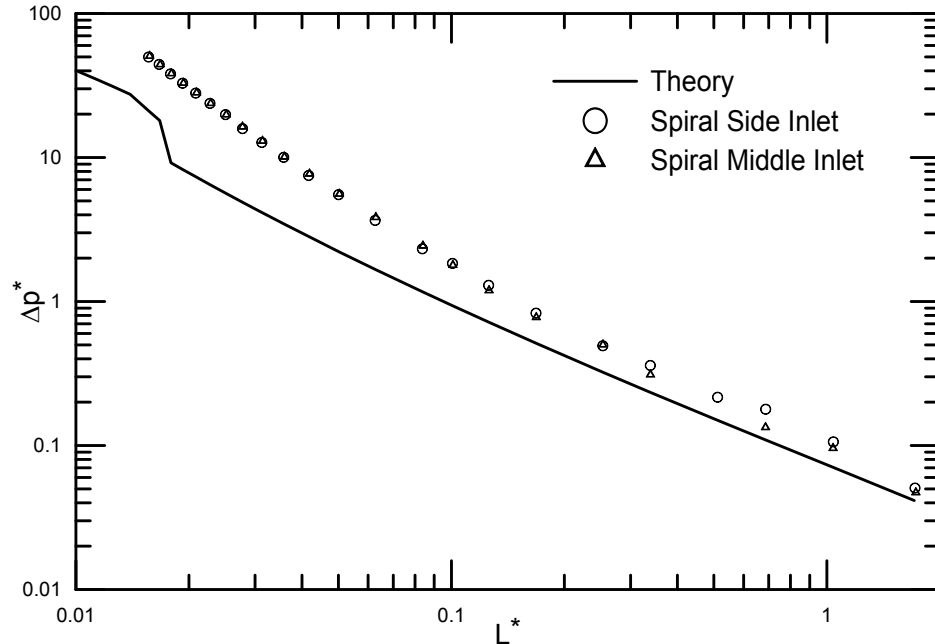


Figure 3.10: Pressure drop for the spiral channel with middle and side inlet comparison to the straight channel of an identical size

Figure 3.11 shows the pressure drop and heat transfer comparison between the spiral heat sink and the straight channel of an identical cross section and length. It can be observed that for a constant pressure drop, better heat transfer can be obtained using the straight channel. However, one should note that in the case of removing the heat from a finite area, having a straight channel is impossible, and the pressure drop penalty due the channel geometry is inevitable.

### 3.9 Conclusion

Heat transfer and pressure drop performance of a spiral square channel were studied by employing water and four different silicone oils. In one set of experiments, fluids entered from the side of the spiral, and in the other they entered from the center. The heat transfer for all the fluids and the pressure drop for the water were examined

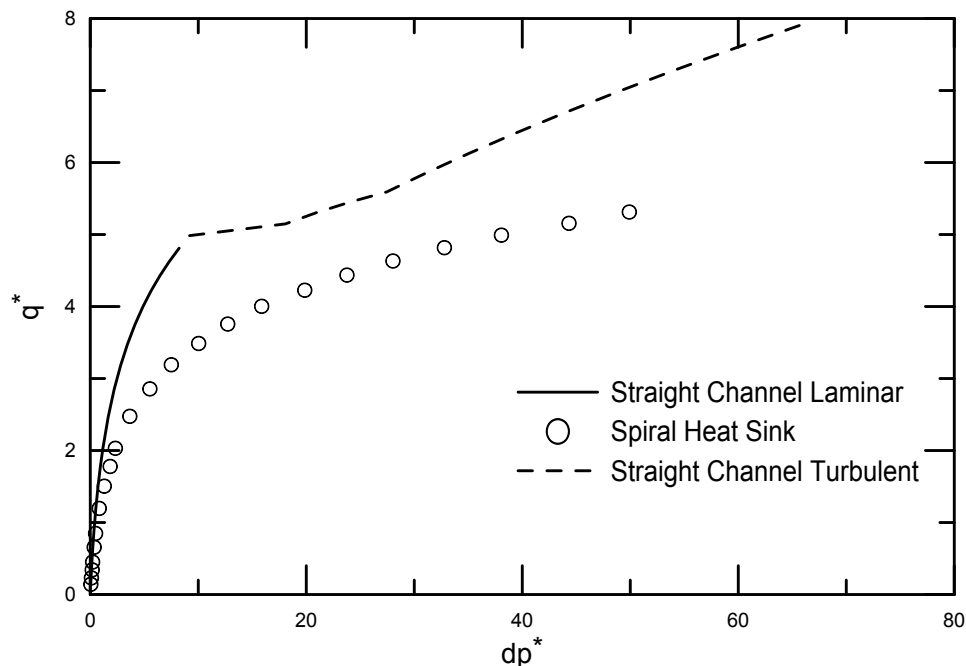


Figure 3.11: Pressure drop and heat transfer performance comparison of spiral channel and an identical straight channel

experimentally. The results were normalized and compared to those for a continuous straight channel with the identical size.

It was shown that 0.65 cSt silicone oil enhances the heat transfer better than other fluids and with less pressure drop penalty. It has been observed that, in general, the spiral geometry is able to significantly enhance heat transfer compared to a straight channel. Furthermore, from Figs. 3-4, one may conclude that the spiral channel does not increase the augmentation significantly in low flow rates. Nevertheless, the pressure drop penalty becomes more significant as the flow rate increases. These results show that there is no difference in feeding the heat sink from the side or the middle. One should note that entrance effects in short spiral channels could influence the pressure drop.

Dravid et al. correlation [35] has been used to predict the heat transfer results. The length of the spiral was discretized into small cells, so the curvature in each cell was

assumed to be constant. The comparison showed good agreement for the Dravid et al. model [35] for Prandtl numbers greater than 5.

The present study highlights many areas which are in need of further investigation so as to properly develop systems which utilize spiral geometry for thermal enhancement. While greater flow rates have shown better thermal augmentation, greater pressure drop is expected simultaneously.

### **Acknowledgement**

The authors acknowledge the financial support of the Natural Sciences and Engineering Research Council of Canada (NSERC) and Auto 21 NCE.

## **3.10 References**

- [1] A. P. Sudarsan and V. M. Ugaz, Fluid Mixing in Planar Spiral Microchannels, Royal Society of Chemistry, vol. 6, pp. 74-82, 2005.
- [2] S. Wongwises and P. Naphon, A Review of Flow and Heat Transfer Characteristic in Curved Tubes, Journal of Renewable and Sustainable Energy Reviews, vol. 10, pp. 463-490, 2006.
- [3] M. H. Oddy, J. G. Santiago, J. C Mikkelsen, Electrokinetic Instability Micromixing, Analytical Chemistry , vol. 73, pp. 5822-5832, 2001.
- [4] L. H. Lu, Ryu K. S., Liu C., J., Fabrication of a 3D Active Mixer Based on Deformable Fe-Doped PDMS Cones With Magnetic Actuation, Journal of Microelectromechanical Systems, vol. 11, pp. 462-469, 2002.
- [5] R. H. Liu., J. Yang, M. Z. Pindera, M. Athavale, P. Grodzinski, Microfluidic Chip Based Microarray Analysis, Lab on a Chip, vol. 2, p. 151, 2002.
- [6] C. Bartoli and F. Baffigi, Effects of Ultrasonic Waves on The Heat Transfer Enhancement in Subcooled Boiling, Experimental Thermal and Fluid Science, vol. 35

- (3), pp. 423-432, 2011.
- [7] R. L. Webb and N. H. Kim, Principles of Enhanced Heat Transfer, Taylor and Francis, Philadelphia, 2005.
- [8] J. Thompson, On The Origin of Windings of River and Alluvial Planes, with Remarks on The Flow of Water Round Bends in Pipes, Proceedings of the Royal Society of London, vol. 5, Ser. A. 1876.
- [9] G. S. Williams, C. W. Hubbell, G. H. Fenkell, Experiments at Detroit, Michigan on the effect of curvature on the flow of water pipes, Transactions of the American Society of Civil Engineers, vol. 1, p. 47, 1902.
- [10] J. H. Grindley and A. H. Gibson, On the Frictional Resistance of Air through a Pipe, Proceedings of the Royal Society of London, Ser. A80, p. 114, 1908.
- [11] J. Eustice, Experiments of Streamline Motion in Curved Pipes, Proc. of Royal Society of London, Ser. A, pp. 85-119, 1911.
- [12] A. Boothroyd, Spiral Heat Exchanger, Int. Enc. Of Heat Transfer, G. Hewitt, Y. Pulezhaev, eds., CRC Press, New York, p. 1044, 1997.
- [13] K. Chonwdhury, H. Linkmeyer, M. Kh. Bassiouny, Analytical Studies on The Temperature Distribution in Spiral Plate Heat Exchangers: Straightforward Design Formulate for Efficiency and Mean Temperature Difference, Journal Chemistry Engineering Process, vol. 19, pp. 183-190, 1985.
- [14] L. C. Burmeister., Effectiveness of Spiral-Plate Heat Exchanger with Equal Capacitance Rate, ASME Journal of Heat Transfer, vol. 128, pp. 195-301, 2006.
- [15] W. R. Dean, Note on the Motion of Fluid in a Curved Pipe, The London, Edinburgh and Dublin Philosophical Magazine and Journal of Sci., vol. 4, pp. 208-223, 1927.
- [16] W. R. Dean. The Streamline Flow through Curved Pipes, The London, Edinburgh and Dublin Philosophical Magazine and Journal of Science, vol. 5 (7), pp. 673-695,

1928.

[17] C. M. White, Streamline Flow through Curved Pipes, Proc. of Royal Society of London, Series A: Mathematical and Physical Science, vol. 123, pp. 645-663, 1929.

[18] K. C. Cheng and M. Akiyama, Laminar Forced Convection Heat Transfer in Curved Rectangular Channels, International Journal of Heat and Mass Transfer, vol. 13, pp. 471-490, 1970.

[19] M. Akiyama and K. C. Cheng, Graetz Problem in Curved Pipes with Uniform Wall Heat Flux, Journal of Applied Sciences Research, vol. 29, pp. 401-417, 1974.

[20] Y. Mori, Y. Uchida, T. Ukon, Forced Convective Heat Transfer in a Curved Channel with a Square Cross Section, International Journal of Heat and Mass Transfer, vol. 14, pp. 1787-1805, 1971.

[21] G. Yee, R. Chilukuri, J. Humphrey, Developing Flow and Heat Transfer in Strongly Curved Ducts of Rectangular Cross Section, ASME Journal of Heat Transfer, vol. 102, pp. 285-291, 1980.

[22] K. Nigam, S. Vashisth, V. Kumar, A Review on the Potential Applications of Curved Geometries Ion Process Industry, Industrial and Engineering Chemistry Research, vol. 47, pp. 3291-3337, 2008.

[23] K. C. Cheng, R. C. Lin, J. W. Ou, Fully Developed Laminar Flow in Curved Rectangular Channels, ASME Journal of Fluids Engineering, vol. 98, pp. 41-48, 1976.

[24] R. L. Manlapaz and S. W. Churchill, Fully Developed Laminar Convection from Helical Coil, Chemical Engineering Communications, vol. 9, pp.185-200, 1980.

[25] Y. Aoyama, K. Futagami, Velocity Distribution and Turbulence Structure of Fully Developed Flow in a Curved Tube, Experimental Heat Transfer, vol. 2, pp. 353-370, 1989.

[26] D. S. K. Tinga, K. C. Cheng, Relaminarization of Developing Turbulent Flow in

- a 180° Curved Square Channel: A Study Based on Temperature Fluctuation Measurements, *Experimental Heat Transfer*, vol. 9, pp. 267-285, 1996.
- [27] K. C. Cheng, Instability and Transition to Turbulent in a Curved Square Duct by Temperature Fluctuation Measurements, *Experimental Heat Transfer*, vol. 12, pp. 53-71, 1999.
- [28] L. C. Burmeister and M. W. Egner, Heat Transfer for Laminar Flow in Spiral Ducts of Rectangular, *ASME Journal of Heat Transfer*, vol. 127, pp. 352-356, 2005.
- [29] S. M. Hashemi and M. A. Akhavan-Behbahani, An Empirical Study on Heat Transfer and Pressure Drop Characteristics of CuO-base Oil Nanofluid Flow in a Horizontal Helically Coiled Tube Under Constant Flux, *International Communications in Heat and Mass Transfer*, vol. 14, pp. 1787-1805, 2012.
- [30] S. J. Kline and F. A. McClintock, Describing Uncertainties in Single-Sample Experiments, *Mechanical Engineering*, P. 3, 1953.
- [31] Y. S. Muzychka, E. Walsh, P. Walsh, Heat Transfer Enhancement Using Laminar Gas-Liquid Segmented Fluid Stream, *Proceeding of Inter Pack. 2009*, San Francisco, July 19-23, 2009.
- [32] Y. S. Muzychka and M. M. Yovanovich, Laminar Forced Convection Heat Transfer in Combined Entry Region of Non-Circular Ducts, *ASME Journal of Heat Transfer*, vol. 126, pp. 54-62, 2004.
- [33] S. Kakac, W. Aung, R. K. Shah, *Handbook of Single Phase Convective Heat Transfer*, Wiley, 1987.
- [34] A. Bejan, *Convective Heat Transfer*, Wiley, 2005.
- [35] A. N. Dravid, K. A. Smith, E.W. Merrill, P. L. Brain, Effect of Secondary Fluid Motion Flow Heat Transfer in Helically Coiled Pipes, *AIChE Journal*, vol. 17 (5), pp. 1114-1122, 1971.
- [36] J. D. Seader, C. E. Kalb, Fully Developed Viscous-Flow Heat Transfer in Curved

Circular Tubes with Uniform Wall Temperature, *AIChE Journal*, vol. 20, No. 2, pp. 340-346, 1974.

[36] P. S. Srinivasan, S. S. Nandapurkar, F. Holland, Friction factors for coils, *Transactions of the Institution of Chemical Engineers*, vol. 48, pp. T156-T161, 1970.

# Chapter 4

## Heat Transfer and Pressure Drop in Mini Channel Heat Sinks\*

**M.Ghobadi and Y.S. Muzychka**

Microfluidics and Multiphase Flow Lab, Faculty of Engineering and Applied Science,  
Memorial University of Newfoundland, St. John's, NL, Canada, A1B 3X5

### **ABSTRACT**

Heat transfer and pressure drop for two types of square mini-channel heat sinks for the purpose of cooling are investigated: one with spiral geometry and other with straight geometry which has 90 degree bends. The cross section of the channels for both heat sinks is a 1 mm square channel and fabricated on a copper base plate. A copper cap plate is used to seal the channel. Water and five low viscosity silicon oils (0.65 cSt, 1 cSt, 3 cSt, 10 cSt and 100 cSt) were used as a coolant; thus a Prandtl number from 5 to 100 was examined. Heat transfer behavior over a range of flow rates from laminar to turbulent has been examined for all the fluids; only water was examined as a working fluid for pressure drop measurements. It has been shown that heat transfer is increased in comparison to the straight channel of similar length due to the disturbance of the boundary layer. This disturbance also results in increasing the pressure drop. The dimensionless mean wall flux and the dimensionless thermal flow length were used to analyze the experimental data instead of conventional Nusselt number and channel length.

**Keywords:** Heat Sink, Heat Transfer, Pressure drop, Dean Number, Graetz Flow

\* *Accepted for Publication in Heat Transfer Engineering*

## 4.1 Introduction

The prevailing trend of miniaturization in electronic devices is aligned with the increasing demand for higher performance and reliability, requires new methods for the removal of heat. Thermal management of these miniature electronic devices has attracted many researchers to develop efficient and cost competitive heat removal systems. Thermal management for heat fluxes up to  $10,000 W/cm^2$  which are generated by state-of-the-art chips in very small volume is needed. Conventional air-cooled heat sinks have limited the heat transfer coefficient that should be improved. Liquid cooled micro channel flow networks, as heat sinks are known to be a promising approach to this heat transfer problem because of its ease of manufacture at the chip level. Micro-fabrication technologies also allow production of miniature liquid cooled heat sinks that are suitable for microprocessor cooling. However, even the upper range of heat fluxes achieved in such micro-channel heat sinks will not meet the increasing demands of the electronics industry.

A micro-channel or mini channel heat sink is a device that removes heat by fluid flowing in channels over a heated substrate (e.g. a computer chip). Single-phase flow in micro-channels and mini channels is often laminar, and additional means to increase the mass and heat transfer rates in micro-channels is desired. Tuckerman and Pease [1] were pioneers to introduce the micro-channel heat sink cooling concept. A rectangular micro-channel with a width of  $50 \mu m$  and depth of  $302 \mu m$  was fabricated on  $1 \times 1 cm^2$  silicon wafer. Using water as working fluid, they demonstrated an impressive heat removal rate of  $790 W/cm^2$  with their integrated single phase microchannel heat sink, however at the expense of significant pressure losses of over 2 bar for one square

centimeter of chip.

This topic attracted many other researchers who mainly worked analytically [2-8], numerically [9-14], and experimentally [10, 15-24]. Keyes [2] analytically studied a heat sink with fins on it which was inspired by the study by Tuckerman and Pease [1]. Knight et al. [5] prepared an optimization method based on the basic equations of fluid mechanics and combined conduction/convection heat transfer in a heat sink in dimensionless form for both laminar and turbulent, and applied the method to the heat sink analyzed by Pease and Tuckerman [1]. Bejan and Morega [6] reported the optimal geometry of an array of fins that minimizes the thermal resistance between the substrate and the laminar flow forced through the fins. Bau et al. [8] analyzed micro channel heat sinks by solving numerically a conjugate heat transfer problem consisting of the simultaneous determination of the temperature fields and proposed an algorithm for the selection of the heat exchanger's dimensions.

Fedorov and Viskanta [9] developed a three-dimensional model to investigate flow and conjugate heat transfer in the micro channel based heat sink for electronic packing. They solved the equations numerically and compared the results with the available experimental results. Peterson et al. [11] simulated the forced convection heat transfer occurring in silicon-based micro channel heat sinks by using a simplified three dimensional conjugate heat transfer model (2D for the fluid flow and 3D for the heat transfer).

Tao et al. [12] considered a mini-channel heat sink with the bottom size of  $20\text{ mm} \times 20\text{ mm}$  cooled with a laminar flow of water and a constant heat flux boundary condition. They studied the effects of the channel dimensions, the channel wall thickness, the bottom thickness and the inlet velocity on the pressure drop, the thermal resistance and the maximum allowable heat flux. Their results indicated that a narrow and deep channel with thin bottom thickness and relatively thin channel wall thickness

improved the heat transfer. They optimized the configuration to design a heat sink that can cool a chip with heat flux of  $256 \text{ W/cm}^2$  at the pumping power of  $0.205 \text{ W}$ . Chein and Chen [13] performed a numerical analysis on the effects of inlet/outlet arrangement micro-channel heat sink efficiency. The fluid flow and heat transfer were considered inside the heat sinks. Using the averaged velocities and fluid temperatures in each channel to quantify the fluid flow and temperature misdistributions, they found better uniformities in velocity, and temperature can be found in the heat sinks having a coolant supply and collection vertically via inlet/ outlet ports opened on the heat sink cover plate. While Zhang et al. [14] used two flip chip ball grid array packages (FCBGA) with different chip foot prints,  $12 \text{ mm} \times 12 \text{ mm}$  and  $10 \text{ mm} \times 10 \text{ mm}$  for high heat flux characterizations. Using an analytical method, they predicted the pressure drop and thermal resistance.

Sasaki and Kishimoto [15] experimentally evaluated the relationship between the cooling capability and the channel width with a constant pressure drop for micro grooved cooling fins, and found that there are optimal channel widths which give rise to the maximum allowable power density.

A thermal module to transfer heat efficiently from high power dissipation chips to a liquid via forced convection was designed by Nayak [16]. Channel geometries for deep channels ( $1000 \mu\text{m}$  deep, and used for turbulent flow), and shallow channels ( $100 \mu\text{m}$  deep, and used for laminar flow) were optimized for high heat transfer coefficient. For the deep channel design, the maximum device temperature rise on the module was  $18^\circ \text{C}$  for a power dissipation of  $42 \text{ W/chip}$ , and a flow rate of  $126 \text{ cm}^3/\text{s}$ . For the shallow channel design, the temperature rise was  $19^\circ \text{C}$  for a flow rate of  $19 \text{ cm}^3/\text{s}$ , and a power dissipation level of  $42 \text{ W/chip}$ . Rahman and Gui [17] designed, fabricated, and tested micro-channels heat sinks for aircraft avionics cooling.

Harmes et al. [18] collected experimental results for single-phase laminar forced con-

vection in rectangular micro-channels. The heat sinks had a total projected area of  $1.0\text{ cm}$  by  $1.0\text{ cm}$  with 64 channels of width  $54\text{ }\mu\text{m}$  and height  $215\text{ }\mu\text{m}$ . Their tests were performed with deionized water as the cooling fluid. The system performance was presented in terms of overall pressure drop and local thermal resistance. Also, the associated convective heat transfer was reported in terms of the friction factor and the Nusselt number. Their experimental results were reported to be in good agreement with classical developing channel theory.

Another noticeable experimental investigation for single-phase forced convection in deep rectangular micro-channels was performed by Harmes et al. [20]. They tested two configuration systems: a single channel system and a multiple channel system. They were both identical except for the lack of extended surface in the single channel system. Deionized water was used as the cooling liquid. In terms of flow and heat transfer characteristics, the micro-channel system designed for developing laminar flow outperforms the comparable single channel system designed for turbulent flow. Rahman [21] experimentally measured the pressure drop and heat transfer coefficient in micro channel heat sinks. He used two different channel patterns. A parallel pattern distributed the fluid through several parallel passages between the inlet and the outlet headers located at two ends of the wafer. The series pattern carried the fluid through a longer winding channel between the inlet and the outlet headers. Different aspect ratios were studied with water as a working fluid for all. The Nusselt number and coefficient of friction in the device for different flow rate, channel size and channel configurations were measured and compared. Further experimental study on micro-channel heat sinks was performed by Naphon and Khonseur [22]. They just studied laminar flow in Reynolds number range of  $200 - 1000$  and power of  $0.180 - 0.540\text{ W/cm}^2$ . The effect of using different geometrical configurations and roughness of the channel were studied.

Forced convection heat transfer and pressure drop through the porous structure were studied at  $Re < 408$  with water as the coolant by Singh et al [23]. They were able to remove the heat flux of  $290 \text{ W/cm}^2$  at the source with the coolant pressure drop of  $34 \text{ KPa}$  across the porous sample while maintaining the heater junction temperature below the permissible limit of  $100 \pm 5^\circ\text{C}$  for chipsets. Their investigation classified the sintered porous heat sink as a potential thermal management device for high end microprocessors.

A geometrical optimization of the micro heat sink with straight circular micro-channels with inner diameter of  $D_i = 900 \mu\text{m}$  was performed by Dorin [24]. He compared the results with the results obtained for conventional channel configuration with lateral inlet/outlet cross section. Hydrodynamic and heat transfer performance were considered in his work.

In this paper two mini channel heat sinks with different channel geometries are investigated. One straight heat sink which the channel has sharp 90 degree bends at each end and one spiral heat sink. The inlet/outlet configuration for the spiral heat sink is also studied. Both heat sinks have the same size projection area and cross section. Heat transfer for water and five silicon oils with different viscosities (0.65 cSt, 1 cSt, 3 cSt, 10 cSt and 100 cSt) is investigated. The pressure drop of water in both heat sinks also analyzed. The results are reduced in dimensionless form and presented graphically to make the comparison easier. The heat transfer enhancement and pressure drop increase for the heat sinks and are compared to a straight channel with the identical cross section size and length.



Figure 4.1: Spiral and straight heat sinks used in the experiments

## 4.2 Heat Sinks and Experimental Setup

Fig. 4.1 shows the two heat sinks, used for the experiments. The square  $1\text{ mm}$  channel was fabricated on a copper base plate. A flat copper cap plate of identical size was bolted tight to seal the channel. Five Cole-Palmer T type thermocouples were employed to measure the surface temperature; one at the dead center and four at the center of each quadrant on one surface. Two additional thermocouples measured the inlet and outlet bulk temperature using a simple T junction with a thermocouple embedded into the stream. Three Omega differential pressure transducers with different ranges were used to measure the pressure drop of the water flow passing through the heat sink. A Keithley Data Acquisition system (DAQ) collected the temperatures and the pressure drop during the experiments. The thermal conductivity of the copper is high enough to consider a uniform temperature distribution for the heat sink; thus, the five measured temperatures which were very close in value were averaged to calculate the mean surface temperature.

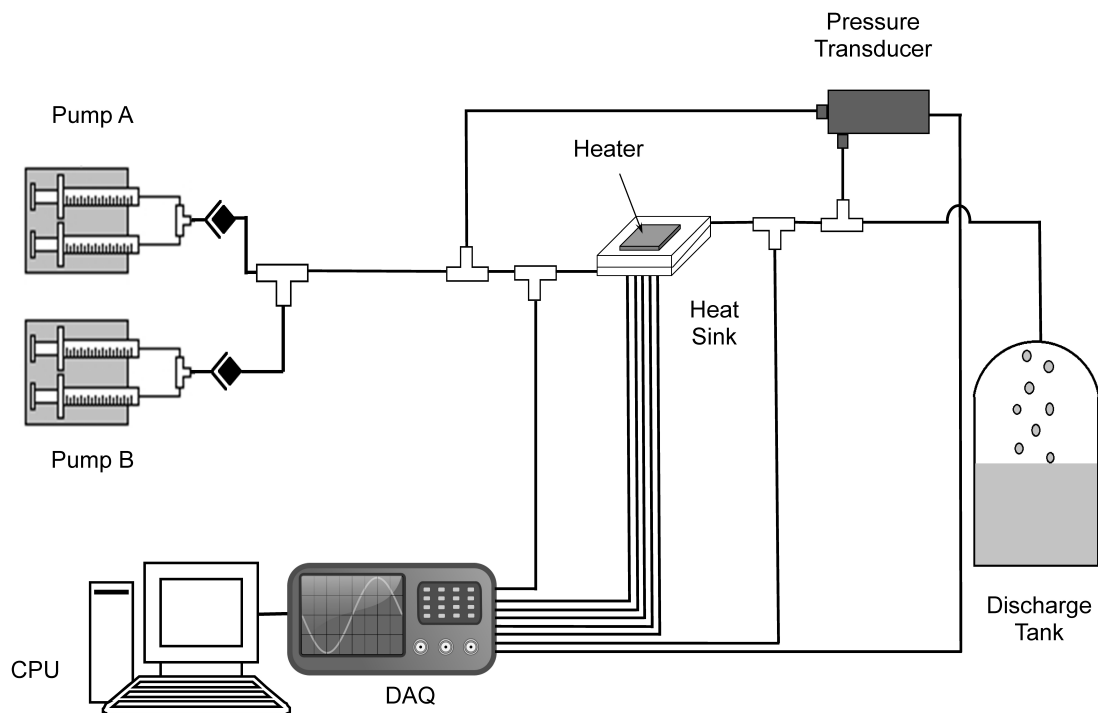


Figure 4.2: Experimental test setup

Fig. 4.2 shows a schematic configuration of the test setup. Four syringes (Hamilton Glass Gas Tight) were filled with the test fluid, and the pumps (Harvard Pump 33) were set to the desirable flow rate. The total power provided to the heaters (Watlow Film Heaters) was adjusted for each flow rate to avoid exceeding maximum temperature limits which can damage the heaters. When water was used as the test fluid in the experiment, it was disposed after leaving the heat sink, whereas, the silicone oils were recycled. Ten readings for each flow rate were made and averaged to account for local fluctuations.

### 4.3 Benchmarking and Uncertainty

In general, the uncertainty of the thermocouple reading was verified to be within  $0.1^\circ C$  using an ice bath and boiling water. The uncertainty in volumetric flow rates provided by the syringe pumps was measured at low and high flow rates and found to be on the order of  $\pm 1$  percent or better. The uncertainty of the pressure drop measurements is reported to be  $\pm 1\%$  of full scale. A simple uncertainty analysis was conducted using the method outlined by Kline and McClintock [25]. The result  $F$  is a given function of independent variables  $x_1, x_2, \dots, x_n$ , and  $w_F$  is the uncertainty in the result and  $w_1, w_2, \dots, w_n$  are uncertainties in the independent variables. Then the uncertainties in the result can be calculated as follow:

$$w_F = \left[ \left( \frac{\delta F}{\delta x_1} w_1 \right)^2 + \left( \frac{\delta F}{\delta x_2} w_2 \right)^2 + \dots + \left( \frac{\delta F}{\delta x_n} w_n \right)^2 \right]^{1/2} \quad (4.1)$$

This yields an uncertainty using the root mean squares method of  $\pm 6.36 - 7.91\%$  in the dimensionless heat transfer  $q^*$ ,  $\pm 6.04 - 7.60\%$  for  $L^*$  and  $\pm 1 - 5\%$  for  $dp^*$ .

Fig. 4.3 depicts the pressure drop and the heat transfer benchmarking test. The pressure drop test was performed on a straight tube with  $1.6\text{mm}$  diameter and  $314\text{cm}$  length, and  $163\text{mm}$  long straight copper tubing with hydraulic diameter of  $1.65\text{mm}$  was used for the heat transfer test. The main purpose of benchmarking tests is to determine the uncertainty of our apparatus used for the measurements. Friction factor is plotted versus Reynolds number. The uncertainty in the measurements was found to be less than  $5\%$  in comparison to the straight tube pressure drop theory. Three different sensors have been used to accomplish the test according to the pressure drop, which was measured. The experimental results are compared with theoretical results for laminar flow in straight tubing.

The manufacturer supplied viscosity and other silicone oil properties. However, the

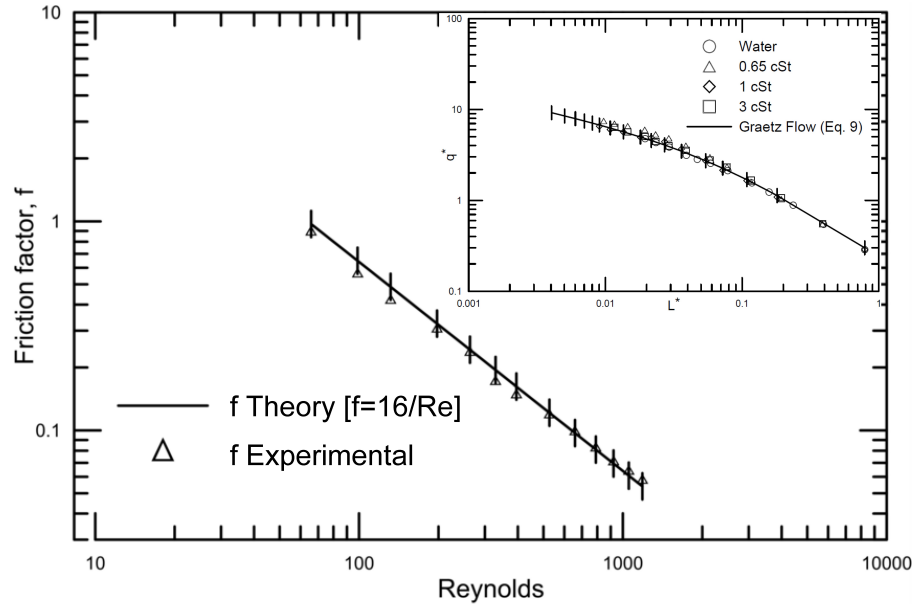


Figure 4.3: Pressure drop and heat transfer benchmarking test in straight circular tubes

viscosity of the oils and water were measured with an accurate viscometer. Water was used as a reference fluid. The deviations between the reported viscosity, and measured viscosity were found to be less than 5%. Temperature effects on the properties have also been considered.

## 4.4 Analytical Model

In this section we begin by summarizing the expressions which have been used to present the data in terms of dimensionless heat transfer rate. The experimental results will be compared to the results for a straight channel having the same cross section, length and boundary condition.

The temperature difference in a channel or duct can be defined in number of ways. The most commonly used form for defining the local heat transfer coefficient in an

internal flow for constant temperature has traditionally been in terms of the bulk temperature,  $T_m = T_m(z)$ . In a single fluid heat sink with isothermal condition, however, it is not feasible to calculate the bulk temperature at each cross section easily. Hence, the easier approach is to use the wall to inlet temperature difference,  $T_w - T_i$ .

Nusselt number has been traditionally used to present heat transfer coefficient in non-dimensionalized format. In the heat sink with a uniform constant wall temperature  $T_w$ , the local Nusselt number may be defined as:

$$Nu_{D_h} = \frac{q_z D_h}{k(T_w - T_m)} = \frac{h D_h}{k} \quad (4.2)$$

This is based on the wall to bulk mean fluid temperature. If a mean Nusselt number is desired, then we must integrate along the duct length:

$$\overline{Nu}_{D_h} = \frac{1}{L} \int_0^L Nu_{D_h} dz = \frac{\bar{q} D_h}{k \Delta T_{LMTD}} \quad (4.3)$$

However, as mentioned before, finding the bulk temperature at each length is not practical. Alternatively, one may utilize the dimensionless heat transfer rate which is based on the mean wall to inlet temperature difference. This approach is more natural and more practical in the analysis of single fluid devices. The dimensionless mean wall flux can be defined as:

$$q^* = \frac{\bar{q} D_h}{k(T_w - T_i)} \quad (4.4)$$

We may also be interested to introduce the dimensionless thermal length instead of traditional Reynolds number to present our data.

$$L^* = Gz^{-1} = \frac{L/D_h}{Pe_{D_h}} \quad (4.5)$$

The dimensionless mean wall flux can be related to the Nusselt number using single fluid heat exchanger theory, e.g. the  $\epsilon - NTU$  method for constant wall temperature. This leads to the following expression relating the two:

$$q^* = \frac{1}{4L^*} [1 - \exp(-4\overline{Nu}L^*)] \quad (4.6)$$

As mentioned before, we are interested in comparing the experimental results with the model for an identical straight channel in a same condition. For non-circular straight micro-channels and mini-channels, we can use an alternative form of the Muzychka and Yovanovich [26] model:

$$q^* = \left[ \left( 0.641 \left( \frac{fRe_{D_h}}{L^*} \right)^{1/3} \right)^{-3/2} + \left( \frac{1}{4L^*} \right)^{-3/2} \right]^{-2/3} \quad (4.7)$$

where  $fRe_{D_h}$  is the friction factor Reynolds number group for laminar flow, see Kakac et al. [27] or Bejan [28]. For a rectangular mini-channel, Muzychka and Yovanovich [26] proposed using the first term of the exact series solution:

$$fRe_{D_h} = \frac{24}{(1 + \beta)^2 \left[ 1 - \frac{192}{\pi^5} \tanh \frac{\pi}{2\beta} \right]} \quad (4.8)$$

where  $\beta = b/a$  is the aspect ratio of the rectangular channel such that  $0 < \beta < 1$ . For a square channel  $fRe_{D_h} = 14.23$ .

## 4.5 Data Analysis

In all experiments, fluid enters the heat sink as a single phase liquid flow, is heated up and leaves in the same condition; hence the total heat removed by the fluid can be calculated as:

$$Q_{bulk} = \dot{m}C_p(T_o - T_i) \quad (4.9)$$

The heat sink was insulated to minimize the heat leakage due to the convection, but conduction heat transfer is still present. The amount of heat received by the fluid is still different from the heat provided by the heaters:

$$Q_{bulk} = P - \frac{(T_w - T_a)}{R_{thermal}} \quad (4.10)$$

Where P is the power input, and  $R_{thermal}$  is the thermal resistant of the insulated box around the heat sink when no liquid flow is present. It was measured experimentally. The second term represents the heat loss to the surroundings. The overall bulk heat transfer using the two approaches was in good agreement.

For a square channel, the characteristic length (hydraulic diameter) is the side length  $D_h = a$ ; thus the dimensionless characteristics are:

$$q^* = \frac{\left(\frac{Q_{bulk}}{4aL}\right) D_h}{k(T_w - T_i)} \quad (4.11)$$

$$L^* = Gz^{-1} = \frac{L/D_h}{Pe_{D_h}} \quad (4.12)$$

It is also desirable to present the pressure drop of the flow through the heat sink in non-dimensionlized format. A definition based on Bejan number is used; however the characteristic length of the channel is used instead of the duct length.

$$dp^* = \frac{\Delta p D_h^2}{\alpha \mu} \quad (4.13)$$

## 4.6 Results and Discussion

Water and four different silicone oils with the viscosity of 0.65 cSt, 1 cSt, 3 cSt and 10 cSt have been used as a cooling medium. Prandtl numbers from 5.7 up to 108 were tested during the experiments. Flow rates from 1.5 *ml/min* up to 200 *ml/min* were adjusted according to the viscosity of the fluid and the pump power. The Reynolds number was reported to vary from mainly laminar flow to slightly turbulent flow. Table 4.1 shows the average Prandtl number and range of Reynolds numbers for the fluids examined during the tests. Power adjustment was conducted due to the flow rate to avoid exceeding the allowable temperature of the heaters, which is about 80°C. It ranged from 5 W for the lower flow rate and increased to maximum power of (20 W) for the higher flow rates. All fluid properties have been calculated using the mean of the inlet and outlet temperature. Properties were obtained from the supplier of the silicone oils (Clear Co.).

Table 4.1: Prandtl, Reynolds, and Peclet Numbers for Examined Fluids

Fluid	$Pr$	$Re$	$Pe$
Water	5.7	34 – 3715	193.8 – 21175
0.65 cSt	8.6	44 – 4481	378 – 38536
1 cSt	13.9	430 – 2907	417 – 40407
3 cSt	38.5	9.68 – 767	373 – 29529
10 cSt	108.6	2.79 – 151.42	303 – 16444
100 cSt	830	0.31 – 1.88	248 – 1635

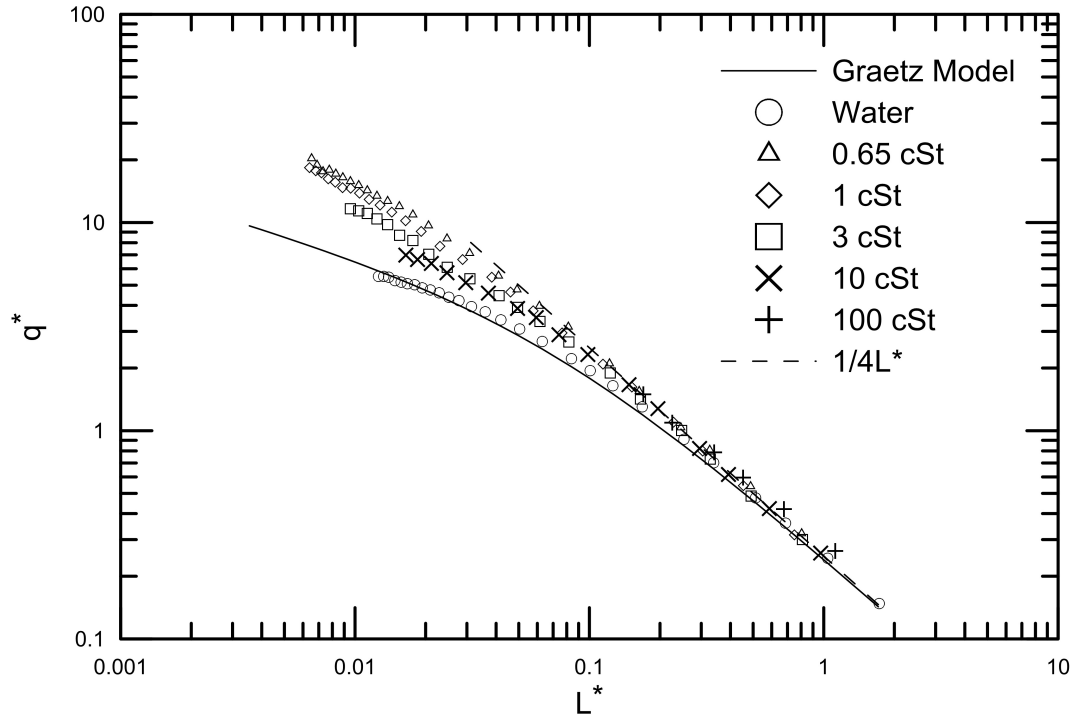


Figure 4.4: Different fluid performance for the middle inlet spiral channel heat sink

#### 4.6.1 Heat Transfer

As discussed before the effect of inlet configuration in the spiral heat sink is also considered in this study. The fluids entered from the middle and exited from the side and, or they entered from the side and exited from the middle. Figures 4.4 and 4.5 show the heat transfer results for all the fluids in both configurations. The logarithmic scale is used for both axes. Increasing the flow rate means decreasing the  $L^*$ . The simple Graetz model for a straight channel with the identical cross section size and length is plotted to show how the curvature in the spiral heat sink enhances the heat transfer. An augmentation is observed in heat transfer for both entrance configurations.

As expected, the results for all fluids merge to one for fully developed ( $1/4L^*$ ) flow and the different behaviour only occurs in higher flow rates where the secondary flow

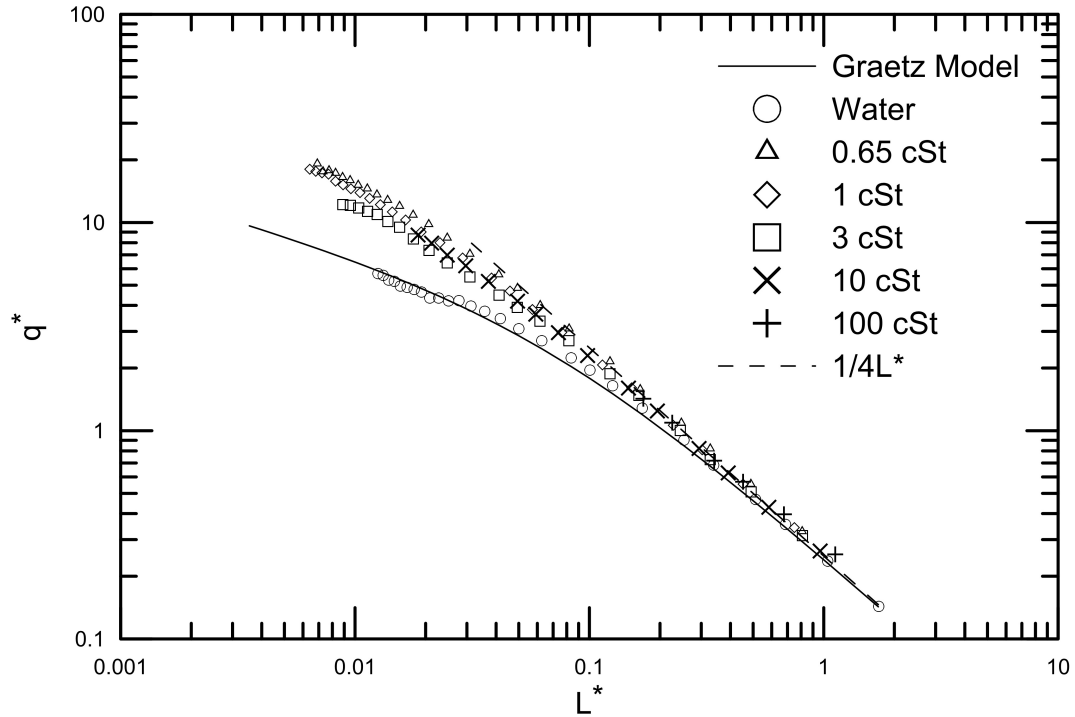


Figure 4.5: Different fluid performance for the side inlet spiral channel heat sink

is initiated and affects the radial mass and heat transfer occur. In other words, the curvature does not improve the heat transfer when fluid moves at very low speed. The secondary flow which enhances heat transfer in curved channels does not appear for the low flow rates. With increasing flow rate, heat transfer augmentation is observed, as compared to the equivalent straight channel. The heat transfer behaviour follows the same trend for all the fluids.

Figure 4.6 depicts the experimental results for the straight heat sink. Again water, 0.65 cSt, 1 cSt, 3 cSt, 10 cSt and 100 cSt silicone oils are examined. Unlike the spiral heat sink, water shows better enhancement even in high flow rates (small  $L^*$ ) and augmentation is observed as compared to the Graetz model.

Comparisons are made between the results for spiral middle inlet, side inlet and straight heat sink. The comparisons showed that the total heat transfer is equal

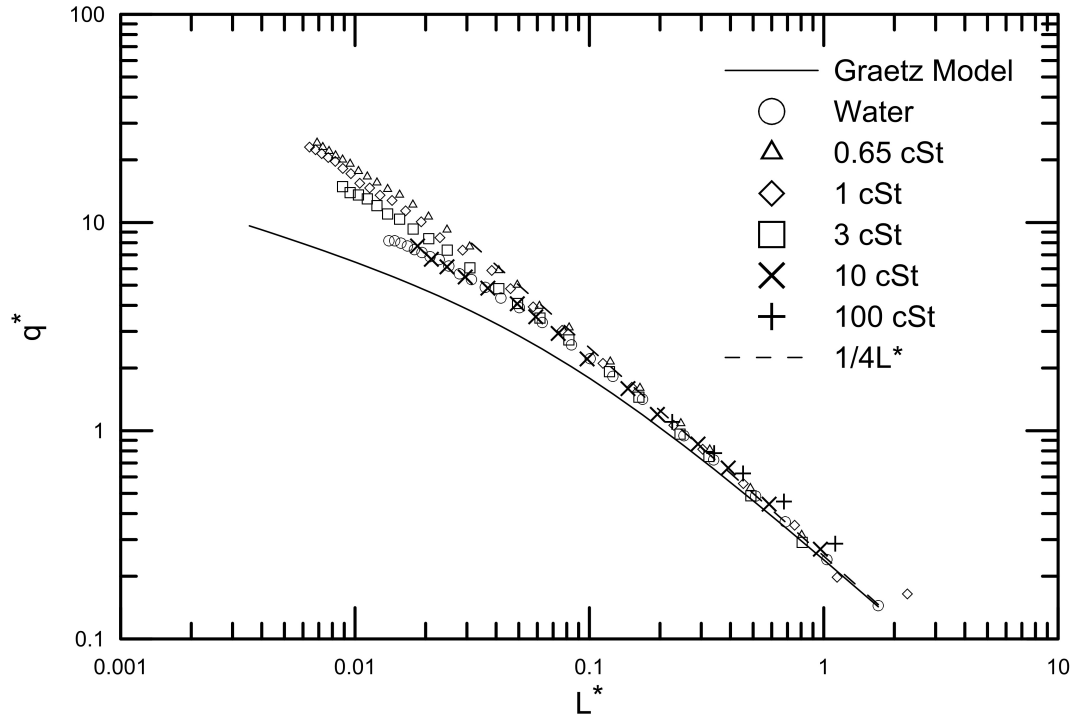


Figure 4.6: Different fluid performance for the straight channel heat sink

whether the Dean number decreases or increases through the flow path. Figure 4.7 shows the spiral entrance configuration effect for 1 cSt silicon oil. The equivalent points for both configurations are showing the same enhancement compared to the Graetz model for the identical straight channel. The straight heat sink is also included in the figure and it can be seen that it shows better enhancement compared to the spiral geometry. Experimental results show that there is no significant difference between the spiral and the straight geometries and the inlet configurations, except that at very low flow rates the straight geometry is preferable. Figure 4.8 shows the entrance effect comparison for 10 cSt silicon oil. It can be seen that the two inlets start deviating from each other by reduction of  $L^*$ , i.e. increasing of the flow rate. Inserting the fluid from the side shows around 25% better heat removal. This happens because inserting the fluid in the side causes the heated-fluid to reach the

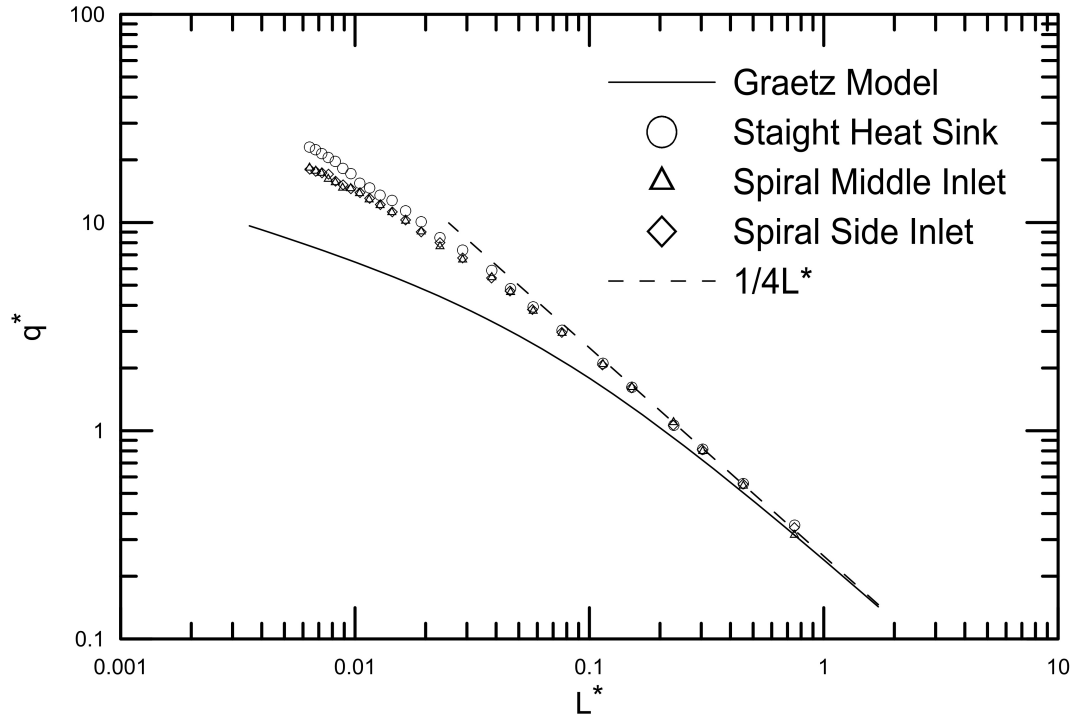


Figure 4.7: The configuration effect of channel pattern for 1 cSt silicon oil

end of the path, which has more curvature and has higher Dean number, which has been proven to increase the heat transfer. In the side inlet heat sink, the heated fluid flows inside a less curved path that implies having less heat transfer augmentation. At the beginning, however, the heat transfer is high enough regardless of the Dean number of the path.

#### 4.6.2 Pressure Drop

Figure 4.9 depicts the pressure drop of water passing through the heat sinks. Both inlet/outlet configurations are considered in this graph. Analytical results for a straight channel with identical size are also shown here. The discrepancy in the pressure drop for the straight channel is due to the change of correlation from laminar to turbulent. The analytical results are based on both laminar and turbulent flow inside a straight

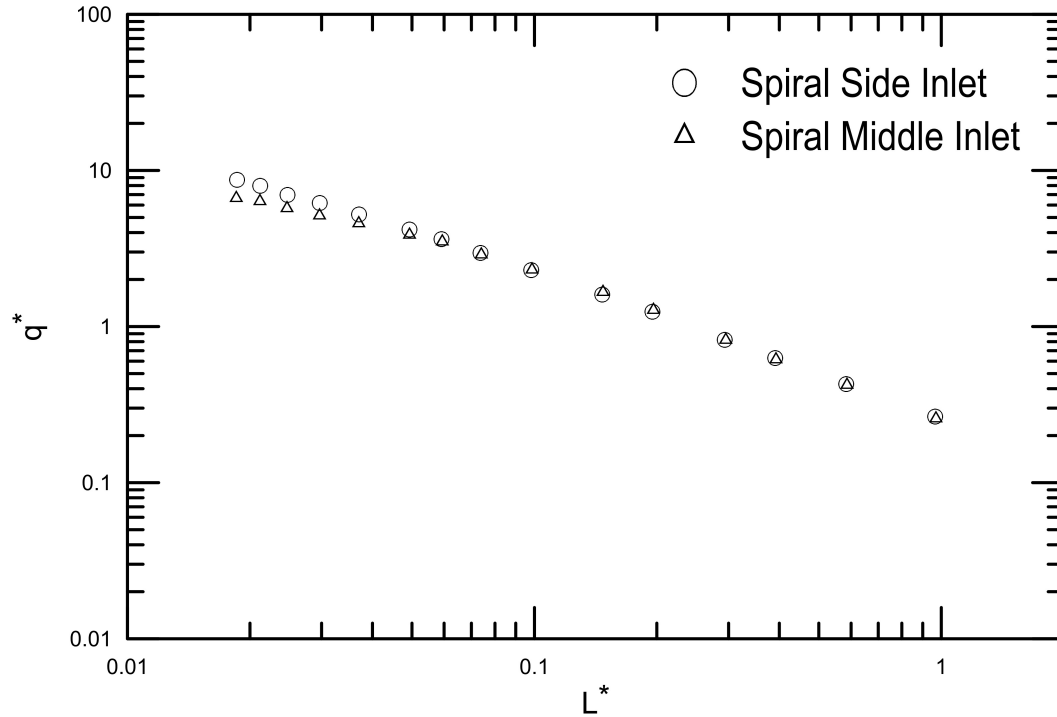


Figure 4.8: The entrance effect in the spiral heat sink for 10 cSt silicon oil

channel. It can be seen that the pressure drop for both heat sinks follow the trend for a straight channel in low flow rates, which means that secondary flow and circulation do not affect the flow sufficiently to increase the pressure drop. By increasing the flow rate (decreasing  $L^*$ ), one may observe an increase in the pressure drop for both heat sinks. Unlike the heat transfer, the pressure drop for both configurations in the spiral heat sink is the same. However, the pressure drop for the straight heat sink shows a 30% increase compared to the spiral heat sink. One may conclude that the effect of disturbed flow at bends in the straight heat sink can increase the heat transfer more than the effect of the secondary flow in the spiral heat sink, however at the same time the pressure drop is also increased more in the straight heat sink.

In order to show the increase in the pressure drop in comparison to a straight channel, it may be helpful to illustrate the fraction of these two pressure drops. Figure 4.10

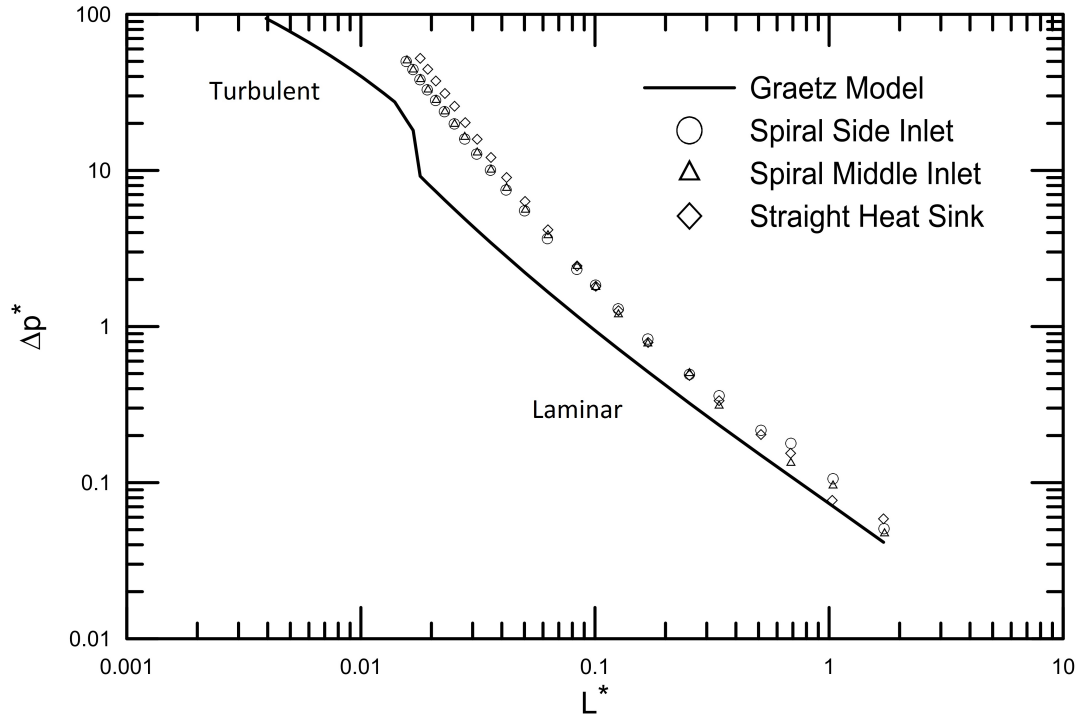


Figure 4.9: Dimensionless pressure drop comparison between the heat sinks

depicts the comparison versus the speed of water inside the channel. The speed for both channels is the same as the cross sections are identical. It can be seen that the fractions for both heat sinks start from a quantity more than one and from a similar number (1.3). The pressure fraction for both inlet/outlet configuration is equal with the maximum error of 7% when  $U = 0.33 \text{ m/s}$ . The pressure drop fraction increases as the velocity is increased and reaches the maximum of 4.5 for  $U = 2.63 \text{ m/s}$ . The pressure drop fraction for water inside the straight heat sink is obviously greater than the pressure drop fraction passing through the spiral heat sink. It reaches up to 5.69 for  $U = 2.33 \text{ m/s}$  which is 37% higher than the pressure drop fraction for the spiral heat sink.

The results showed that both heat transfer and pressure drop are increased in the spiral and straight geometries. The question at this point is how much pressure drop

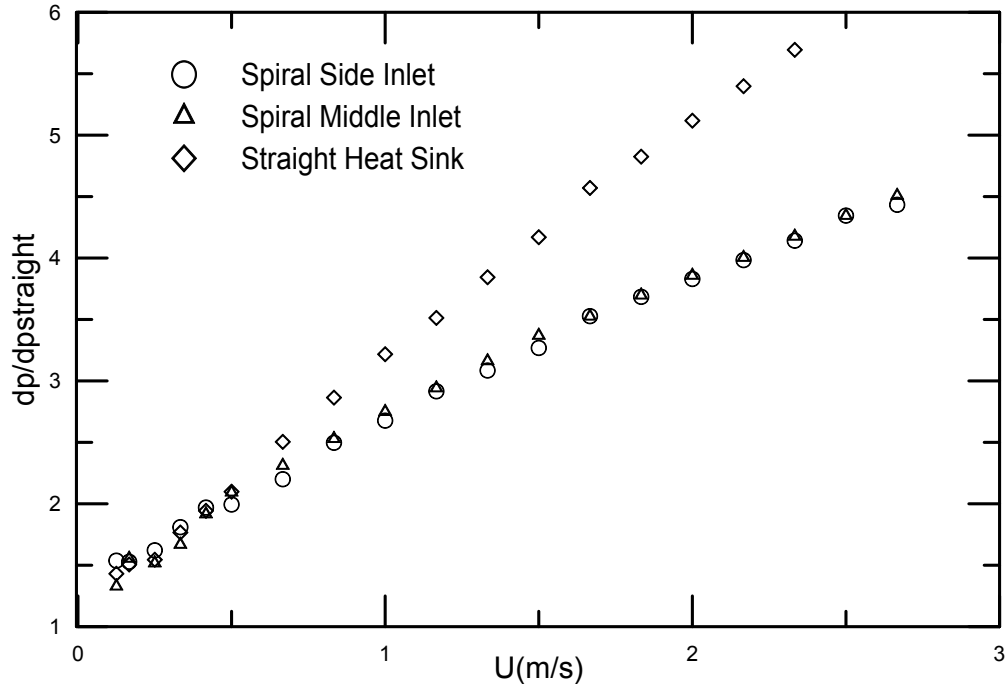


Figure 4.10: Pressure drop comparison of the heat sinks versus water velocity

penalty should be paid for the heat transfer augmentation or how much improvement can be reached with a constant pressure drop in case a pump with a constant pumping force is going to be used.

Figure 4.11 shows the dimensionless heat transfer versus dimensionless pressure drop. Both terms have been defined in the previous section. The inconsistency in the straight channel pressure drop is due to the transition from laminar to turbulent which was considered to occur at  $Re = 2500$ . Before the transition point, both spiral and straight heat sinks give less heat transfer for a constant pressure. Whereas, in turbulent flow region for the straight channel, the straight heat sink shows augmentation in a constant pressure drop of the flow compared to the straight channel, but the spiral channel still shows less heat transfer compared to the straight heat sink. It should be noted that although the heat transfer for a straight channel is better in low flow rates,

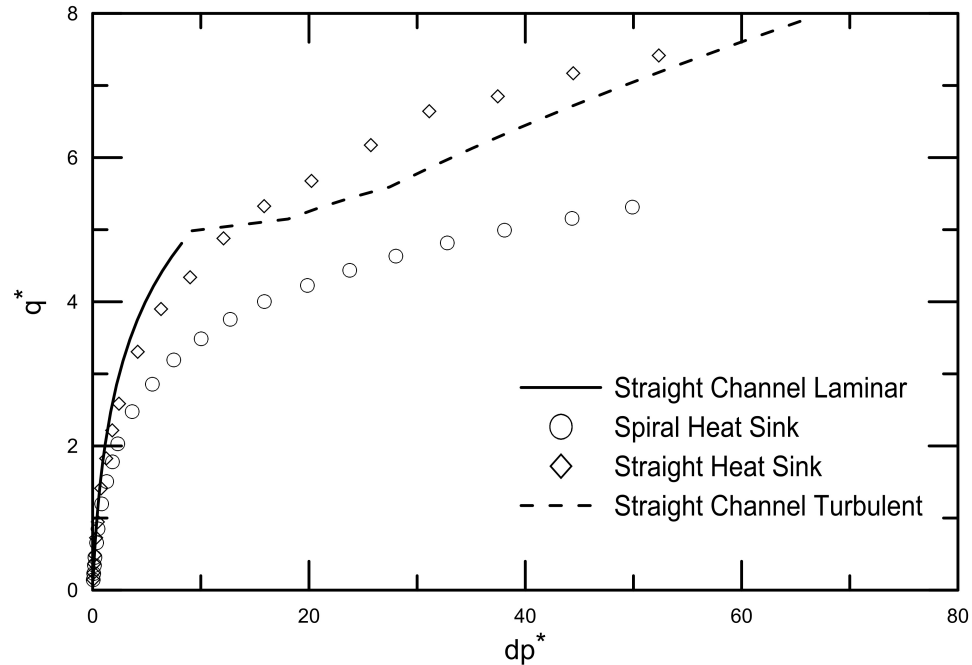


Figure 4.11: Dimensionless heat transfer versus dimensionless pressure drop comparison

it is impossible to have such a channel in a small area without any bend. Hence, in a small area, one should choose between the straight and spiral heat sinks according to the situation and application. One should also note that in a straight channel of the same cross section and length, higher velocities are needed to have the same heat removal which can be obtained at lower velocities. It can be seen that the flow in the straight channel transits to turbulent flow, whereas, the flow remains in laminar region for during the tests.

## 4.7 Conclusion

Water and five silicone oils with different viscosities were examined as a coolant in two heat sinks with different geometries. A spiral heat sink with different inlet/outlet configurations and a straight heat sink with sharp bends at each end were fabricated

on base plates of copper. The results were normalized and compared to the results for a straight channel with the identical size.

These early results furnish a number of important observations, namely which kind of fluid is the most efficient and in which range of flow rate the heat transfer is enhanced. It was shown that increasing the viscosity doesn't increase the heat transfer enhancement, but only increases the pressure drop, and consequently the pumping cost. It has been shown that, in general, the spiral and straight heat sinks are able to enhance the heat transfer compared to a straight channel. Furthermore, from Figures 4.4-4.5, one may conclude that the heat transfer for both heat sinks is not enhanced significantly in low flow rates and at higher flow rates conclude a better enhancement. However, the pressure drop penalty becomes more significant as the flow rate increases. Early results for the spiral geometry show that there is no difference in feeding the heat sink from the side or the middle.

Figure 4.11 showed a complete conclusion for the pressure drop and heat transfer in the heat sinks. It revealed that while the flow is laminar in the straight channel, and at a constant pressure drop, both heat sinks have lower heat transfer rate in comparison to a straight channel having the same cross section. However, it is impossible to have a straight channel inside a heat sink and one should use another geometry and configuration to cool down a system. Whereas, having turbulent flow in the straight channel, the straight heat sink shows a better heat transfer at a constant pressure drop in comparison to the straight channel.

It was shown that for a constant pressure drop, heat transfer inside a straight channel is higher when one uses laminar flow, whereas, in turbulent flow, the straight heat sink shows a better enhancement compared to a simple channel.

Further investigations on the heat transfer enhancement and pressure drop in curved channels and flow through 90 degree bends are needed. The mechanism of augmen-

tation at each geometry should be found to find a technique that enhances the heat transfer in low flow rates to reduce the pumping cost.

### **Acknowledgement**

The authors acknowledge the financial support of the Natural Sciences and Engineering Research Council of Canada (NSERC) and Auto 21 NCE.

## **4.8 References**

- [1] Tuckerman, D. B., and Pease, R. F. W., High-performance heat sinking for VLSI, *Electron Device Letters, IEEE*, vol. 2, pp. 126-129, 1981.
- [2] Keyes, R. W. Heat transfer in forced convection through fins, *Electron Devices, IEEE Transactions*, vol. 31, pp. 1218-1221, 1984.
- [3] Samalam, V. K., Convective heat transfer in microchannels, *J. Electron Mater*, vol. 18, pp. 611-617, 1989.
- [4] Knight, R. W., Goodling, J. S., Hall, D. J. Optimal thermal design of forced convection heat sinks-analytical. *J. Electron Package, Trans ASME*, vol. 113, pp. 313-321, 1991.
- [5] Knight, R. W., Hall, D. J., Goodling, J. S., Jaeger, R. C., Heat sink optimization with application to microchannels Components, Hybrids, and Manufacturing Technology, *IEEE Transactions*, vol. 15, pp. 832-842, 1992.
- [6] Bejan, A., and Morega, A. M., Optimal arrays of pin fins and plate fins in laminar forced convection, *TRANSACTIONS - ASME: JOURNAL OF HEAT TRANSFER*, vol. 115, pp. 75-81, 1993.
- [7] Lee, D., and Vafai, K., Comparative analysis of jet impingement and microchannel cooling for high heat flux applications, *Int. J. Heat Mass Transfer*, vol. 42, pp. 1555-1568, 1999.

- [8] Weisberg, A., Bau, H. H., Zemel, J. N., Analysis of microchannels for integrated cooling, *Int. J. Heat Mass Transfer*, vol. 35, pp. 2465-2474, 1992.
- [9] Fedorov, A. G., and Viskanta, R., Three-dimensional conjugate heat transfer in the microchannel heat sink for electronic packaging, *Int. J. Heat Mass Transfer*, vol. 43, pp. 399-415, 2000.
- [10] Qu, W., and Mudawar, I., Experimental and numerical study of pressure drop and heat transfer in a single-phase micro-channel heat sink, *Int. J. Heat Mass Transfer*, vol. 45, pp. 2549-2565, 2002.
- [11] Li, J., Peterson, G. P., Cheng, P., Three-dimensional analysis of heat transfer in a micro-heat sink with single phase flow, *Int. J. Heat Mass Transfer*, vol. 47, pp. 4215-4231, 2004.
- [12] Xie, X. L., Liu, Z. J., He, Y. L., Tao, W. Q., Numerical study of laminar heat transfer and pressure drop characteristics in a water-cooled minichannel heat sink, *Appl. Therm. Eng.*, vol. 29, pp. 64-74, 2009.
- [13] Chein, R., and Chen, J., Numerical study of the inlet/outlet arrangement effect on microchannel heat sink performance, *International Journal of Thermal Sciences*, vol. 48, pp. 1627-1638, 2009.
- [14] Zhang, H. Y., Pinjala, D., Wong, T. N., Toh, K. C., Joshi, Y. K., Single-phase liquid cooled microchannel heat sink for electronic packages, *Appl. Therm. Eng.*, vol. 25, pp. 1472-1487, 2005.
- [15] Sasaki, S., and Kishimoto, T., Optimal structure for microgrooved cooling fin for high-power LSI devices, *Electron. Lett.*, vol. 22, pp. 1332-1334, 1986.
- [16] Nayak, D., Hwang, L., Turlik, I., Reisman, A. A high-performance thermal module for computer packaging. *J. Electron Mater.*, vol. 16, pp. 357-364, 1987.
- [17] Rahman, M. M., Gui, F., In Design, fabrication, and testing of microchannel heat sinks for aircraft avionics cooling, *Proceedings of the Intersociety Energy Conversion*

Engineering Conference, vol. 1, pp 1-6, 1993.

[18] Harms, T. M., Kazmierczak, M., Gerner, F. M., Hölke, A., Henderson, H. T., Pilchowski, J., Baker, K., Experimental investigation of heat transfer and pressure drop through deep microchannels in A (110) silicon substrate, ASME Heat Transfer Div. Publ. HTD, vol. 351, pp. 347-357, 1997.

[19] Kawano, K., Minakami, K., Iwasaki, H., Ishizuka, M., In Micro channel heat exchanger for cooling electrical equipment, American Society of Mechanical Engineers, Heat Transfer Division, vol. 361-3, pp. 173-180, 1998.

[20] Harms, T. M., Kazmierczak, M. J., Gerner, F. M., Developing convective heat transfer in deep rectangular microchannels, Int. J Heat Fluid Flow, vol. 20, pp. 149-157, 1999.

[21] Rahman, M. M., Measurements of heat transfer in microchannel heat sinks, Int. Commun. Heat Mass Transfer, vol. 27, pp. 495-506, 2000.

[22] Naphon, P., and Khonseur, O., Study on the convective heat transfer and pressure drop in the micro-channel heat sink, Int. Commun. Heat Mass Transfer, vol. 36, pp. 39-44, 2009.

[23] Singh, R., Akbarzadeh, A., Mochizuki, M., Sintered porous heat sink for cooling of high-powered microprocessors for server applications. Int. J. Heat Mass Transfer, vol. 52, pp. 2289-2299, 2009.

[24] Dorin, L., Effects of inlet geometry on heat transfer and fluid flow of tangential micro-heat sink, Int. J. Heat Mass Transfer, vol. 53, pp. 3562-3569, 2010.

[25] S. J. Kline and F. A. McClintock, Describing Uncertainties in Single-Sample Experiments, Mech. Eng., P. 3, 1953.

[26] Y. S. Muzychka and M. M. Yovanovich, Laminar Forced Convection Heat Transfer in Combined Entry Region of Non-Circular Ducts, ASME J. Heat Transfer, vol. 126, pp. 54-62, 2004.

[27] S. Kakac, W. Aung, R. K. Shah, Handbook of Single Phase Convective Heat Transfer, Wiley, 1987.

[28] A. Bejan, Convective Heat Transfer, Wiley, 2005.

# Chapter 5

## Effect of Entrance Region and Curvature on Heat Transfer in Mini Scale Curved Tubing at Constant Wall Temperature\*

**M.Ghobadi and Y.S. Muzychka**

Microfluidics and Multiphase Flow Lab, Faculty of Engineering and Applied Science,  
Memorial University of Newfoundland, St. John's, NL, Canada, A1B 3X5

### **ABSTRACT**

An experimental study on heat transfer enhancement in short curved tubes for the constant wall temperature boundary condition is presented. Copper tubing with four different radii of curvature (1 cm, 2 cm, 4 cm, and 8 cm) and in four lengths were used. Tubing radii were chosen, so that a constant tube length occurs in different curvatures. Hence, the effect of curvature on heat transfer at a constant length can be studied as well as the effect of heat transfer enhancement by changing the length in a constant curvature. Experimental results are also compared with an existing model for curved tubing. Water and three different silicone oils (0.65 cSt, 1 cSt and 3 cSt) were used in the experiments to examine the effect of Prandtl number on curved tubing heat transfer augmentation.

**Keywords:** Heat Transfer, Curved Tubing, Passive Heat Transfer Enhancement, Entrance Region

\* *International Journal of Heat and Mass Transfer*; 2013; 65: 357-365

## 5.1 Introduction

Using curved geometry is one of the most effective passive heat transfer enhancement methods which fit several heat transfer applications. Curved tubes are an essential component of nearly all industrial processes, ranging from power production, chemical and food industries, electronics, environment engineering, waste heat recovery, manufacturing, air-conditioning, refrigeration, and space applications. The use of curved tubes in continuous processes is an attractive alternative to conventional agitation since similar and sometimes better performance can be achieved at lower energy consumption and reduced maintenance requirement because of no moving parts. For heat and mass-transfer applications, they have the two-fold advantages of increasing the transfer rate due to secondary flow and providing high heat and mass-transfer area per unit volume of space. Curved tubes can provide homogenization of feed streams with a minimum residence time and are available in most materials of construction. Early investigations on curved geometries were conducted by Thomson [1], Williams [2], Grindley and Gibson [3] and Eustic [4].

Spiral geometry is one of the applications of curved geometry. The idea of using spiral geometry was first used in spiral plate heat exchangers in late 19th century [5] and further investigations conducted in the 1930s in Sweden [6,7].

The concept is also being used in coiled tubes. The most popular use for coiled tubing is circulation or deliquification. Coiled tube heat exchangers, logging and perforating, and drilling are other applications of coiled tubing [8,9]. From a heat transfer point of view, helically coiled exchangers offer certain advantages. Compact size provides a distinct benefit. Higher film coefficients, the rate at which heat is transferred through

a wall from one fluid to another, and more effective use of available pressure drop result in efficient and less-expensive designs. True counter-current flow fully utilizes available LMTD (logarithmic mean temperature difference). Helical geometry permits handling of high temperatures and extreme temperature differentials without high induced stresses or costly expansion joints. High-pressure capability and the ability to fully clean the service-fluid flow area added to the exchanger's advantages. Neglecting the effect of coiled tube pitch Rennie [10] examined the double-pipe helical heat exchangers numerically and experimentally. Kumar et al. [11] studied a tube-in-tube helically coiled heat exchanger for turbulent flow regime numerically. Shokouhmand et al. [12] experimentally investigated the shell and helically coiled tube heat exchangers in both parallel-flow and counter-flow configuration. They used the Wilson plot method [13] to calculate the overall heat transfer coefficient.

Unlike the flow in straight pipes, fluid motion in a curved pipe is not parallel to the curved axis of the bend, owing to the presence of a secondary motion caused by secondary flow. As the flow enters a curved bend, centrifugal forces act outward from the center of curvature on the fluid elements. Because of the no-slip condition at the wall, the axial velocity in the core region is much greater than that near the wall. To maintain the momentum balance between the centrifugal forces and pressure gradient, slower moving fluid elements move toward the inner wall of the curved tube. This leads to the onset of a secondary flow such that fluid near the wall moves along the upper and lower halves of the torus wall while fluid far from it flows to the outer wall. The curvature,  $1/R$ , affects the flow patterns, and even slight curvature was observed to modify the critical velocity of the fluid [14].

Dean [15,16] conducted the first analytical studies of fully developed laminar flow in a curved tube. He developed a series solution as a perturbation of the Poiseuille flow in a straight pipe for low values of Dean number ( $De < 17$ ). He reported that

the relation between pressure gradient and the rate of flow is not dependent on the curvature to the first approximation. In order to show its dependence, he modified the analysis by including the higher-order terms and was able to show that a reduction in flow due to curvature depends on a single variable (now known as the Dean number), equal to  $Re\sqrt{(D/2R)}$  (where  $Re$  is the Reynolds number,  $D$  is the tube diameter, and  $R$  is the radius of curvature of curved tube in Dean's notation). Various other authors have used different definitions of the Dean number for curved tube studies. It was reported that, for low Dean numbers, the axial-velocity profile was parabolic and unaltered from the fully developed straight tube flow. As the Dean number is increased, the maximum velocity begins to be skewed toward the outer periphery. Similarly, for high curvatures, the secondary flow intensity is very high while for lower curvatures, the secondary flow intensity is much less [14].

White [17] numerically studied the pressure drop through a coil of constant curvature. A complete investigation on heat transfer has been provided by Akiyama and Cheng [18, 19] on curved rectangular channels and curved pipes with uniform heat flux and a peripherally uniform wall temperature. Using a numerical method, they found solutions up to a reasonably high Dean number for different aspect ratios. They also showed that the perturbation method is only applicable for a relatively low Dean number region and a boundary-layer technique is valid only for high Dean number regimes. The effect of Dean number on velocity and temperature field was also studied in their work.

Mori et al. [20] studied the effect of viscosity and secondary flow. At the central part of the flow passage, when the intensity of the secondary flow is strong, it is possible to neglect the effect of the viscosity and heat conduction compared with a stress analogous to the Reynolds stress and heat convection due to the secondary flow components. According to their paper, the effect of the viscosity and heat conduction

are confined within a thin layer along a wall of the passage, where the intensity of the secondary flow is weakened. They proved that because of this effect one can consider the existence of the boundary layer along the wall of the passage for a flow which is strongly affected by the secondary flow. They divided the flow and temperature fields in their curved channel into two regions: i) the core region about the central part of the passage where the effect of the secondary flow is dominant over viscosity and ii) the boundary layer region along the wall where the effect of the viscosity and heat conduction cannot be ignored. They proved the existence of such a boundary layer experimentally. Their method is also applicable to non-circular cross sections as well as circular cross sections.

Nigam [14] accomplished a comprehensive review on the papers related to the application of curved geometry in the process industry up to 2008. The primary objective of this work is to provide an overview of the perspective on evolution of curved tube technology and introduction to a new class of curved tubes. The paper is divided into four parts. The first part discusses the fundamentals involved in enhancing the mixing performance and local phenomena in curved tubes to better understand how mixing and heat, and mass transfer proceed for single-phase flow. In the second part, the chemistry of two-phase flow in curved tubes is discussed and reported. Both the first and second parts also review the well established models available for pressure drop, heat transfer, mixing, and mass-transfer in the curved tubes. Methods for estimating the performance of curved tubes from experimental data, empirical correlations, and computational fluid dynamics are also discussed. The third part discusses the development of a new class of curved chaotic geometries (bent coils) as a course of technological development. The hydrodynamics, heat transfer, and mass-transfer performance in curved chaotic configurations have been discussed and compared against curved tubes. More experimental [21,22] and numerical [23,24] studies have been

conducted since this time.

Cheng [25] reported that the number of the vortices inside a curved channel depend on the Dean number. Two vortices have been reported for  $De < 100$ , whereas for  $100 < De < 500$ , four vortices appear in a square curved channel. These extra vortices vanish at about  $De \approx 500$ . The channel aspect ratio determines the exact value of the disappearance.

Burmeister and Egner [26] numerically studied laminar flow and heat transfer in three-dimensional spiral ducts of a rectangular cross section with different aspect ratios. The boundary conditions were assumed to be axially and peripherally uniform wall heat flux and a peripheral uniform wall temperature. They presented average Nusselt number as a function of distance from inlet and Dean number. Their results are applicable to spiral plate heat exchangers.

Hashemi and Akhavan-Behabadi [27] experimentally investigated the heat transfer and pressure drop characteristics of nanofluid flow inside horizontal helical tubes under constant wall flux. They studied the effect of different parameters such as Reynolds number, fluid temperature and nanofluid particle weight concentration on heat transfer coefficient and pressure drop of the flow.

Chang et al. [28] conducted an experimental study that examines the Nusselt number (Nu), friction factor (f) and thermal performance factor (TPF) for a square spiral channel with two opposite end walls roughened by in-line 45 degree ribs.

This paper mainly focuses on studying the heat transfer inside short curved tubing under constant wall temperature boundary conditions. Short curved tubes find application in heat sinks, serpentine tube, or using in nanofluids. Curvature and length effects are considered in this paper. The copper tube was curved with four radii 1, 2, 4, and 8 cm and in different lengths. Fig. 5.1 depicts the four examined shapes for different radii and lengths. Hence, we consider different lengths with the same



Figure 5.1: Curved tubing in different lengths

curvature, and different curvatures for a constant length. The effect of Dean number change at a constant length has been studied. The results have also been compared with an identical straight tube for a similar constant wall temperature condition. Table 5.1 shows the curvatures and lengths of the curved tubes used in the experiment. One may notice that the radii have been picked in such a way that the lengths of different curvatures match together.

Table 5.1: Curved tubes lengths in cm

<i>Radius</i>	$\theta = 90$	$\theta = 180$	$\theta = 270$	$\theta = 360$
1 cm	-	3.14	4.71	6.28
2 cm	3.14	6.28	9.42	12.56
4 cm	6.28	12.56	18.84	25.12
8 cm	-	25.12	-	-

The effect of Prandtl number has been also considered in this study, since water and three silicone oils with low viscosities, 0.65 cSt, 1cSt and 3 cSt have been used in

all of the configurations. Prandtl numbers from 5 to 40 are covered in this paper. The effect of Prandtl on each configuration is also considered to show which fluid can better enhance the heat transfer in curve tubing. Finally, the experimental results have been compared with an existing model by Dravid [29].

## 5.2 Experimental Setup

Fig. 5.2 shows the configuration of the experimental setup. Depending on the flow rate, two or four syringes (Hamilton Glass Gas Tight) were filled with the test fluid, and the pumps (Harvard Pump 33) were set to the desirable flow rate. Each syringe can hold 100 ml; hence total 400 ml of the working fluid was available for each run of the experiment. Considering the maximum volumetric rate at 100 ml/min, the system had at least 4 minutes or more time to become thermally stable. The flow from four syringes merged together and flow into the curved copper tubing. Thermocouples were placed at each end with the least distance from the copper tubing. The copper tubing were cut with smooth edges so that the flow was not disturbed entering the tubing. Plastic tubing was used to connect the flow tube to the curved tubing. A Keithley Data Acquisition system (DAQ) collected the temperatures. Five readings were taken and averaged for inlet and outlet temperature to minimize the error in reading. The curved tubes were placed horizontally inside the constant temperature water bath, so that the gravitational effect can be neglected. The constant temperature bath maintained the temperature at the set point within  $\pm 0.1^{\circ}C$  uncertainty. The water temperature and consequently the surface temperature of the curved tubing were set  $40^{\circ} C$ , whereas the fluid inlet temperature was measured to be around  $23^{\circ} C$ . The estimated uncertainty of the LMTD temperature was  $\approx 0.2^{\circ}C$ .

The viscosity of the silicone oils, as well as their temperature dependence were given

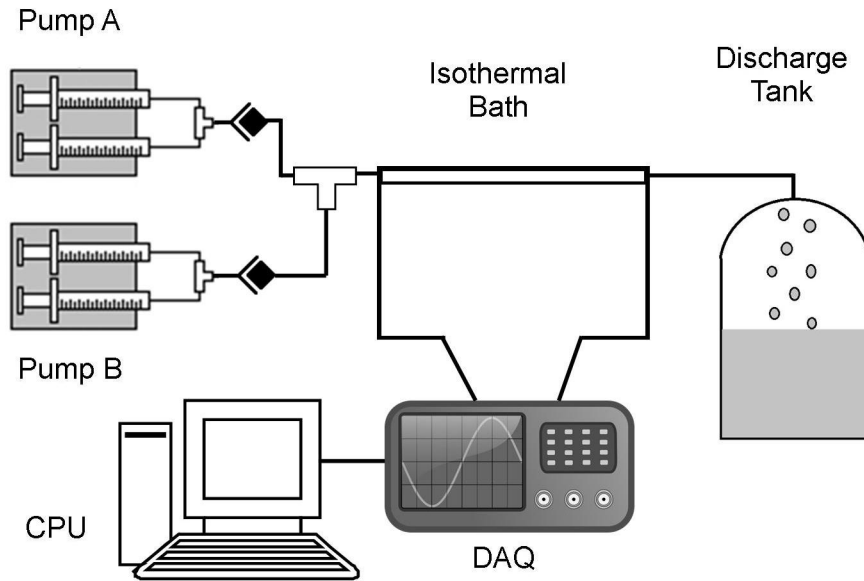


Figure 5.2: System configuration

by the manufacturer. However, we measured the viscosities of the oils with an accurate apparatus (Physica MCR 301 from Rheosys Company) at room temperature to confirm the reported data. The data were found to be inside the 5% range of the reported data. The accuracy of the device was also benchmarked by measuring the viscosity of water.

In order to confirm the accuracy of the experimental procedure, benchmarking tests have been done on a straight tube with the same copper tubing. The tests were done with a 163 mm long segment of straight copper tubing with the diameter of 1.65 mm. The tubing was cut precisely and the edges were filed to have smooth ends. Finally, two plastic tubes were glued to the ends to avoid any leakage. Two thermocouples were placed in the same manner as the original experiments as near as possible to the entrance and exit. The constant wall temperature condition was considered with surface temperature of  $40^{\circ}\text{C}$ . The ambient temperature was around  $25^{\circ}\text{C}$ . The tube was placed in the thermal bath horizontally, so gravity doesn't affect the results.

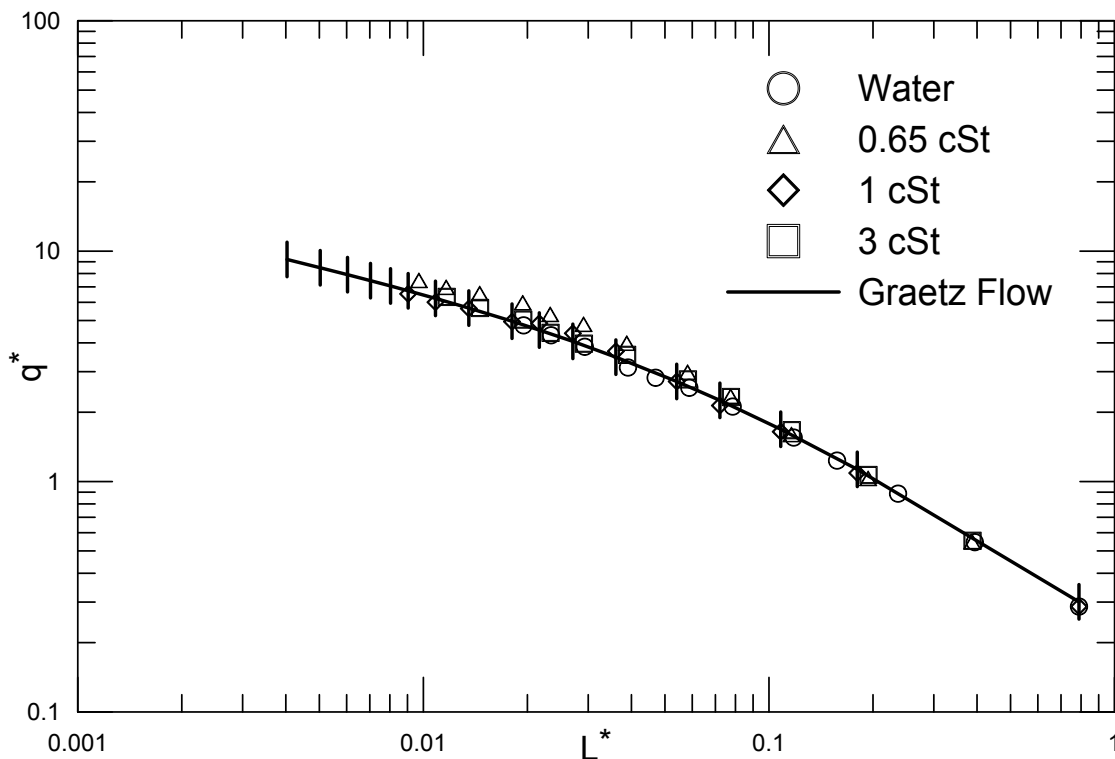


Figure 5.3: Benchmarking results with 10 percent error bars

The flow was assumed to be hydrodynamically developed and thermally developing. Water, 0.65 cSt oil, 1 cSt and 3 cSt oil were examined as the working fluids. Fig. 5.3 shows the benchmarking results for all of the working fluid in comparison to the Graetz model for straight tubes. The accuracy of the experiments can be verified by comparing the gathered data with the model. The rms error was found to be less than 7 percent for all the fluids and test conditions.

### 5.3 Data Analysis

In this section we review the equations which have been used to reduce the data collected from the DAQ. The total heat removed by the fluid can be obtained by writing the energy balance for each fluid as a single phase liquid flow:

$$Q = \dot{m}C_p(T_o - T_i) \quad (5.1)$$

The mean heat transfer rate is also the heat transfer per unit area of the coiled tubing:

$$\bar{q} = \frac{Q}{PL} \quad (5.2)$$

Since we are interested in the average value of  $h$  or the Nusselt number for the entire tube, and the boundary condition is constant wall temperature, we use log mean temperature difference:

$$\Delta T_{lm} = \frac{\Delta T_o - \Delta T_i}{\ln \frac{\Delta T_o}{\Delta T_i}} \quad (5.3)$$

Finally one may find  $\bar{h}$  and Nusselt number by the following equations:

$$\bar{h} = \frac{\bar{q}}{\Delta T_{lm}} \quad (5.4)$$

$$\overline{Nu} = \frac{\bar{q}D}{k_f \Delta T_{lm}} \quad (5.5)$$

One may want to use Nusselt number, which requires defining the LMTD temperature. Another approach is to use the wall to inlet temperature difference,  $T_w - T_i$ . In this paper we also adopt a dimensionless heat transfer rate which is based on the mean wall to inlet temperature difference rather than the traditional heat transfer coefficient approach which utilizes the log mean wall to bulk temperature difference. This alternative approach is more natural and more practical in the analysis of single fluid devices.

Two dimensionless parameters of interest which need to be defined are the dimensionless mean wall flux:

$$q^* = \frac{\bar{q}D}{k(T_w - T_i)} \quad (5.6)$$

and the dimensionless thermal length:

$$L^* = \frac{L/D}{Pe_D} \quad (5.7)$$

The dimensionless mean wall flux can be related to the Nusselt number using single fluid heat exchanger theory, e.g. the  $\varepsilon - NTU$  method for constant wall temperature. This leads to the following expression relating the two:

$$q^* = \frac{1}{4L^*} [1 - \exp(-4\overline{Nu}L^*)] \quad (5.8)$$

In the case of a Graetz flow in a circular tube, Muzychka et al. [30] obtained:

$$q^* = \left[ \left( \frac{1.614}{L^{*1/3}} \right)^{-3/2} + \left( \frac{1}{4L^*} \right)^{-3/2} \right]^{-2/3} \quad (5.9)$$

For curved tubes, the experimental results are compared to the model by Dravid [29] who experimentally showed the effect of the secondary flow effect on heat transfer enhancement. He proposed the following correlation for the fully developed Nusselt number and constant curvature:

$$Nu = (0.65\sqrt{De} + 0.76)Pr^{0.175} \quad (5.10)$$

The equation is valid in the range of  $50 < De < 2000$  and  $5 < Pr < 175$ . The validity of the model in the mentioned range is examined based on the experimental results.

## 5.4 Results and Discussion

As stated before, water and three different silicone oils were used in the experiments. Hence, a broad range of Prandtl numbers, Dean numbers and Reynolds numbers have been examined in the experiments. Table 5.2 summarizes the range for these different dimensionless numbers. Prandtl number which depends on the fluid properties, particularly, heat capacity, viscosity and conductivity, changes mostly with the viscosity change as the other two parameters are almost the same for different silicone oils. As viscosity is a strong function of temperature, the correlations given by the provider were used to calculate the viscosity in each experiment (the average of the entrance and the exit temperature were used). Since it is independent of curvature and flow rate directly, only one average of Prandtl number is presented for all curvatures and flow rates. On the other hand, Reynolds number which depends on the velocity, hydraulic diameter and viscosity, changes noticeably by changing the flow rate and consequently the flow velocity. Considering the fact that the curvature changes don't affect the Reynolds number, one may conclude that Reynolds number range for a fluid inside channels with different curvature is the same. Thus, for a liquid at the same flow rate the Reynolds number is the same for different curvature. However, Dean number is proportional to the channel curvature and changes when changing both flow rate and curvature. It implies that the range for Dean number for the same fluid is different in different curvature ranges.

In this section, the experimental results are presented based on four different conditions. First, the experimental results are compared with the model by Dravid [29]. Second, we examine the effect of curvature and length change in curved tubing. Finally, the Prandtl number effect on the heat transfer enhancement in curved tubes is examined.

Fig. 5.4 shows the heat transfer results for water inside the curved tubing with 4 cm

Table 5.2: Prandtl, Reynolds and Dean range for the different fluids

<i>Fluid</i>	<i>Pr</i>	<i>Re</i>	<i>Radii</i>	<i>De</i>
<i>water</i>	5 – 6.3	30 – 2000	1	5 – 400
			2	5.5 – 350
			4	4.1 – 280
			8	3 – 172
<i>0.65cSt</i>	7.9 – 9.2	30 – 2000	1	9.3 – 570
			2	6.4 – 440
			4	4.7 – 295
			8	3.3 – 200
<i>1cSt</i>	12.6 – 14	20 – 1260	1	6.34 – 355
			2	4.3 – 255
			4	3.11 – 188
			8	2.2 – 133
<i>3cSt</i>	35 – 40	7 – 260	1	2 – 73
			2	1.4 – 52
			4	1 – 38
			8	0.7 – 25

radius with the length of 25.12 cm. The plot is in Log-Log base. The x axis shows the dimensionless thermal length,  $L^*$ . The y axis is the dimensionless mean wall flux, which represents the convection heat transfer between the fluid and the tube wall. The Graetz model represents the heat transfer inside straight tubing with the same cross section. The points above this line show augmentation in comparison to straight tubing. The asymptote of  $q^* = 1/4L^*$  shows the maximum heat transfer which may occur in tubing due to the energy balance, when  $T_o \approx T_w$ . Any point above this dashed line cannot satisfy the energy balance and is not likely accurate.

The Prandtl number is  $Pr \approx 5$  and the constant wall temperature condition was set to  $50^\circ C$ . The experimental results are compared with the Dravid model [31], and have shown an average deviation of 6.8 percent. The Graetz model for a straight tube with an identical cross section and length and the same constant wall temperature

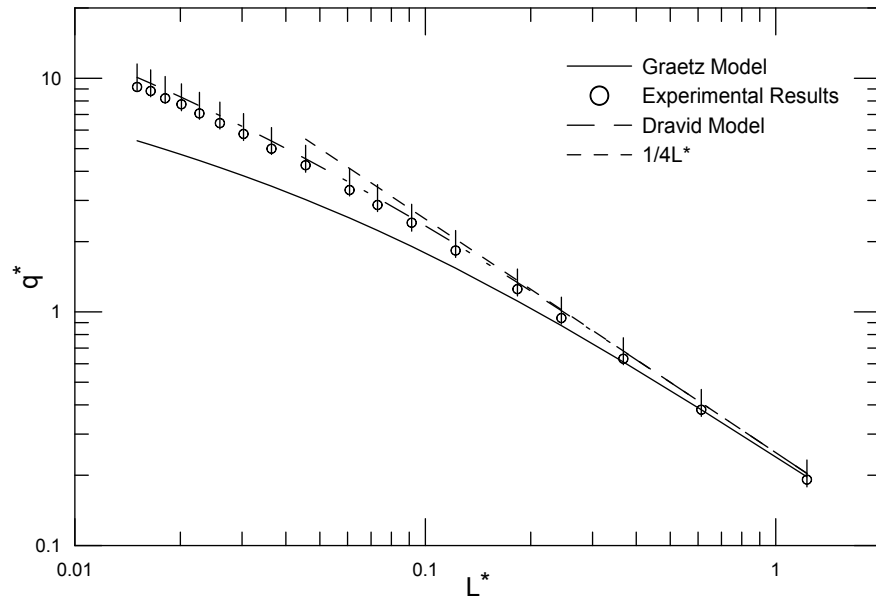


Figure 5.4: Dravid model comparison for the experimental results for water  $R=4$  cm,  $L=25.12$  cm with 10 percent error bars

condition is also drawn in the figure. One may observe a noticeable heat transfer enhancement by using short curved tubing in comparison to straight tubing.

Fig. 5.5 depicts the same configuration for 1cSt silicone oil flowing inside a 2 cm radius with 9.42 cm length. The Prandtl number is an average of 37.5. The wall temperature was set to  $40^{\circ} C$ . A good agreement between the model and experimental results is observed with an average error of 5 percent. Other comparisons of the experimental results have also shown the same precision.

Now that we have shown that short curved tubing can enhance the heat transfer in comparison to straight tubing, it is helpful to investigate the effect of changing the curvature in same length. We are expecting an increase in the heat transfer by increasing the curvature which follows by increasing the Dean number.

Fig. 5.6 shows the results for different curvatures of copper tubing for the constant length of 6.28 cm. The working fluid is water with the average Prandtl number of 5, and the wall temperature was  $50^{\circ} C$ . The results are presented in terms of

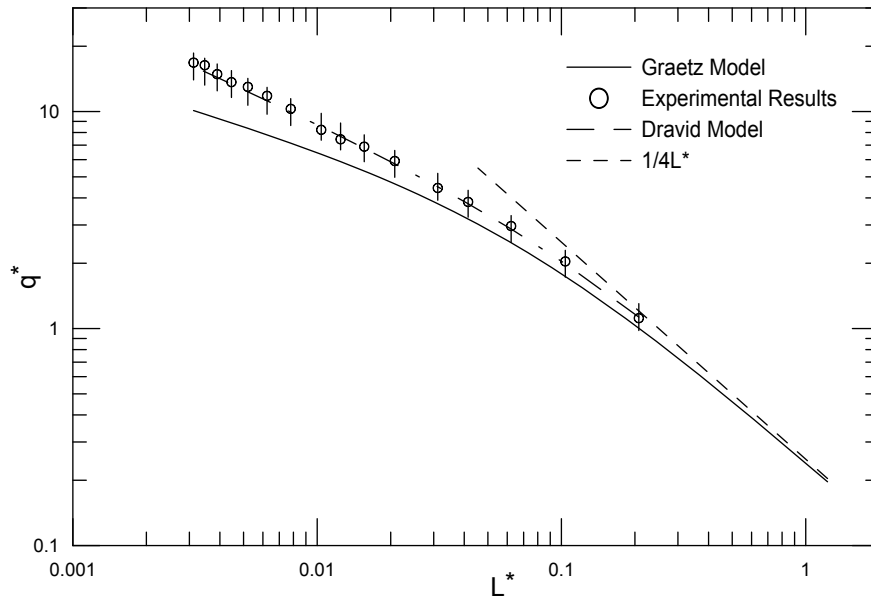


Figure 5.5: Dravid model comparison for 1 cSt silicone oil  $R=2$  cm,  $L=9.42$  cm with 10 percent error bars

radius of curvature ( $R$ ), and curve angle ( $\theta$ ). As we expected for the curvature effect, smaller radius of curvature (higher curvature) results in increased heat transfer. The dimensionless mean wall flux is the highest for 1 cm radius, and it is higher in 2 cm radius in comparison to 4 cm radius. Such results were predictable due to the nature of enhancement which implies the main reason for the enhancement is the secondary flow initiation inside the tubing which increases by increasing the curvature.

Fig. 5.7 is the similar plot showing the results for 1 cSt silicone oil in a curved tubes having the constant length of 25.12 cm. This length may be reached by a full circle with 4 cm radius, or a half circle with 8 cm radius. The similar trend is also observed in this plot. The 4 cm radius shows better augmentation than the 8 cm radius one. However, both curved tubes show the heat transfer augmentation in comparison to the straight tube. Figs. 5.6 and 5-7 also depict that at very low flow rates, all the points for Graetz model, curved tubes and the maximum heat transfer merge together. This happens because the secondary flow can only become effective when the flow velocity

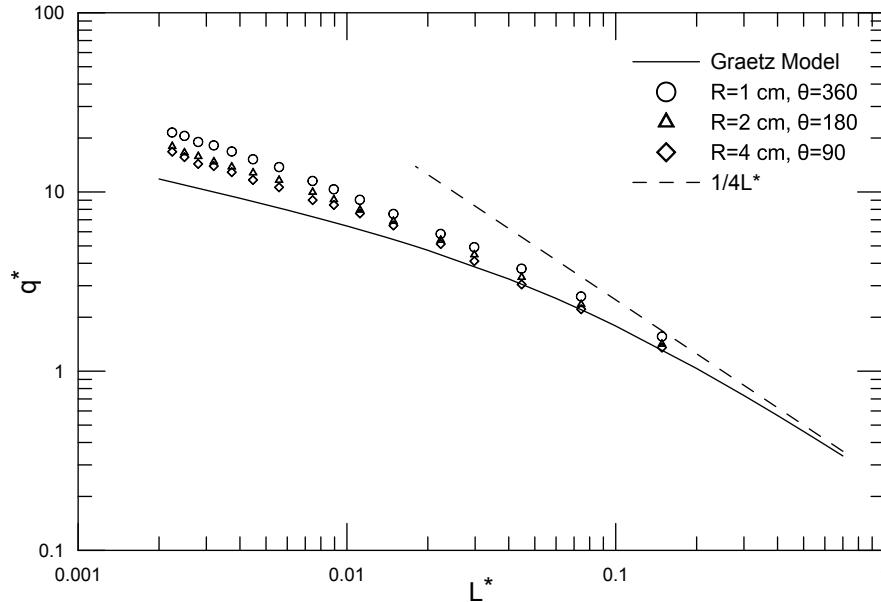


Figure 5.6: Different radius of curvature for water with  $L=6.28$  cm

is high enough to initiate it, otherwise, the flow acts like a flow in straight tubing. One may be interested in Nusselt number comparison instead of dimensionless mean wall flux. Figs. 5.8 and 5.9 show the Nusselt data for the conditions which have been examined in Figs. 5.6 and 5.7 respectively. Since the length of the tubes being discussed are the same, and the curvature is the only parameter which is being changed, the Graetz model for any equivalent length of curved tubes, is a single line and the comparison is valid. Nusselt number for fully developed flow with constant wall temperature remains constant,  $Nu = 3.66$ , for any Reynolds number, and is shown for lower Reynolds. The Nusselt versus Reynolds comparison shows the similar result which was obtained in the previous analysis. The insert figures show the Nusselt versus Dean number. As discussed before Dean number is the parameter that accounts for the secondary flow. Therefore, as the length and Prandtl number is the same for each Figure, the expectation is having the same Nusselt for a constant Dean number, which is satisfied according to the experimental results. However, one should note

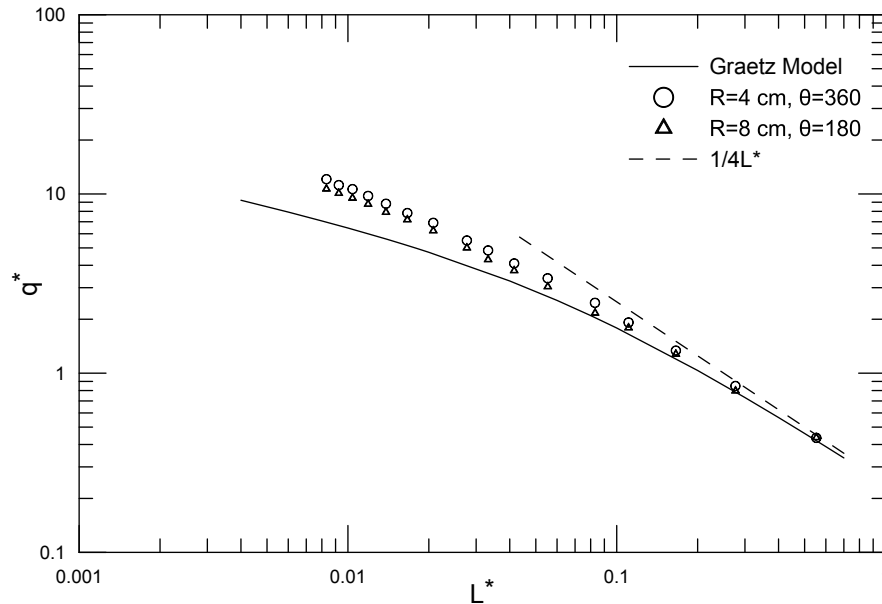


Figure 5.7: Different radius of curvature for 1 cSt silicone oil with  $L=25.12$  cm

that comparing two curved tubes with a same length, the one with lower curvature (bigger radius of curvature) requires higher Reynolds and consequently higher fluid velocity to have the same Dean number as the one with greater curvature.

The next set of investigations examine the length effect of the tubes on a constant curvature in mini scale curved tubes. We examine the effect of the tube length on heat transfer augmentation by considering 4 different lengths from a quarter, half, three quarter and full circle with a same radius. Hence, convection heat transfer is compared in three different lengths for the same curvature. Considering the same flow speed, Reynolds and Dean numbers in each flow are the same for all the lengths. Thus, one may conclude that the difference in the heat transfer augmentation is only due to the change in the length.

Figs. 5.10 and 5.11 show the length effect at a constant curvature for two different conditions. Fig. 5.10 depicts the length effect on the 4 cm radius of curvature tube employing 0.65 cSt silicone oil as a working fluid. The constant temperature bath

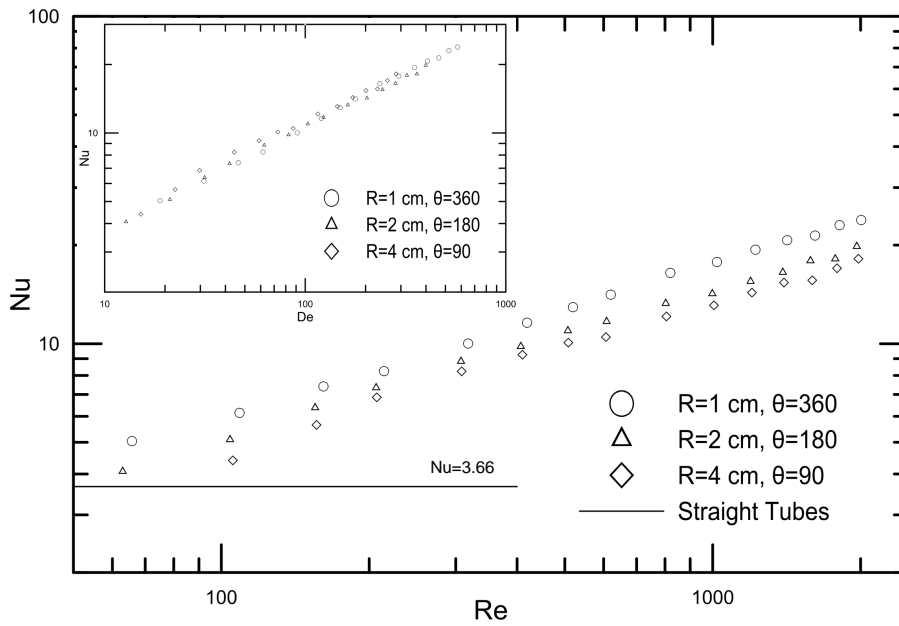


Figure 5.8: Nusselt analysis for different radius of curvature for water at  $L=6.28$  cm

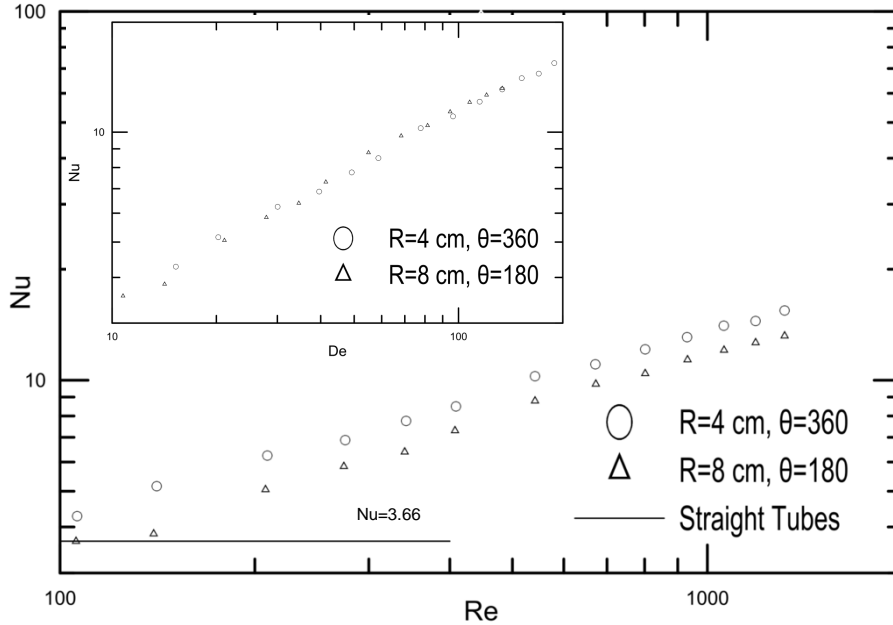


Figure 5.9: Nusselt analysis for different radius of curvature for 1 cSt silicone oil with  $L=25.12$  cm

temperature and consequently the wall temperature was set to  $40^{\circ}\text{C}$ , and the average Prandtl number is 8.3. Fig. 5.11 shows the length effect on the 2 cm radius of curvature with 3 cSt silicone oil which has the average Prandtl number of 38. The wall temperature was set to  $40^{\circ}\text{C}$ . Since, there is a linear correlation between Reynolds number and Dean number, the range of both dimensionless numbers are the same for all four lengths, and Nusselt number versus Dean number show the same trend as employing Reynolds number instead of Dean number. One may conclude that the Nusselt number slightly increases by decreasing the length. However, one should note that Nusselt number analysis for the constant curvature curved tubes requires extra attention, where the tube length differs for each curve angle with a same radius of curvature. Hence, we cannot have a single line to depict the Nusselt for the straight tubes. The insert Figures show the Graetz model for the straight tubes of the equivalent length of the mentioned curved tubes. It can be seen that the Nusselt number increases by decreasing the length. It happens due to the nature of Nusselt number that accounts the entrance effects.

Nusselt number for the curved tubes in the case of constant curvature and different lengths depicts the length effects as well as the secondary flows initiated by curving the tube. Consequently, employing Nusselt number versus Reynolds number or Dean number accounts the entrance effect as well as the secondary flow. It can be seen that the insert Figures show that the Nusselt number is higher for the straight tubes having shorter length. In other words, in Figs. 5.10 and 5.11 enhancement as a result of both the secondary and the entrance effect is reflected. Obviously, the entrance effect dominates the enhancement at shorter lengths, and it can be seen that the difference between the longer curved tubes (270 and 360 degree) is smaller in both Figures, which reflects the vanishing of the entrance effect on the total Nusselt number having longer curved tubes.

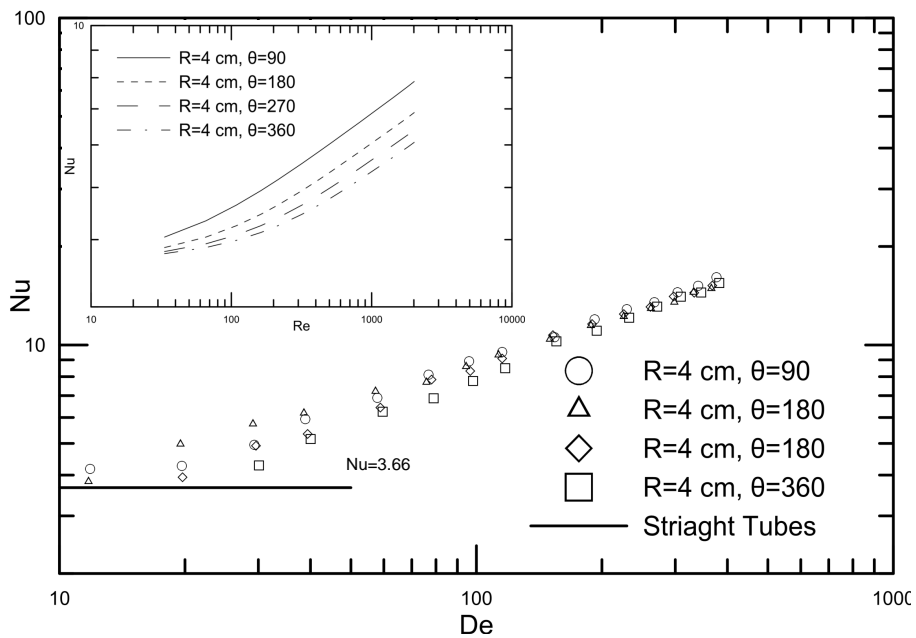


Figure 5.10: Nusselt analysis for different lengths for 0.65 cSt silicone oil with  $R=4$  cm

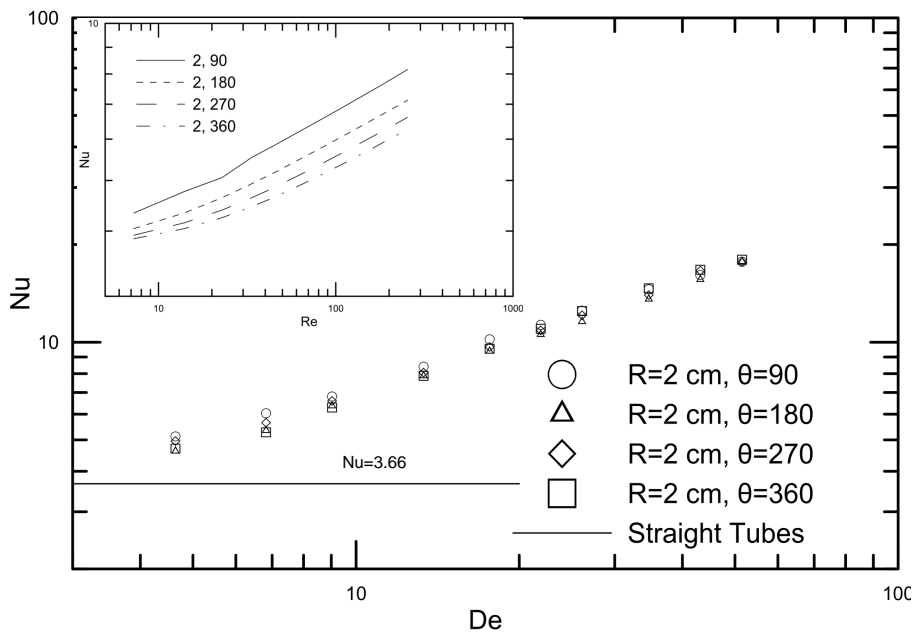


Figure 5.11: Nusselt analysis for different lengths for 3 cSt silicone oil with  $R=2$  cm

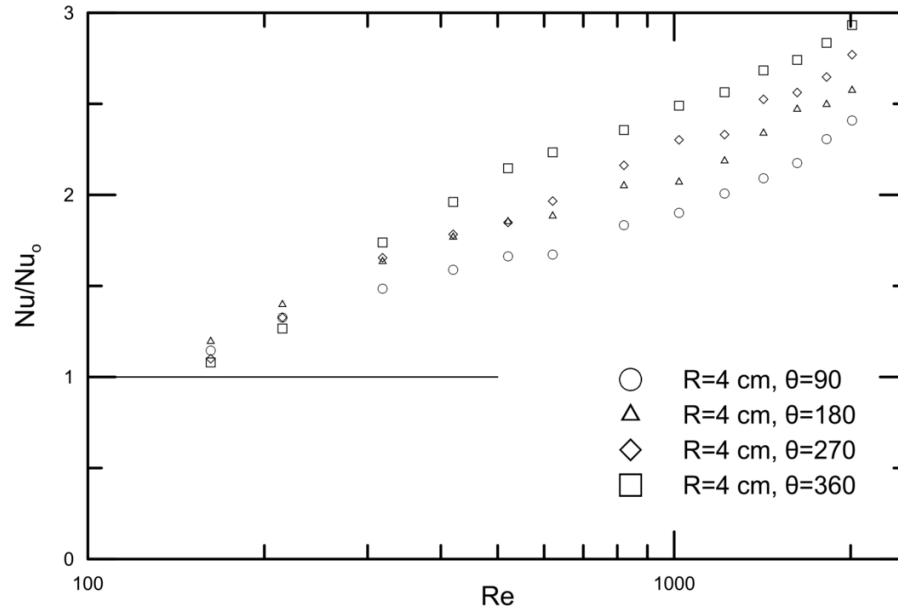


Figure 5.12: Normalized Reynolds analysis for different lengths for 0.65 cSt silicone oil with  $R=4$  cm

In order to examine the secondary effect on heat transfer enhancement, the Nusselt can be normalized according to the Nusselt for the straight tubing of the equivalent length ( $Nu/Nu_0$ ). Figs. 5.12 and 5.13 representing the results of this normalization. The trend is similar to what have been seen in Figs. 5.10 and 5.11, and they show that the longer curved tubing is required to allow the secondary flow becomes effective. From Figs. 5.12 and 5.13 one may conclude that for the shorter tubing, heat transfer enhancement is dominated by the entrance effect, however, further investigation is required for longer curved tubing which requires coiling the tubes.

$q^*$  versus  $L^*$  analysis can not be applied for a constant curvature and different lengths due to the definition of  $L^*$ , which contains the length, Reynolds number and Prandtl number. Consequently, a constant  $L^*$  with different lengths at a same curvature means the shorter duct should either have a higher Prandtl number working fluid, which is not the case, or higher Reynolds number. Hence, any observed augmentation for a

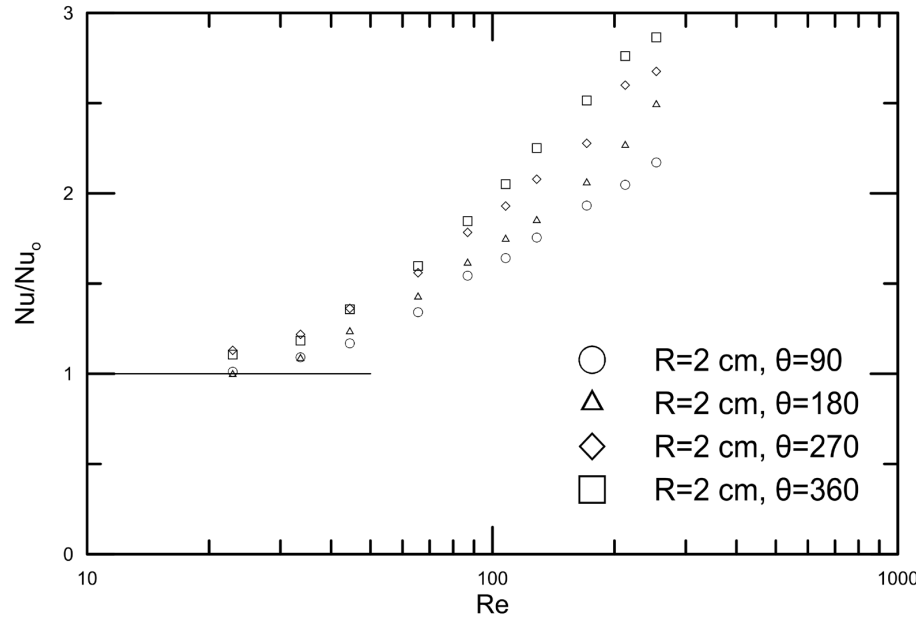


Figure 5.13: Normalized Reynolds analysis for different lengths for 3 cSt silicone oil with  $R=2$  cm

longer tube in comparison to a shorter one may be due the higher Reynolds number. The effect of Prandtl number on the augmentation is another important issue that should be investigated. Fig. 5.14 shows the dimensionless mean wall flux versus the dimensionless thermal length for the 2 cm radius. Examined fluids are water and silicone oils with different viscosities: 0.65 cSt, 1 cSt and 3 cSt. The comparison shows that the highest heat transfer augmentation is reached by using the water and the least viscous silicone oil which show the best enhancement. Water with the average Prandtl number of 5.5 shows the best enhancement, and it is followed by 0.65 cSt silicone oil with Prandtl number of 8.2. 1 cSt silicone oil with  $Pr = 13$  falls behind the 0.65 cSt silicone oil. Finally, 3 cSt silicone oil with  $Pr = 38$  shows the least heat transfer enhancement.

The augmentation decreases with increasing the viscosity. Hence, the less viscous the fluid is in curved tubing, the greater enhancement is reached. This difference

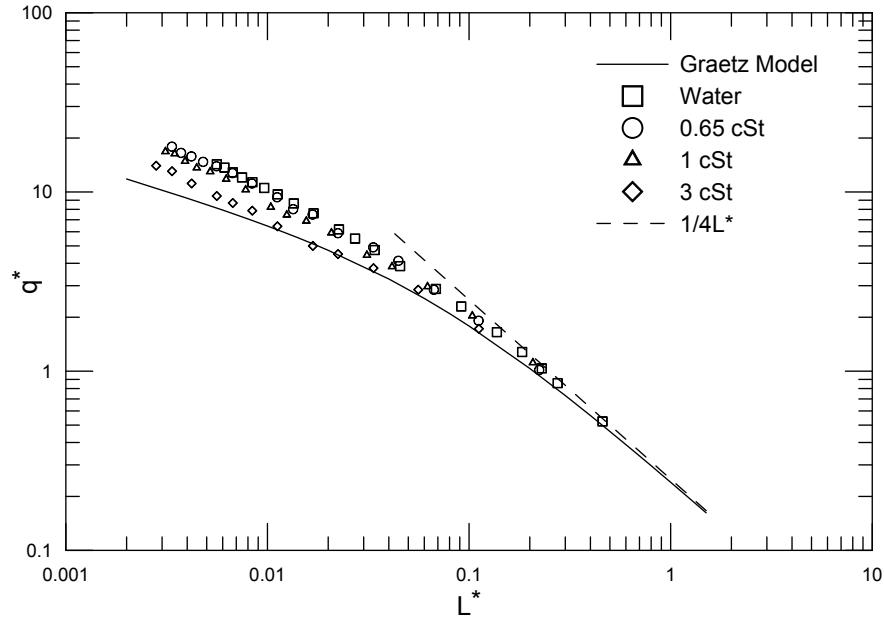


Figure 5.14: Viscosity effect on the curved tube with  $R=2$  cm and  $L=9.42$  cm

in the heat transfer augmentation becomes more noticeable by increasing the flow rate (smaller  $L^*$ ). The secondary flow initiation strongly depends on the viscosity of the working fluid, and the lower viscosity results in an increase in the intensity of the secondary flow which as discussed before is the main reason for the heat transfer augmentation.

Fig. 5.15 is another viscosity comparison inside the curved tubing with 8 cm radius. This curvature was the highest curvature we could examine in the constant temperature bath. The results for this geometry agree very well with the one at Fig. 5.14. Water shows the best heat transfer performance in increasing the heat transfer, and the enhancement decreases by increasing the Prandtl number.

## 5.5 Conclusion

Experimental studies have been done on the heat transfer inside short mini scale curved tubes at the constant wall temperature boundary condition. Water and three

low viscosity silicone oils were used to investigate the enhancement effect of curved tubing. The dimensionless mean wall flux and the dimensionless thermal length were used instead of conventional Nusselt number.

First, the Dravid model [29] was used to predict the heat transfer behavior for a constant wall temperature wall with good accuracy. The criteria for the Dean number and Prandtl number were checked to make sure that it is applicable under the current condition. The experimental results were predicted with 10 percent accuracy.

Second, the effect of curvature on the heat transfer was studied by examining the heat transfer in curved tubes with a constant length and different curvatures. It was observed that the heat transfer is increased by decreasing the radius of curvature (increasing the curvature). It was shown that short mini-scale curved tubes are capable of greater enhancing the heat transfer. It also has been shown that the augmentation is fairly constant for a constant length and Dean number. However, a higher Reynolds number is required when the curvature is smaller to have the same Dean number.

Third, a set of short curved tubes with constant curvature and different lengths were used to study the effect of length on augmentation. The experimental results reveal that increasing the length at the same curvature results in significantly increasing the total heat transfer. This means that the enhancement mechanism needs some length to become effective. The Nusselt analysis revealed more interesting results, showing that the entrance effect dominates the augmentation in short lengths, however the secondary flow effect becomes greater by increasing the curved tubing length. The normalized results which eliminated the entrance effect have shown that the enhancement is increased by increasing the length.

Finally, the effect of Prandtl number on the heat transfer was studied. Similar tests were conducted with different working fluids. It has been shown that fluids with lower Prandtl number, namely water and 0.65 cSt silicone oil, are able to enhance the

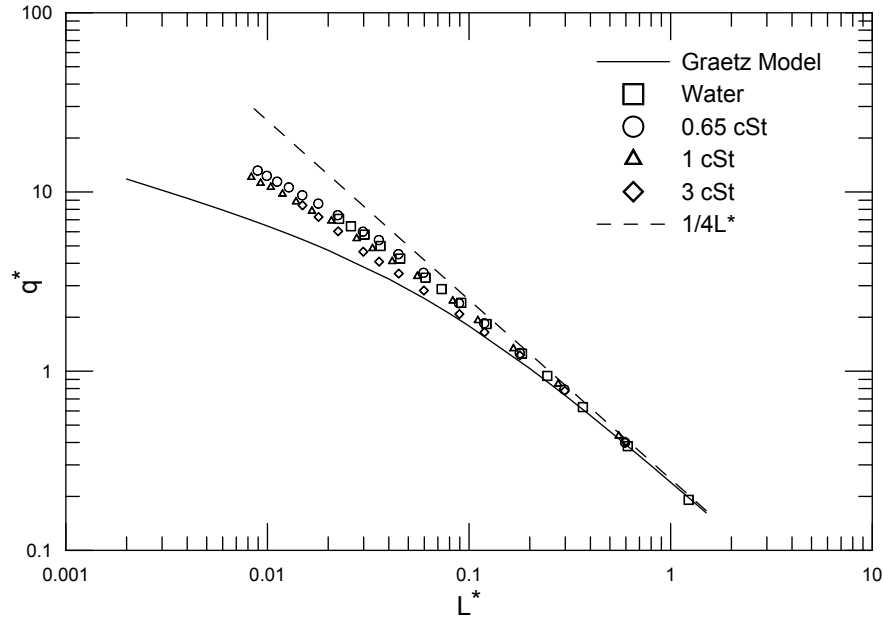


Figure 5.15: Viscosity effect on the curved tube with  $R=8$  cm and  $L=25.12$  cm

heat transfer better than the fluid with higher viscosity and Prandtl number. Further investigations on curved tubing are required to investigate the heat transfer enhancement inside the curved tubing with greater curvatures and lengths. Furthermore, as there is always a trade off between the heat transfer and pressure drop in a system, the same study for pressure drop is useful to find ways to minimize the pressure drop and maximize the heat transfer in a curved tubing system.

### Acknowledgement

The authors acknowledge the financial support of the Natural Sciences and Engineering Research Council of Canada (NSERC) and Auto 21 NCE.

## 5.6 References

- [1] J. Thompson, On the origin of windings of river and alluvial planes, with remarks on the flow of water round bends in pipes, *Proc. R. Soc. London. Ser. A*, 1 (1976).

- [2] G. S. Williams, C. W. Hubbell, G. H. Fenkell, On the effect of curvature on the flow of water pipes, *Trans. Am. Soc. Civ. Eng* 47 (1902).
- [3] J. H. Grindley, A. H. Gibson, On the frictional resistance of air through a pipe, *Proc. R. Soc. London, Ser. A*, 80, 114 47 (1902).
- [4] J. Eustice, Experiments of streamline motion in curved pipes, Lab on a Chip, *Proc. R. Soc. London, Ser. A*, 85, 119, (1911).
- [5] A. Boothroyd, Spiral heat exchanger", *Int. Enc. Of Heat Transfer*, G. Hewitt, Y. Pulezhaev, eds., CRC Press, New York (2005) 1044.
- [6] K. Chonwddury, H. Linkemeyer, M. Kh. Bassiouny, Analytical studies on the temperature distribution in spiral plate heat exchangers: straightforward design formulate for efficiency and mean temperature difference, *J. of Chemical Process* 29 (2008) 183-190.
- [7] L. C. Burmeister, Effectiveness of spiral-plate heat exchanger with equal capacitance rate, *J. of Heat Transfer* 128 (2010) 195-301.
- [8] I. Mudawar, M. Visarisa, Coiled-tube heat exchanger for high-pressure metal hybrid hydrogen storage systems- Part 1. Experimental study, *Int. J. of Heat and Mass Transfer* 55 (2012) 1782-1795.
- [9] I. Mudawar, M. Visarisa, Coiled-tube heat exchanger for high-pressure metal hybrid hydrogen storage systems- Part 2. Computational model, *Int. J. of Heat and Mass Transfer* 55 (2012) 1782-1795.
- [10] T. J. Rennie, Numerical and experimental studies of a double-pipe helical heat exchanger, *Ph.D. Thesis, McGill University, Montreal, Canada*, 2004.
- [11] V. Kumar, B. Faizee, M. Mridha, K. D. P. Nigam, Numerical studies of a tube-in tube helically coiled heat exchange, *Chem. Eng. Process* 47(12) (2008) 2287-229.
- [12] H. Shokouhmand , M.R. Salimpour, M.A. Akhavan-Behabadi, Experimental investigation of shell and coiled tube heat exchangers using Wilson plots, *Int. Comm.*

*in Heat and Mass Transfer* 35 (2011) 84-92.

[13] J. W. Rose, Wilson plot and accuracy of thermal measurements, *Exp. Thermal and Fluid Sci.* 28 (2004) 77-86.

[14] K. Nigam, S. Vashisth, V. Kumar, A review on the potential applications of curved geometries ion process industry, *Ind. Eng. Chem. Fund., Ind. Eng. Chem. Res.* 47 (2008) 3291-3337.

[15] W. R. Dean, Note on the motion of fluid in a curved pipe, *The London, Edinburgh and Dublin Philosophical Magazine and Journal of Science* 4 (1927) 208-223.

[16] W. R. Dean, The streamline flow through curved pipes, 6th International Conference on Multiphase flow, *The London, Edinburgh and Dublin Philosophical Magazine and Journal of Science* 5 (1928) 673-695.

[17] C. M. White, Streamline flow through curved pipes, *Proceedings of Royal Society of London, Series A: Mathematical and Physical Science* 123 (1929) 645-663.

[18] K. C. Cheng, M. Akiyama, Laminar forced convection heat transfer in curved rectangular channels, *Microfluid Nanofluid, J. of Heat Transfer* 13 (1970) 471-490.

[19] K. C. Cheng, M. Akiyama, Graetz problem in curved pipes with uniform wall heat flux, *Int. J. of Applied Science Re.* 29 (1974) 401-417.

[20] Y. Mori, Y. Uchida, T. Ukon, Forced convective heat transfer in a curved channel with a square cross section, *Int. J. of Heat and Mass Transfer* 14 (1971) 1787-1805.

[21] J. M. MacInnes, J. Ortiz-Osorio, P. J. Jordan, G. H. Priesman, R. W. K. Allen, Experimental demonstration of rotating spiral microchannel distillation, *Chemical Engineering Journal*, *Chemical Engineering Journal* (2010).

[22] X. Wang, X. Yin, C. Heyong, Microflow injection chemiluminescence system with spiral micro channel for the determination of cisplatin in human serum, *Analytical Chemical Acta* 678 (2) (2010) 135-139.

[23] J. Zhu, X. Xuan, lectrophoresis and dielectrophoresis in curved micro channels,

*J. of Colloid and Interface Science* 340 (2009) 285-290.

[24] S. Sarkar, A. Dalal, G. Biswas, Mixed convective heat transfer from two identical square cylinders in cross flow at  $Re = 100$ , *Int. J. of Heat and Mass Transfer* 53 (2010) 2628-2642.

[25] K. C. Cheng, R. C. Lin, J. W. Ou, Fully developed laminar flow in curved rectangular channels, *J. of Fluids Eng.* 98 (1976) 41-48.

[26] L. C. Burmeister, M. W. Egner, Heat transfer for laminar flow in spiral ducts of rectangular, *Trans. of the ASME* 127 (2005) 352-356.

[27] S. M. Hashemi, M. A. Akhavan-Behbahani, "An empirical study on heat transfer and pressure drop characteristics of CuO-base oil nanofluid flow in a horizontal helically coiled tube under constant flux", *Int. J. of Com. Heat and Mass Transfer* 14 (2012) 1787-1805.

[28] S. W. Chang, K. F. Chiang, J. K. Kao, Heat transfer and pressure drop in a square spiral channel roughened by in-line skew ribs", *Int. J. of Heat and Mass Transfer* 54 (2004) 3167-3178.

[29] A. N. Dravid, K. A. Smith, E. W., P. L. Brain, "Effect of secondary fluid motion flow heat transfer in helically coiled pipes", *J. AICHE* 17 No. 5 (1971) 1114-1122.

[30] Y. S. Muzychka, M. M. Yovanovich, "Laminar forced convection heat transfer in combined entry region of non-circular ducts", *J. of Heat Transfer* 126 (2004) 54-62.

# Chapter 6

## Pressure Drop in Mini-Scale Coiled Tubing\*

**M.Ghobadi and Y.S. Muzychka**

Microfluidics and Multiphase Flow Lab, Faculty of Engineering and Applied Science,  
Memorial University of Newfoundland, St. John's, NL, Canada, A1B 3X5

### **ABSTRACT**

In the present study, laminar, steady state flow in mini-scale coiled tubes was studied experimentally. Three different tube diameters: 1.59 mm, 1.27 mm and 1.016 mm with different lengths of 1 m and 0.5 m were coiled with different radius of curvature to provide data over a wide range of Reynolds numbers from 5 to 2300. An asymptotic model is developed based on the experimental results to predict the pressure drop increase based on Dean number. The results and simple model are also compared to a well-known existing model for circular tubing. The coiled tube lengths used in this study were long enough to consider the flow to be fully developed. The effects of varying curvature and tube length are also studied. The pitch of the coils is restricted to the diameter of the tube to minimize the effect of coiling. Dean number is used instead of Coiled number (modified Dean number) which allows the results to be expanded to spiral and curved tubing.

**Keywords:** Pressure Drop, Fanning Friction Factor, Dean Number, Curved Tubing

\* *Submitted to Experimental Thermal and Fluid Science*

## 6.1 Introduction

Coiled tubing finds application in oil pipeline systems, heat exchangers, steam generators, chemical plants, etc, because of the practical importance of their high efficiency in heat transfer, compactness in structure, eases of manufacture and arrangement. Curved geometry is one of the passive heat transfer enhancement methods that fits several heat transfer applications. Secondary flow is created in curved geometry which enhances the radial fluid transport and consequently heat transfer. However, as the existing boundary layer is disturbed, pressure drop also increases in passive techniques. Consequently, their net effectiveness depends upon the balance between the increase in pump power and the increase in heat transfer.

Unlike flow in straight pipes, fluid motion in a curved pipe is not parallel to the curved axis of the bend, owing to the presence of a secondary flows caused by the curvature of the duct. As the flow enters a curved duct, centrifugal forces act outward from the center of curvature on the fluid elements. Pressure gradients parallel to the axis of symmetry are almost uniform along lines normal to that of the symmetry axis. Because of the no-slip condition at the wall, the axial velocity in the core region is much greater than that near the wall. To maintain the momentum balance between the centrifugal forces and pressure gradient, slower moving fluid elements move toward the inner wall of the curved tube. This leads to the onset of a secondary flow such that fluid near the wall moves along upper and lower halves of the curved duct while fluid far from it flows to the outer wall.

Early investigations on curved geometries were conducted by Thomson [1], Williams [2], Grindley and Gibson [3] and Eustic [4]. The idea of using spiral geometry was first

used in spiral plate heat exchangers in late 19th century [5] and further investigations conducted in the 1930s in Sweden [6, 7].

Dean [8, 9] conducted the first analytical studies of fully developed laminar flow in a curved tube of circular cross section. He developed a series solution as a perturbation of the Poiseuille flow in a straight pipe for low values of Dean number ( $De < 17$ ). He reported that the relation between pressure gradient and the rate of flow is not dependent on the curvature to the first approximation. In order to show its dependence, he modified the analysis by including the higher-order terms and was able to show that reduction in flow due to curvature depends on a single variable (now known as the Dean number), equal to  $Re\sqrt{(D/2R)}$  (where  $Re$  is the Reynolds number,  $D$  is the tube diameter, and  $R$  is the radius of curvature of the curved tube using Dean's notation). Various other authors have used different definitions of the Dean number for curved tube studies. It was reported that for low Dean numbers, the axial-velocity profile was parabolic and unaltered from the fully developed straight tube flow. As the Dean number is increased, the maximum velocity begins to be skewed toward the outer periphery. Similarly, for large values of curvature ratio,  $D/2R$ , the secondary flow intensity is very high while for small values of the curvature ratio the secondary flow intensity is much less [10].

White [11] numerically studied the pressure drop through a coil of constant curvature. A complete investigation on heat transfer has been provided by Akiyama and Cheng [12, 13] on curved rectangular channels and curved pipes with uniform heat flux and a peripherally uniform wall temperature. Using a numerical method, they found solutions up to a reasonably high Dean number for different aspect ratios. They also showed that the perturbation method is only applicable for a relatively low Dean number region and a boundary-layer technique is valid only for high Dean number regime. The effect of Dean number on velocity and temperature field was also studied

in their work.

Cheng [12] reported that the number of the vortices inside a curved channel depend on the Dean number. Two vortices have been reported for  $De < 100$ , whereas for  $100 < De < 500$ , four vortices appear in a square curved channel. These extra vortices vanish at about  $De \approx 500$ . The channel aspect ratio determines the exact value of the disappearance.

Mori et al. [14] studied the effect of viscosity and secondary flow. At the central part of the flow passage, when the intensity of the secondary flow is strong, it is possible to neglect the affect of the viscosity and heat conduction compared with a stress analogous to the Reynolds stress and heat convection due to the secondary flow components. According to their paper, the effect of the viscosity and heat conduction are confined within a thin layer along a wall of the passage, where the intensity of the secondary flow is weakened. They proved that because of this effect one can consider the existence of the boundary layer along the wall of the passage for a flow which is strongly affected by the secondary flow. They divided the flow and temperature fields in their curved channel into two regions: i) the core region about the central part of the passage where the effect of the secondary flow is dominant over viscosity and ii) the boundary layer region along the wall where the effect of the viscosity and heat conduction cannot be ignored. They proved the existence of such a boundary layer experimentally. Their method is also applicable to non-circular cross sections as well as circular cross sections.

Nigam [15] accomplished a comprehensive review on the papers related to the application of curved geometry in the process industry up to 2008. The primary objective of their work is to provide an overview of the perspective on evolution of curved tube technology and introduction to a new class of curved tubes. The paper is divided into four parts. The first part discusses the fundamentals involved in enhancing the mixing

performance and local phenomena in curved tubes to better understand how mixing and heat and mass transfer proceed for single-phase flow. In the second part, the chemistry of two-phase flow in curved tubes is discussed and reported. Both the first and second parts also review the well established models available for pressure drop, heat transfer, mixing, and mass-transfer in the curved tubes. Methods for estimating the performance of curved tubes from experimental data, empirical correlations, and computational fluid dynamics are also discussed. The third part discusses the development of a new class of curved chaotic geometries (bent coils) as a course of technological development. The hydrodynamics, heat transfer, and mass-transfer performance in curved chaotic configurations have been discussed and compared against curved tubes.

Hashemi and Akhavan-Behabadi [16] experimentally investigated the heat transfer and pressure drop characteristics of nanofluid flow inside horizontal helical tube under constant flux. They studied effect of different parameters such as Reynolds number, fluid temperature and nanofluid particle weight concentration on heat transfer coefficient and pressure drop of the flow. Akhavan-Behabadi et al. [17] conducted another experimental study using a double-pipe counter flow heat exchanger with engine oil as working fluid inside the internal copper tube. They used saturated steam for heating the oil to achieve a constant wall temperature condition.

Chang et al. [18] conducted an experimental study that examines the detailed Nusselt number (Nu) distributions, pressure drop coefficients ( $f$ ) and thermal performance factor (TPF) for a square spiral channel with two opposite end walls roughened by in-line 45 degree ribs.

Abassi et al. [19] experimentally and numerically studied the pressure drop and convective heat transfer behavior of nano fluid in laminar, steady state flow in helically coiled tube at a constant wall temperature. They designed a heat exchanger capable

of providing constant wall temperature for coils. The numerical study was carried out with three dimensional governing equations. However, using constant effective properties, the difference between numerical and experimental results was significant. They used a dispersion model to make this difference negligible.

Manlapaz and Churchill [20] studied steady, fully developed, laminar flow of an incompressible fluid through a helically coiled tube of finite pitch. They reviewed available experimental data and theoretical predictions and recommended using a piecewise correlation for the Fanning friction factor ratio. Their correlation is also compared to the experimental results. However, good agreement is not observed.

Austin and Soliman [21] showed that the pitch changes affect the low Reynolds flow more than high Reynolds flow. Yamamoto et al. [22,23] showed that at a constant  $R/a$ , the friction factor deviates from that of the torodial curved tube as torsion due to the pitch decreases toward that of the straight tube as torsion further increases. Yamamoto et al. [24] studied the secondary flow structure and stability of flow in a helical pipe with large torsion by using a numerical calculation of a fluid particle trajectory. They found an acceptable agreement with the existing experimental results.

Grundman [25] presented a practical friction diagram of helically coiled tube, which accounts for the effect of curvature ratios. Takahashi and Momazaki [26] experimentally measured the pressure drop of mercury flow inside a helical coil tube and showed that the pressure drop was almost the same as the pressure drop of the mercury flow in a straight tube.

## 6.2 Experimental Setup

This paper mainly focuses on studying the pressure drop inside mini-scale coiled plastic tubing. Tygon flexible plastic tubes from Saint-Gobain Co. in 1 m and 0.5 m

length were cut and coiled in different radii of curvature. Table 6.1 shows the ID and OD of tubes which were employed. Five radii of curvature were used to investigate different curvatures,  $1/R$ , and diameter to radius of curvature ratio  $D/2R$ . The tubes were coiled and glued around cylinders with radii of 8.15 mm, 10.625, 12.125 mm and 14.175 mm. A cylinder with radius of curvature of 36 mm was also used only for the tube with diameter of 1.59 mm and 1 m length. For each of these radius of curvature we also added the tube diameter to the nominal radius of curvature of the cylinders to calculate the Dean number. The tubes wall was firm enough due to the large thickness to remain circular while they were coiled.

Critical Reynolds number for transition to turbulent flow is discussed and checked to assure the flow is laminar in all of the experiments. Two pressure sensors with pressure ranges of 0-1 psi and 0-5 psi were used to obtain accurate results. Data were used to calculate the Fanning friction factor. An empirical correlation is proposed to calculate the Fanning friction factor ratio in comparison to straight tubes,  $f_c/f_s$ .

Table 6.1: Tubing outer and Inside Diameter

Number	Outer Diameter	Inside Diameter
1	1.59 mm	3.175 mm
2	1.27 mm	2.286 mm
3	1.016 mm	1.778 mm

Fig. 6.1 shows the configuration of the system used to measure friction factors. The working fluid was pushed through the coils with different flow rates and consequently different Reynolds numbers. Depending on the flow rate, two or four syringes (Hamilton Glass Gas Tight) were filled with the test fluid, and the pumps (Harvard Pump 33) were set to the desirable flow rate. Each syringe can hold 100 ml; hence total 400 ml of the working fluid was available for each run of the experiment. The flow from

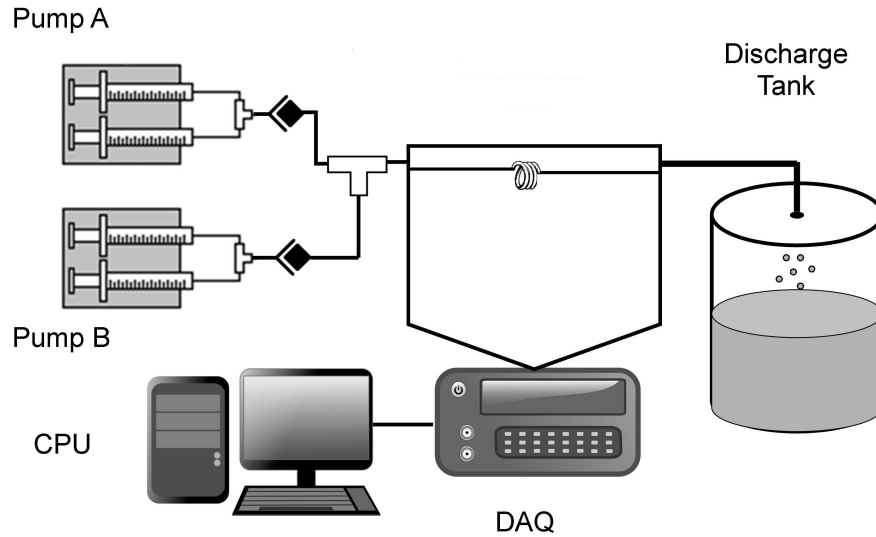


Figure 6.1: Experimental Setup

four syringes merged together and flow into the coiled plastic tubing. The accuracy of the pumping system was benchmarked by collecting the pumped fluid and weighing it in a time period. The uncertainty of the pumping system was found to be less than 1%.

Water was used for most of the experiments, whereas, 3 cSt silicone oil was used for shorter coils to make the pressure drop measurement easier and more precise. Room temperature was measured consistently, and the fluid properties were updated based on the room (bulk) temperature. We measured the viscosities of the 3 cSt silicone oil and water with an accurate apparatus (Physica MCR 301 from Rheosys Company) at the room temperature to confirm the reported data. The data were found to be inside the 5% range of the reported data.

In order to assure the accuracy of the experiments a benchmarking test was first done with a straight tube that we could predict the pressure drop with the well-known Darcy-Weisbach equation. Fig. 6.2 depicts the pressure drop benchmarking test results. The pressure drop test was performed on a straight tube with 1.59 mm

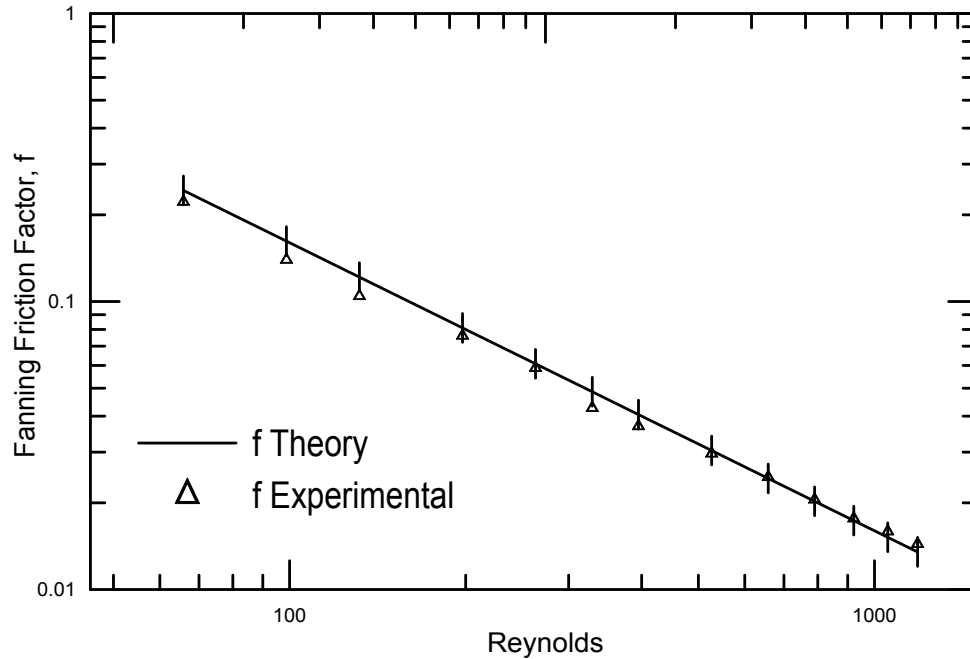


Figure 6.2: Benchmarking results for a straight tube, with error bars represent  $\pm 10\%$

diameter and 314 cm length. The main purpose of benchmarking tests is to determine the uncertainty of our apparatus used for the measurements. Friction factor is plotted versus Reynolds number.

Three different sensors have been used to accomplish the tests according to the pressure drop range, which was measured. 10 readings for each pressure drop were collected to assure that there is no noise effect on the readings. The sensors were attached as near as possible to the coiled tubes, and were calibrated before each run. The experimental results are compared with Darcy-Weisbach equation for laminar flow in straight tubing. The uncertainty of the pressure gauges are 1 percent of the full scale. Using the Kline and McClintock method [27], the uncertainty of the friction factor measurements was found to be between 1.29 – 5.09%.

### 6.3 Data Analysis

As discussed before, the Dean number accounts the secondary flow in a curved tube and introduced as:

$$De = Re\sqrt{\frac{D}{2R}} \quad (6.1)$$

In a helical coil, the effective radius of curvature  $R_c$  of each turn is influenced by the coil pitch  $b$ , and is given by:

$$R_c = R \left[ 1 + \left( \frac{b}{2\pi R} \right)^2 \right] \quad (6.2)$$

Use of  $R_c$  instead of  $R$  in Dean number definition results in a new number, referred to as a helical coil number  $He$ , defined as:

$$He = Re\sqrt{\frac{D}{2R_c}} = De \left[ 1 + \left( \frac{b}{2\pi R} \right)^2 \right]^{-1/2} \quad (6.3)$$

In all the experimental tests reported in this paper, the pitch was minimized to the external diameter of the copper tubing. Hence, the effective radius  $R_c$  mostly affects the tube with the lowest curvature:

$$R_c = R \left[ 1 + \left( \frac{0.0016}{2\pi \cdot 0.00875} \right)^2 \right] = 1.00085R \quad (6.4)$$

which can be neglected. So for this study we use the Dean number instead of Helical number. So the results presented in this paper can be also used in spiral geometries. Another important criterion for internal flows is the critical Reynolds number. A transition from laminar to turbulent flow is identified by critical Reynolds number,  $Re_{crit}$ . In curved duct flows, it is difficult to identify  $Re_{crit}$  by a change in the slope of the curve for friction factor versus Reynolds number, because of the gradual change.

However Holland et al. [28] recommended the following correlation for design purposes:

$$Re_{crit} = 2100 \left[ 1 + 12 \left( \frac{R}{D} \right)^{-0.5} \right] \quad (6.5)$$

The lowest  $Re_{crit}$  which can be used in our experiments can be expressed as:

$$Re_{crit} = 2100 \left[ 1 + 12 \left( \frac{0.01475}{0.00105} \right)^{-0.5} \right] = 8,823 \quad (6.6)$$

which indicates that in the present work transition to turbulent flow doesn't happen until the Reynolds number is almost four times greater than the critical Reynolds for straight tubes. Since all of our results are at  $Re < 2200$ , we can consider the results to be in the laminar region.

Most of the available correlations for coiled tubes are based on the ratio of the friction factor for curve tubing relative to the friction factor for straight tubes,  $f_c/f_s$ . Using a regression analysis, Manlapaz and Churchill [20] recommended a correlation for the fully developed laminar flow in a helical coiled tube of finite pitch. They reviewed the available experimental data and theoretical predictions of coiled tubing with zero pitch, and proposed the following correlation:

$$\frac{f_c}{f_s} = \sqrt{\left( 1.0 - \frac{0.18}{[1 + (35/De)^2]^{0.5}} \right)^m + \left( \frac{De}{88.33} \right) \left( 1 + \frac{D/R}{3} \right)^2} \quad (6.7)$$

where  $m=2$  for  $De < 20$ ,  $m=1$  for  $20 < De < 40$ , and  $m=0$  for  $De > 40$ . The correlation is valid when  $2R/D > 7$ . In the present study  $10 < 2R/D < 45$ , and the correlation can be applied. We used this correlation to compare with the experimental results at mini scale, and the proposed correlation.

## 6.4 Results and Discussion

In this section we consider the new data obtained for mini-scale coiled tubing. Different range of Reynolds numbers and Dean numbers are covered in this study. Table 6.2 summarizes the range for Reynolds number and Dean number, for the different tube diameters and curvatures examined. Since the length doesn't affect Reynolds number and Dean number at a constant flow rate, the range for dimensionless number is given for each tube diameter. The Reynolds number depends on the velocity, diameter, and viscosity, and changes noticeably by changing the flow rate, and consequently the flow velocity, and it is independent of curvature. Thus, for a liquid at the same flow rate, the Reynolds number is the same for different curvatures. However, the Dean number is proportional to the channel curvature and changes when changing both flow rate and curvature.

Table 6.2: Tubing outer and Inside Diameter

Tube Diameter [mm]	$Re$	Radii[mm]	$De$
1.59	60 – 2200	8.15	20 – 700
		10.63	17 – 600
		12.13	16 – 500
		14.18	14 – 460
		36	20 – 270
1.27	50 – 1900	8.15	13 – 500
		10.63	11.7 – 450
		12.13	11 – 420
		14.18	10 – 370
1.016	40 – 110	8.15	10 – 260
		10.63	9 – 230
		12.13	8 – 215
		14.18	7 – 295

We use Fanning friction factor-Reynolds number product,  $(f_c Re)$  for the pressure

drop presentation. First,  $f_c Re$  for one mini tube with a constant length and different radius of curvature are presented. Later, the results are plotted versus Dean number to normalize them based on the curvature. The proposed correlation is then used to predict the results and comparisons with the Manlapaz and Churchill [20] model are made.

Fig. 6.3 presents the experimental results for the coil tubes with 1.016 mm diameter and 0.5 m length. The plot shows  $f_c Re$  versus Reynolds number to depict the effect of curvature on the Fanning friction factor. Different radii of curvature are depicted:  $R=8.15$  mm,  $R=10.625$  mm,  $R=12.125$  mm and  $R=14.74$  mm. The  $f_c Re$  for straight tubes is also plotted to show the pressure drop increase in coil tubes.  $f_s Re$  remains constant,  $f_s Re = 16$ , for any Reynolds number, because Fanning friction is defined as  $16/Re$  for laminar flows. Obviously, increasing curvature,  $1/R$ , causes an increase in the pressure drop for all of the coiled tubes. The maximum pressure drop is achieved using the coiled tubing with the largest curvature, i.e. when  $R=8.15$  mm, and is followed by  $R=10.625$  mm, etc. Coiled tubes with  $R=12.125$  mm and  $R=14.75$  show the least pressure drop gain. Increasing the curvature intensifies the secondary flow and has been proved to increase heat and mass transfer. However, the additional momentum transport causes the pressure drop increase.

It has been observed that for Dean numbers less than  $De < 5$ , the pressure drop is close to the pressure drop inside straight tubes of equivalent length. In order to predict such behaviour, one may employ an asymptotic correlation to account the curvature effect on high Dean fluid flow, and neglect the curvature effect on low Dean number fluid flow.

Figs. 6.4, 6.5, 6.6 and 6.7 show the pressure drop increase due to the curvature effect for different tube diameters and lengths. Figs. 6.4 and 6.5 illustrate the pressure drop increase of the flow inside a tube having 1.27 mm diameter and 1 m and 0.5 m

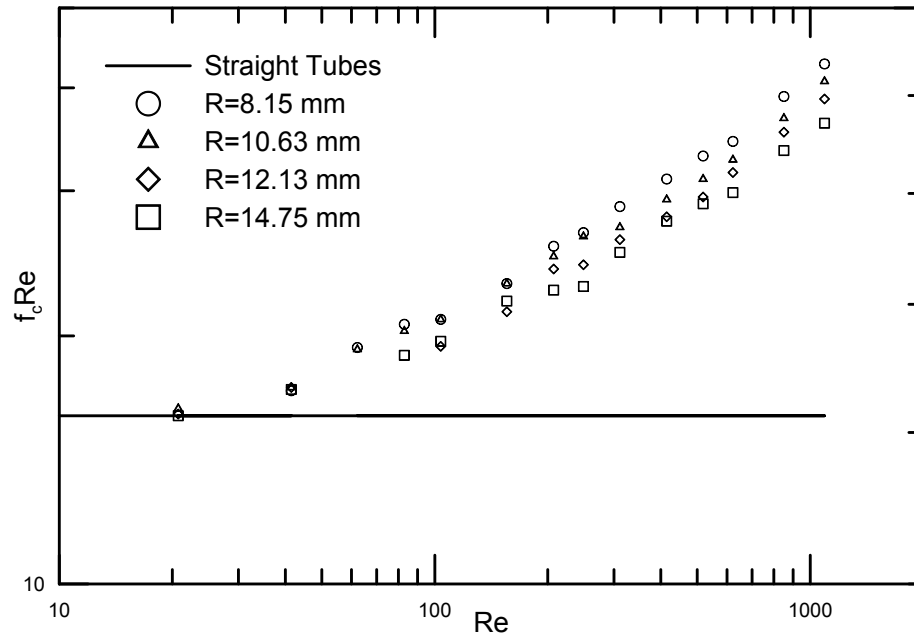


Figure 6.3:  $f_c Re$  vs  $Re$  for 1.016 mm tube diameter and 0.5 m length

length respectively. At a constant Reynolds number, the tube with the least radius of curvature, i.e.  $R = 8.15$  mm, shows the most pressure drop and the least pressure drop is achieved with the tube having the maximum radius of curvature, i.e.  $R = 14.75$  mm.

Figs. 6.6 and 6.7 depict the pressure drop results for coiled tubes having 1.59 mm diameter with 1 m and 0.5 m length, respectively. Besides the tube curvatures used in Figs. 6.3 and 6.4,  $R = 36$  mm is also used for the 1 m length to show how the pressure drop decreases at a same Dean number using a significantly lower curvature  $1/R$ . Similar behaviour is also observed for Figures 6.6 and 6.7 and curvature is found to increase the pressure drop in comparison to straight tubes.

The results are also presented against Dean number instead of Reynolds. We expected that the pressure drop at a constant Dean number should be the same regardless of its curvature. However, reducing the curvature  $1/R$  indicates that higher flow rate

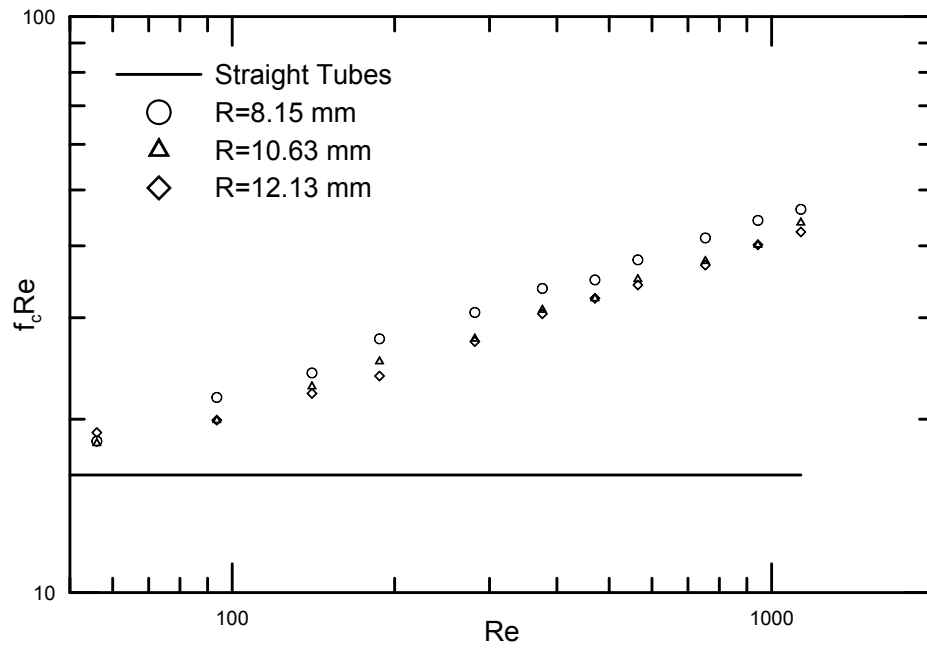


Figure 6.4:  $f_c Re$  vs  $Re$  for 1.27 mm tube diameter and 1 m length

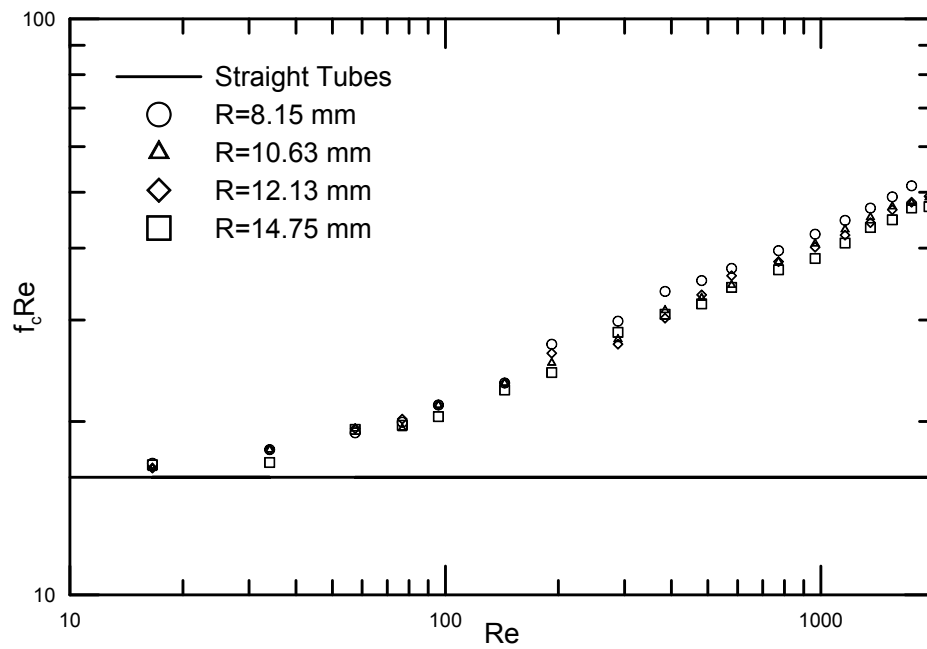


Figure 6.5:  $f_c Re$  vs  $Re$  for 1.27 mm tube diameter and 0.5 m length

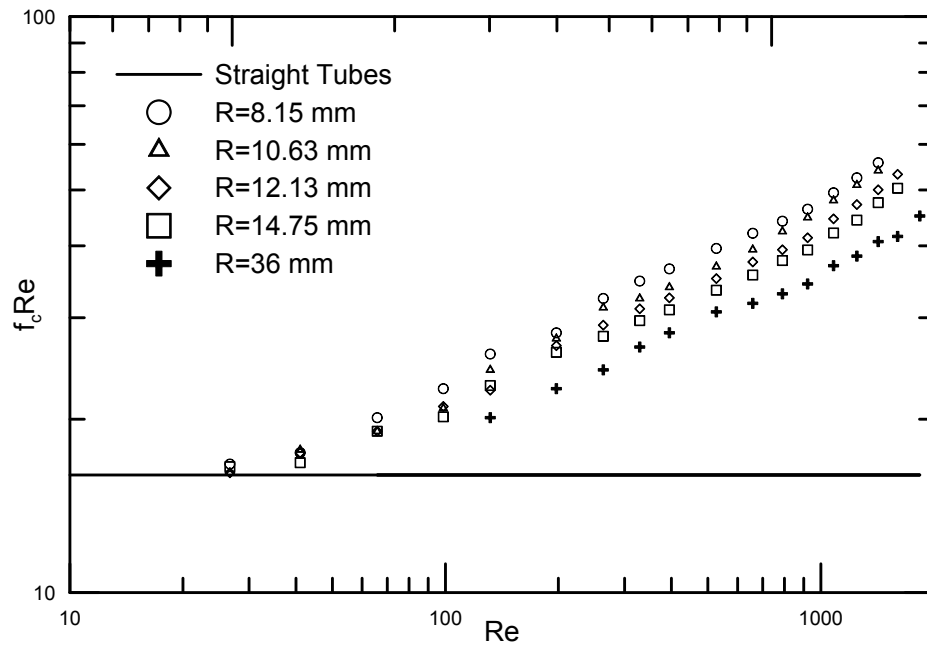


Figure 6.6:  $f_c Re$  vs  $Re$  for 1.59 mm tube diameter and 1 m length

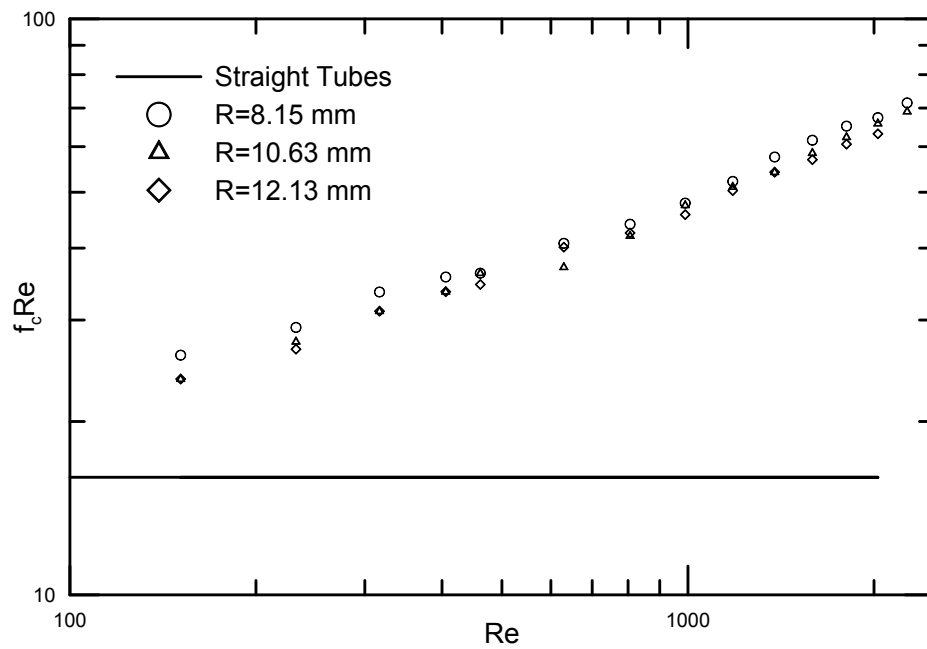


Figure 6.7:  $f_c Re$  vs  $Re$  for 1.59 mm tube diameter and 0.5 m length

(Reynolds number) is required to achieve the same Dean number. Reviewing the collected experimental results, we observed that the flow inside curved tubes can be divided to three main regions: low Dean number flow  $De < 5$ , high Dean number flows  $De > 50$ , and transition flow  $5 < De < 50$ . It was found that the pressure drop for flow with  $De < 5$  is identical to the pressure drop of the flow in straight tubes. For the high Dean number flows, based on the collected results, we were able to develop a simple empirical prediction for the friction factor ratio in curved and coiled tubes with small pitches for fully developed flows. Employing an empirical approach and using an algebraic expression of the form:

$$\frac{f_c}{f_s} = CDe^m \quad (6.8)$$

Finding the constants, C and m, based on the results for high number flows, the following friction factor ratio correlation is obtained:

$$\frac{f_c}{f_s} = 0.45De^{1/3} \quad (6.9)$$

where  $f_c$  is the curved tubes friction factor, and  $f_s$  is the straight tubes friction factor. Consequently, the following asymptotes are found:

$$\frac{f_c}{f_s} = \begin{cases} 1 & \text{if } De < 5 \\ 0.45De^{1/3} & \text{if } De \geq 50 \end{cases} \quad (6.10)$$

The two asymptotes can be blended as:

$$\frac{f_c}{f_s} = \left[ 1 + \left( 0.45De^{1/3} \right)^n \right]^{1/n} \quad (6.11)$$

Finally, using the results in the transition flow, the power was found as  $n = 5$ , and the following correlation is proposed to calculate friction factor ratio:

$$\frac{f_c}{f_s} = \left[ 1 + \left( 0.45De^{1/3} \right)^5 \right]^{1/5} \quad (6.12)$$

The validity of the correlation is examined for Dean numbers up to 700 based on the present experimental results.

Most of the results for the pressure drop are presented in the form of  $fRe$ . The friction factor for curved tubes can be written as:

$$f_c \times Re = 16 \left[ 1 + \left( 0.45De^{1/3} \right)^5 \right]^{1/5} \quad (6.13)$$

The presented results versus the Dean number can be compared to the proposed correlation and the model of Manlapaz and Churchill [20]. Comparing the two models, it can be observed that the Manlapaz and Churchill model [20] is the function of Dean number and  $D/R$ , whereas, the presented model is only the function of Dean number. Fig. 6.8 depicts the Manlapaz-Churchill [20] correlation for different  $D/R$  that has been used for the first set of results that will be presented. It can be seen that the Manlapaz and Churchill model is a weak function of  $D/R$  in the range of one millimeter. Hence, instead of using separate lines to present the Manlapaz and Churchill correlation [20], only one line will be depicted for all  $D/R$ . Later, it can be observed that this simplification is negligible in comparison to the deviation the model shows from the collected results.

Fig. 6.9 illustrates  $f_c Re$  versus Dean number for coiled tubes having 1.016 mm diameter and 0.5 m length. The  $f_c Re$  for different radii of curvature of  $R=8.15$  mm, 10.625 mm, 12.125 mm and 14.75 mm are plotted versus Dean number to show what happens for coiled tubes with different curvatures, but a same Dean number, having different Reynolds. It has been observed that pressure drop is fairly similar for coiled tubes with a similar Dean number.

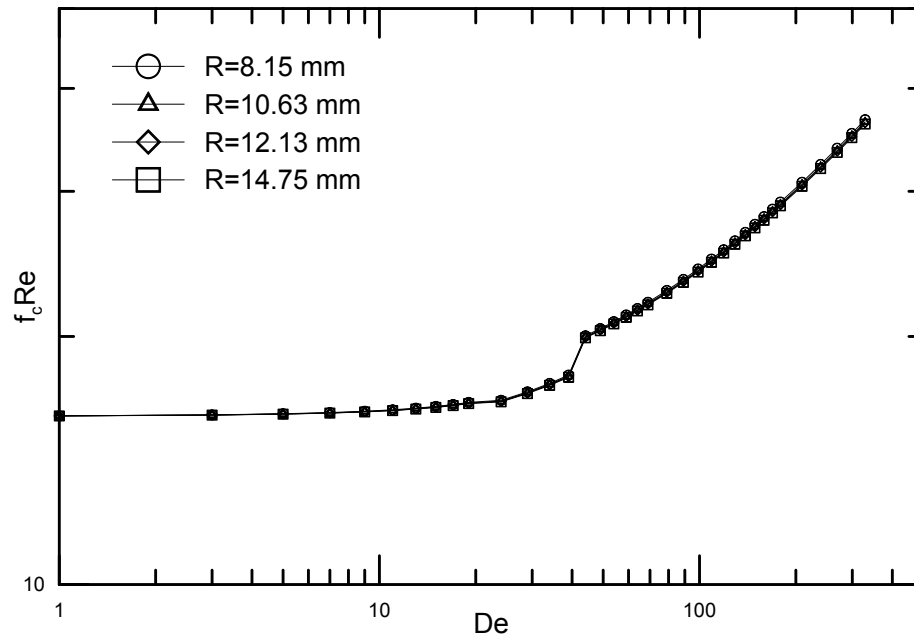


Figure 6.8: Manlapaz-Churchill correlation for different  $D/R$  ratios

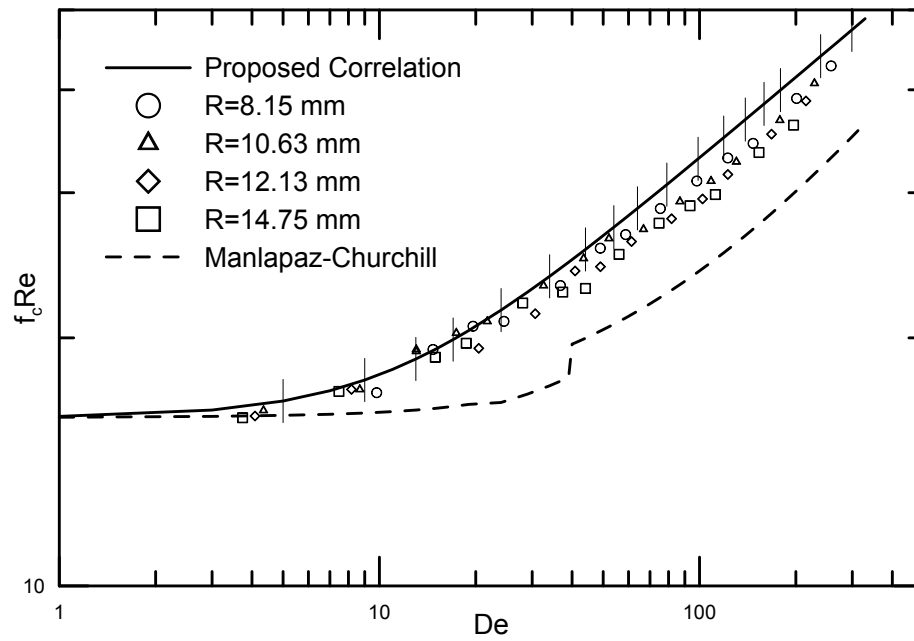


Figure 6.9:  $f_c Re$  vs  $De$  for 1.016 mm tube diameter and 0.5 m length

The continuous line depicts the proposed model for the friction factor ratio prediction. It was found that the pressure drop results follow two asymptotic line: one that approaches  $f_c Re = 16$ , the same as the flow in straight tubes, and another asymptote is  $f_c Re = 16 \times 0.45 De^{1/3}$ . The flows between  $5 < De < 50$  are found to show a transitional behaviour. Hence, combining the two models using the asymptotic correlation method,  $n = 5$  was found to predict the transitional results with the best accuracy. The correlation is found to predict the experimental results in mini scale with rms error range of 1 – 19 percent and the average of 5 percent. The maximum deviation was found to be 10 percent. The dashed line shows the Manlapaz-Churchill [20] model which was introduced earlier. Their correlation predicts  $f_c Re$  in low Dean numbers,  $De < 5$ , similar to the proposed correlation, whereas, it is unable to predict the friction factor in higher Dean number flows, and in the transition from low Dean flows to high Dean flows.

Figs. 6.10 and 6.11 show the proposed correlation prediction for coiled tubes having 1.27 mm diameter, and 1 m and 0.5 m length. A better agreement in comparison to the results for 1.016 is observed. The experimental results are predicted with the average of less than 5 percent rms error by using the proposed correlation, whereas, the Manlapaz-Churchill [20] model is unable to predict the present experimental results. It can also be observed that for high Dean number flows the proposed model predict the results better than the Manlapaz-Churchill [20] model.

Figs. 6.12 and 6.13 show the results for coiled tubes created by employing 1.59 mm tubes with 1 m and 0.5 m length shaped for different radii of curvature. The proposed model predicts the friction factor with less than 5 percent error in this condition, and we were also able to measure  $f_c Re \approx 16$  for  $De \approx 5$ . Whereas, for the 0.5 m long tube, it was hard to obtain the points in the transition and low Dean number flows. Fig. 6.14 shows all the experimental results in the form of  $f_c Re$  versus Dean number.

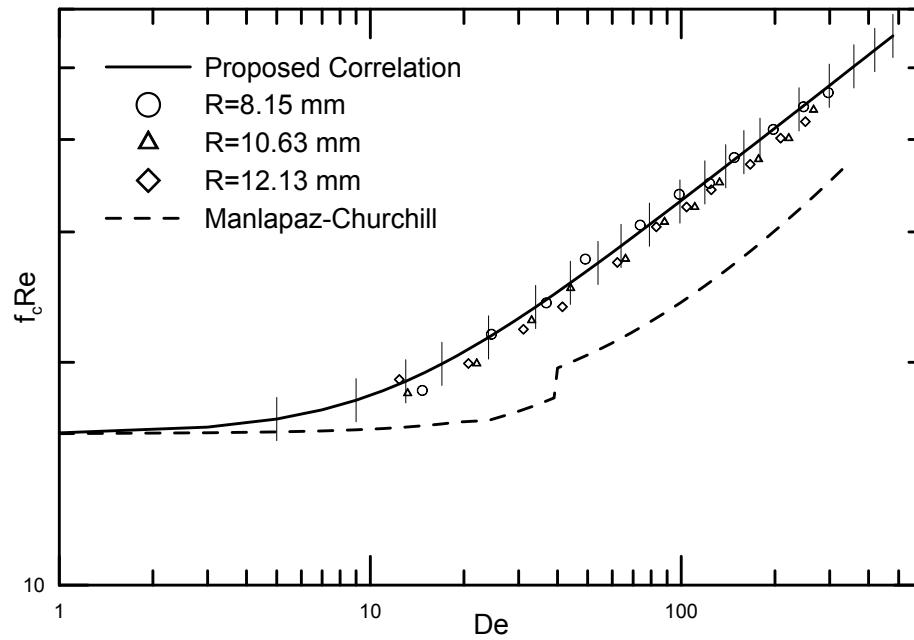


Figure 6.10:  $f_c Re$  vs  $De$  for 1.27 mm tube diameter and 1 m length

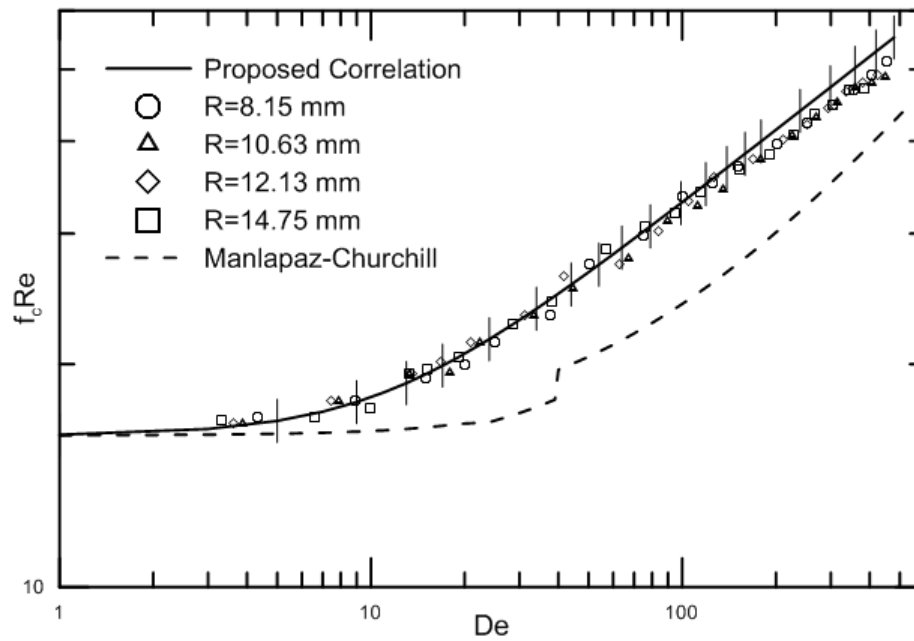


Figure 6.11:  $f_c Re$  vs  $De$  for 1.27 mm tube diameter and 0.5 m length

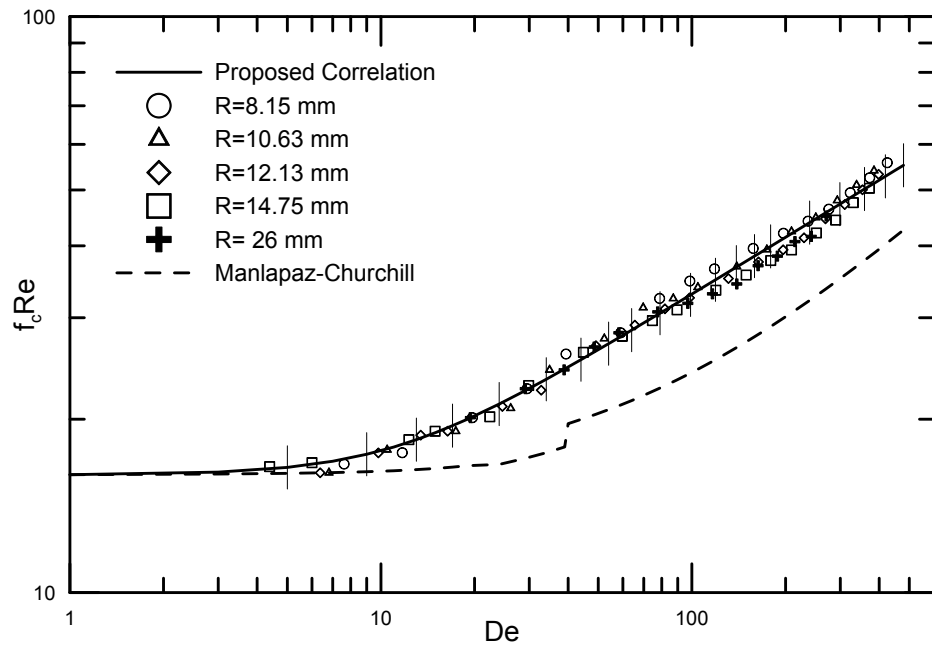


Figure 6.12:  $f_c Re$  vs  $De$  for 1.59 mm tube diameter and 1 m length

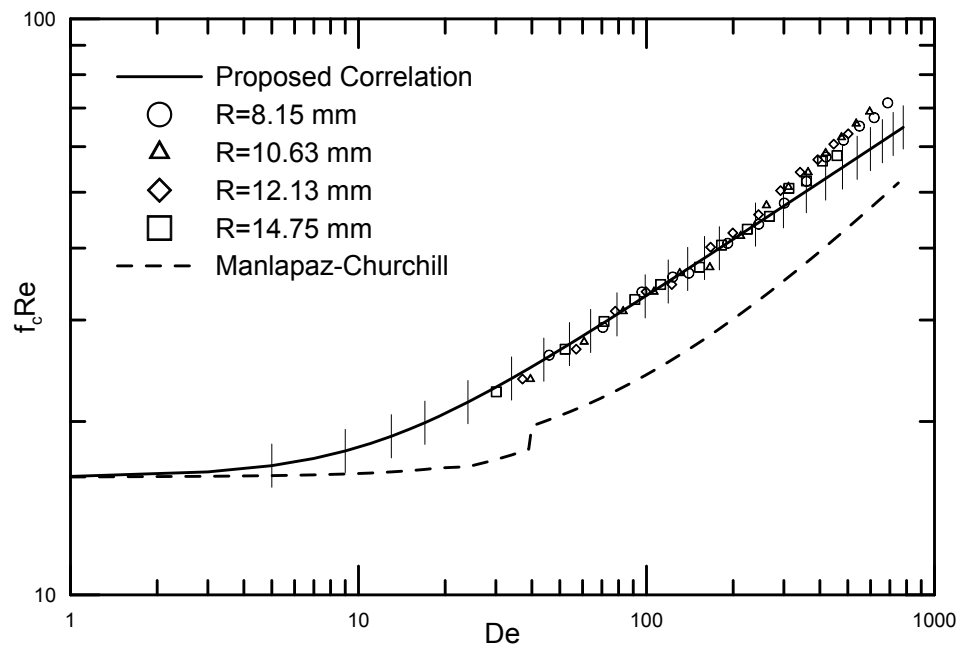


Figure 6.13:  $f_c Re$  vs  $De$  for 1.59 mm tube diameter and 0.5 m length

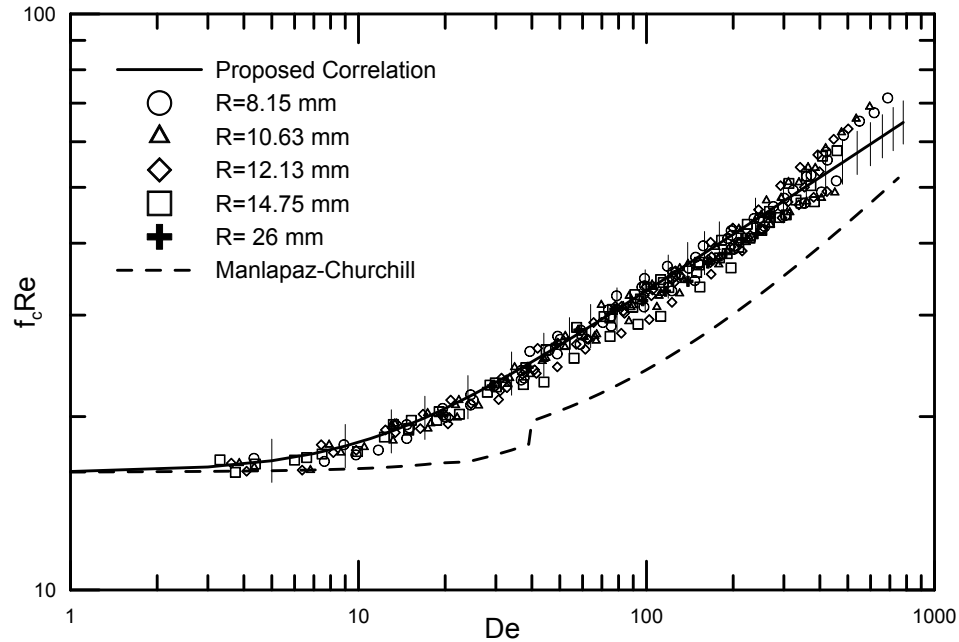


Figure 6.14:  $f_c Re$  vs  $De$  for all of the experimental results

The proposed model and Manlapaz-Churchill [20] model are depicted to predict the results as well. It can be seen that the results follow the trend of the proposed model, and good agreement is observed between the proposed model and the measured results.

## 6.5 Conclusion

Using curved tubes as a passive heat transfer enhancement is attractive in many industries, however, the increased pressure drop is recognized as the main drawback for the systems employing curved tubes. Experimental studies have been conducted on the pressure drop inside mini scale coiled tubes. Plastic tubes with three different mini scale diameter were cut in 1 m and 0.5 m lengths and were coiled around the cylinder with different radius of curvature. A wide range of Reynolds numbers, 40-220, and Dean numbers, 7-560, were studied.

It was shown that the curved tubes increase the pressure drop in comparison to straight tubes. It has also been shown that the pressure drop for the flow inside the tubes with greater curvature  $1/R$  is larger than for flow inside less curved tubes as expected.

Based on the present experimental results, we found that flows with low Dean number,  $De < 5$ , behave the same as flows inside straight tubes, and pressure drop was almost similar to straight tubes. For the flows with high Dean number,  $De > 50$ , the pressure drop was found to follow another asymptote in the format of a simple power law, where using curved tubes, Reynolds number is replaced by Dean number. Combining the two asymptotes and using the results in the transition region,  $5 < De < 50$ , a new asymptotic correlation is proposed to predict the pressure drop in curved tubes, and coiled tubes with small pitch.

The correlation was able to predict the results at mini scale and in the Dean number range of the present experiments with less than 5 percent error, and the maximum error was found to be 10 percent. The Manlapaz and Churchill [20] model was also used in the comparisons and it was shown that the error for their predictions is unacceptable at mini scale.

Further investigations are required for the pressure drop of coiled tubes in mini scale for higher Reynolds and Dean numbers to find a correlation that can predict the pressure drop when turbulence becomes important. Finding the optimal curvature to maximize the heat transfer and minimize the pressure drop needs further experimental and numerical study.

### **Acknowledgement**

The authors acknowledge the financial support of the Natural Sciences and Engineering Research Council of Canada (NSERC) and Auto 21 NCE.

## 6.6 References

- [1] Thompson J., 1986, "On the origin of windings of river and alluvial planes, with remarks on the flow of water round bends in pipes," Proc. R. Soc. London, Serial A 5 (1).
- [2] Williams, G. S., Hubbell, C. W., and Fenkell, G. H., 1902, "Michigan on the effect of curvature on the flow of water pipes," Trans. Am. Soc. Civil Eng., 47.
- [3] Grindley, J. H., and Gibson A. H., 1908, "On the frictional resistance of air through a pipe," Proc. R. Soc. London, Ser. A, 80, pp.114-139.
- [4] Eustice J., 1911, "Experiments of streamline motion in curved pipes," Proc. R. Soc. London, Ser. A, 85, pp. 119-131.
- [5] Boothroyd A., 1997, "Spiral heat exchanger," Int. Enc. of Heat Transfer, G. Hewitt, Y. Pulezhaev, eds., CRC Press, New York.
- [6] Chonwdhury K., Linkmeyer H., and Bassiouny M. Kh., 1985, "Analytical studies on the temperature distribution in spiral plate heat exchangers: straightforward design formulate for efficiency and mean temperature difference," J. Chemical Eng. Process, 19, pp. 183-190.
- [7] Burmeister L. C., 2006, "Effectiveness of spiral-plate heat exchanger with equal capacitance rate," J. of Heat Transfer, 128, pp. 195-301.
- [8] Dean W. R., 1927, "Note on the motion of fluid in a curved pipe," The London, Edinburgh and Dublin Philosophical Magazine and Journal of Science, 4, pp. 208-223.
- [9] Dean W. R., 1928, "The streamline flow through curved pipes," The London, Edinburgh and Dublin Philosophical Magazine and Journal of Science, 5, pp. 673-695.
- [10] Nigam K., Vashisth S., and Kumar V., 2008, "A review on the potential applications of curved geometries ion process industry," Ind. Eng. Chem. Res., 47, pp. 3291-3337.

- [11] White C. M., 1929, "Streamline flow through curved pipes," Proceedings of Royal Society of London, Series A: Mathematical and Physical Science, 123, pp. 645-663.
- [12] Cheng K. C., and Akiyama M., 1970, "Laminar forced convection heat transfer in curved rectangular channels," J. of Heat Transfer, 13, pp. 471-490.
- [13] Akiyama M., and Cheng K. C., 1974, "Graetz problem in curved pipes with uniform wall heat flux," Int. J. of Applied Science Re., 29, pp. 401-417.
- [14] Mori Y., Uchida Y., Ukon T., 1971, "Forced convective heat transfer in a curved channel with a square cross section," Int. J. of Heat and Mass Transfer, 14, pp. 1787-1805.
- [15] Nigam K., Vashisth S., Kumar V., and Burhanuddin F. 2008, "Numerical Studies of a Tube-in-Tube Helically Coiled Heat Exchanger," Chemical Engineering and Processing: Process Intensification, 47, pp. 2287-2295.
- [16] Hashemi S. M., and Akhavan-Behabadi M. A., 2012, "An empirical study on heat transfer and pressure drop characteristics of CuO-base oil nanofluid flow in a horizontal helically coiled tube under constant flux," International Journal of Communication in Heat and Mass Transfer, 14, pp. 1787-1805.
- [17] Fakoor-Pakdaman M., Akhavan-Behabadi M. A., and Razi P., 2013, "An empirical study on the pressure drop characteristics of nanofluid flow inside helically coiled tubes," International Journal of Thermal Science, 65, pp. 206-213.
- [18] Chang S. W., Chiang K. F., and Kao J. K., 2012, "An empirical study on heat transfer and pressure drop characteristics of CuO-base oil nanofluid flow in a horizontal helically coiled tube under constant flux," International Journal of Communication in Heat and Mass Transfer, 14, pp. 1787-1805.
- [19] Akbaridoust F., Rakhsha M., Abassi A., and Saffar-Avval M., 2013, "Experimental and numerical investigation of nanofluid heat transfer in helically coiled tubes at constant wall temperature using dispersion model," International Journal of Heat and

Mass Transfer, 58, pp. 480-491.

[20] Manlapaz R. L., and Churchill S. W., 1980, "Fully developed laminar flow in a helically coiled tube of finite pitch," *Chemical Engineering Communication*, 7, pp. 57-78.

[21] Austen D. S., and Soliman H. M., 1980, "Laminar Flow and Heat Transfer in Helically Coiled Tubes with Substantial Pitch", *Experimental Thermal Fluid Science*, 1, pp. 183-194.

[22] Yamamoto K., Yanase S., Yoshida T., 1994, "Torsion Effect on the Flow in a Helical Pipe", *Journal of Fluid Dynamics Research*, 14, pp. 259-273.

[23] Yamamoto K., Akita T., Ikeuchi H., Kita Y., 1995 "Experimental Studies of the Flow in Helical Circular Tube", *Journal of Fluid Dynamics Research*, 16, pp. 237-249.

[24] Yamamoto K., Aribowo A., Hayamizu Y., Hirose T., Kawahara K., 2002 "Visualization of The Flow in a Helical Pipe", *Journal of Fluid Dynamics Research*, 30, pp. 251-167.

[25] Grundman R., 1985, "Friction Diagram of The Helically Coiled Tube", *Chemical Engineering and Processing: Process Intensification*, vol. 19, pp. 113-115.

[26] Takahashi M., and Momozaki Y., 2000, "Pressure Drop and Heat Transfer of a Mercury Single-Phase Flow and an Air-Mercury Two-Phase Flow in a Helical Tube Under a Strong Magnetic Field", *Chemical Engineering and Processing: Process Intensification*, 51, pp. 869-877.

[27] Kline S. J., and McClintock F. A., 1953, "Describing uncertainties in single-sample experiments," *Mech. Eng.*, 75, pp. 3-8.

[28] Srinivasan P. S., Nandapurkar S. S., and Holland F. A., 1970, "Friction factors for coils," *Tran. Inst. Chem. Eng.*, 48, pp.T156-T161.

# Chapter 7

## Fully Developed Heat Transfer in Mini Scale Coiled Tubing for Constant Wall Temperature\*

**M.Ghobadi and Y.S. Muzychka**

Microfluidics and Multiphase Flow Lab, Faculty of Engineering and Applied Science,  
Memorial University of Newfoundland, St. John's, NL, Canada, A1B 3X5

### **ABSTRACT**

An experimental study on heat transfer enhancement in mini scale coiled tubing for constant wall temperature conditions is conducted. Copper coils with three different radii of curvature (1 cm, 2 cm, and 4 cm), and in four lengths (1, 2, 3 and 4 coil turns) were used. The tube length is long enough to consider the flow to be hydro-dynamically fully developed. Hence, the effects of varying curvatures and lengths on heat transfer are studied. The pitch of the coil is restricted to diameter of the tube to minimize the effect of coiling. Dean number is used instead of Coiled number (modified Dean number), and hence, the results can be expanded to spiral and curved tubing. Water and two different silicone oils (0.65 cSt, 1 cSt) were used in the experiments to examine the effect of Prandtl number on coiled tubing heat transfer augmentation. Prandtl number from 5 to 15 is covered in this paper. A new asymptotic correlation is proposed to calculate Nusselt number in fully developed coiled tubing based on the current results. In addition, dimensionless mean wall flux and dimensionless thermal length are also considered besides Nusselt, Reynolds, and Dean numbers.

**Keywords:** Heat Transfer, Curved Tubing, Asymptotic Analysis, Passive Heat Transfer Enhancement

\* *Accepted for Publication in International Journal of Heat and Mass Transfer*

## 7.1 Introduction

In general, there are two methods to improve heat transfer rates: active and passive techniques [1, 2]. Active techniques are based on external forces such as electro-osmosis [3], magnetic stirring [4], bubble induced acoustic actuation [5] and ultrasonic effects [6] to perform the augmentation. Active techniques are effective; however, it is not always easy to perform the compatible design with other components in a system. They also increase the total cost of the system manufacturing.

On the other hand, passive techniques employ fluid additives or special surface geometry. Using the surface geometry approach is easier, cheaper and does not interfere with other components in the system. Surface modification, adding additives to the fluid or additional devices, incorporated in the stream are three passive augmentation techniques. In these techniques, the existing boundary layer is disturbed and the heat transfer performance is improved; however, pressure drop is also increased [7]. Consequently, their net effectiveness depends upon the balance between the increase in heat transfer augmentation and the pressure drop penalty.

Curved geometry is one of the passive heat transfer enhancement methods that fits several heat transfer applications such as power production, chemical and food industries, electronics, environment engineering, etc. Centrifugal force generates a pair or two pairs of cross-sectional secondary flow (based on the Dean number), which are known as the Dean vortices, improves the overall heat transfer performance with an amplified peripheral Nu variation. The velocity near the outer wall is greater than the flow in straight pipes, whereas, to maintain the momentum balance between the centrifugal force and pressure gradient, slower moving fluid elements move toward the inner wall of the curved tube.

Dean [9, 10] conducted the first analytical studies of fully developed laminar flow in a curved tube of circular cross section. He developed a series solution as a perturbation

of the Poiseuille flow in a straight pipe for low values of Dean number ( $De < 17$ ). He reported that the relation between pressure gradient and the rate of flow is not dependent on the curvature to the first approximation. In order to show its dependence, he modified the analysis by including the higher-order terms and was able to show that reduction in flow due to curvature depends on a single variable (now known as the Dean number), equal to  $Re\sqrt{(D/2R)}$  (where  $Re$  is the Reynolds number,  $D$  is the tube diameter, and  $R$  is the radius of curvature of the curved tube in Dean's notation). Various other authors have used different definitions of the Dean number for curved tube studies. It was reported that, for low Dean numbers, the axial-velocity profile was parabolic and unaltered from the fully developed straight tube flow. As the Dean number is increased, the maximum velocity begins to be skewed toward the outer periphery. Similarly, for low values of curvature ratio, the secondary flow intensity is very high while for high values of the curvature ratio the secondary flow intensity is much less [11].

Due to volumetric constraints, a wide range of curved tubing applications are in coiled shape format. The most popular use for coiled tubing is circulation or deliquification. Coiled tube heat exchangers, logging and perforating, and drilling are other applications of coiled tubing [12, 13]. From a heat transfer point of view, helically coiled exchangers offer certain advantages. Compact size provides a distinct benefit. True counter-current flow fully utilizes available LMTD (logarithmic mean temperature difference). Helical geometry permits the handling of high temperatures and extreme temperature differentials without high induced stresses or costly expansion joints. High-pressure capability and the ability to fully clean the service-fluid flow area add to the heat exchanger's advantages. Neglecting the effect of coiled tube pitch, Rennie [14] examined the double-pipe helical heat exchangers numerically and experimentally. Kumar et al. [15] studied a tube-in-tube helically coiled heat exchanger for

turbulent flow regime numerically. Shokouhmand et al. [16] experimentally investigated the shell and helically coiled tube heat exchangers in both parallel-flow and counter-flow configuration. They used Wilson Plots [17] to calculate the overall heat transfer coefficient.

A complete investigation on heat transfer has been provided by Akiyama and Cheng [18, 19] on curved rectangular channels and curved pipes with uniform heat flux and a peripherally uniform wall temperature. Using a numerical method, they found solutions up to a reasonably high Dean number for different aspect ratios. They also showed that the perturbation method is only applicable for a relatively low Dean number region and a boundary-layer technique is valid only for high Dean number regime. The effect of Dean number on velocity and temperature field was also studied in their work.

Nigam [11] accomplished a comprehensive review on the papers related to the application of curved geometry in the process industry up to 2008. The primary objective of their work is to provide an overview of the perspective on evolution of curved tube technology and introduction to a new class of curved tubes. The Nigam's paper [11] is divided into four parts. The first part discusses the fundamentals involved in enhancing the mixing performance and local phenomena in curved tubes to better understand how mixing and heat- and mass-transfer proceed for single-phase flow. In the second part, the chemistry of two-phase flow in curved tubes is discussed and reported. The third part discusses the development of a new class of curved chaotic geometries (bent coils) as a course of technological development. The hydrodynamics and heat and mass transfer performance in curved chaotic configurations have been discussed and compared against curved tube.

Cheng [20] reported that the number of the vortices inside a curved channel depend on the Dean number. Two vortices have been reported for  $De < 100$ , whereas for

$100 < De < 500$ , four vortices appear in a square curved channel. These extra vortices vanish at about  $De \approx 500$ . The channel aspect ratio determines the exact value of the disappearance.

Burmeister and Egner [21] numerically studied laminar flow heat transfer in three-dimensional spiral ducts of a rectangular cross section with different aspect ratios. The boundary conditions were assumed to be axially and peripherally uniform wall heat flux and a peripheral uniform wall temperature. They presented average Nusselt number as a function of distance from inlet and Dean number. Their results are applicable to spiral plate heat exchangers.

Chang et al. [22] conducted an experimental study that examines the detailed Nusselt number (Nu) distributions, pressure drop coefficients ( $f$ ) and thermal performance factor (TPF) for a square spiral channel with two opposite end walls roughened by in-line 45 degree ribs.

Hashemi and Akhavan-Behabadi [23] experimentally investigated the heat transfer and pressure drop characteristics of nanofluid flow inside horizontal helical tube under constant wall flux. They studied effect of different parameters such as Reynolds number, fluid temperature and nanofluid particle weight concentration on heat transfer coefficient and pressure drop of the flow.

Ghobadi and Muzychka [24] studied the heat transfer augmentation inside short curved mini tubes. They showed that increasing the curvature,  $1/R$ , leads to heat transfer enhancement. They showed that the entrance effect dominates the augmentation in short lengths, however the secondary flow effect becomes greater by increasing the curved tubing length. It has been shown that the lower the Prandtl number is, the better enhancement is observed.

Manlapaz and Churchill [25] developed a general correlation for fully developed laminar convection from a helical coil for all Prandtl and Dean numbers. Their model was

constructed by joining the theoretical Nusselt number for a straight tube, a theoretical asymptote for the regime of creeping secondary flow, a semi-theoretical expression for the boundary layer regime and an asymptotic value of  $Nu$  for the intermediate regime of flow. Their model is also used to predict the experimental results. However, agreement was not observed between their correlation and the present experimental results in the mentioned Prandtl number range. Subsequently, a new correlation is proposed for the heat transfer prediction in the region of  $5 < Pr < 15$  and  $5 < De < 700$ .

This paper mainly focuses on studying the heat transfer inside coiled copper tubing under constant wall temperature boundary condition. The radius of curvature and length effects have been considered in this paper. The copper tube was coiled into three 1, 2, and 4 cm radii and in one, two, three and four full turns. Table 7.1 shows the radius of curvature and the lengths of the curved tubes used in the experiment. One may notice that the diameters have been picked in such a way that the lengths of different curvatures match together. Hence, we have examined different lengths with the same curvature, and different curvatures with the same length. The coils are long enough to consider the the flow to be hydro-dynamically fully developed. The effect of Dean number for the fixed length has also been studied. The results have been also compared to an identical straight tube in the similar constant wall temperature condition, where  $Nu = 3.66$ .

Table 7.1: Tubing outer and Inside Diameter

<i>Radius</i>	1 turn	2 turns	3 turns	4 turns
1 cm	-	12.56	18.84	25.12
2 cm	12.56	25.12	37.68	50.24
4 cm	25.12	50.24	75.36	-

Showing that the Manlapaz and Churchill correlation [25] can not predict the heat transfer within the examined Prandtl region, a new asymptotic correlation is proposed.

The proposed correlation is obtained by dividing the curved tubes flow into three regions: low curvature region  $De < 10$ , high curvature region  $De > 50$ , transitional region  $10 < De < 50$ . Knowing that the heat transfer behaviour in the low curvature region is similar to the one for straight tubes, and employing the empirical correlation format to develop an empirical correlation in high curvature region, two asymptotes for the low curvature and the high curvature regions is obtained. According to the experimental results asymptotic analysis was used to blend the two asymptotes and predict the heat transfer in the transitional region.

Finally, the effect of Prandtl number has been considered in this study, since water and two silicone oils with low viscosities, 0.65 cSt, and 1 cSt have been used in all of the configurations. Prandtl number from 5 to 15 are considered in this paper. The heat transfer augmentation change by changing the working fluid is depicted.

## 7.2 Experimental Setup

Fig. 7.1 shows the configuration of the system used to measure heat transfer rates. Depending on the flow rate, two or four syringes (Hamilton Glass Gas Tight) were filled with the test fluid, and the pumps (Harvard Pump 33) were set to the desirable flow rate. Each syringe can hold 100 ml; hence total 400 ml of the working fluid was available for each run of the experiment. Considering the maximum volumetric rate at 100 ml/min, the system had 4 minutes or more to become thermally stable. The flow from four syringes merged together and flow into the coiled copper tubes. Thermocouples were placed at each end with the least distance from the copper tubing. The copper tubes were cut with smooth edges so that the flow was not disturbed while entering the tubing. Plastic tubing was used to connect the flow tube to the coiled tubes. A Keithley Data Acquisition system (DAQ) recorded the

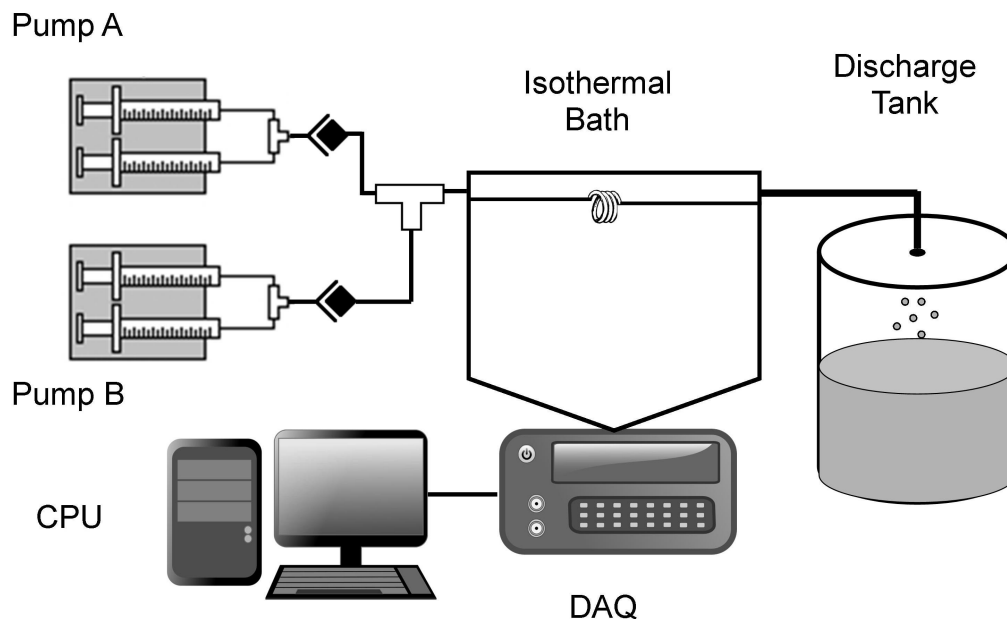


Figure 7.1: System configuration

temperatures. Five readings were taken and averaged for inlet and outlet temperature to minimize the error in reading. The curved tubes were placed horizontally inside an isothermal water bath, so that the gravitational effect can be neglected. The water temperature and consequently the surface temperature of the coiled tubes were set as  $40^{\circ}\text{C}$ , whereas the fluid inlet temperature was measured to be around  $23^{\circ}\text{C}$ .

The isothermal bath maintained the temperature at the set point within  $\pm 0.1^{\circ}\text{C}$  deviation. Using the Kline and MacClintock method [26], the uncertainty of the calculated Nusselt is found to be 1.6%–4.8% of the reported Nusselt. The accuracy of the pumps was also measured to be 1% of the adjusted volume, which gives 0.7%–0.8% uncertainty for the calculated Reynolds number.

The viscosity of the silicone oils, as well as their temperature dependence were given by the manufacturer. However, we also measured the viscosities of the oils with an accurate apparatus (Physica MCR 301 from Rheosys Company) at the room temperature to confirm the reported data. The data were found to be inside the 5% uncertainty

range of the reported data. The accuracy of the device was also benchmarked by measuring the viscosity of water.

In order to confirm the accuracy of the experimental procedure, bench marking tests have been done on a straight tube of the same copper and cross section. The tests were done with a 163 mm long straight copper tube with a diameter of 1.65 mm (the same as the curved tubing). The tubing was cut precisely and the edges were filed to have smooth ends. Finally, two plastic tubes were glued to the ends to avoid any leakage. Two thermocouples were placed in the same manner as the original experiments as near as possible to the entrance and exit. The tube was placed in the thermal bath horizontally, so gravity doesn't affect the results. The flow was assumed to be hydrodynamically developed and thermally developing. Water, 0.65 cSt oil, 1 cSt and 3 cSt oil were examined as the working fluids. Fig. 7.2 shows the benchmarking results for all the working fluids in comparison to Graetz model for straight tubes. The accuracy of the experiments can be verified by comparing the gathered data with the model. The rms error was found to be less than 7 percent for all the fluids and test conditions.

### 7.3 Data Analysis

The Data Acquisition (DAQ) system collects the inlet and outlet temperatures of the fluid. The heat transfer rate can be obtained by writing the energy balance for the working fluid as a single phase liquid flow.

$$Q = \dot{m}C_p(T_o - T_i) \quad (7.1)$$

The mean heat flux is:

$$\bar{q} = \frac{Q}{PL} \quad (7.2)$$

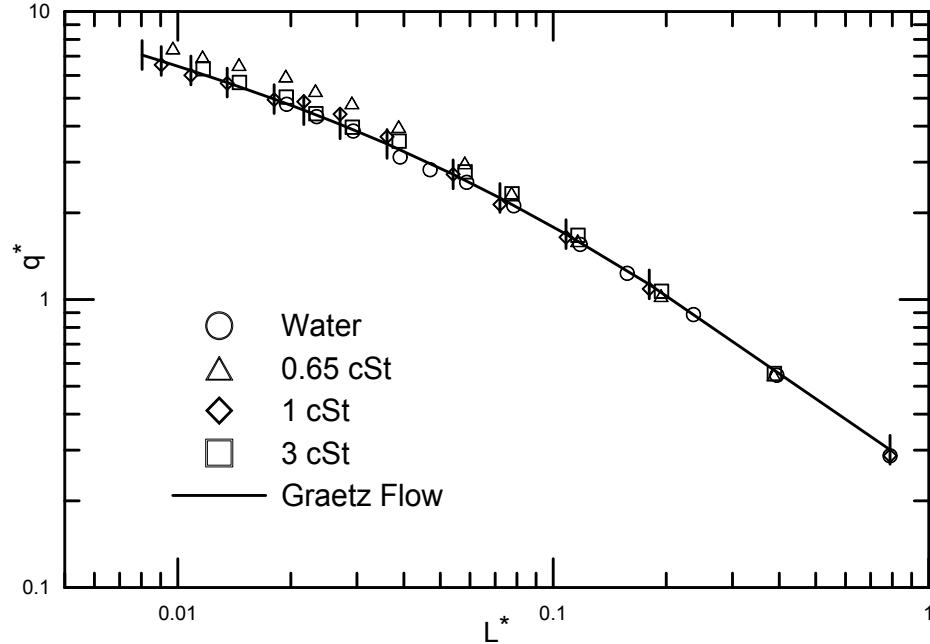


Figure 7.2: Benchmarking results for a straight tube, with error bars represent  $\pm 10\%$

Since we are interested in the average value of  $h$  and Nusselt number for the entire tube, and the boundary condition is constant wall temperature, we use logarithmic mean temperature difference:

$$\Delta T_{lm} = \frac{\Delta T_o - \Delta T_i}{\ln \frac{\Delta T_o}{\Delta T_i}} \quad (7.3)$$

Finally one may simply find  $\bar{h}$ , and  $\overline{Nu}$  from the following equations:

$$\bar{h} = \frac{\bar{q}}{\Delta T_{lm}} \quad (7.4)$$

$$\overline{Nu} = \frac{\bar{h}D}{k_f} \quad (7.5)$$

Nusselt number versus Reynolds number is the most common procedure to reduce the heat transfer results, however, the dimensionless thermal length, which reflects the

tube length as well as flow speed, can be used instead of Reynolds number:

$$L^* = Gz^{-1} = \frac{L/D}{Pe_D} \quad (7.6)$$

In addition to Nusselt number, it is also useful to consider the dimensionless mean wall flux along with the dimensionless thermal length:

$$q^* = \frac{\bar{q}D}{k(T_w - T_i)} \quad (7.7)$$

The dimensionless mean wall flux and the dimensionless thermal length were employed earlier for the benchmarking results presentation. In the case of a Graetz flow in a circular tube, the dimensionless mean wall flux can be related to the Nusselt number. Muzychka et al. [27] employed single fluid heat exchanger theory, e.g. the  $\varepsilon - NTU$  method for constant wall temperature condition to derive the following correlation:

$$q^* = \left[ \left( \frac{1.614}{L^{*1/3}} \right)^{-3/2} + \left( \frac{1}{4L^*} \right)^{-3/2} \right]^{-2/3} \quad (7.8)$$

As discussed before, the Dean number accounts for the secondary flow in a curved tube and introduced as:

$$De = Re \sqrt{\frac{D}{2R}} \quad (7.9)$$

In a helical coil, the effective radius of curvature  $R_c$  of each turn is influenced by the coil pitch  $b$ , and is given by:

$$R_c = R \left[ 1 + \left( \frac{b}{2\pi R} \right)^2 \right] \quad (7.10)$$

Use of  $R_c$  instead of  $R$  in Dean number definition results in a new number, referred to as a helical coil number  $He$ , defined as:

$$He = Re\sqrt{\frac{D}{2R_c}} = De \left[ 1 + \left( \frac{b}{2\pi R} \right)^2 \right]^{-1/2} \quad (7.11)$$

In all the experimental tests reported in this paper, the pitch was minimized to the external diameter of the copper tubing. Hence, the effective curvature  $R_c$  mostly affects the tube with the lowest radius of curvature:

$$R_c = R \left[ 1 + \left( \frac{0.0016}{2\pi \cdot 0.01125} \right)^2 \right] = 1.0005R \quad (7.12)$$

So for this study we use Dean number instead of Helical number. Thus, the results presented in this paper can be also used for spiral geometries.

It has been shown that there are significant Nusselt number oscillations in the entrance region, and therefore, thermal entry length should be calculated to check whether the flow is in the fully developed region or not. The thermal entrance region of a helical coil is about 20 to 50 percent shorter than that of a straight tube. Janssen and Hoogendoorn [28] provide the following equation for the thermal entry length which is based on dimensionless thermal length:

$$L_{th}^* = \frac{L_{th}/D}{Pe_D} < \frac{15.7Pr^{-0.8}}{De} \quad (7.13)$$

Calculating the thermal entrance region, and comparing it to the coiled tubes length, the flow can be considered as fully developed without significant errors.

As a part of this study the collected results are compared to the well known correlation of Manlapaz and Churchill [25] for the fully developed laminar convection from a helical coil derived by joining several asymptotes. However, based on the presented results, their model cannot predict the Nusselt number in the mini-scale coil tubing in the Prandtl range of 5-15. Their model is:

$$Nu_T = \left[ \left( 3.657 + \frac{4.343}{x_1} \right)^3 + 1.158 \left( \frac{De}{x_2} \right)^{3/2} \right]^{1/3} \quad (7.14)$$

where:

$$x_1 = \left( 1 + \frac{957}{De^2 Pr} \right)^2 \quad (7.15)$$

and

$$x_2 = 1 + \frac{0.477}{Pr} \quad (7.16)$$

## 7.4 Results and Discussion

As stated before, water and two different silicone oils were used, and a broad range of Reynolds numbers and Dean numbers have been examined in the present experiments. Table 7.2 summarizes the range for different dimensionless numbers. As viscosity is a strong function of temperature, the correlations given by the manufacturer were used to calculate the viscosity for each experiment (the average of the entrance and the exit temperature were used to find the mean temperature), and Prandtl number range is given for all curvatures. On the other hand, Reynolds number which depends on the velocity, diameter and viscosity, changes noticeably by changing the flow rate, and consequently the flow velocity, and is also independent of curvature. Thus, for a liquid at the same flow rate, the Reynolds number is the same for different curvatures. However, the Dean number is proportional to both flow rate and curvature. This means that the range for Dean number for the same fluid varies in different curvature ranges.

In this section, the experimental results will be presented based for three different

Table 7.2: Prandtl, Reynolds and Dean Range for the Different Fluids

<i>Fluid</i>	<i>Pr</i>	<i>Re</i>	<i>Radii[cm]</i>	<i>De</i>
<i>water</i>	5 – 6.3	30 – 2500	1	5 – 500
			2	5.5 – 370
			4	4.1 – 280
0.65 <i>cSt</i>	7.9 – 9.2	30 – 2500	1	9.3 – 700
			2	6.4 – 500
			4	4.7 – 295
1 <i>cSt</i>	12.6 – 15	20 – 1260	1	6.34 – 455
			2	4.3 – 330
			4	3.11 – 240

conditions. First, we examine the effect the curvature on the heat transfer augmentation. The effect of different lengths with the same curvature is also studied with different turns of coil for each curvature. Finally, the Prandtl number effect on the heat transfer enhancement in curved tubing is studied.

Fig. 7.3 shows the heat transfer analysis (Nusselt number versus Reynolds number) for a constant length, 0.26 m, of copper coiled tubing using 0.65 cSt silicone oil as the working fluid. The Prandtl number is an average of 8.5 and the wall temperature was set to 40°C. Different radii of curvature were employed with various turns of the coil to make the equal lengths. The Nusselt number for the fully developed flow inside a straight tube,  $Nu = 3.66$ , is also plotted to show the heat transfer enhancement of different curvatures. Since the Prandtl number and length are the same for all three curvatures, curvature is the only varying parameter between the presented results. Heat transfer for all three radii of curvature (1 cm, 2 cm, and 4 cm) is enhanced in comparison to the straight tubing heat transfer; however, the smallest radii of curvature,  $R = 1\text{cm}$ , augments the heat transfer more than the heat transfer for  $R = 2\text{cm}$  and  $R = 4\text{cm}$ . Such a result was predictable due to the nature of the

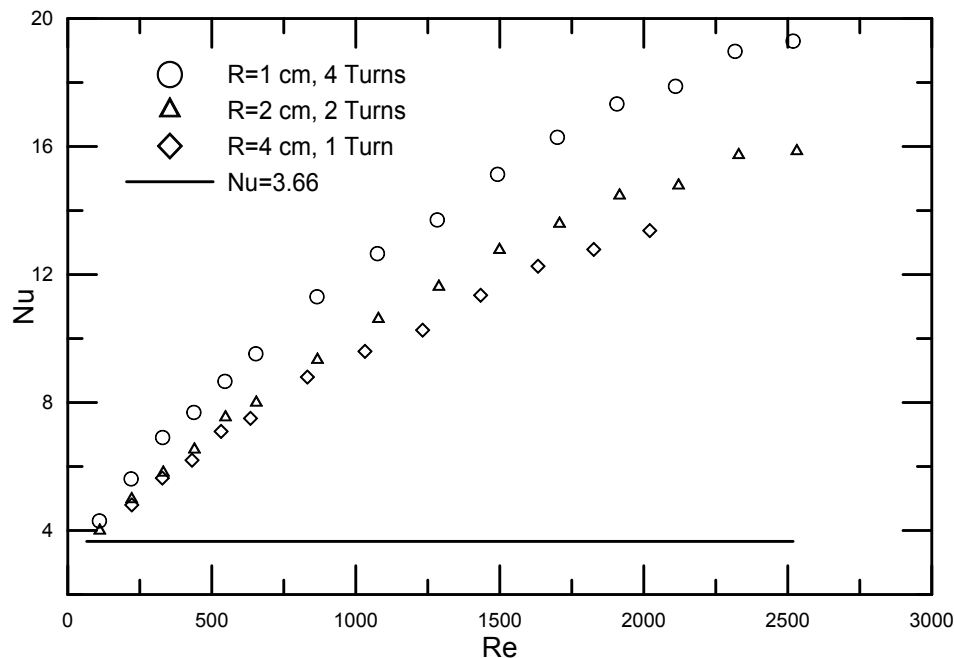


Figure 7.3: Heat transfer performance of different curvatures for constant length of 0.26 m with 0.65 cSt oil

enhancement mechanism, which implies the main reason for the enhancement is the secondary flow initiation inside the tubing which increases by increasing the curvature  $1/R$ .

Figs. 7.4 and 7.5 depict the same comparison for 1 cSt silicone oil and water as working fluids. In Fig 4 the length is constant at 0.13 m and radii of curvature of 1 cm and 2 cm were employed with different coil turns to make the constant length of 0.13 m. In Fig. 7.5 we exploited 1 cm, 2 cm and 4 cm radii of curvature to obtain the 0.26 cm length of copper tubing. At this point we can conclude that increasing the Dean number leads to an increase in the heat transfer coefficient, however, one should note that Prandtl number is also important in the enhancement.

The heat transfer results are also presented against Dean number instead of Reynolds. We expected that the Nusselt number at a constant Dean number should be the same for a same working fluid, for different radii of curvature. However, reducing

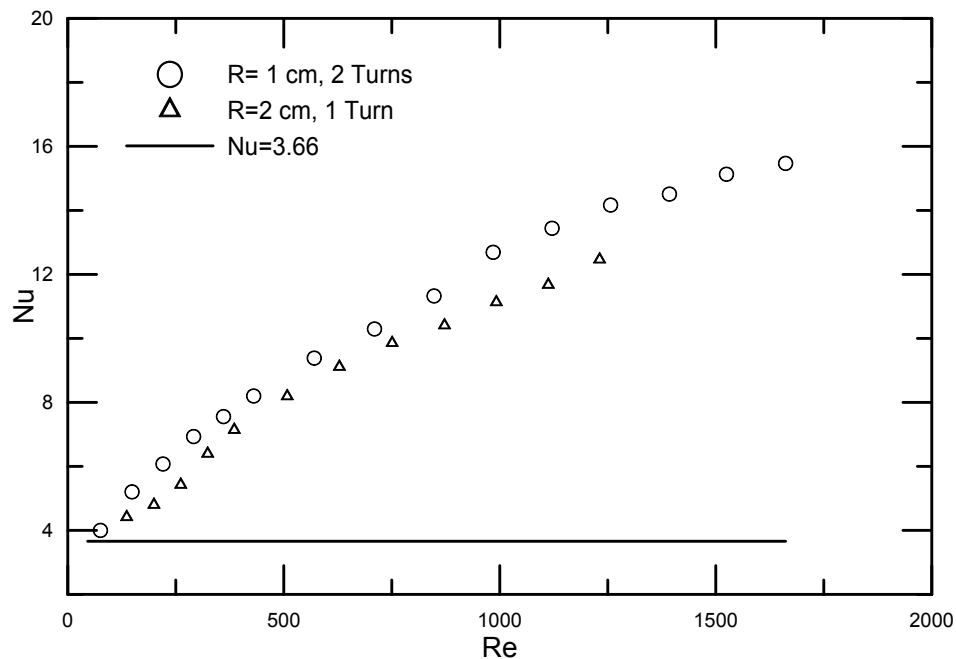


Figure 7.4: Heat transfer performance of different curvatures for constant length of 0.13 m with 1 cSt oil

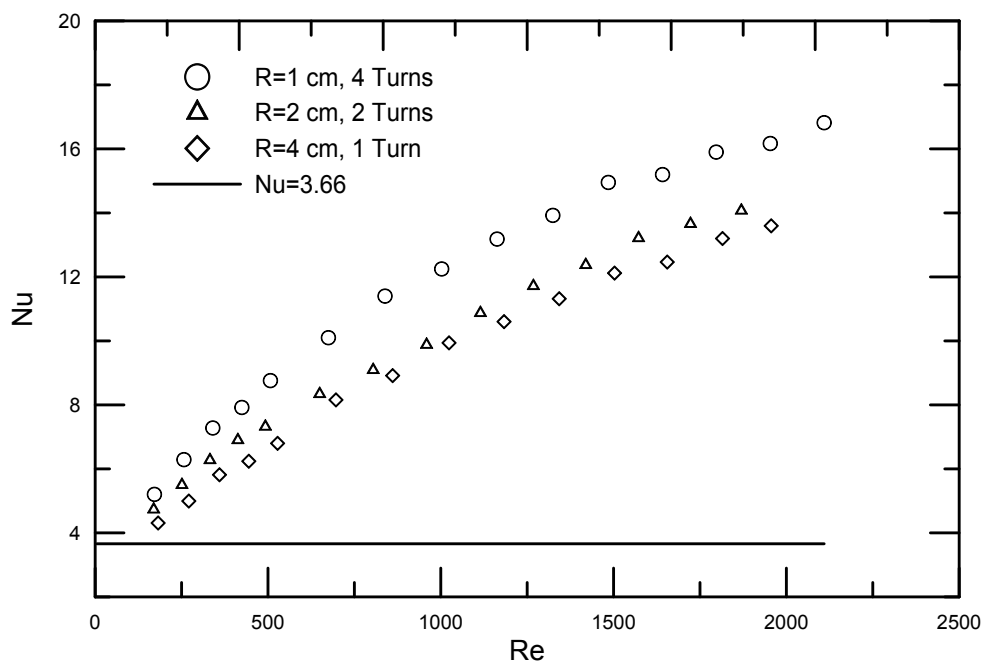


Figure 7.5: Heat transfer performance of different curvatures for constant length of 0.26 m with water

the curvature,  $1/R$ , indicates that higher flow rate (Reynolds number) is required to achieve the same Dean number. The mentioned thermal behaviour can be used to derive a correlation to predict the heat transfer correlation based on Dean number and Prandtl number.

Reviewing the collected experimental results, we observed that the flow inside curved tubes can be divided to three main regions: low curvature region  $De < 10$ , high curvature region  $De > 50$ , and transitional region  $10 < De < 50$ . It was found that the heat transfer coefficient for flow with  $De < 10$  is identical to the fully developed pressure drop of the flow in straight tubes in constant wall temperature boundary condition,  $Nu = 3.66$ . In other words, the viscous forces resist against the secondary flow initiation inside curved tubes.

For the high Dean number flows, based on the collected results, we were able to develop a simple empirical prediction for the Nusselt number in curved and coiled tubes with small pitches for fully developed flows. Employing an empirical approach and using an algebraic expression of the form:

$$Nu = CDe^{m_1}Pr^{m_2} \quad (7.17)$$

Finding the constants,  $C$ ,  $m_1$  and  $m_2$ , based on the results for high number flows, the following correlation is obtained:

$$Nu_c = 0.91375\sqrt{De}Pr^{-0.1} \quad (7.18)$$

where  $Nu_c$  is the curved tubes Nusselt number. Consequently, the following asymptotes are found:

$$Nu_c = \begin{cases} 3.66 & \text{if } De < 10 \\ 0.91375\sqrt{De}Pr^{-0.1} & \text{if } De \geq 50 \end{cases} \quad (7.19)$$

The two asymptotes can be blended as:

$$Nu_c = \left[ 3.66^n + \left( 0.91375\sqrt{De}Pr^{-0.1} \right)^n \right]^{1/n} \quad (7.20)$$

Finally, using the results in the transitional flow, the power was found as  $n = 4$ , and the following correlation is proposed to calculate friction factor ratio:

$$Nu_c = \left[ 3.66^4 + \left( 0.91375\sqrt{De}Pr^{-0.1} \right)^4 \right]^{1/4} \quad (7.21)$$

The validity of the correlation is examined for Dean numbers up to 700 based on the present experimental results.

Now we can compare the experimental results with the proposed correlation. In each of the experiment sets the working fluid was the same, and the working fluid properties were updated based on the average working temperature, however Prandtl number during the experiment was found to be fairly constant. Consequently, by plotting Nusselt number versus Dean number, we are expecting that the heat transfer for all curvatures at a constant Dean number should be the same. We can also plot the proposed model based on the average Prandtl number for each set. Fig. 7.6 shows the proposed model prediction for the constant length of 0.26 m with 0.65 cSt silicone oil as the working fluid. The solid line shows the proposed correlation, and the Nusselt number results for the copper tubing with 1 cm, 2 cm and 4 cm radii of curvature in the constant length of 0.26 m. All of the experimental results are in good agreement with the model, and are within 10% of the predicted Nusselt.

Figs. 7.7 and 7.8 are the correlation prediction results for 1 cSt silicone oil and water

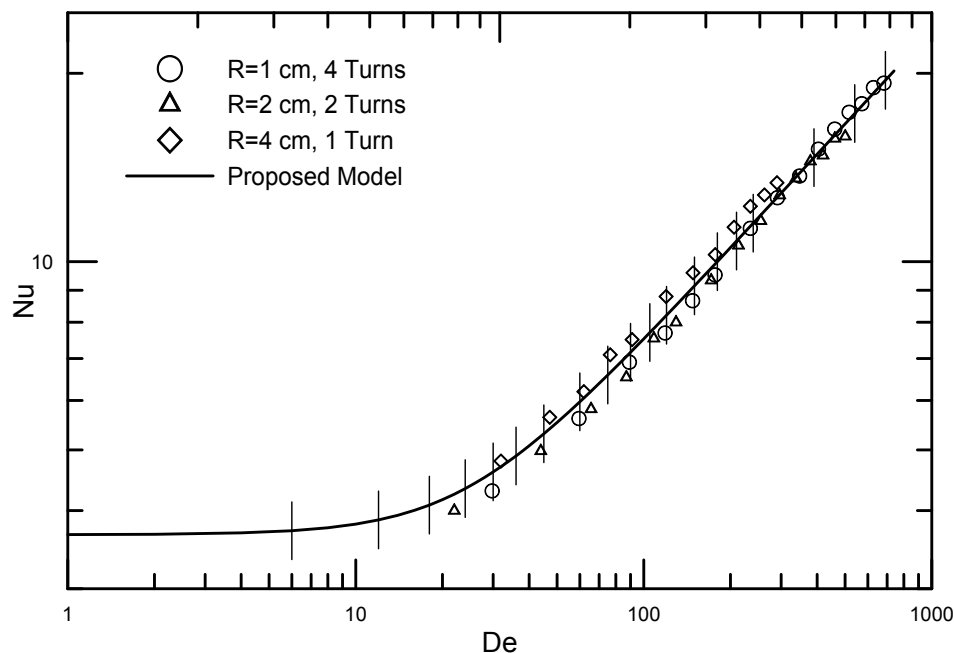


Figure 7.6: Proposed model prediction for constant length of 0.26 m and different curvatures with 0.65 cSt oil

inside the constant lengths of 0.13 m and 0.26 respectively. Fig. 7.7 depicts the results for 1 cSt silicone oil as working fluid and 2 cm and 4 cm radius of curvature. The experimental results follow the trend especially in higher Dean numbers, when the entrance effect becomes more negligible. Fig. 7.8 shows the correlation prediction for water and 1 cm, 2 cm and 4 cm of radius of curvature which make the constant length of 0.26 m. The correlation is found to be able to predict the Nusselt number with less than 10 percent error for all three working fluids.

The next set of investigations examine the effect of tube length with a constant radius of curvature. We investigated the effect of length on heat transfer augmentation by considering three or four different lengths from 1, 2, 3 and 4 turns of coils with a same radius. Hence, convection heat transfer is compared in at least three different lengths for a same curvature. Considering the same flow rate, Reynolds and Dean numbers in each flow are the same for all the lengths. Thus, one may conclude that the difference

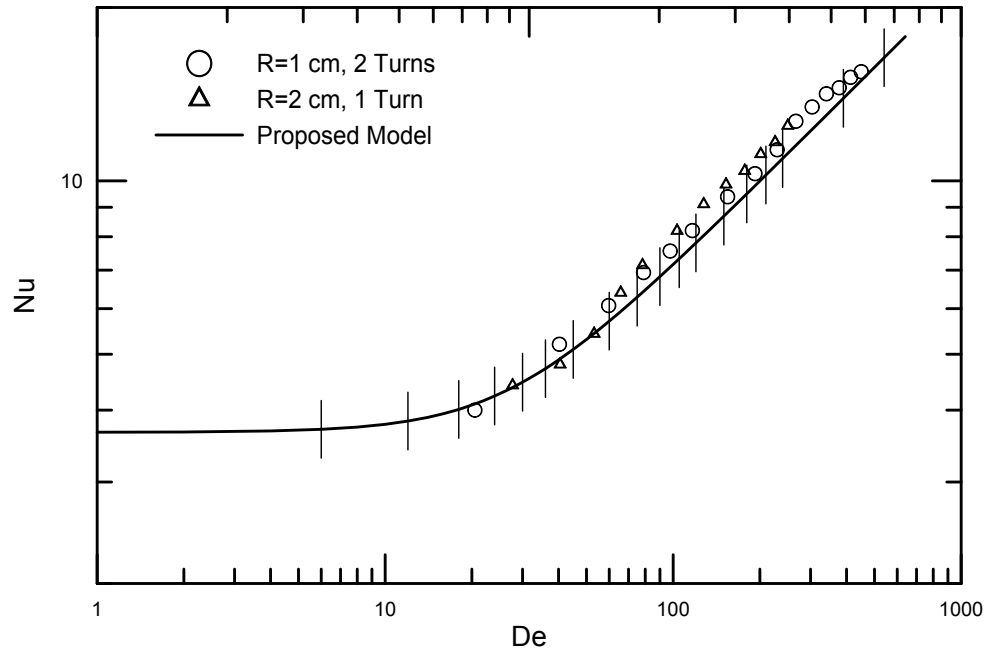


Figure 7.7: Proposed model prediction for constant length of 0.13 m and different curvatures with 1 cSt oil

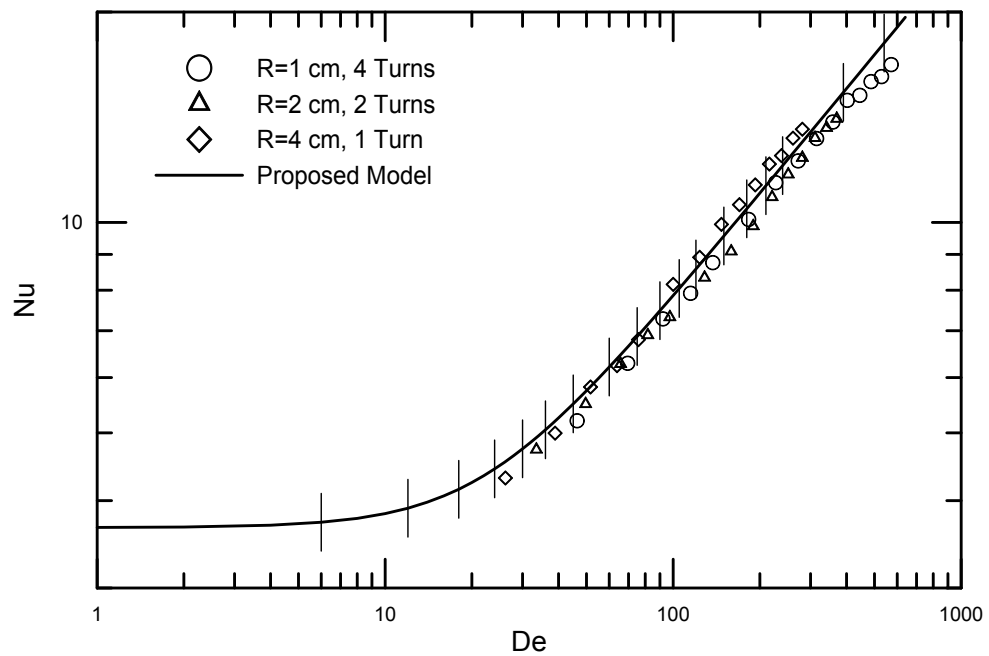


Figure 7.8: Proposed model prediction for constant length of 0.26 m and different curvatures with water

in the heat transfer augmentation is only due to the change in the length, which is not expected.

Fig. 7.9 shows the model prediction for the constant radius of curvature of 1 cm and four lengths created by 1, 2, 3 and 4 full rounds of coiled tubing. Again the model is able to predict the results well. Figs. 7.10 and 7.11 show correlation predictions for constant radius of curvature of 4 cm and 2 cm and 1 cSt silicone oil and water as working fluids respectively. The experimental results were found to be within 10 percent of correlation prediction range. As we expected, since all tests were done in the fully developed region and fluid was not thermally saturated, Nusselt number for a same Dean number and Prandtl number is constant regardless of the coil tube length until the fluid becomes thermally fully saturated. The Churchill and Manlapaz model [25] is also plotted in Figures 7.9, 7.10 and 7.11. It can be seen that the Churchill-Manlapaz model prediction are outside of the uncertainty range of the collected results.

Nusselt number analysis for a constant curvature curved tubing requires extra attention as the length is different for each experimental data set. There is a linear correlation between Reynolds number and Dean number, which means the range of both numbers are the same for all four lengths. Whereas, having different lengths implies that a different Graetz models are valid in Nusselt number versus Reynolds number plots, and the reported Reynolds numbers do not reflect the length effect. As a result, for the heat transfer analysis in the constant curvature analysis, we employ dimensionless mean flux analysis instead of Nusselt number; since, there is only one line for Graetz model, regardless of the straight tube length, we can plot all the results on a same graph and compare them to the Graetz model.

The effect of Prandtl number on the augmentation is another important issue that should be investigated. Fig. 7.12 shows the Nusselt number versus the Reynolds

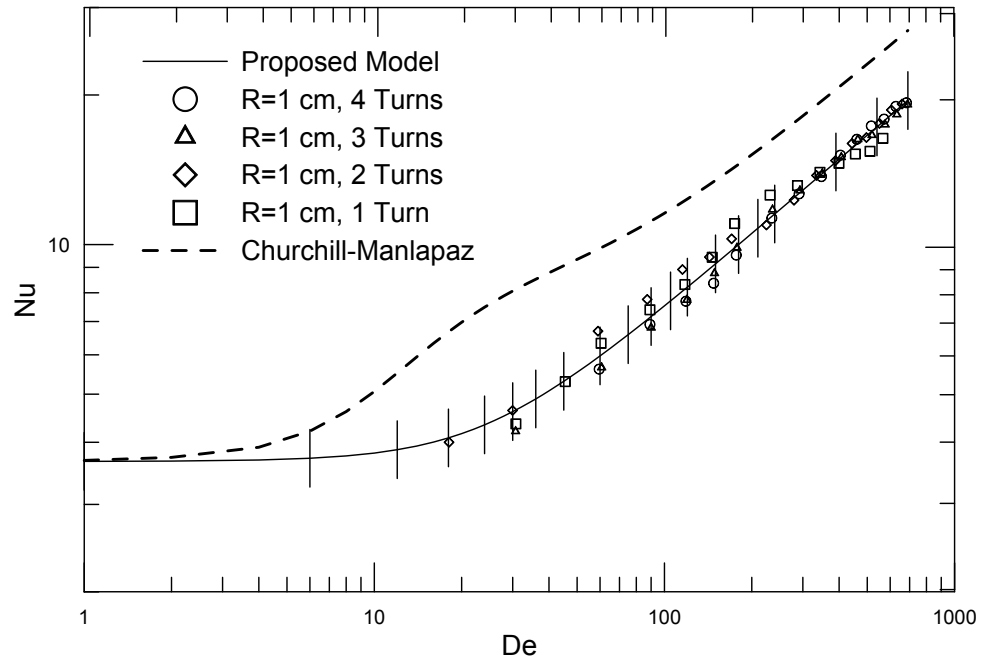


Figure 7.9: Model prediction for 1 cm curvature and 0.65 cSt oil

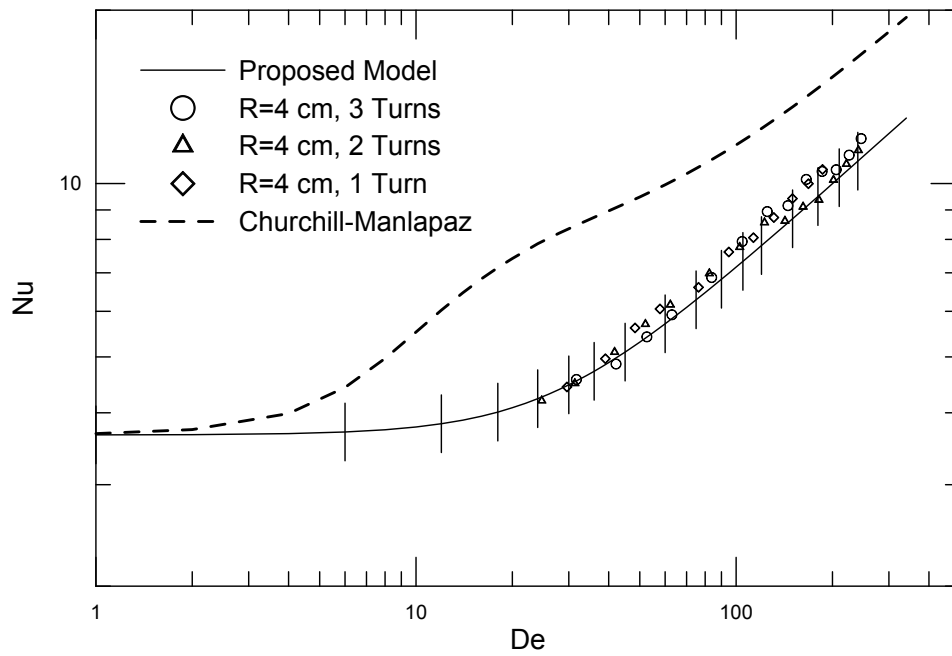


Figure 7.10: Model prediction for 4 cm curvature and 1 cSt oil

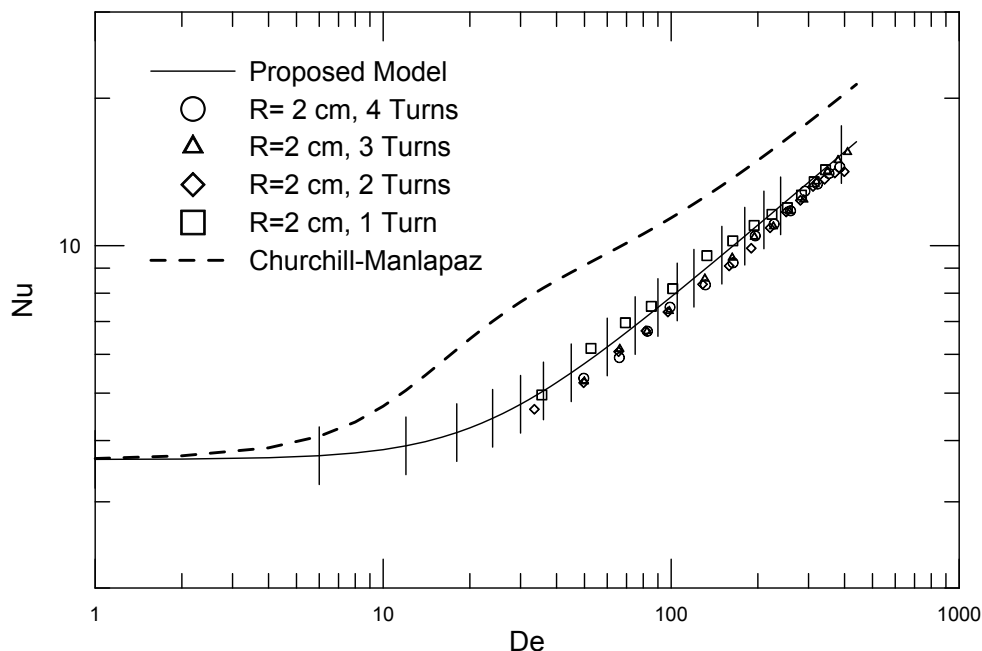


Figure 7.11: Model prediction for 2 cm curvature and water

number for 3 turns of coiled tubing with 2 cm radius of curvature. Examined fluids are water, 0.65 cSt and 1 cSt silicone oils. The comparison shows that the highest heat transfer augmentation is reached by using the water and the least viscous silicone oil, which shows the best enhancement. Water with the average Prandtl number of 5.5 shows the best enhancement, and it is followed by 0.65 cSt silicone oil with Prandtl number of 8.2. 1 cSt silicone oil with Prandtl number of 15 falls behind the 0.65 cSt silicone oil.

The augmentation decreases with increasing the viscosity. Hence, the less viscous the working fluid is in coiled tubing, the greater enhancement is reached. This difference in the heat transfer augmentation becomes more noticeable by increasing the flow rate. The secondary flow initiation strongly depends on the viscosity of the working fluid; the lower viscosity results in an increase of the intensity of the secondary flow, which as discussed before is the main reason for the heat transfer augmentation.

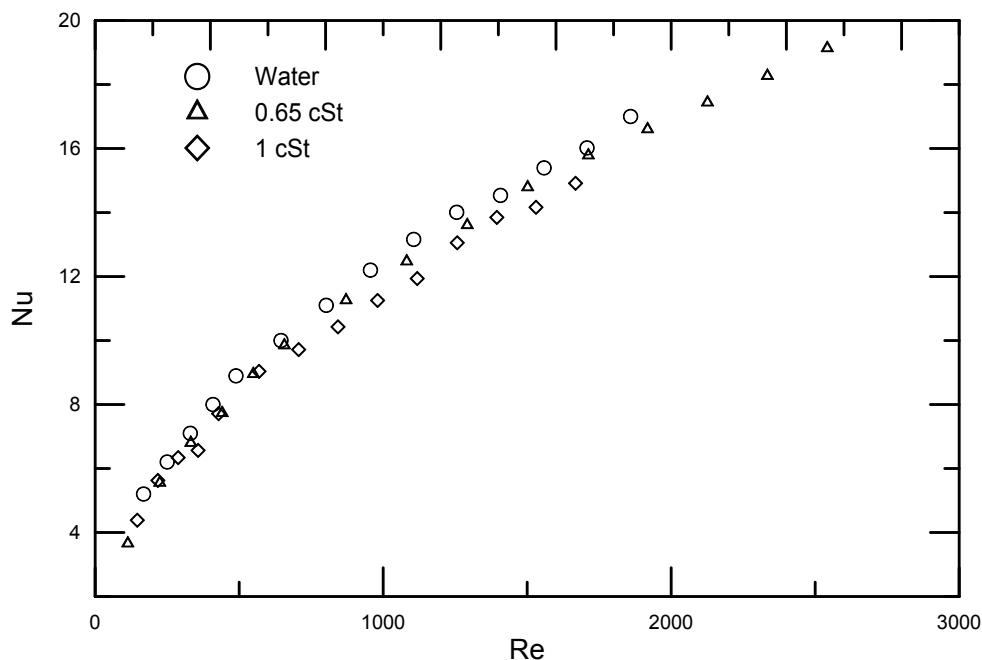


Figure 7.12: Viscosity effect on the curved tubing with three turns of 2 cm radius

Fig. 7.13 is another viscosity comparison inside the curved tubing with 1 cm radius and 3 turns of coil. This radius of curvature was the highest curvature we could examine in the constant temperature bath. The results for this geometry are in good agreement with that of Fig. 7.12. Water shows the best heat transfer performance in increasing the heat transfer, and the enhancement decreases by increasing the Prandtl number.

## 7.5 Conclusion

An experimental study has been conducted on the heat transfer inside mini scale coiled tubing for constant wall temperature condition. Water and two low viscosity silicone oils were used to investigate the enhancement effect of curved tubing. The flow inside curved tubes were categorized into three regions: low curvature region  $De < 10$ , where the heat transfer behaviour resembles the one in straight tubes,

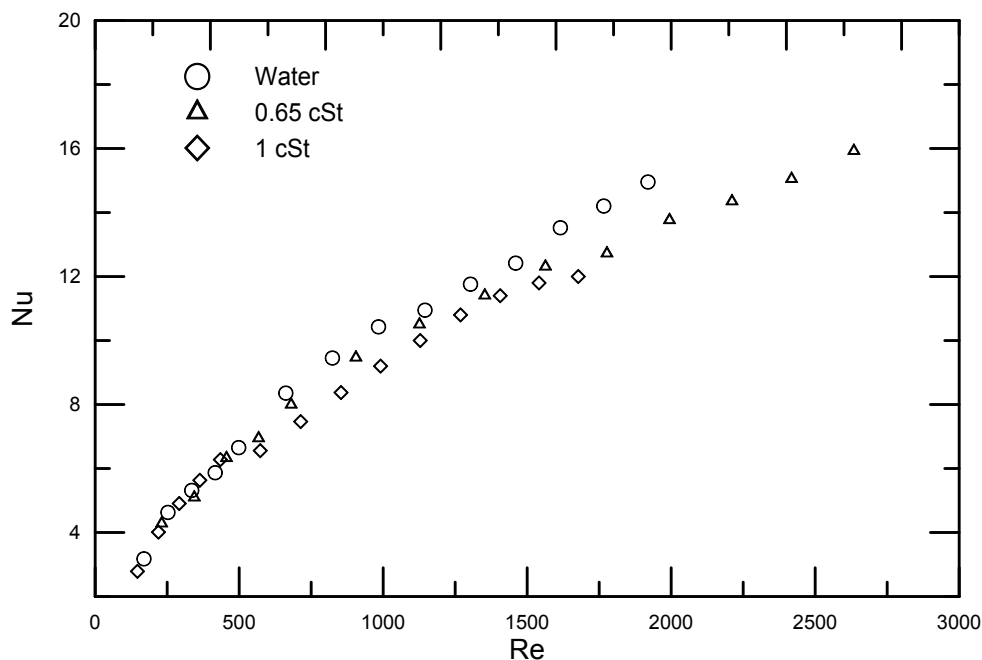


Figure 7.13: Viscosity effect on the curved tubing with three turns of 1 cm radius

high curvature region  $De > 50$  and transitional region  $10 < De < 50$ . Using an empirical method, a correlation is found to predict the heat transfer in high curvature region. Blending the two, and using the experimental results, an asymptotic model is proposed to predict the Nusselt number in the Prandtl number range of  $5 < Pr < 15$ , and Dean number range of  $40 < De < 700$ . The experimental results fall within the  $\pm 10\%$  range of the proposed model prediction.

The effect of curvature on the heat transfer was studied by examining the heat transfer in curved tubes with a constant length and different radii of curvature. It was shown that curved tubes are capable of enhancing the heat transfer at mini scale, and the heat transfer is increased by decreasing the radius of curvature (increasing the curvature  $1/R$ ). It has been shown that the augmentation remains the same for a constant Dean number, if a working fluid is not changed. However, obviously, a higher velocity is required when the curvature  $1/R$  is smaller to have the same Nusselt number.

In another part of this study, a set of coiled tubes with a constant radius of curvature and different lengths were used to study the effect of length on augmentation. The results for constant radius of curvature and different working fluids were compared to the proposed model and the model by Churchill and Manlapaz. The dimensionless mean wall flux and the dimensionless thermal length were also employed instead of conventional Nusselt number and Reynolds number analysis to reduce the results, in order to show the length effects on the heat transfer in coiled tubes. It was found that the Nusselt number in fully developed region is not affected by the length of coiled tubing.

Finally, the effect of Prandtl number on the heat transfer was studied. Similar tests were conducted with different working fluids. It has been shown that fluids with lower Prandtl number, namely water and 0.65 cSt silicone oil enhance the heat transfer better than the fluid with higher viscosity and Prandtl number.

Further investigations on curved tubing are required to investigate the heat transfer enhancement inside the coiled tubing with higher curvatures and lengths. As there is always a trade off between the heat transfer and pressure drop in a system, the same study for pressure drop is useful to find way to minimize the pressure drop and maximize the heat transfer in a curved tubing system.

### **Acknowledgments**

The authors acknowledge the financial support of the Natural Sciences and Engineering Research Council of Canada (NSERC) and Auto 21 NCE.

## **7.6 References**

- [1] A. P. Sudarsan , V. M. Ugaz, Fluid mixing in planar spiral microchannels, Journal of The Royal Society of Chemistry 6 (2005) 74-82.

- [2] S. Wongwises, P. Naphon, A review of flow and heat transfer characteristic in curved tubes, *Renewable and Sustainable energy reviews* 10 (2006) 463-490.
- [3] M. H. Oddy, J. G. Santiago, J. C. Mikkelsen, Electrokinetic Instability Micromixing, *Analytical Chemistry* 73 (2001) 5822-5832.
- [4] M. Riahi, E. Alizadeh, Fabrication of a 3D active mixer based on deformable Fe-doped PDMS cones with magnetic actuation, *Journal of Micromechanics and Micro-Engineering* 22 (11) (2012): 115001.
- [5] Q. Xiagemeng, L. Rongsheng, C. Hong, Microfluidic Chip Based Microarray Analysis, *Progress in Chemistry* 23 (01) (2011) 221-230.
- [6] C. Bartoli, F. Baffigi, Effects of ultrasonic waves on the heat transfer enhancement in subcooled boiling, *Experimental Thermal and Fluid Science* 35 (3) (2011) 423-432.
- [7] R. L. Webb, N. H. Kim, *Principles of enhanced heat transfer*, Taylor and Francis, Philadelphia, 2005.
- [8] Y. Mori, Y. Uchida, T. Ukon, Forced convective heat transfer in a curved channel with a square cross section, *International Journal of Heat and Mass Transfer* 14 (1971)1787-1805.
- [9] W. R. Dean, Note on the motion of fluid in a curved pipe, *The London, Edinburgh and Dublin Philosophical Magazine and Journal of Science* 4 (1927) 208-223.
- [10] W. R. Dean, The streamline flow through curved pipes, *The London, Edinburgh and Dublin Philosophical Magazine and Journal of Science* 5 (1928) 673-695.
- [11] K. Nigam, S. Vashisth, V. Kumar, A review on the potential applications of curved geometries ion process industry, *Industrial and Engineering Chemistry Research* 47 (2008) 3291-3337.
- [12] I. Mudawar, M. Visaria, Coiled-tube heat exchanger for high-pressure metal hybrid hydrogen storage systems- Part 1. Experimental study, *International Journal of Heat and Mass Transfer* 55 (2012)1782-1795.

- [13] I. Mudawar, M. Visaria, Part II: Coiled-tube heat exchanger for high-pressure metal hybrid hydrogen storage systems- Part 1. Experimental study, *International Journal of Heat and Mass Transfer* 55 (2012) 1796-1805
- [14] T. J. Rennie, Numerical and experimental studies of a double-pipe helical heat exchanger, Ph.D. Thesis, McGill University, Montreal, Canada, 2004.
- [15] K. Nigam, S. Vashisth, V. Kumar, F. Burhanuddin, Numerical Studies of a Tube-in-Tube Helically Coiled Heat Exchanger, *Chemical Engineering and Processing: Process Intensification* 47 (2008) 2287-2295.
- [16] H. Shokouhmand, M.R. Salimpour, M.A. Akhavan-Behabadi, Experimental investigation of shell and coiled tube heat exchangers using Wilson plots, *International Journal of Communications in Heat and Mass Transfer* 35 (2008) 84-92.
- [17] J. W. Rose, Wilson plot and accuracy of thermal measurements, *Experimental Thermal and Fluid Science* 28 (2004) 77-86.
- [17] C. M. White, Streamline flow through curved pipes, *Proceedings of Royal Society of London, Series A: Mathematical and Physical Science* 123 (1929) 645-663.
- [18] K. C. Cheng, M. Akiyama, Laminar forced convection heat transfer in curved rectangular channels, *Journal of Heat Transfer* 13 (1970) 471-490.
- [19] M. Akiyama, K. C. Cheng, Graetz problem in curved pipes with uniform wall heat flux, *International Journal of Research and Reviews in Applied Sciences* 29 (1974) 401-417.
- [20] K. C. Cheng, R. C. Lin, J. W. Ou, Fully developed laminar flow in curved rectangular channels, *Journal of Fluids Engineering* 98 (1976) 41-48.
- [21] L. C. Burmeister, M. W. Egner, Heat transfer for laminar flow in spiral ducts of rectangular, *Transaction of the ASME* 127 (2005) 352-356.
- [22] S. W. Chang, K. F. Chiang, J. K. Kao, Heat transfer and pressure drop in a square spiral channel roughened by in-line skew ribs, *International Journal of Heat*

and Mass Transfer 54 (2004) 3167-3178.

[23] S. M. Hashemi, M. A. Akhavan-Behbahani, An empirical study on heat transfer and pressure drop characteristics of CuO-base oil nanofluid flow in a horizontal helically coiled tube under constant flux, International Journal of Communications in Heat and Mass Transfer 14 (2012) 1787-1805.

[24] M. Ghobadi, Y. S. Muzychka, Effect of entrance region and curvature on heat transfer in mini scale curved tubing at constant wall temperature, International Journal of Heat and Mass Transfer 65 (2013) 357-365.

[25] R. L. Manlapaz, S. W. Churchill, Fully developed laminar convection from helical coil, Chemical Engineering Communication 9 (1980) 185-200.

[26] S. J. Kline, F. A. McClintock, Describing uncertainties in single-sample experiments, Journal of Mechanical Engineering 75 (1953) 3-8.

[27] Y. S. Muzychka, M. M. Yovanovich, Laminar forced convection heat transfer in combined entry region of non-circular ducts, Journal of Heat Transfer 126 (2004) 54-62.

[28] L. A. M. Jansen, C. J. Hoogendoorn, Laminar convective heat transfer in helical coiled tubes, International Journal of Heat and Mass Transfer 21 (2010) 1197-1206.

# Chapter 8

## Summary and Conclusions

The current thesis can be divided to three main parts. In the first part a summary of relevant correlations for the heat transfer and the pressure drop inside curved circular tubes are presented. In the second part (Chapters 3 and 4) two spiral and straight heat sinks were thermally and hydro dynamically investigated. In Chapters 5, 6 and 7 pressure drop and heat transfer in short and long curved tubes are studied.

## 8.1 Objectives of The Present Thesis

The main objectives of each chapter are listed as follow:

### 8.1.1 Heat Transfer and Pressure Drop in a Spiral Square Channel

Heat transfer and pressure drop performance of spiral square channel were studied by employing water and four different silicone oils. In one set of experiments fluids entered from the side of the spiral, and in the other they entered from the center. The heat transfer for all the fluids and the pressure drop for the water were examined experimentally. The results were normalized and compared to those for a continuous straight channel with the identical size.

The results furnished a number of important observations, namely which kind of fluid is the most efficient fluid and in which range of flow rate the heat transfer is enhanced. It was shown that 0.65 cSt silicone oil,  $Pr = 8$ , enhances the heat transfer better than other fluids and with less pressure drop penalty. It was observed that, in general, the spiral geometry is able to enhance heat transfer compared to a straight channel. Furthermore, it has been shown that spiral channel does not increase the augmentation significantly in low flow rates. Nevertheless, the pressure drop penalty becomes more significant as the flow rate increases. These results show that there is no difference in feeding the heat sink from the side or the middle. One should note that the entrance effects in short spiral channels could influence the pressure drop. Two models by Dravid [1] and Seader and Kalb [2] were used to predict the heat transfer results. The length of the spiral was discretized in to small cells, so the curvature in each cell was assumed to be constant. The comparison showed good agreement for the Dravid model [1] for Prandtl numbers greater than 5. However, the Seader and Kalb [2] correlation predicts the heat transfer augmentation with higher accuracy for water. Consequently, the Seader and Kalb correlation [2] was recommended for water and fluids with  $Pr < 5$ , and the Dravid correlation [1] was recommended for fluids with  $Pr > 5$ . The accuracy of the both models were questioned in the region  $5 < Pr < 15$ . Consequently, further studies were performed to generate a new model to predict the Nusselt number in mentioned Prandtl region.

### **8.1.2 Heat Transfer and Pressure Drop in Mini Channel Heat Sinks**

Water and five silicone oils with different viscosities were examined as a coolant in two heat sinks with different geometries. A spiral heat sink with different inlet/outlet configurations and a straight heat sink with sharp bends at each end were fabricated

on base plates of copper. The results were normalized and compared to the results for a straight channel with the identical size.

It has been shown that, in general, the spiral and straight heat sinks are able to enhance the heat transfer compared to a straight channel. Furthermore, It has been observed that the heat transfer for both heat sinks is not enhanced significantly in low flow rates and at higher flow rates conclude a better enhancement. However, the pressure drop penalty becomes more significant as the flow rate increases. Reviewing the results for the spiral geometry shows that there is no difference in feeding the heat sink from the side or the middle.

Comparing the pressure drop and heat transfer in the heat sinks revealed that while the flow is laminar in the straight channel, and at a constant pressure drop, both heat sinks have lower heat transfer rate in comparison to a straight channel having the same cross section. However, it is impossible to have a straight channel inside a heat sink and one should use another geometry and configuration to cool down a system. Whereas, having turbulent flow in the straight channel, the straight heat sink shows a better heat transfer at a constant pressure drop in comparison to the straight channel. It was shown that for a constant pressure drop, heat transfer inside a straight channel is higher when one uses laminar flow, whereas, in turbulent flow, the straight heat sink shows a better enhancement compared to a simple channel.

### **8.1.3 Effect of Entrance Region and Curvature on Heat Transfer in Mini Scale Curved Tubing at Constant Wall Temperature**

Experimental studies have been done on the heat transfer inside short mini scale curved tubes at the constant wall temperature boundary condition. Water and three

low viscosity silicone oils were used to investigate the enhancement effect of curved tubing. The dimensionless mean wall flux and the dimensionless thermal length were used instead of conventional Nusselt number.

First, the Dravid model [1] was used to predict the heat transfer behavior for a constant wall temperature wall with good accuracy. The criteria for the Dean number and Prandtl number were checked to make sure that it is applicable under the current condition. The experimental results were predicted with 10 percent accuracy.

Second, the effect of curvature on the heat transfer was studied by examining the heat transfer in curved tubes with a constant length and different curvatures. It was observed that the heat transfer is increased by decreasing the radius of curvature (increasing the curvature). It was shown that short mini-scale curved tubes are capable of greater enhancing the heat transfer. It also has been shown that the augmentation is fairly constant for a constant length and Dean number. However, a higher Reynolds number is required when the curvature is smaller to have the same Dean number.

Third, a set of short curved tubes with constant curvature and different lengths were used to study the effect of length on augmentation. The experimental results reveal that increasing the length at the same curvature results in significantly increasing the total heat transfer. This means that the enhancement mechanism needs some length to become effective. The Nusselt number analysis revealed more interesting results, showing that the entrance effect dominates the augmentation in short lengths, however the secondary flow effect becomes greater by increasing the curved tubing length. The normalized results which eliminated the entrance effect have shown that the enhancement is increased by increasing the length.

### 8.1.4 Pressure Drop in Mini-Scale Coiled Tubing

Using curved tubes as a passive heat transfer enhancement is attractive in many industries, however, the increased pressure drop is recognized as the main drawback for the systems employing curved tubes. Experimental studies have been conducted on the pressure drop inside mini scale coiled tubes. Plastic tubes with three different mini scale diameter were cut in 1 m and 0.5 m lengths and were coiled around the cylinder with different radius of curvature. A wide range of Reynolds numbers, 40-220, and Dean numbers, 7-560, were studied.

It was shown that the curved tubes increase the pressure drop in comparison to straight tubes. It has also been shown that the pressure drop for the flows inside the tubes with greater curvature  $1/R$  is larger than for flow inside less curved tubes as expected.

Based on the present experimental results, we found that flows with low Dean number,  $De < 5$ , behave the same as flows inside straight tubes, and pressure drop was almost similar to straight tubes. For the flows with high Dean number,  $De > 50$ , the pressure drop was found to follow another asymptote in the format of a simple power law, where using curved tubes, Reynolds number is replaced by Dean number. Combining the two asymptotes and using the results in the transition region,  $5 < De < 50$ , a new asymptotic correlation is proposed to predict the pressure drop in curved tubes, and coiled tubes with small pitch.

The correlation was able to predict the results at mini scale and in the Dean number range of the present experiments with less than 5 percent error, and the maximum error was found to be 10 percent. The Manlapaz and Churchill model [3] was also used in the comparisons and it was shown that the error for their predictions is unacceptable at mini scale.

### 8.1.5 Fully Developed Heat Transfer in Mini Scale Coiled Tubing for Constant Wall Temperature

Comparing the collected experimental results with the existing models, no model could predict the Nusselt number for the working fluid with  $5 < Pr < 15$ . An experimental study has been conducted on the heat transfer inside mini scale coiled tubing for constant wall temperature condition. Water and two low viscosity silicone oils were used to investigate the enhancement effect of curved tubing. The flow inside curved tubes were categorized into three regions: low curvature region  $De < 10$ , where the heat transfer behaviour resembles the one in straight tubes, high curvature region  $De > 50$  and transitional region  $10 < De < 50$ . Using an empirical method, a correlation is found to predict the heat transfer in high curvature region. Blending the two asymptotes, and using the experimental results, an asymptotic model is proposed to predict the Nusselt number in the Prandtl number range of  $5 < Pr < 15$ , and Dean number range of  $40 < De < 700$ . The experimental results fall within  $\pm 10\%$  of the proposed model prediction.

The effect of curvature on the heat transfer was studied by examining the heat transfer in curved tubes with a constant length and different radii of curvature. It was shown that curved tubes are capable of enhancing the heat transfer at mini scale, and the heat transfer is increased by decreasing the radius of curvature (increasing the curvature  $1/R$ ). It has been shown that the augmentation remains the same for a constant Dean number, if a working fluid is not changed. However, obviously, a higher velocity is required when the curvature  $1/R$  is smaller to have the same Nusselt number.

In another part of this study, a set of coiled tubes with a constant radius of curvature and different lengths were used to study the effect of length on augmentation. The results for constant radius of curvature and different working fluids were compared to

the proposed model and the model by Churchill and Manlapaz. The dimensionless mean wall flux and the dimensionless thermal length were also employed instead of conventional Nusselt number and Reynolds number analysis to reduce the results, in order to show the length effects on the heat transfer in coiled tubes. It was found that the Nusselt number in fully developed region is not affected by the length of coiled tubing.

## **8.2 Recommendations for Future Studies**

Based on the results of the present thesis, there are still many open questions and discussions on heat transfer in two phase slug flows in curved geometry. The followings are the most important ones which could be considered and addressed in future studies:

### **8.2.1 Two-Phase Flow inside Curved Ducts**

Two-phase segmented flow, Taylor flow, is known as an effective method to enhance heat transfer, however, it increases the pressure drop at the same time. Combining the curved geometry and the slug flow can furnish further heat transfer enhancement methods. The slug flow can be liquid-gas or liquid-liquid flow.

### **8.2.2 Particle Image Velocimetry**

Although many investigations have been conducted using PIV, there are still many gaps that need to be filled. Curved geometry is known as an efficient way for heat transfer augmentation in heat sinks and few studies were performed to understand the nature of the flow in a curved channel from heat transfer point of view and also hydrodynamic point. Micro-PIV observation is needed to find the flow field change

for different Reynolds number, curvatures and cross sections.

### 8.2.3 Flow in Micro Scale Curved Ducts

All of the results presented in this dissertation were in the mini scale range. However, with the recent advancement in micro fabrication technologies, the size of electronic devices is decreasing. At the same time, the high density of circuits and related heat generation requires a simultaneous increase in the performance of a cooling system to keep the electronics operating at optimum temperature. Conventional air-based heat sinks have limited heat transfer coefficient which needs to be extended. Liquid cooled micro channel networks or heat sinks are known to be a promising approach to this heat transfer problem because of its plausible manufacturability at the chip level. Micro-fabrication technologies allow us to produce miniature liquid cooled heat sinks which are suitable for microprocessor cooling purpose. Heat transfer enhancement using curved geometries in the micro scale has many challenges for future studies.

## 8.3 References

- [1] Dravid, A. N., Smith, K. A., Merrill, E. W., Brian, P. L. T., Effect of Secondary Fluid Motion on Laminar Flow Heat Transfer in Helically Coiled Tubes, *American Institution of Chemical Engineers*, vol. 17, no. 5, pp. 1114-1122, 1971.
- [2] Kalb, C. E., and Seader, J. D., Fully Developed Viscous Flow, Heat Transfer in Curved Tubes with Uniform Wall Temperatures, *American Institute of Chemical Engineers Journal*, vol. 20, pp. 340-346, 1974.
- [3] Manlapaz, R. L., and Churchill, S. W. Fully Developed Laminar Convection From a Helical Coil. *Chemical Engineering Communication*, vol. 97, pp. 185-200, 1981.

# Appendix A

## Appendix

### A.1 Experimental Method

The general configurations of the experiments were explained briefly in the corresponding chapters. In this section I describe more details about the different experimental setup used during my PhD studies, and add more pictures to illustrate the experimental setup.

#### A.1.1 Heat Sinks

Fig. A.1 shows the two heat sinks, used for the experiments. The square 1 *mm* channel was fabricated on a copper base plate. The following equation defines the radius of curvature at each distance from the center of spiral heat sink,  $x$ :

$$R = 2 + \frac{2x + x^2/2}{\pi} \quad (\text{A.1})$$

A flat copper cap plate with the identical size was bolted tight to seal the channel. The total heat provided by two heaters (Watlow Film Heaters), one placed on the cap, and one on the plate, which contains the channel. Five T type thermocouples were



Figure A.1: Heat sinks channel patterns

placed near the spiral channel wall to measure the surface temperature; one at the dead center and four at the center of each quadrant on one surface. Two additional thermocouples were used to measure the inlet and outlet bulk temperature using a simple T junction with a thermocouple embedded into the stream. A Keithley Data Acquisition system (DAQ) collected the temperatures during the experiments. 10 readings were collected within 10 time steps, and averaged to give me the temperature of the four corners and the middle of the heat sinks. The five measured temperatures from the wall were averaged to calculate the mean surface temperature. The maximum temperature difference between the five readings was found to be less than  $2^{\circ} C$ , which means less than 5% maximum deviation from the average surface temperature. Two heaters were also glued to the both surfaces of the heat sinks in order to provide a symmetric heat flux to the heat sink. Fig. A.2 depicts the schematic configuration of the system.

The heat sinks were placed inside boxes surrounded by insulation material were to

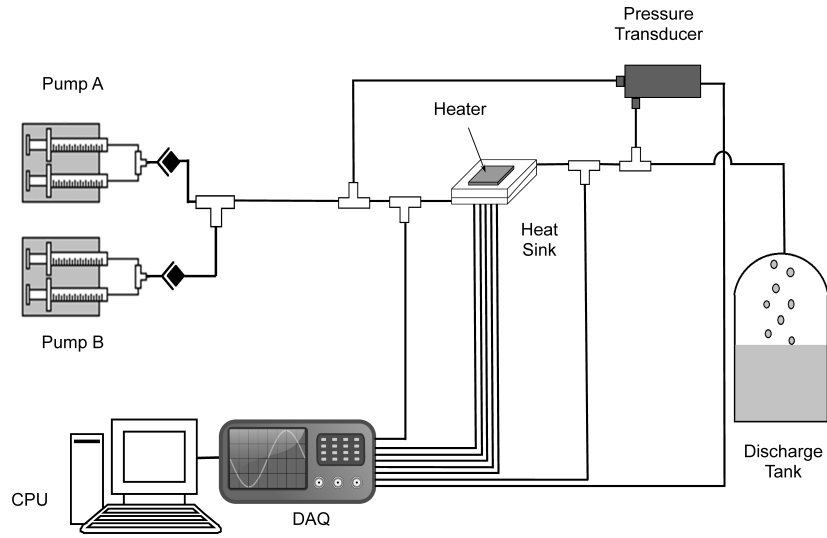


Figure A.2: Experiment configurations of the heat sinks tests

minimize the effect of natural convection and radiation (Fig. A.3). The thermal resistance of the system was measured, and used to calculate the heat transfer to the surrounding. In order to calculate the thermal resistance of the box, different power levels were applied to the heat sinks without having any flow inside them. Hence, the only mode of heat transfer from the heat sink assumed to be the conduction through the insulation box to the ambient temperature. The surface temperature was read for each applied power. The thermal resistance for each applied power may be found as:

$$R_{thermal} = \frac{P}{T_w - T_a} \quad (\text{A.2})$$

By averaging the calculated thermal resistance for different applied powers, the thermal resistance of the insulation box was calculated ( $R_{thermal} = 47.25 \text{ m}^2\text{K/W}$ ). Consequently, I could measure the heat removed by the working fluid and ambient, and found the heat transfer coefficient of the fluid.

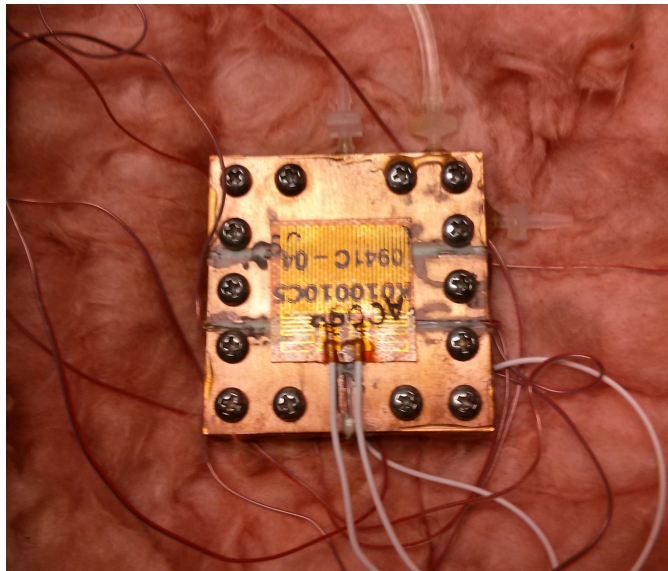


Figure A.3: A heat sink inside the insulation box

### A.1.2 Curved and Coiled Tubes

Generally, two types of coiled and curved tubing were employed during the experiments: copper tubing and plastic tubing. Copper tubes were mostly used for the heat transfer calculation purpose, and plastic ones were used to measure the pressure drop. In the first part of the experiments, I began with short curved tubes that were explained and depicted in Chapter 5. The tubes were cut and curved in the MUN shop, and the ends were polished to minimize the effect of entrance disturbance. The coil tubes used in Chapter 7 were curved in the same way. The number of turns was chosen short enough so that the working fluid does not become saturated. A few number of the coiled tubes are depicted in Fig. A.4.

Mini scale plastic tubes were curved around cylinders with different diameter to investigate the pressure drop inside mini scale coiled tubes. The results were presented in Chapter 6. Fig. A.5 shows how the tubes for the pressure drop measurement purpose were coiled.



Figure A.4: Coiled tubes used for the heat transfer experiments in Chapter 7



Figure A.5: A coiled tube used for the pressure drop tests

## A.2 Benchmarking Tests

Benchmarking is defined as the process of comparing one's process and performance metrics to industry bests or best practice from other industries. Dimensions typically measured are quality, time and cost. Benchmarking in the current case is applied to redo the tests under conditions which the correct answers are already known and by comparing the obtained experimental results with the expected answers I could verify the experimental procedure. In the most cases, a straight tubing or a channel is used, since the exact results for straight tubes/channels are widely available.

In this section, I briefly describe how I have benchmarked the experiment procedure. There are two tests regarding the benchmarking: 1) Heat transfer, 2) Pressure drop. Both tests were done on a straight tube and under different working conditions.

### A.2.1 Heat Transfer

The test was done with a 163 mm long straight copper tubing with the diameter of 1.65 mm. the tubing was cut precisely and the edges were filed to have smooth ends. Finally, two plastic tubes were glued to the ends to avoid any leakage. Thermocouples were placed at each side with the minimum distance from the copper tubing. As the conductivity of the plastic tubing is too low (in comparison to copper) we assume that the exit temperatures that were measured are equal to the temperature of the fluids at the end of the copper tubing. The constant wall temperature condition was considered with surface temperature of 40° C. The ambient temperature was around 25° C.

The tube was placed in the thermal bath horizontally, so gravity doesn't affect the results. Fig. A.6 shows the tube and connections used for the heat transfer benchmarking test. The flow assumed to be hydrodynamically developed and thermally



Figure A.6: The straight tube used for the heat transfer benchmarking test

developing at the copper tube entrance. Water, 0.65 cSt oil, 1 cSt and 3 cSt oil were examined as working fluid.

A good agreement was observed between the measured heat transfer coefficient and the calculated coefficient. Fig. A.7 depicts the comparison of the Graetz model and the examined fluids. The RMS error calculation based on the following correlation was done and the results are shown in table A.1.

Table A.1: RMS of heat transfer benchmarking test

Fluid	Water	0.65 cSt	1 cSt	3 cSt
RMS	3.29%	9.35%	8.05%	2.85%

### A.2.2 Pressure Drop

The pressure drop verification was done on a 3 meter piece of plastic pipe. The diameter of the pipe was 3.14 mm and the flow was assumed to reach the fully developed condition (based on the hydrodynamic entrance length). Water was used as the working fluid at the room temperature (22° C). Reynolds numbers from 65 up to 1200 was

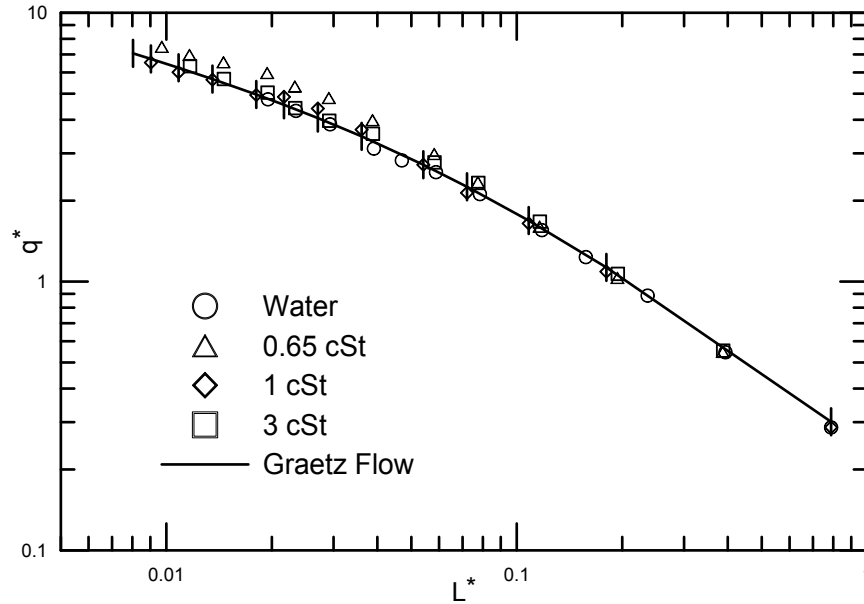


Figure A.7: Heat transfer benchmarking results for water and different silicone oils with 10% error bars

examined; hence, the flow remained laminar:

$$\Delta p = \frac{128\mu L Q}{\pi D^4} = 32 \frac{L}{D} \frac{\mu \bar{u}}{D} \quad (\text{A.3})$$

Three different pressure sensors with different range were used to measure the pressure drop: 0-1 psi, 0-10 psi and 0-50 psi. Therefore, pressure drop at each velocity was measured with the most accurate sensor. Fig. A.8 shows the benchmarking summary inside the 3 meter straight tube. The collected points are within the 5% range of the straight tube model.

### A.2.3 Viscosity Benchmarking

As a part of my experimental verification, I also measured the reported qualities of working fluids with a precise instrument to verify the reported values by the provider companies. The viscosity of the silicone oils, as well as their temperature dependence

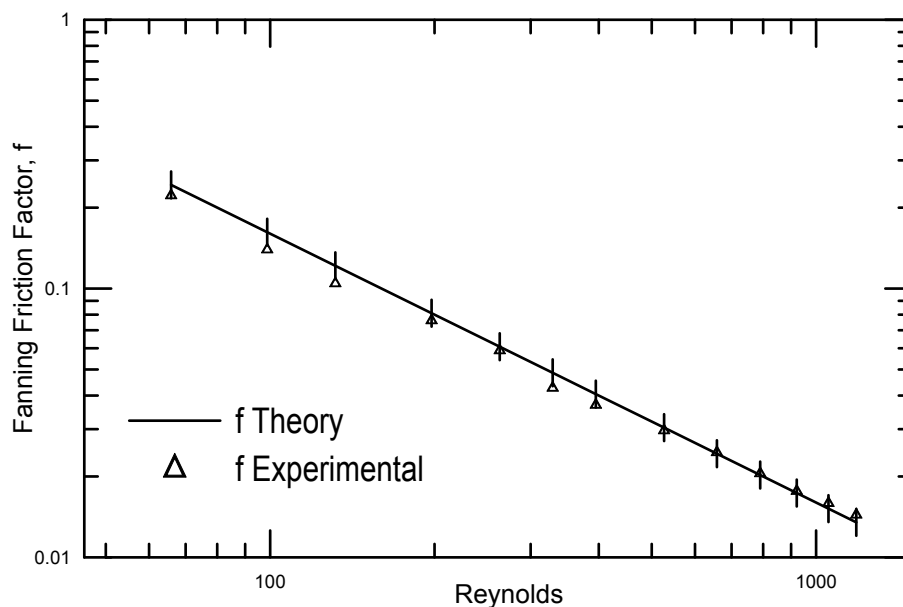


Figure A.8: Pressure drop benchmarking results for water with 10% error bars

were given by the manufacturer (Fig. A.9). However, we also measured the viscosities of the oils with an accurate apparatus (Physica MCR 301 from Rheosys Company) at room temperature to confirm the reported data. Different rates of rotational speed were applied to the disk rotating on a film of the fluid, and the required torque was measured. Finally, the apparatus converted the given torque to the viscosity for each speed. The mean viscosity of a fluid can be calculated from of the collected data. The accuracy of the device was also benchmarked by measuring the viscosity of water. Reported viscosity at temperature of 22° C by the company, measured viscosity at temperature of 22° C and deviation are shown in table A.2

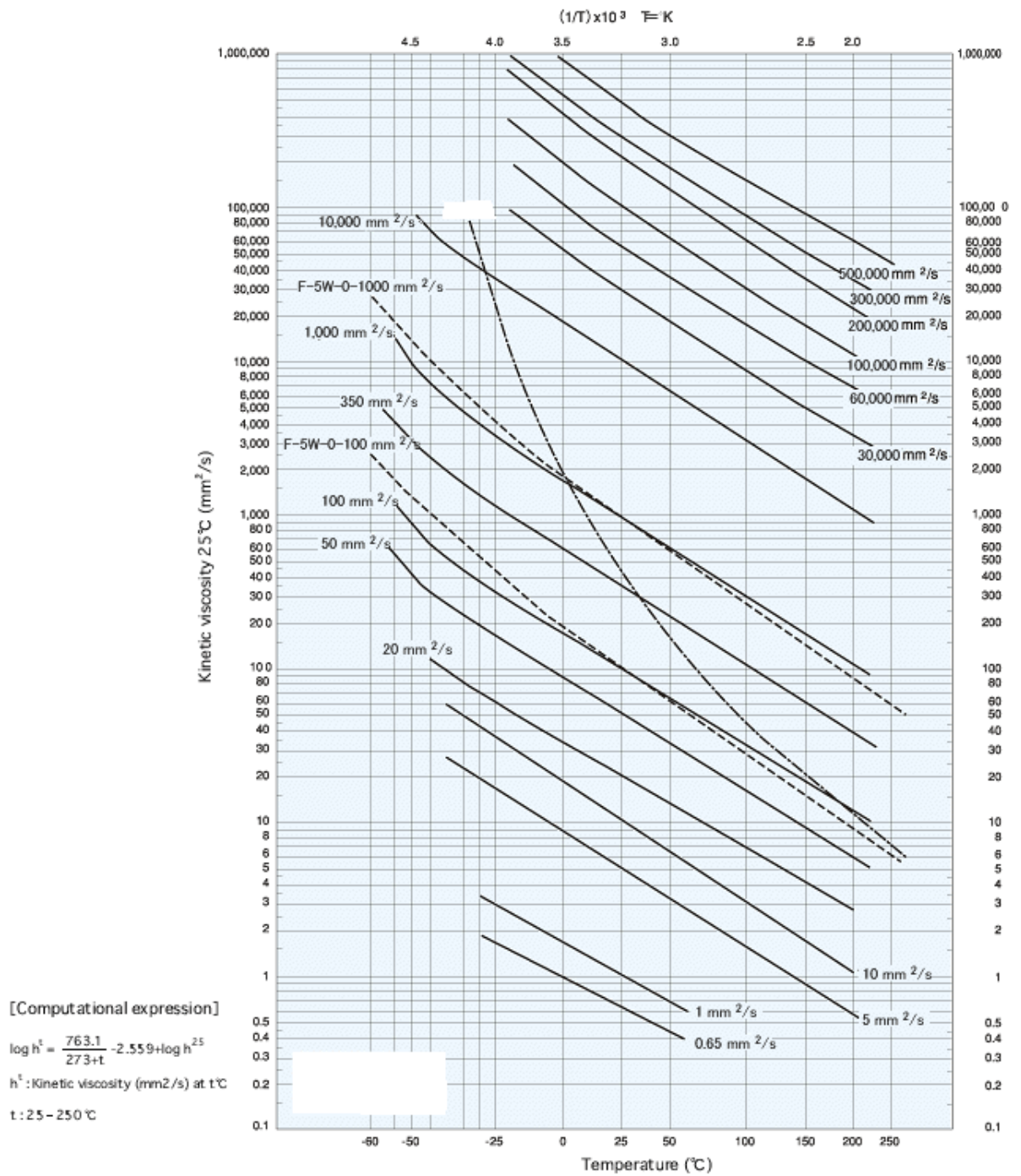


Figure A.9: Viscosity of the silicon Oils given by the company (Clear Co.)

Table A.2: Silicone oils benchmarking results

Fluid	Measured Viscosity	Reported Viscosity	Difference
0.65 cSt	0.505 cSt	0.526 cSt	4.18 %
1 cSt	0.895 cSt	0.872 cSt	2.51 %
3 cSt	2.616 cSt	2.717 cSt	3.87 %
10 cSt	9.415 cSt	9.406 cSt	1.02 %
100 cSt	101 cSt	99.398 cSt	1.58 %

### A.3 Uncertainty Analysis

Uncertainty of the reported quantities have been reported in each chapter, and the method by Kline and McClintock [1] was introduced to calculate it.

$$w_F = \left[ \left( \frac{\delta F}{\delta x_1} w_1 \right)^2 + \left( \frac{\delta F}{\delta x_2} w_2 \right)^2 + \dots + \left( \frac{\delta F}{\delta x_n} w_n \right)^2 \right]^{1/2} \quad (\text{A.4})$$

where  $F$  is a given function of the independent variables  $x_1, x_2, \dots, x_n$ , and  $w_F$  is the uncertainty in the result and  $w_1, w_2, \dots, w_n$  are uncertainties in the independent variables.

In this section I will calculate uncertainties for three parameters as samples: Reynolds number,  $L^*$  and  $q^*$ . In each case an amount for each independent variable is assigned and depending on the uncertainties of each variable, the uncertainty of the results is calculated.

#### A.3.1 Reynolds Number Uncertainty

Reynolds number can be defined as:

$$Re = \frac{\rho U D}{\mu} \quad (\text{A.5})$$

Considering  $\rho = 996 \frac{Kg}{m^3}$  and  $U = 1 m/s$  with 1% uncertainty for  $\rho U$ ,  $\mu = 8.7 \times 10^{-4}$  with 2% uncertainty and  $D = 1.6 mm \pm 0.02 mm$ . Calculating Reynolds number for this case as:  $Re = 1,31.7$ , we can calculate the uncertainty for the Reynolds number as:

$$w_{Re} = \left[ \left[ \left( \frac{D}{\mu} \right) \times 0.01 \times 996 \right]^2 + \left[ \left( \frac{\rho U}{\mu} \right) \times 2 \times 10^{-5} \right]^2 + \left[ \left( \rho U D \frac{-1}{\mu^2} \right) \times 0.02 \times 8.7 \times 10^{-4} \right]^2 \right]^{1/2} \quad (A.6)$$

$$w_{Re} = [335 + 524 + 1,341.7]^{1/2} = 46.91 \quad (A.7)$$

It means that the uncertainty of the calculation is  $Re = 1,831.7 \pm 46.9$  or 2.56%.

### A.3.2 $L^*$ Uncertainty

$L^*$  can be defined as:

$$L^* = \frac{L/D}{PrRe} \quad (A.8)$$

Considering  $\rho = 996 \frac{Kg}{m^3}$  and  $U = 1 m/s$  with 1% uncertainty for  $\rho U$ ,  $\mu = 8.7 \times 10^{-4}$  *Pa.s* with 2% uncertainty,  $D = 1.6 mm \pm 0.02 mm$ , Length of  $L = 100 mm \pm 0.01 mm$  and Prantdl number of 5. Calculating Reynolds number for this case as:  $Re = 1,31.7 \pm 46.91$ , and  $L^* = 0.00682$ , we can calculate the uncertainty for the  $L^*$  as:

$$w_{L^*} = \left[ \left[ \left( \frac{1/D}{PrRe} \right) \times 10^{-5} \right]^2 + \left[ \left( \frac{L}{PrRe D^2} \right) \times 10^{-5} \right]^2 + \left[ \left( \frac{L}{PrD Re^2} \right) \times 46.91 \right]^2 \right]^{1/2} \quad (A.9)$$

$$w_{L^*} = [4.65 \times 10^{-13} + 10^{-9} + 3 \times 10^{-8}]^{1/2} = 0.0002846 \quad (A.10)$$

The uncertainty of the  $L^*$  is calculated as  $L^* = 0.00682 \pm 0.0002846$  or 4.1%.

### A.3.3 $q^*$ Uncertainty

$q^*$  can be defined as:

$$q^* = \frac{\bar{q}D_h}{K(T_w - T_i)} \quad (\text{A.11})$$

The uncertainty of  $q^*$  is calculated for the case of the spiral channel explained in Chapters 3 and 4. The spiral channel has the length of  $278 \text{ mm} \pm 0.01 \text{ mm}$  and the square cross section with  $1 \text{ mm} \pm 0.01 \text{ mm}$  side. The uncertainty of  $q^*$  will be calculated for the case where  $T_w = 26.91^\circ \text{ C} \pm 0.1^\circ \text{ C}$ ,  $T_i = 24.39^\circ \text{ C} \pm 0.1^\circ \text{ C}$ . Other properties of water are:  $C_p = 4072 \text{ J/K}$  and  $K = 0.613 \text{ W/mK}$ .

$$\bar{q} = \frac{Q_{net}}{4D_hL} \quad (\text{A.12})$$

We measured  $Q_{net} = 7.44 \text{ W}$ , and calculated  $q^* = 4.34$ . One may plug in  $\bar{q}$  in the main equation and eliminate  $D_h$ . However, one should note that the uncertainty of  $D_h$  would be eliminated in this case. Thus, in order to apply consider the uncertainties of  $D_h$ , we may write  $q^*$  as:

$$q^* = \frac{\frac{Q_{net}}{4D_hL} D_h}{K(T_w - T_i)} \quad (\text{A.13})$$

Consequently, we may calculate the  $q^*$  uncertainty components as:

$$\left[ \left( \frac{Q_{net}}{4KLD_h(T_w - T_i)} \right) \times 10^{-5} \right]^2 = 0.001876 \quad (\text{A.14})$$

$$\left[ \left( \frac{Q_{net}D_h}{4KL(T_w - T_i)D_h^2} - 1 \right) \times 10^{-5} \right]^2 = 0.001867 \quad (\text{A.15})$$

$$\left[ \left( \frac{Q_{net}D_h}{4LKD_hT_w^2} - 1 \right) \times 0.1 \right]^2 = 1.469 \times 10^{-10} \quad (\text{A.16})$$

$$\left[ \left( \frac{Q_{net} D_h}{4LK D_h} \frac{1}{T_i^2} \right) \times 0.1 \right]^2 = 1.51 \times 10^{-10} \quad (\text{A.17})$$

$$\left[ \left( \frac{Q_{net} D_h}{4LK D_h (T_w - T_i)} \frac{-1}{L^2} \right) \times 10^{-5} \right]^2 = 2.4 \times 10^{-8} \quad (\text{A.18})$$

and the uncertainty of the calculation becomes:

$$w_{q^*} = \left[ 0.001876 + 0.001876 + 1.47 \times 10^{-10} + 1.51 \times 10^{-10} + 2.4 \times 10^{-8} \right]^{1/2} = 0.0612 \quad (\text{A.19})$$

The  $q^*$  uncertainty can be written as:  $q^* = 4.34 \pm 0.0612$  or 1.41%.